Development of $Au/TiO_2/SiO_2$ photocatalysts and their application as self-cleaning and depolluting coatings for building materials

Manuel Luna

María Jesús Mosquera Díaz, Catedrática del Departamento de Química Física de la Universidad de Cádiz y José Manuel Gatica Casas, Profesor Titular del Departamento de Ciencia de los Materiales e Ingeniería Metalúrgica y Química Inorgánica de la Universidad de Cádiz.

Certifican:

> Que la presente Tesis Doctoral titulada «Development of $Au/TiO_2/SiO_2$ photocatalysts and their application as self-cleaning and depolluting coatings for building materials» elaborada por el licenciado en química Manuel Jesús Luna Aguilera ha sido realizada bajo nuestra dirección y que, hallándose concluida, autorizamos su presentación a fin de que pueda ser evaluada.

Y para que conste, expedimos y firmamos el presente informe en Puerto Real (Cádiz) a 29 de marzo de 2019.

Fdo. María Jesús Mosquera Díaz

Fdo. José Manuel Gatica Casas

Agradecimientos

Primero agradecer a mis directores María Jesús Mosquera Díaz y José Manuel Gatica Casas porque sin su dirección y ayuda no habría sido posible realizar esta Tesis.

También quiero agradecer a:

-Hilario Vidal por su colaboración en varios de los trabajos de investigación que conforman está Tesis y por ofrecerse a revisar el resto de la Tesis.

-Juan José Delgado por su participación en el primer trabajo de esta Tesis.

-Almoraima Gil ya que gracias a ella comencé esta Tesis por ayudarme siempre que lo he necesitado.

-Los miembros del grupo de investigación en el momento de mi llegada, Luis, Dario y Farid, por enseñarme todo lo necesario para comenzar mi trabajo en la Tesis.

-El resto de miembros del grupo, Giada, Marina (aunque ya no esté y nos caigamos mal), Souad, Jorge, y en especial a Luis y Rafa, con los que llevo desde el comienzo de la aventura universitaria.

-El profesor Mills de la Queen's University of Belfast por permitirme realizar una estancia en su grupo que ha supuesto una experiencia y unos resultados de gran valor para esta tesis. También a Steph por enseñarme toda la metodología de trabajo. Y a todos los miembros del grupo por su amabilidad y hacerme sentir uno más.

-Mis padres que sin ellos no hubiera llegado a donde estoy y siempre han estado ahí para apoyarme.

-A mi pareja con la que he vivido y sufrido todo este periodo, que siempre ha estado ahí y que sin su ayuda y en especial la de estos últimos meses no habría sido capaz de finalizar esta Tesis de la manera adecuada.

-A mis amigos, que hemos tenido que hacer malabares para poder vernos y pasar ratos juntos e incluso tirar de juego online para no perder el contacto.

-Y por último a Akira Toriyama, he crecido de la mano de Dragon Ball y me ha hecho eternamente feliz que después de tantos años decidiera continuar su obra durante este periodo tan importante de mi vida

Esta tesis ha sido realizada bajo la financiación del Gobierno de España asociada a los proyectos de investigación *MAT2013-42934 y MAT2017-84228-R y al contrato predoctoral* BES-2014-068031 *concedido en la convocatoria «A*yudas para contratos predoctorales para la formación de doctores 2014»

Index

Resumen

Actualmente, la contaminación del aire es uno de los principales problemas de la población mundial, por lo que hay un creciente interés en el desarrollo de tecnologías para su mitigación. TiO_2 es un fotocatalizador que ha mostrado tener capacidad para dotar a los materiales de construcción de propiedades autolimpiantes y descontaminantes. Sin embargo, la efectividad del TiO_2 se encuentra limitada bajo iluminación solar debido a su exclusiva absorción de luz ultravioleta, por lo que resulta imprescindible, para estos fines, modificar los fotocatalizadores de TiO_2 para aprovechar más eficientemente la luz solar.

Esta Tesis Doctoral se centra en el desarrollo y estudio de fotocatalizadores de $Au/TiO_2/SiO_2$, específicamente diseñados para ser aplicados en materiales de construcción, dotándoles propiedades autolimpiantes y descontaminantes. El oro mejora la fotoactividad del TiO_2 y la matriz de SiO_2 promueve la adhesión del TiO_2 al sustrato. En particular, se han estudiado diferentes parámetros para optimizar la actividad de estos fotocatalizadores, siendo los más relevantes: (i) el método de incorporación de las nanopartículas de oro (AuNPs), (ii) su tamaño y su relación respecto al TiO_2, (iii) el tipo y la relación TiO_2/SiO_2, y (iv) la combinación de las AuNPs con TiO_2 dopado con nitrógeno. Se ha llevado a cabo una caracterización en detalle de los fotocatalizadores desarrollados con objeto de correlacionar sus propiedades químicas, texturales y estructurales con su actividad fotocatalítica.

Esta estrategia permite la aplicación de los soles de $Au/TiO_2/SiO_2$ en materiales de construcción, penetrando el sol en el sustrato y produciendo recubrimiento fotocatalíticos firmemente adheridos. La fotoactividad del recubrimiento origina materiales de construcción con propiedades autolimpiantes y descontaminantes que son considerablemente mejoradas cuando se integran las AuNPs en los recubrimientos.

Abstract

Air pollution is one of the major problems of the current world, thus, there is an increasing focus on the development of technologies for its mitigation. TiO_2 is a photocatalyst that has demonstrated to have the capacity of promote self-cleaning and de-polluting properties on building materials. However, the TiO_2 performance is limited in outdoor conditions due to its exclusive UV absorption and modified-TiO_2 photocatalysts are necessary to take advantage of the sunlight.

In this Doctoral Thesis $Au/TiO_2/SiO_2$ photocatalysts specifically designed to be applied on building materials for producing self-cleaning and depolluting properties have been synthetized. The gold improves the TiO_2 photoactivity and the SiO_2 matrix promotes the adhesion TiO_2-substrate. In particular, different parameters have been studied in order to optimize these photocatalysts. The most relevant being: (i) the method of incorporation of the gold nanoparticles (AuNPs), (ii) their size and loading, (iii) the type of TiO_2 particles and their loading, and (iv) the combination of AuNPs and nitrogen doping of TiO_2. An in-depth characterization of the developed photocatalysts has been carried out in order to correlate their chemical, textural and structural properties with their photocatalytic performance.

This strategy allows the application of the $Au/TiO_2/SiO_2$ sols on building materials by common methods, penetrating the sols in the substrates and producing well-adhered photocatalytic coatings. The photoactivity of the coatings results in obtaining building materials with self-cleaning and depolluting properties, which are considerably enhanced when AuNPs are present in the coating.

Chapter 1

Introduction

1.1. TiO_2 photoactivity

The starting point of the TiO_2 use as photocatalyst was the year 1972 when Fujishima and Honda discovered the TiO_2-mediated electrochemical photolysis of water [1]. Since them, the TiO_2 has become the most widely employed and investigated photocatalyst due to its high photoactivity, good physicochemical stability, low cost and the lack of toxicity [2,3]. The abundant number of researches about TiO_2 has demonstrated its versatility showing effectiveness for photocatalytic water splitting and hydrogen production, photoelectrochemistry applications, dye sensitization and solar energy conversion and photochemical air and water treatments [4]. These applications take place according to different mechanisms, but all of them has the same origin, being initiated when TiO_2 received radiation with energy higher than its band gap. The TiO_2 excitation promote its electrons in the valence band to the conduction band, resulting in the formation of electron-hole pairs. These photoinduced charge carriers are the responsible of the photoelectrical properties of TiO_2, but they can also react with adsorbed species or with O_2 and water to produce radicals triggering different chemical process, as represented in Figure 1.

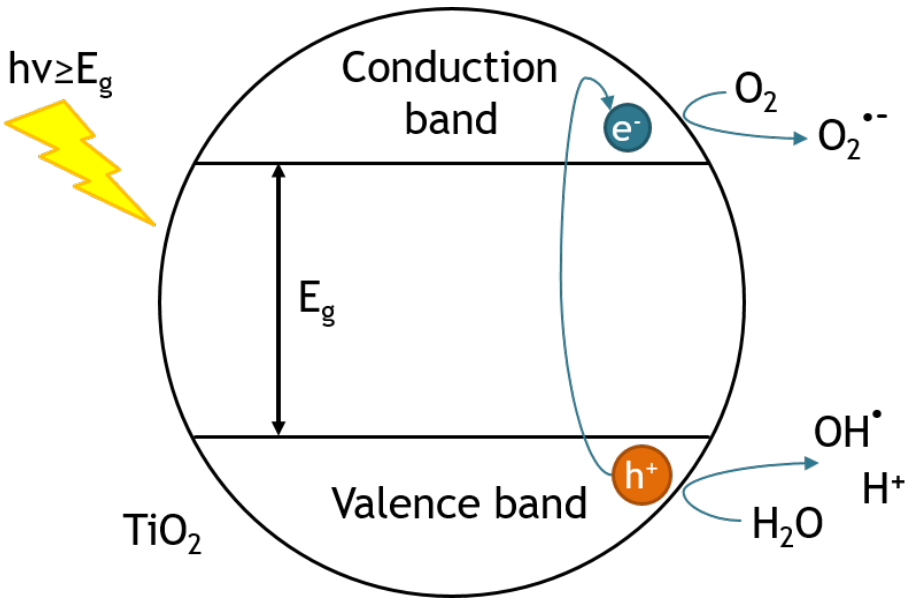

Figure 1. Schematic representation of TiO_2 photo-activation.

The amorphous TiO_2 is not photoactive whereas the crystalline TiO_2, which mainly occurs in three polymorphic forms, rutile (tetragonal), anatase (tetragonal) and brookite (orthorhombic), presents photoactivity [5,6]. Rutile is the most stable phase and it has a direct-type band gap of 3.0 eV. Even though anatase has a band gap of 3.2 eV, its photocatalytic properties are higher than those of rutile due to its indirect-type band gap that promotes the lifetime of electron-hole pairs. Brookite is a better photocatalytic material than anatase and rutile because this structure traps the generated electrons reducing the electron-hole recombination rate. However, the brookite synthesis is technically difficult being only possible its preparation by hydrothermal methods due to its narrower stability range compared to the other TiO_2 polymorphs. Frequently, the TiO_2 photocatalysts are not crystallinity pure and they are composed by several phases and, even amorphous fractions, such as the well known P25 particles, consisting in more than 70% anatase with a minor amount of rutile and a small amount of amorphous phase [7].

The photocatalysts properties are also modified by the morphology of the material, and consequently the TiO_2 has been prepared in a wide variety of shapes, including nanoparticles, nanorods, nanowires, nanotubes, nanosheets or porous nanostructures [8]. Numerous syntheses has been developed for preparing TiO_2 photocatalysts, thus preparation methods can be classifiable as: sol and sol-gel, micelle and inverse micelle, hydrothermal, solvothermal, direct oxidation, chemical or physical deposition, electrodeposition, sonochemical and microwave-assisted [9]. This huge research effort is based on the aim of optimizing the TiO_2 photocatalysts for specifics uses and the improvement of the preparation methods taking into account their real applications. This growing scientific interest in TiO_2 photocatalysis is demonstrated when the number of publications related to TiO_2 phocatalysts in the last 40 years and its relative proportions respect to the total number publications about photocatalysis are presented (Figure 2).

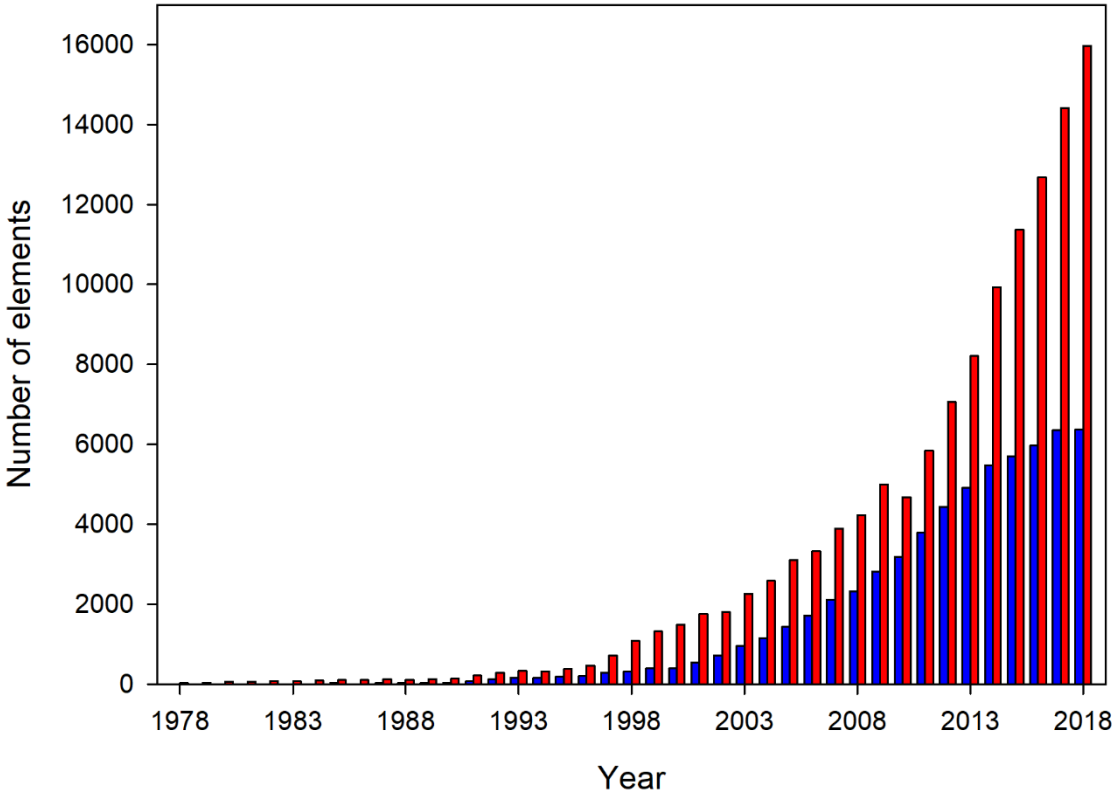

Figure 2. Numbers of research publications per year, search results in the period of 1978-2018 in the ‘‘Web of Science’’ using the keywords ‘‘photocataly∗’’ (red bars) and ‘‘TiO_2 AND photocataly*’’ (blue bars).

1.2. TiO_2 photocatalysts for building materials

In the field of photocatalytic construction and building materials TiO_2 has been extensively employed due to their characteristic and their good compatibility with traditional construction materials [10]. The use of TiO_2 on building materials started from the early 1990s being applied on all type of construction materials, such as glass [11], ceramics [12], roof tiles [13], stones [14], mortars [15], concrete [16] and asphalt [17]. Specifically, the photocatalytic properties of TiO_2 allow the production of photocatalytic materials for three major applications, air-depolluting, self-cleaning and self-sterilization.

The organic pollutants and gases, such as NO, NO_2 and SO_2, present in the air of urban environments, can be degraded by TiO_2, which make it an effective tool to curb the atmospheric

pollution. In the specific case of the nitrogen oxides (NO_x) more than 7000 tons are emitted yearly in Europe [18]. Emissions of NO_x to the atmosphere contribute with a volume of gases which is similar to that of CO, moreover, their toxicity is even four times higher. The problem is particularly worrying in urban areas mainly due to the intensification of industrial activity and the increasing number of motor vehicles in circulation [19]. As well known, NO_x not only affect human health but also are responsible for the increase of the greenhouse effect and, consequently, planetary climatic change. However, no matter the progress in energy and environmental efficiency of transport means, as well as the ever more restrictive limits to industrial discharges, our society is still far away from avoiding these hazardous emissions. Therefore, much research has been focussed on the NO_x photo-oxidation by TiO_2 to non-toxic nitrate forms that can be removed by rain water, being the involved mechanism as follows [17]:

TiO_2 photo-activation

$$TiO_2 \xrightarrow{h\nu} h^+ + e^-$$

Radicals formation

$$h^+ + OH^- \rightarrow OH^\bullet$$

$$e^- + O_2 \rightarrow O_2^{\bullet -}$$

$$H^+ + O_2^{\bullet -} \rightarrow HO_2^\bullet$$

NO and NO_2 oxidation

$$NO + HO_2^\bullet \rightarrow NO_2 + OH^\bullet$$

$$NO_2 + OH^\bullet \rightarrow HNO_3$$

The pollution, but also the animal, microorganism and human action, produces visible alterations on buildings in the form of staining, moist areas, soiling or graffiti [20]. The proliferation and accumulation of these alterations over time can constitute an important impact on the aesthetic value of the buildings and large costs of remediation. A large proportion of

these stains are produced by soot or organic compounds, alone or acting as binder of dirt particles, that can be effectively degraded by TiO_2 [15,21]. The oxidation process of these species to CO_2 and H_2O can take place according different to mechanisms in which the holes or the radicals produced by the TiO_2 photo-activation are the oxidizing agents [22,23].

Despite all the benefits described above, the use of TiO_2 on building materials presents certain limitations. First, the activity of ordinary TiO_2 photocatalysts both in outdoor and indoor applications is restricted due to its absorption of light mainly located in the UV range which is scarce in the light of sun and common lamps. Second, TiO_2 photocatalysts must be integrated on buildings using methods that preserve their photocatalytic properties and ensure a suitable durability. TiO_2 can be directly incorporated during the fabrication of certain construction materials, as in the case of tiles, mortars and concrete [13,24–26], but other strategies for integration on existing structures are necessary.

1.3. Modifications of TiO_2 photocatalysts

One of the most important goals of TiO_2 research is the improvement of its photocatalytic performance, having developed several ways to achieve this purpose, such as doping both with metals [27] or non-metals [28], noble metal deposition [29], dye sensitization [30], semiconductor heterojunction [31], graphene addition [32], among others. The TiO_2 modifications can be classified in two groups, bulk modifications and surface modifications [9]. The bulk modifications correspond to doping and they constitute chemical changes in the TiO_2 composition that produce alterations in the electronic TiO_2 structure, (as shown in Figure 3), which in turn modify its photocatalytic properties. The surface modifications correspond to metal deposition, dye sensitization, semiconductor heterojunction or other strategies where a substance is placed in contact with TiO_2. In this case, the TiO_2 is not chemically modified but

the deposited substance and the TiO_2 interact transferring energy or charge carriers between them.

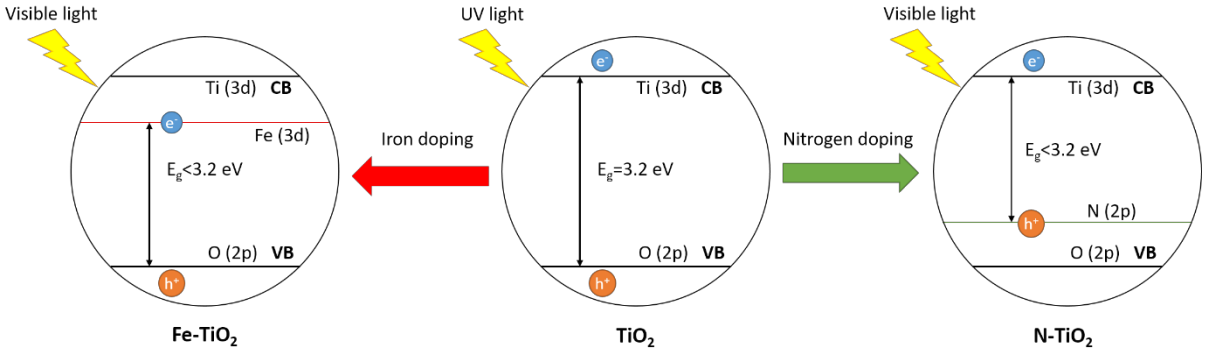

Figure 3. Schematic representation of bulk modification of TiO_2, by means of metal (Fe) and non-metal (N) doping rendering the TiO_2 energy levels modifications.

Each TiO_2 modification promotes the photoactivity in a different way, but two main general mechanisms can be described:

1-As explained before, the electron-hole pairs produced by the TiO_2 photo-activation are the responsible of the photocatalytic properties, but they can react between them producing heat or radiation, which is known as electron-hole pair recombination, so stopping the photo-process. Some TiO_2 modifications act promoting the trapping of the photogenerated charge carriers reducing the electron-hole pair recombination rate and, in this way, enhancing the photoactivity [33].

2-The modified TiO_2 have absorption in the visible range allowing the visible light activation of TiO_2 by band-gap reduction [34] or by sensitization [35,36]. This allows the TiO_2 photoactivity under visible light and promotes the photolytic process under solar radiation.

1.3.1 AuNPs deposition

The gold nanoparticles (AuNPs) deposition on TiO_2 has been reported to significantly promote the TiO_2 performance, acting in several ways. First, the TiO_2-Au contact modifies the energy levels and the charge transfer phenomena in TiO_2 surface. The AuNPs can act as reservoir of photogenerated charge carriers and they equilibrate the Fermi level, decreasing the electron-hole pair recombination [37–39]. On the other hand, the localized surface plasmon resonance (LSPR) effect of the AuNPs enhances the TiO_2 photoactivity under visible radiation [40]. The major mechanism taking place is the TiO_2 sensitization. The visible radiation excites the AuNPs electrons and they can be injected in the TiO_2 conduction band triggering the photocatalytic process (as illustrated in Figure 4) [41]. In addition, other LSPR mediated processes that can enhance the TiO_2 photoactivity have been proposed: (1) The excited AuNPs electrons colliding in the TiO_2-Au contact area can have enough kinetic energy for promoting the TiO_2 electrons to the valence band [42,43]; (2) the LRSP excitation produces a local heating and the surrounding AuNPs can reach temperatures up to 100 °C favouring the photodegradation processes [44]; and (3) the LRSP increases the electric field around the AuNPs promoting the electron-hole pairs formation [45].

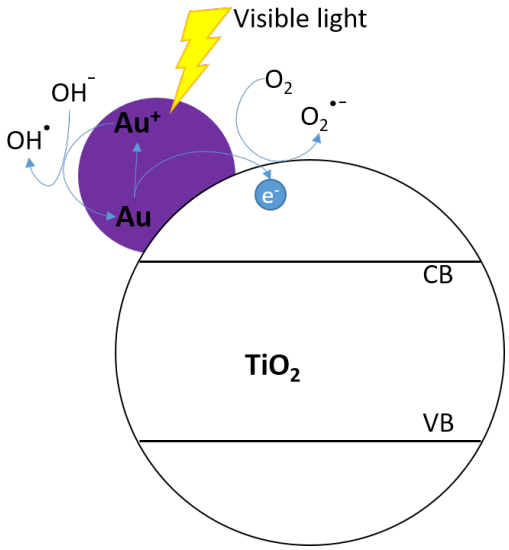

Figure 4. Schematic representation of Au-TiO_2 photocatalyst under visible light activation.

Other noble metals, like silver, can also produce the described effects, but AuNPs presents several advantages over silver nanoparticles (AgNPs): (1) the maximum absorption of LSPR of AgNPs is localized around 400 nm, close to UV light, whereas the LSPR of AuNPs is between 500 and 600 nm, the range where solar light is more intense [46]; (2) AgNPs are highly reactive and they can be oxidized in the presence of O_2 being this oxidation promoted as AgNPs are in contact with TiO_2 with its higher reduction potential [47], whereas AuNPs are considered inert [48]; and (3) AuNPs also show catalytic properties by themselves [49] as reported for NO_x photo-oxidation [50,51].

1.3.2 Nitrogen doping

Nitrogen can be incorporated into TiO_2 structure in different ways. According to its situation in the TiO_2 lattice, nitrogen can substitute oxygen atoms or it can be placed in interstitial positions [28,52]. Regarding its chemical form, nitrogen can be incorporated as nitrogen or as oxidized nitrogen species [28,52,53]. As previously explained and illustrated in Figure 3, the nitrogen doping modifies the TiO_2 electronic levels reducing the band gap, which promotes the photoactivity [54]. Additionally, the nitrogen doping promotes the charge carriers trapping, so reducing the recombination [55].

Another interesting effect of nitrogen doping is that it can be used together the AuNPs deposition for producing Au/N-TiO_2 photocatalysts. In this way the effects induced by gold and nitrogen are synergetic, obtaining higher photoactivities than those corresponding to N-TiO_2 or Au/TiO_2 photocatalysts alone [56–58].

1.4. TiO_2/SiO_2 photocatalysts for building materials

Going back to the issue of TiO_2 photocatalysts application on buildings, TiO_2 nanomaterials can be easily dispersed in water or organic solvents and applied in situ for producing TiO_2 coatings after solvent evaporation. Although these coatings show a proper performance, they are composed by an agglomeration of particles that can be easily detached by the weathering [59–63]. The use of a binder can mitigate this problem, in particular silica presents affinity for the common building materials and it has been reported that promotes the TiO_2 adhesion to the substrate [64–66]. Silica can present porous structure with large surface area that allows the diffusion of substances to the photoactive centres promoting the photoactivity in comparison with a non-porous matrix [63].

For the last few years, the research group TEP243 at the University of Cadiz has developed a sol-gel technique that has been reported to provide an effective methodlogy for the treatment of building materials [67] for several reasons: (1) the obtained sols have low viscosities that allow their in situ application by using common and low cost methods; (2) they penetrate in the porous structure of the substrate and xerogels coatings with high adhesion to the substrate are spontaneously produced; and (3) the presence of a surfactant, n-octylamine, in the synthesis promotes the formation of a crack-free mesoporous material. This last aspect, the absence of fractures, is fundamental to get a durable coating on building materials [62,68,69].

Recently, it has been proposed a inverse micelle mechanism that explains the silica formation in this sol-gel synthesis (see Figure 5) [70]. The ultrasonic shaking allows the formation of a microemulsion of water in the silica oligomer, thanks to the n-octylamine reverse micelles. These micelles are composed by the water necessary for silica oligomer and the catalyst, n-octylamine, for the condensation reaction, thus they act as nanoreactor for the silica formation

producing silica seeds. The formed seeds can grow reacting with the silica oligomer until the silica nanoparticles are aggregated together, producing a material constituted by the packing of amorphous silica particles. The interparticle spacing of the silica packing produces a mesoporous structure that reduces the capillarity pressure during the gel drying and prevents the cracking.

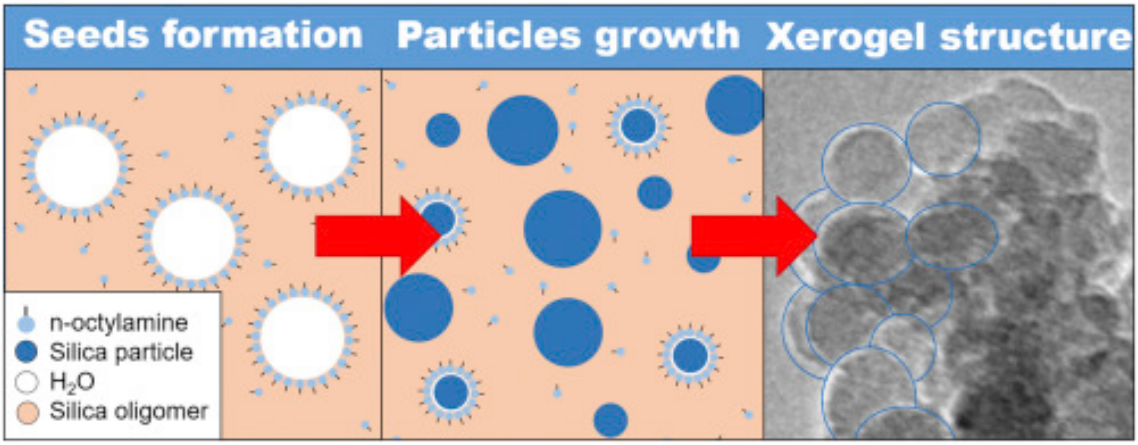

Figure 5. Silica formation via inverse micelle mechanism proposed for the sol-gel route developed by the research group TEP243. Reprinted from D.S. Facio, M. Luna, M.J. Mosquera, Facile preparation of mesoporous silica monoliths by an inverse micelle mechanism, Microporous Mesoporous Mater. 247 (2017) 166–176.

The integration of preformed TiO_2 particles in this sol-gel route has made it possible to develop TiO_2/SiO_2 that can be easily applied on building materials for producing effective photocatalytic coatings (see Figure 6) [60,63,71]. The commercial titania particles applied as a water dispersion on stone did not create an effective coating, whereas the TiO_2/SiO_2 coating were firmly adhered to the stone surface ensuring that photocatalytic properties of the coating have a long-term effect. In addition, the mesoporous structure of the TiO_2/SiO_2 photocatalysts enhance the photoactivity properties of the coating, compared with the effect produced by a material comprising similar particles embedded in a microporous silica matrix.

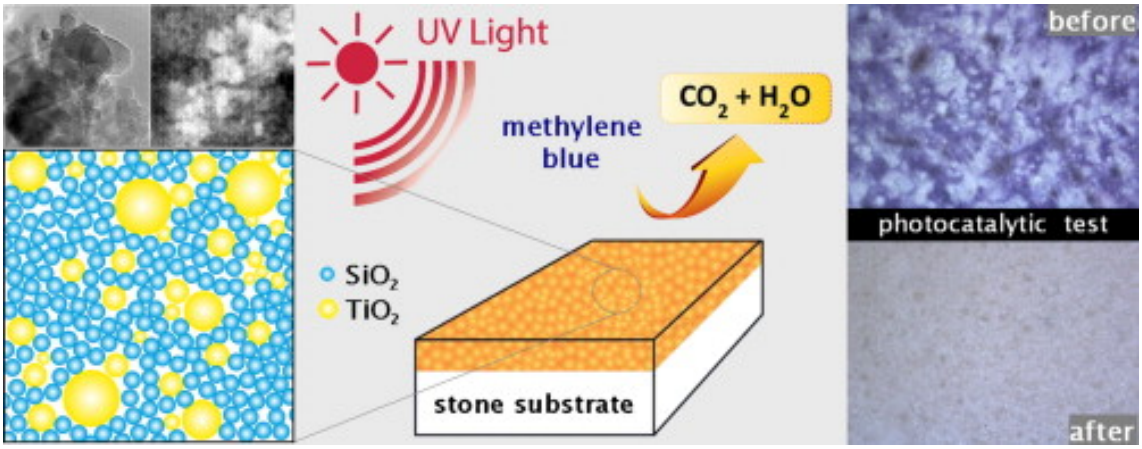

Figure 6. Structure and performance of TiO_2/SiO_2 coating developed the research group TEP243.Reprinted from Pinho, M.J. Mosquera, Photocatalytic activity of TiO_2-SiO_2 nanocomposites applied to buildings: Influence of particle size and loading, Appl. Catal. B Environ. 134–135 (2013) 205–221.

1.5. TiO_2 modifications for enhancing the performance on building materials

Although the performance of TiO_2 photocatalysts for building materials is limited by its low absorption under solar light, few research focussed on the enhancement of the TiO_2 photoactivity for building application can be found in the literature. The nitrogen doping [24,72] and the AgNPs [73,74] are the only approaches employed for promoting the TiO_2 performance on construction materials. In particular, the effect of incorporating silver to the TiO_2/SiO_2 photocatalyst described in the previous epigraph was also investigated demonstrating that enhances their photocatalytic performance [75]. In spite of the benefits of gold over silver, the application of Au/TiO_2 photocatalysts on building materials has not investigated with the exception of a work from Bergamonti et al. [76]. They prepared a TiO_2 sol containing AuNPs that was applied on stone, but photoactivity was not significantly increased due to the addition of gold, probably due to the big size of AuNPs (60-150 nm) compared with the TiO_2 crystallite size (3-6 nm)

According to these finding, we propose the topic of this Thesis, the integration of Au/TiO_2 nanomaterials in the previously described sol-gel synthesis as an innovative strategy to produce Au/TiO_2/SiO_2 photocatalysts, as reflected in Figure 7. These photocatalysts can solve the two mains drawbacks associated to the TiO_2 employment for producing photocatalytic building materials. The AuNPs can promote the TiO_2 photoactivity under solar light and the silica matrix provides a suitable adhesion TiO_2-substrate. Therefore, building materials with promoted self-cleaning and depolluting properties would be obtained.

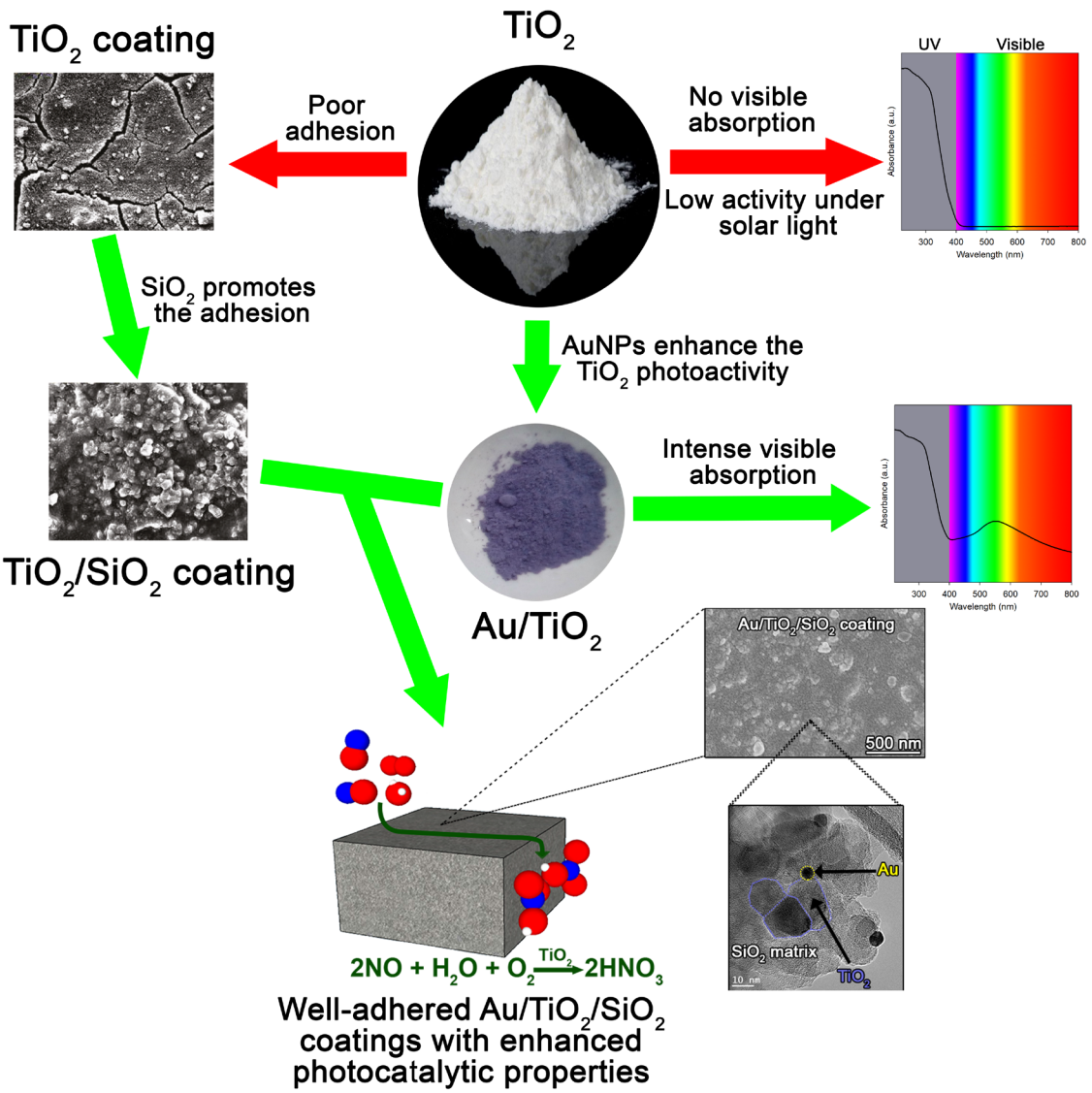

Figure 7. Graphic illustration of the main objective of the present Thesis, the solution of the drawbacks associated to the use of TiO2 on building materials developing Au/TiO_2/SiO_2 photocatalysts.

1.6. References

[1] A. Fujishima, K. Honda, Electrochemical Photolysis of Water at a Semiconductor Electrode, Nature. 238 (1972) 37–38.

[2] M. Pelaez, N.T. Nolan, S.C. Pillai, M.K. Seery, P. Falaras, A.G. Kontos, P.S.M.M. Dunlop, J.W.J.J. Hamilton, J.A. Byrne, K. O'Shea, M.H. Entezari, D.D. Dionysiou, A review on the visible light active titanium dioxide photocatalysts for environmental applications, Appl. Catal. B Environ. 125 (2012) 331–349.

[3] J. Carbajo, A. Tolosana-Moranchel, J.A. Casas, M. Faraldos, A. Bahamonde, Analysis of photoefficiency in TiO_2 aqueous suspensions: Effect of titania hydrodynamic particle size and catalyst loading on their optical properties, Appl. Catal. B Environ. 221 (2018) 1–8.

[4] M.A. Henderson, A surface science perspective on TiO_2 photocatalysis, Surf. Sci. Rep. 66 (2011) 185–297.

[5] K. Fischer, A. Gawel, D. Rosen, M. Krause, A. Abdul Latif, J. Griebel, A. Prager, A. Schulze, Low-temperature synthesis of anatase/rutile/brookite TiO_2 nanoparticles on a polymer membrane for photocatalysis, Catalysts. 7 (2017) 209.

[6] M. Monai, T. Montini, P. Fornasiero, Brookite: Nothing New under the Sun?, Catalysts. 7 (2017) 304.

[7] B. Ohtani, O.O. Prieto-Mahaney, D. Li, R. Abe, What is Degussa (Evonic) P25? Crystalline composition analysis, reconstruction from isolated pure particles and photocatalytic activity test, J. Photochem. Photobiol. A Chem. 216 (2010) 179–182.

[8] M.T. Noman, M.A. Ashraf, A. Ali, Synthesis and applications of nano-TiO_2: a review, Environ. Sci. Pollut. Res. 26 (2019) 3262–3291.

[9] X. Chen, S.S. Mao, Titanium dioxide nanomaterials: Synthesis, properties, modifications and applications, Chem. Rev. 107 (2007) 2891–2959.

[10] J. Chen, C.S. Poon, Photocatalytic construction and building materials: From fundamentals to applications, Build. Environ. 44 (2009) 1899–1906.

[11] T. Watanabe, A. Nakajima, R. Wang, M. Minabe, S. Koizumi, A. Fujishima, K. Hashimoto, Photocatalytic activity and photoinduced hydrophilicity of titanium dioxide coated glass, Thin Solid Films. 351 (1999) 260–263.

[12] W. Xiaohong, J. Zhaohua, L. Huiling, L. Xuandong, H. Xinguo, TiO_2 ceramic films prepared by micro-plasma oxidation method for photodegradation of rhodamine B, Mater. Chem. Phys. 80 (2003) 39–43.

[13] M. Radeka, S. Markov, E. Lončar, O. Rudić, S. Vučetić, J. Ranogajec, Photocatalytic effects of TiO_2 mesoporous coating immobilized on clay roofing tiles, J. Eur. Ceram. Soc. 34 (2014) 127–136.

[14] F. Gherardi, A. Colombo, M. D'Arienzo, B. Di Credico, S. Goidanich, F. Morazzoni, R. Simonutti, L. Toniolo, Efficient self-cleaning treatments for built heritage based on highly photo-active and well-dispersible TiO_2 nanocrystals, Microchem. J. 126 (2016) 54–62.

[15] J.M. De la Rosa, A.Z. Miller, J.S. Pozo-Antonio, J.A. González-Pérez, N.T. Jiménez-Morillo, A. Dionisio, Assessing the effects of UVA photocatalysis on soot-coated TiO_2-containing mortars, Sci. Total Environ. 605–606 (2017) 147–157.

[16] M. Faraldos, R. Kropp, M.A. Anderson, K. Sobolev, Photocatalytic hydrophobic concrete coatings to combat air pollution, Catal. Today. 259 (2016) 228–236.

[17] W. Fan, K.Y. Chan, C. Zhang, K. Zhang, Z. Ning, M.K.H. Leung, Solar photocatalytic asphalt for removal of vehicular NOx: A feasibility study, Appl. Energy. 225 (2018) 535–541.

[18] European Environment Agency, European Union emission inventory report 1990–2014 under the UNECE Convention on Long-range Transboundary Air Pollution (LRTAP), 2016.

[19] J. Colls, A. Tiwary, Air Pollution, 3rd ed., CRC Press, London, 2010. https://www.taylorfrancis.com/books/9781351988926.

[20] ICOMOS International Scientific Committe for Stone (ISCS), Illustrated Glossary on Stone Deterioration Patterns, 2010.

[21] L. Peruchon, E. Puzenat, A. Girard-Egrot, L. Blum, J.M. Herrmann, C. Guillard, Characterization of self-cleaning glasses using Langmuir-Blodgett technique to control thickness of stearic acid multilayers. Importance of spectral emission to define standard test, J. Photochem. Photobiol. A Chem. 197 (2008) 170–176.

[22] A. Fujishima, X. Zhang, D. Tryk, TiO_2 photocatalysis and related surface phenomena, Surf. Sci. Rep. 63 (2008) 515–582.

[23] T. Ochiai, A. Fujishima, Photoelectrochemical properties of TiO_2 photocatalyst and its applications for environmental purification, J. Photochem. Photobiol. C Photochem. Rev. 13 (2012) 247–262.

[24] V. Vaiano, G. Sarno, P. Ciambelli, D. Sannino, Functionalization of ceramic tiles with

N-doped TiO_2 and their photocatalytic function under UV or visible light irradiation, J. Adv. Oxid. Technol. 17 (2014) 193–201.

[25] J.S. Pozo-Antonio, A. Dionísio, Self-cleaning property of mortars with TiO_2 addition using real diesel exhaust soot, J. Clean. Prod. 161 (2017) 850–859.

[26] M.M. Hassan, H. Dylla, L.N. Mohammad, T. Rupnow, Evaluation of the durability of titanium dioxide photocatalyst coating for concrete pavement, Constr. Build. Mater. 24 (2010) 1456–1461.

[27] S. Saroj, L. Singh, S.V. Singh, Photodegradation of Direct Blue-199 in carpet industry wastewater using iron-doped TiO_2 nanoparticles and regenerated photocatalyst, Int. J. Chem. Kinet. 51 (2019) 189–205.

[28] Y.-C. Yen, S. Ou, K.-J. Lin, One-pot synthesis of nitrogen-doped TiO_2 nanowires with enhanced photocurrent generation, J. Chinese Chem. Soc. 64 (2017) 1392–1398.

[29] F.J. López-Tenllado, J. Hidalgo-Carrillo, V. Montes-Jiménez, E. Sánchez-López, F.J. Urbano, A. Marinas, Photocatalytic production of hydrogen from binary mixtures of C-3 alcohols on Pt/TiO_2: Influence of alcohol structure, Catal. Today. 328 (2019) 2–7.

[30] Z. Youssef, L. Colombeau, N. Yesmurzayeva, F. Baros, R. Vanderesse, T. Hamieh, J. Toufaily, C. Frochot, T. Roques-Carmes, S. Acherar, Dye-sensitized nanoparticles for heterogeneous photocatalysis: Cases studies with TiO_2, ZnO, fullerene and graphene for water purification, Dye. Pigment. 159 (2018) 49–71.

[31] J.K. Lee, Y.K. Kim, B.J. Choi, T.M. Chung, J.H. Han, SnO-decorated TiO_2 nanoparticle with enhanced photocatalytic performance for methylene blue degradation, Appl. Surf. Sci. 480 (2019) 1089–1092.

[32] Á. Tolosana-Moranchel, A. Manassero, M.L. Satuf, O.M. Alfano, J.A. Casas, A. Bahamonde, Influence of TiO_2-rGO optical properties on the photocatalytic activity and efficiency to photodegrade an emerging pollutant, Appl. Catal. B Environ. 246 (2019) 1–11.

[33] R. Katoh, A. Furube, K. Yamanaka, T. Morikawa, Charge separation and trapping in N-Doped TiO_2 photocatalysts: A time-resolved microwave conductivity study, J. Phys. Chem. Lett. 1 (2010) 3261–3265.

[34] R. Asahi, T. Morikawa, T. Ohwaki, K. Aoki, Y. Taga, Visible-light photocatalysis in nitrogen-doped titanium oxides, Science. 293 (2001) 269–271.

[35] Y. Xu, C.H. Langford, UV- or visible-light-induced degradation of X3B on TiO_2 nanoparticles: The influence of adsorption, Langmuir. 17 (2001) 897–902.

[36] N.T. Nolan, M.K. Seery, S.J. Hinder, L.F. Healy, S.C. Pillai, A systematic study of the effect of silver on the chelation of formic acid to a titanium precursor and the resulting effect on the anatase to rutile transformation of TiO_2, J. Phys. Chem. C. 114 (2010) 13026–13034.

[37] V. Subramanian, E.E. Wolf, P. V. Kamat, Catalysis with TiO_2/gold manocomposites. effect of metal particle size on the fermi level equilibration, J. Am. Chem. Soc. 126 (2004) 4943–4950.

[38] P. V Kamat, D. Meisel, Nanoparticles in advanced oxidation processes, Curr. Opin. Colloid Interface Sci. 7 (2002) 282–287.

[39] Y. Zhou, D.M. King, X. Liang, J. Li, A.W. Weimer, Optimal preparation of Pt/TiO_2 photocatalysts using atomic layer deposition, Appl. Catal. B Environ. 101 (2010) 54–60.

[40] X. Zhang, Y.L. Chen, R.S. Liu, D.P. Tsai, Plasmonic photocatalysis., Rep. Prog. Phys. 76 (2013) 046401.

[41] S. Mubeen, G. Hernandez-Sosa, D. Moses, J. Lee, M. Moskovits, Plasmonic photosensitization of a wide band gap semiconductor: converting plasmons to charge carriers, Nano Lett. 11 (2011) 5548–5552.

[42] C. Langhammer, Z. Yuan, I. Zorić, B. Kasemo, Plasmonic properties of supported Pt and Pd nanostructures, Nano Lett. 6 (2006) 833–838.

[43] V.P. Zhdanov, C. Hägglund, B. Kasemo, Relaxation of plasmons in nm-sized metal particles located on or embedded in an amorphous semiconductor, Surf. Sci. 599 (2005) L372–L375.

[44] X. Chen, H. Zhu, J. Zhao, Z. Zheng, X. Gao, Visible-light-driven oxidation of organic contaminants in air with gold nanoparticle catalysts on oxide supports, Angew. Chemie Int. Ed. 47 (2008) 5353–5356.

[45] J. Lee, T. Javed, T. Skeini, A.O. Govorov, G.W. Bryant, N.A. Kotov, Bioconjugated Ag nanoparticles and CdTe nanowires: Metamaterials with field-enhanced light absorption, Angew. Chemie Int. Ed. 45 (2006) 4819–4823.

[46] S. Link, M.A. El-Sayed, Spectral properties and relaxation dynamics of surface plasmon electronic oscillations in gold and silver nanodots and nanorods, J. Phys. Chem. B. 103 (1999) 8410–8426.

[47] K. Awazu, M. Fujimaki, C. Rockstuhl, J. Tominaga, H. Murakami, Y. Ohki, N. Yoshida, T. Watanabe, A plasmonic photocatalyst consisting of silver nanoparticles embedded in titanium dioxide, J. Am. Chem. Soc. 130 (2008) 1676–1680.

[48] A. Desireddy, B.E. Conn, J. Guo, B. Yoon, R.N. Barnett, B.M. Monahan, K. Kirschbaum, W.P. Griffith, R.L. Whetten, U. Landman, T.P. Bigioni, Ultrastable silver nanoparticles., Nature. 501 (2013) 399–402.

[49] M. Haruta, When gold is not noble: Catalysis by nanoparticles, Chem. Rec. 3 (2003) 75–87.

[50] W. Zhu, S. Xiao, D. Zhang, P. Liu, H. Zhou, W. Dai, F. Liu, H. Li, Highly efficient and stable Au/CeO_2–TiO_2 photocatalyst for nitric oxide abatement: Potential application in flue gas treatment, Langmuir. 31 (2015) 10822–10830.

[51] D. Zhang, M. Wen, S. Zhang, P. Liu, W. Zhu, G. Li, H. Li, Au nanoparticles enhanced rutile TiO_2 nanorod bundles with high visible-light photocatalytic performance for NO oxidation, Appl. Catal. B Environ. 147 (2014) 610–616.

[52] F. Peng, L. Cai, H. Yu, H. Wang, J. Yang, Synthesis and characterization of substitutional and interstitial nitrogen-doped titanium dioxides with visible light photocatalytic activity, J. Solid State Chem. 181 (2008) 130–136.

[53] H. Li, J. Li, Y. Huo, Highly active TiO_2N photocatalysts prepared by treating TiO_2 precursors in NH_3/ethanol fluid under supercritical conditions, J. Phys. Chem. B. 110 (2006) 1559–1565.

[54] S.A. Ansari, M.M. Khan, M.O. Ansari, M.H. Cho, Nitrogen-doped titanium dioxide (N-doped TiO_2) for visible light photocatalysis, New J. Chem. 40 (2016) 3000–3009.

[55] K. Yamanaka, T. Morikawa, Charge-carrier dynamics in nitrogen-doped TiO_2 powder studied by femtosecond time-resolved diffuse reflectance spectroscopy, J. Phys. Chem. C. 116 (2012) 1286–1292.

[56] I. Chiu, Z. Shen, R. Wu, Promotion Effect of Au on N/TiO_2 for Hydrogen Generation from Water Splitting, 14 (2014) 7125–7130.

[57] X. Li, T. Fan, H. Zhou, B. Zhu, J. Ding, D. Zhang, Microporous and Mesoporous Materials A facile way to synthesize biomorphic N-TiO_2 incorporated with Au nanoparticles with narrow size distribution and high stability, Microporous Mesoporous Mater. 116 (2008) 478–484.

[58] B. Tian, C. Li, F. Gu, H. Jiang, Synergetic effects of nitrogen doping and Au loading on enhancing the visible-light photocatalytic activity of nano-TiO_2, Catal. Commun. 10 (2009) 925–929.

[59] C. Mendoza, A. Valle, M. Castellote, A. Bahamonde, M. Faraldos, TiO_2 and TiO_2–SiO_2 coated cement: Comparison of mechanic and photocatalytic properties, Appl. Catal. B Environ. 178 (2015) 155–164.

[60] L. Pinho, F. Elhaddad, D.S. Facio, M.J. Mosquera, A novel TiO_2–SiO_2 nanocomposite converts a very friable stone into a self-cleaning building material, Appl. Surf. Sci. 275 (2013) 389–396.

[61] K.V.V.S. Rao, M. Subrahmanyam, P. Boule, Immobilized TiO_2 photocatalyst during long-term use: decrease of its activity, Appl. Catal. B Environ. 49 (2004) 239–249.

[62] A. Calia, M. Lettieri, M. Masieri, Durability assessment of nanostructured TiO_2 coatings applied on limestones to enhance building surface with self-cleaning ability, Build. Environ. 110 (2016) 1–10.

[63] L. Pinho, M.J. Mosquera, Titania-silica nanocomposite photocatalysts with application in stone self-cleaning, J. Phys. Chem. C. 115 (2011) 22851–22862.

[64] R.E. Ramírez-García, J.A. González-Rodríguez, M. Arroyo-Ortega, S.A. Pérez-García, L. Licea-Jiménez, Engineered TiO_2 and SiO_2-TiO_2 films on silica-coated glass for increased thin film durability under abrasive conditions, Int. J. Appl. Ceram. Technol. 14 (2017) 39–49.

[65] V.B. Koli, S. Mavengere, J.-S. Kim, Photocatalytic properties of TiO_2-SiO_2-coated concrete on toluene gas, Mater. Res. Express. 5 (2018) 125006.

[66] A. Rosales, A. Maury Ramírez, R.M. De Gutiérrez, C. Guzmán, K. Esquivel, SiO_2@TiO_2 coating: Synthesis, physical characterization and photocatalytic evaluation, Coatings. 8 (2018) 120.

[67] R. Zarzuela, M. Luna, L.A.M. Carrascosa, M.J. Mosquera, Preserving Cultural Heritage Stone: Innovative Consolidant, Superhydrophobic, Self-Cleaning, and Biocidal Products, in: Adv. Mater. Conserv. Stone, Springer International Publishing, Cham, 2018: pp. 259–275.

[68] A. Licciulli, A. Calia, M. Lettieri, D. Diso, M. Masieri, S. Franza, R. Amadelli, G. Casarano, Photocatalytic TiO_2 coatings on limestone, J. Sol-Gel Sci. Technol. 60 (2011) 437–444.

[69] I. Poulios, P. Spathis, A. Grigoriadou, K. Delidou, P. Tsoumparis, Protection of marbles against corrosion and microbial corrosion with TiO_2 coatings, J. Environ. Sci. Heal. Part A. 34 (1999) 1455–1471.

[70] D.S. Facio, M. Luna, M.J. Mosquera, Facile preparation of mesoporous silica monoliths by an inverse micelle mechanism, Microporous Mesoporous Mater. 247 (2017) 166–176.

[71] L. Pinho, M.J. Mosquera, Photocatalytic activity of TiO_2-SiO_2 nanocomposites applied

to buildings: Influence of particle size and loading, Appl. Catal. B Environ. 134–135 (2013) 205–221.

[72] L. Bergamonti, G. Predieri, Y. Paz, L. Fornasini, P.P. Lottici, F. Bondioli, Enhanced self-cleaning properties of N-doped TiO_2 coating for Cultural Heritage, Microchem. J. 133 (2017) 1–12.

[73] A.R. Nurhamizah, M.R. Zulkifli, J. Mohd Juoi, Effect of additives on the characteristic of Ag-TiO_2 coating deposited on specially made unglazed ceramic tile, Key Eng. Mater. 694 (2016) 160–164.

[74] B. Tryba, M. Piszcz, A.W. Morawski, Photocatalytic and self-cleaning properties of Ag-doped TiO_2, Open Mater. Sci. J. 4 (2010) 5–8.

[75] L. Pinho, M. Rojas, M.J. Mosquera, Ag–SiO_2–TiO_2 nanocomposite coatings with enhanced photoactivity for self-cleaning application on building materials, Appl. Catal. B Environ. 178 (2015) 144–154.

[76] L. Bergamonti, I. Alfieri, M. Franzò, A. Lorenzi, A. Montenero, G. Predieri, M. Raganato, A. Calia, L. Lazzarini, D. Bersani, P.P. Lottici, Synthesis and characterization of nanocrystalline TiO_2 with application as photoactive coating on stones, Environ. Sci. Pollut. Res. 21 (2014) 13264–13277.

Chapter 2

Objectives

The present Doctoral Thesis has been developed within the framework of the two successive research projects with a common research topic, funded by the Spanish Government under the 2013 and 2017 calls focused to Societal Challenges, with the titles *"Ecosustainable building materials for their superhydrophobic, self-cleaning, decontaminating and biocide action (Ref. MAT2013-42934)"* and *"Smart Concrete and other Building Materials for their Self-cleaning, Pollutants Sequestering, Repellent and Biocide action (Ref. MAT2017-84228-R)"*, Therefore, the objectives of this Thesis match with those associated to the mentioned project, being the main one the **Development of ecosustainable nanostructured Au/TiO_2/SiO_2 photocatalysts specifically designed to be applied as depolluting and self-cleaning coatings on building materials.** According to this general objective the following specific objectives were proposed:

1-Synthesis of gold nanoparticles (AuNPs) with plasmonic properties by green routes and their characterization. The AuNPs will be synthesized using gold salts and ecofriendly reducing agents as a plant extract or citrate.

2-Synthesis of photoactive coatings and their characterization. The AuNPs will be incorporated in the sol-gel synthesis that comprises TiO_2 particles, a silica oligomer and a surfactant (n-octylamine). Other alternative will consist of depositing the synthetized AuNPs on the TiO_2 for producing Au/TiO_2 photocatalysts that will be integrated in the described sol. The synthetized sols will gel in laboratory conditions and the resultant Au/TiO_2/SiO_2 photocatalysts will be characterized and evaluated. An in-depth characterization of the developed photocatalysts has been carried out in order to correlate their chemical, textural and structural properties with their photocatalytic performance.

3-Application of photoactive products on building materials, characterization and evaluation of their effectiveness. The sols will be applied on different building materials (limestone, granite and concrete) producing Au/TiO_2/SiO_2 photocatalytic coatings. The coated

building material samples will be characterized paying special attention to those affecting to their photocatalytic properties. The photoactivity will be tested by a model dye degradation. In addition, soot will be employed to evaluate the self-cleaning properties and NO will be the pollutant gas used for determining the depolluting activity.

4-Synthesis of new innovative nanostructures Au/TiO_2, characterization and inclusion in coatings. In order to promote the Au-TiO_2 interaction, new Au/TiO_2 photocatalysts will be prepared by controlled deposition of AuNPs onto TiO_2. The deposition-precipitation synthesis method here proposed also produces nitrogen doping of TiO_2, promoting a synergetic effect in the photoactivity enhancement. These Au/N-TiO_2 photocatalysts will be characterized and evaluated in order to determine the best suited for preparing Au/N-TiO_2/SiO_2 that will applied, characterized and evaluated according to the procedures described in the points 2 and 3.

Chapter 3

TiO_2-SiO_2 coating with a low content of AuNPs for producing self-cleaning building materials

nanomaterials

MDPI

Article

TiO_2-SiO_2 Coatings with a Low Content of AuNPs for Producing Self-Cleaning Building Materials

Manuel Luna [1], Juan J. Delgado [2], M. L. Almoraima Gil [1] and María J. Mosquera [1,*]

[1] TEP-243 Nanomaterials Group, Department of Physical-Chemistry, Faculty of Sciences, University of Cadiz, 11510 Puerto Real, Spain; manuel.luna@uca.es (M.L.); almoraima.gil@uca.es (M.L.A.G.)

[2] Department of Inorganic Chemistry, CASEM, University of Cadiz, 11510 Puerto Real, Spain; juanjose.delgado@uca.es

* Correspondence: mariajesus.mosquera@uca.es; Tel.: +34-956-016-331

Received: 7 February 2018; Accepted: 16 March 2018; Published: 20 March 2018

Abstract: The high pollution levels in our cities are producing a significant increase of dust on buildings. An application of photoactive coatings on building materials can produce buildings with self-cleaning surfaces. In this study, we have developed a simple sol-gel route for producing Au-TiO_2/SiO_2 photocatalysts with application on buildings. The gold nanoparticles (AuNPs) improved the TiO_2 photoactivity under solar radiation because they promoted absorption in the visible range. We varied the content of AuNPs in the sols under study, in order to investigate their effect on self-cleaning properties. The sols obtained were sprayed on a common building stone, producing coatings which adhere firmly to the stone and preserve their aesthetic qualities. We studied the decolourization efficiency of the photocatalysts under study against methylene blue and against soot (a real staining agent for buildings). Finally, we established that the coating with an intermediate Au content presented the best self-cleaning performance, due to the role played by its structure and texture on its photoactivity.

Keywords: photocatalyst; self-cleaning; building; Au-TiO_2/SiO_2

1. Introduction

Today, the concentration of pollutants is significantly high in big cities and industrial environments. Atmospheric aerosol pollutants produce visible stains on buildings. Specifically, small particles and greasy deposits are adhered to building surfaces by organic binders such as hydrocarbons and fatty acids [1]. These pollutants promote a significant change in the aesthetic of historic and modern buildings of our cities and, consequently, it is responsible for costs investments in building conservation.

The use of photoactive building materials provides a possible solution, because organic soiling deposited on their surfaces can be decomposed to water and CO_2 by the action of sun light alone [2]. Since TiO_2 photoactivity was discovered [3], it has become the most popular photocatalyst for several reasons: stability, availability, low cost, lack of toxicity and excellent photocatalytic properties [4]. Regarding the field of construction, TiO_2 has been traditionally employed as a white pigment and as a photocatalyst from 1990 [2]. Photoactive surfaces have been produced on a great variety of building materials, such as glass [5], ceramics [6], roof tiles [7] and especially in stones [8–14], by applying, mainly, TiO_2 nanoparticles (TiO_2NPs) dispersed in a solvent (water or volatile organic compunds (VOCs)), as a coating. It is demonstrated that effective self-cleaning and even depolluting surfaces are achieved. However, not enough attention has been paid to the durability of these coatings, a crucial property because they are exposed to outdoor conditions. As reported in the literature, TiO_2NPs are not suitably adhered to building materials [15–18]. In addition, cracks resulting from the accumulation of TiO_2NPs are commonly produced [11,18,19].

Recently, we have designed long-lasting photoactive coatings for building stones by adding TiO_2NPs into a SiO_2 precursor sol in the presence of n-octylamine [16,20,21]. The low-viscosity sol can penetrate into the pore structure of substrates and its in situ gelling produces a crack-free TiO_2/SiO_2 nanocomposite [16], which is firmly adhered to substrates. The use of siloxanes to immobilize TiO_2 has also been explored by other researchers in order to prepare durable and well-adhered photoactive coatings on concretes [15,22].

Another drawback of TiO_2 for application on building materials can be associated to its absorption, being exclusively localized in the ultraviolet range, which only constitutes 3–5% of solar light. Therefore, enhancing the TiO_2 photoactivity is an important challenge and, moreover, extends its absorption into the visible range, as 45% of solar light is constituted by visible light. Several methods to increase the TiO_2 photoactivity have been described, by using noble metals [23], metal cations [24], non-metal [25] or organic compounds [26]. The use of nanostructured noble metals is one of the most popular choices for improving TiO_2 photoactivity, with silver nanoparticles (AgNPs) and gold nanoparticles (AuNPs) being the most widely used [27–32]. The metal nanoparticles in contact with TiO_2 act as an electron reservoir, reducing the recombination of electron-hole pairs [33]. They also have a high localised surface plasmon resonance (LSPR), the light absorption of which produces effects, such as, generation of electron-hole pairs, local heating, or increasing the electric field around, which can promote the TiO_2 photoactivity [34]. In the specific case of buildings, Ag has been added to TiO_2 to increase the photoactivity of coatings [35–37]. Recently, we have also included a silver precursor to increase the activity of TiO_2-SiO_2 photocatalysts [38].

The use of AuNPs instead of AgNPs, in order to improve TiO_2 photoactivity in coatings applied on buildings, can present significant advantages: (1) The maximum absorption of LSPR of AgNPs is localized around 400 nm, near to UV light, whereas the LSPR of AuNPs is between 500 and 600 nm, the range where solar light is more intense [39]; (2) AgNPs are highly reactive and they can be oxidized in the presence of O_2, as in outdoor conditions, and this oxidation is promoted as AgNPs are in contact with TiO_2 with its higher reduction potential [32], whereas AuNPs are considered inert [40]; and, (3) AuNPs are excellent catalysts alone [41] and consequently they can improve other interesting effects, such as the removal of CO and organic compounds by oxidation.

However, it is important to control the amount of AuNPs in coatings because an excess of gold on a TiO_2 surface can promote some negative effects: (1) a recombination of photo-induced electron-hole pairs [42,43]; (2) a preferential light absorption by gold rather than TiO_2 [44,45]. In both cases, these drawbacks were observed for Au/TiO_2 in a proportion above 2 wt %.

As far as we know, the application of Au-TiO_2 photocatalysts on building materials has scarcely been investigated. Specifically, Bergamonti et al. [46] prepared a sol containing Au-TiO_2 NPs and it was applied on building stone by brushing. The coatings produced on the stone presented significant cracks related to aggregation of NPs. Regarding photoactivity, no increase was observed due to the addition of gold.

The objective of the present work is to develop effective and long-term Au-TiO_2/SiO_2 coatings for building materials. Au and TiO_2 NPs were incorporated into a starting sol containing silica oligomer and n-octylamine. The integration of Au and TiO_2 NPs into a silica matrix produces a well-adhered and continuous coating on the building material surface, promoting a high durability [21]. The surfactant plays several roles: (1) to catalyse sol-gel transition of the silica precursor [47,48], and, (2) to create a mesoporous silica gel network that prevents cracking [47,48] and that provides the access of contaminants to photoactive centres, improving photoactivity [21,49]. The Au content was modified in the study in order to investigate its influence in photoactivity. Since a gold excess produces negative effects [43,45] and increases the photocatalyst price, low Au contents (below 0.25 wt %) were employed in the study.

A complete characterization of structure, texture and optical properties of the photocatalysts was carried out and they were applied on a typical building stone in order to evaluate their properties as self-cleaning coatings. Self-cleaning activity was evaluated by studying the decolourization of

solid dyes deposited on the coated stones. According to the literature [18,50,51], the changes in the coordinates of a color space is the method most used to evaluate the self-cleaning properties of building materials. This is a simple and rapid strategy but it presents a clear subjectivity, because the measure is associated with visual perception [52,53]. In addition, this methodology can promote a misinterpretation because it does not characterize dye degradation. In this work, we compare the color space method and the application of Kubelka-Munk theory, that describes light absorption in a thin layer of dye deposited on a non or low absorbent substrate [54].

2. Materials and Methods

2.1. Synthesis of AuNPs

These were prepared according to a green synthesis route [55] based on a synthesis previously developed by our group [56,57]. This synthesis was selected because it is simple and the AuNPs obtained have a wide LSPR band. Drago leaves (Dracaena Draco) were employed as the reducing and stabilizing agent. Specifically, an aqueous extract of Drago leaves (5% w/v) was prepared under ultrasonic agitation at 50% amplitude, using a Sonopuls HD2200 ultrasonic homogenizer from Bandelin (Berlin, Germany), for 10 min. Next, the extract was filtered.

$KAuCl_4$ was employed as Au precursor. An aqueous 0.47 mM $KAuCl_4$ (Sigma-Aldrich, St. Louis, MO, USA) solution was heated to 60 °C and then the Drago extract was added, with a 4:1 solution/extract ratio (v/v). After 15 min, the dispersion becomes purple, confirming the presence of AuNPs. After 24 h, the Au dispersion was centrifuged at 3000 revolutions per minute (RPM) for 3 min in order to remove the extract residues. The samples were characterized using a JEOL 2010F TEM/STEM microscope (Musahino, Japan) operated at 200 kV. This equipment has a spatial resolution of 0.19 nm in High Resolution Transmission Electron Microscopy (HRTEM) mode. High Angle Annular Dark Field Scanning Transmission Electron Microscopy (HAADF-STEM) images were recorded using an electron probe of 0.5 nm and a camera length of 10 cm. The AuNPs size was determined by measuring more than 300 particles from several HAADF-STEM images at the same magnification. Finally, the AuNPs were precipitated by centrifugation at 13,000 relative centrifugal force (RFC) and re-dispersed in water (Au concentration: 1.5 mg/mL). A scheme of the process is included in Figure 1.

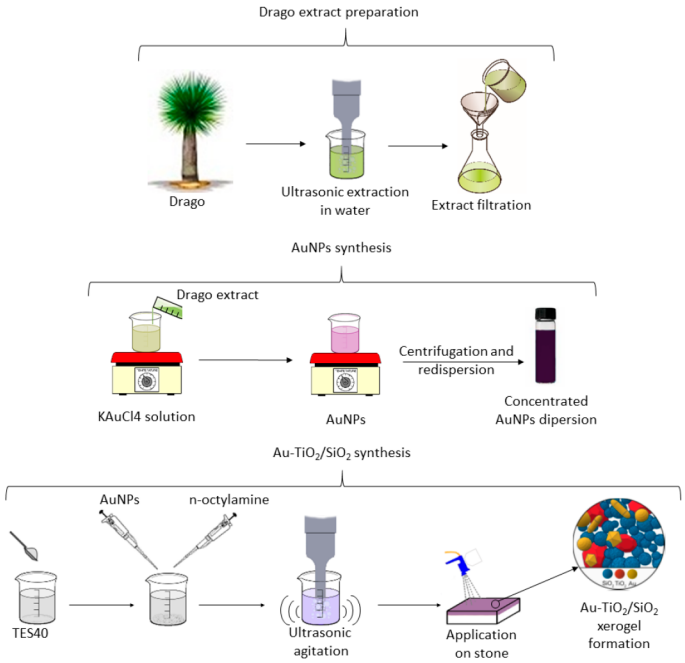

Figure 1. Au-TiO_2/SiO_2 route synthesis and application on the stone samples.

2.2. Au-TiO_2/SiO_2 Synthesis

The following reagents were employed: a silica oligomer, TES40 WN (Wacker, Munich, Germany), an ethoxysilane (average degree of polymerization of 5) providing approximately 41% of silica upon complete hydrolysis, n-octylamine (Sigma-Aldrich, St. Louis, MO, USA), and, commercial TiO_2 particles VP Aeroperl P25/20 (Evonik, Essen, Germany) consisting of a granulated version of P25 TiO_2 particles, with an average particle size of 20 μm, a primary particle size of 21 nm and a surface area of 50 ± 15 m^2. In the synthetic procedure, silica oligomer was mixed with n-octylamine, TiO_2NPs and AuNPs dispersion previously prepared were mixed, under high-power ultrasonic agitation at 125 W, for 10 min by using a Sonopuls HD3200 ultrasonic homogenizer from Bandelin (Berlin, Germany). A schematic of the synthesis route is shown in Figure 1 and the proportions of the reagents employed are compiled in Table 1.

Table 1. Composition of the prepared products.

Product	% TiO_2 [a]	% Water Content [b]	% Au/TiO_2 [c]
S0Au	0	0	0
ST0Au	1	0	0
ST5Au	1	0.33	0.05
ST12Au	1	0.83	0.12
ST25Au	1	1.67	0.25
ST38Au	1	2.50	0.38
ST50Au	1	3.33	0.50

[a] %(w/v) TiO_2/silica oligomer; [b] %(v/v) water/silica oligomer; [c] %(w/w) Au/TiO_2.

The amount of n-octylamine and TiO_2NPs with respect to the silica oligomer were 0.36% v/v and 1% w/v, respectively. The concentration of AuNPs was modified in the range 0–0.50% w/w (Au/TiO_2 ratio). Since Au is added in an aqueous dispersion, the water content was also modified (see Table 1). The synthesized sols were designated ST$Au, where S and T indicate the presence of SiO_2 and TiO_2, respectively, $ is the ‰ w/w of Au/TiO_2.

2.3. Sol-Gel Characterization

Immediately after the synthesis of the sols, their rheological properties were studied using a concentric cylinder viscometer (model DV-II+ with UL/Y adapter) from Brookfield (Middleborough, MA, USA). Experiments were performed at a constant temperature of 25 °C maintained by recirculated water from a thermostatic bath. A shear stress versus shear rate flow curve was generated.

Next, 3 mL of sols were deposited on plastic Petri dishes with a diameter of 85 mm and maintained at room temperature. The spontaneous sol-gel transition took place and the gels were dried at laboratory conditions until constant weight. The obtained xerogels were characterized according to the following procedures:

The UV-visible absorption spectra were recorded on a PG Instruments T92+ spectrophotometer (Leicestershire, UK) with an integrating sphere, and by using $BaSO_4$ powder as white reference. The band-gap values were calculated by using the Kubelka-Munk function and the Tauc plot [58,59].

Textural characterization was performed by N_2 Physisorption at 77 K, using a Quantachrome Autosorb IQ (Boynton Beach, FL, USA). The adsorption data were analysed using a hybrid NLDFT (non-local density functional theory) approach [60] that allows quantification of both micro- and mesopores in order to obtain the pore size distribution of materials containing pores of different geometry.

The previously described TEM/STEM microscope was used to characterize the structure of the materials under study. The samples were prepared by powdered deposition onto lacey carbon coated copper grids.

2.4. Application on Building Material and Characterization

A limestone commonly used in building was chosen. This stone presents a homogeneous structure, composed of a micritic matrix of calcite and has an open porosity of around 12%. The white color of this limestone is ideal for evaluating its color changes. The sols were applied directly (without dilution) on 5 cm × 5 cm × 2 cm samples of stones by spraying onto one of the larger faces until its saturation. The surfaces were maintained wet during 1 min and excess sols were removed by spraying air. Next, the samples were weighed to calculate the uptake of products. Finally, the treated stones were dried under laboratory conditions until their weights were constant (approximately two weeks) and their dry matters were calculated.

Next, we evaluated the changes in stone color induced by the treatments. This effect was determined by using a solid reflection spectrophotometer, Colorflex model, from HunterLab (Reston, VA, USA). The conditions used were: illuminant D65 and observer 10°. CIE$L^*a^*b^*$ color space was used and variations in color were evaluated using the parameter: total color difference (ΔE^*) [61]. $\Delta E^* = \sqrt{\Delta L^{*2} + \Delta a^{*2} + \Delta b^{*2}}$ where ΔL^*, Δa^* and Δb^* are the differences for each colour coordinates.

Scanning electron microscopy (SEM) images of the coatings were taken using a Nova NanoSEM model from the FEI Company (Hillsboro, OR, USA), working at an acceleration voltage of 3 kV.

We evaluated the thickness of the coatings using photographs of transversal cuttings of treated samples dyed with methylene blue for better observation. The images were taken using optical microscope Eclipse LV150 equipped with a camera DS-Fi1, both from Nikon (Minato, Japan).

The adherence of the coating to the stone surface was evaluated by performing a peeling test using Scotch® MagicTM tape (3 M) (Maplewood, MN, USA). The test was carried out by sticking a piece of adhesive tape on the sample surfaces and determining the increase of the tape weight after it is detached, in accordance with a previously reported method [62].

The test for evaluating the self-cleaning activity of the materials under study was adapted from a standard procedure [63]. Firstly, 0.5 mL of a 1 mM solution of methylene blue (MB) in ethanol was deposited, drop by drop, on the treated faces of the samples and on their untreated counterpart. Next, the samples of stones were irradiated in a solar degradation chamber, Solarbox 3000eRH from CO.FO.ME.GRA. (Milan, Italy), equipped with a 2500 W xenon arc lamp and an outdoor UV filter. Incorporated detectors controlled and monitored the temperature, humidity and irradiance (in 300–800 nm range). The conditions in the chamber were 500 W/m^2 of irradiance, 55 °C of temperature and 60 mg/m^3 of absolute humidity. The evolution of color and diffuse reflection spectra with time were determined by using the previously described spectrophotometer. Recently it has been suggested that the photocatalytic degradation of dyes undergo by a sensitization mechanism and the dye would act as a visible light antenna [64,65]. However, we used MB because it is an excellent model to determinate how our coatings will remove coloured pollutants, which is one of the most challenging issues in building conservation.

We evaluated the complete oxidation of MB using a HiCube mass spectrometer from Pfeiffer (Asslar, Germany), employing a 10 mL/min of O_2 (4%)/Ar flow, over a cylindrical (ø5 × 2 cm) stone piece treated with photocatalytic coating and stained with MB. The staining procedure was the same for self-cleaning test. The sample was placed in AISI316 stainless steel reactor (in-house design) over a bed of quartz powder in order to reduce the void volume. Evolution of CO_2 (m/c = 44) and H_2O (m/c = 18) in the gas phase versus time were recorded. After the stabilization period the sample was irradiated with artificial solar light from 300 W Ultra-Vitalux lamp from Osram (Berlin, Germany) located 20 cm above the sample. We used a gas chromatograph Trace 1310 from Thermo Scientific (Waltham, MA, USA) equipped with a pulse discharge detector and a Carboxen 1010 PLOT capillary column from Sigma-Aldrich (St. Louis, MO, USA) to determine the CO_2 concentration in the gas flow from the reactor. In this way, we related the mass spectrometer signal with the CO_2 concentration.

We carried out a self-cleaning test by using soot, a common staining agent of building facades. For soot deposition, according to a previous procedure [66], we exposed the treated faces of stones to the flame of a tealight for 30 s, after, we removed the excess and not adhered soot layer using

compressed air. Next, the stone samples were irradiated in the solar degradation chamber and the evolution of color and diffuse reflection spectra were measured. The operation conditions employed in these photo-catalytic tests were identical to those used in the case of the previously described methylene blue degradation tests.

The hydrophilic properties of the samples were determined by the water contact angle test, using the sessile drop method. The measurements were obtained employing a commercial video-based, software-controlled contact angle analyser (OCA15plus, Dataphysics Instruments, Filderstadt, Germany). The test was carried out before and after light exposure in the solar box, by using the same conditions previously described during 24 h, in order to evaluate the induced hydrophilia phenomenon.

The ability of water to remove stains deposited on the samples was evaluated by the following experiment: a droplet composed of a mixture of terracotta powder and olive oil, simulating a greasy stain, was deposited on the samples. Next, they were subjected to a water stream (to simulate rain action) for 5 s.

3. Results and Discussion

3.1. Sol-Gel Characterization

All the sols showed a nearly Newtonian behaviour in the shear range evaluated. Thus, the viscosities were calculated as the slope of shear stress vs. shear rate curves. The viscosity values obtained for synthetized sols are presented in Table 2.

Table 2. Viscosity and gel time of synthetized sols and textural properties of xerogels obtained.

Product	Viscosity (mPa·s)	Gel Time	S_{total} (m^2/g)	V_{pore} (cm^3/g)
S0Au	4.61	24 h	240	0.32
ST0Au	5.43	12 h	316	0.58
ST5Au	5.80	8 h	217	0.57
ST12Au	6.57	6 h	329	0.74
ST25Au	8.37	3 h	155	0.51
ST38Au	*	5 min	#	#
ST50Au	*	1 min	#	#

* Fast gelation, measurement impossible # material not studied.

ST38Au and ST50Au sols were very viscous and they instantaneously gelled. Thus, the viscosity could not be measured. The viscosity values obtained for the other sols were similar to those corresponding to commercial silica sols employed for protecting building materials (i.e., Tegovakon V100 from Evonik (Essen, Germany), one of the most popular commercial stone consolidants, has a viscosity of 5.25 mPa·s at 25 °C) [16]. It confirms their suitability to be applied by common procedures, such as spraying, brushing, as coatings of building materials, even under outdoor conditions. In addition, a higher viscosity restricts the sol penetration into the substrate porous structure, this imply the reduction of adhesion between coating and substrate.

We observed two trends in the rheological behaviour of the sols under study. Firstly, as we previously observed [20], the inclusion of TiO_2NPs in the sols increased their viscosities. Secondly, we observed a clear direct correlation between viscosity and the gold aqueous dispersion content in the sols. It is well known that the hydrolysis rate of the sol-gel reaction is increased by water concentration [67]. The higher hydrolysis rate produces a higher overall progress of the sol-gel reaction and thus, the viscosity increases.

The sols stored in a closed bottle were maintained as sol for at least 6 months, whereas the sols deposited on plastic Petri dishes gel spontaneously, giving rise to crack-free and homogeneous xerogels. During this sol-gel transition, *N*-octylamine plays several roles: (1) it acts as a basic catalyst of the sol-gel reaction [21]; (2) it promotes formation of a particulated silica mesostructure, preventing cracking [21]

and (3) it adjusts the pH of the media to values above the isoelectric point of TiO_2 NPs, giving rise to negative charges in these NPs that produce mutual repulsive forces. Thus, TiO_2 aggregation is avoided during sol-gel transition and, consequently, a homogeneous gel is produced [21,68,69].

Regarding the gel time, two factors are key. Firstly, the addition of TiO_2NPs reduced the gel time due to the TiO_2NPs acting as seeds, promoting an early nucleation of SiO_2NPs around TiO_2 species and the subsequent faster gel growth [70]. Secondly, the increase of gold aqueous dispersion content also produced a significant decrease in the gel time. In this case, an increase in the hydrolysis rate, due to the higher water content, is responsible for this phenomenon [67].

Gel time is also a key parameter for building materials application, especially when they must be applied in situ, because instantaneous gel times prevent sol penetration into the porous structure of the substrate. Therefore, we discarded the xerogels with higher Au content (ST38Au and ST50Au) due to their previously reported short gel time and high viscosity.

Regarding the appearance of the xerogels, the gel without TiO_2NPs was transparent and those with TiO_2NPs were opaque (ST0Au was white, and gels with AuNPs were purple-blue). The purple-blue color was increased as Au content was raised, highlighting the absorption of visible light. This absorption was due to the LSPR band of AuNPs [39], which was clearly visible in the UV-Vis diffuse reflectance spectra (Figure 2), whereas the photocatalyst without Au (ST0Au) did not present any absorption in the visible range. We also calculated the band gap of the photocatalysts from reflectance spectra and we obtained a band gap of around 3.25 eV for all the materials prepared, close to the TiO_2 anatase band gap (3.2 eV).

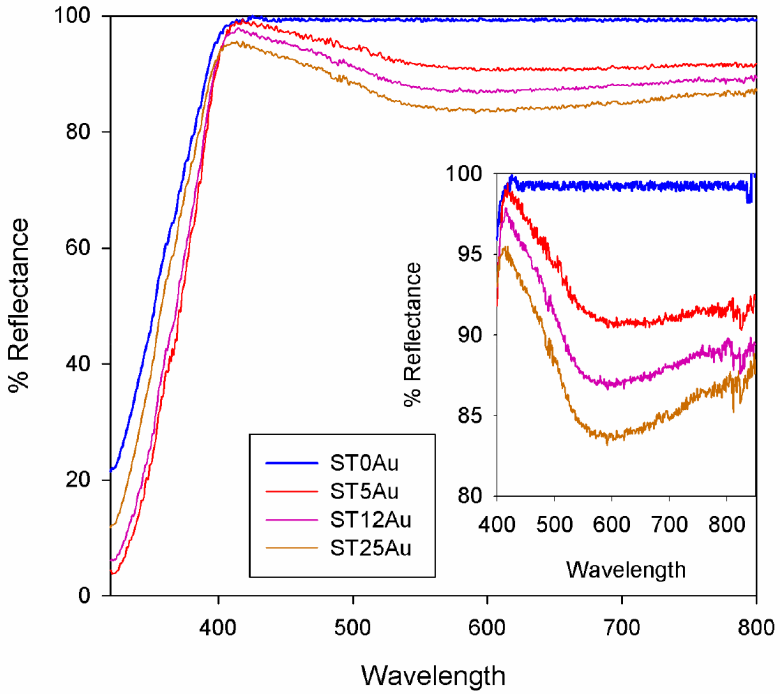

Figure 2. Reflectance UV-Vis spectra of powdered photocatalysts. Inset, detail of visible range.

In order to investigate the porous structure of these materials, N_2 physisorption tests were carried out. Adsorption–desorption isotherms and NLDFT pore size distributions, obtained from the adsorption branches for the materials under study, are shown in Figure 3. The textural data are compiled in Table 2. All materials show type IV(a) isotherms [71], characteristic of mesoporous materials due to the role played by n-octylamine [48]. Other similar TiO_2/SiO_2 composites prepared previously in our laboratory presented similar isotherms [20,21,38].

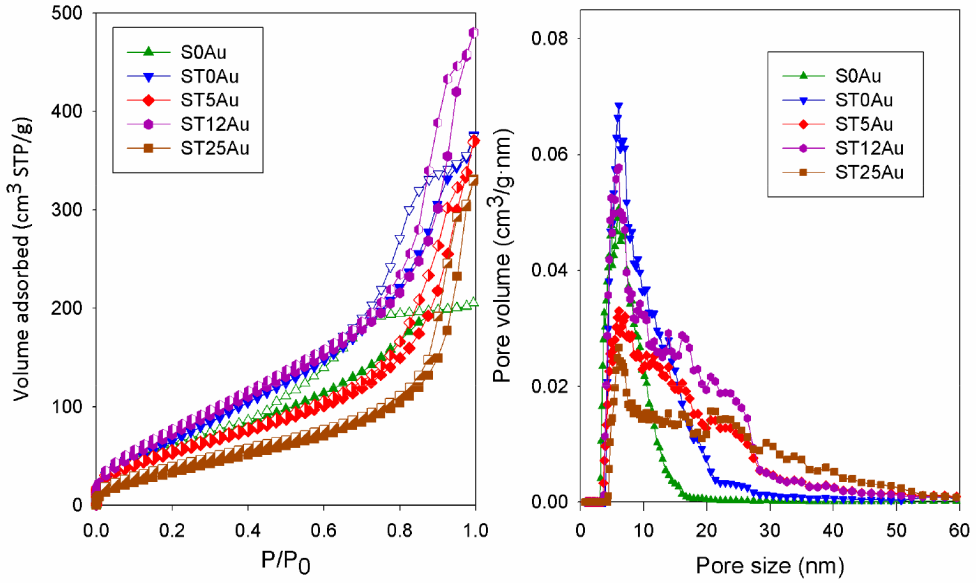

Figure 3. Isotherms and NLDFT (non-local density functional theory) pore size distributions obtained for the photocatalysts under study.

Regarding the hysteresis, S0Au (without TiO_2NPs and without AuNPs) had a triangular hysteresis loop classifiable as H2(b). ST0Au (with TiO_2NPs but without AuNPs) had a hysteresis with an elongated triangular shape, an intermediate situation between H1 and H2. The materials with gold had a H1 hysteresis (characterized by parallel and vertical branches). Hysteresis types H1 and H2 are characteristic of particulate materials formed by aggregation of spherical SiO_2 particles. H1 presents a better connectivity between pores than the H2 isotherm [71,72]. In conclusion, the trend observed in the xerogels under study indicates that the addition of aqueous dispersions of TiO_2NPs and AuNPs increase the interconnectivity of the pores of the original SiO_2 matrix. In the case of AuNPs, we think the increase in porous connectivity was produced by the water increase, since the NPs are inert and their low concentration cannot modify the material structure. In order to confirm the water effect, we prepared xerogels equivalent to ST5Au, ST12Au and ST25Au by replacing aqueous dispersion of AuNPs with water. We obtained isotherms very similar to those corresponding to the materials with AuNPs (Figure S1), confirming the role played by water in the mesostructure of the xerogels.

All the materials presented similar pore size distributions with a maximum at 6 nm, and a tail fitting to larger sizes. We found the greatest differences in the width of the pore distributions. S0Au exhibited the narrowest distribution (≈3–16 nm). The addition of TiO_2 caused the appearance of larger pores (≈4–30 nm), and materials with AuNPs further increased the pore size (≈3.5–55 nm). These results will be discussed together with the TEM data. In addition, the presence of larger pores can be responsible for an increase in pore connectivity and the subsequent transition of the previously described hysteresis shape.

Regarding the textural data, the addition of TiO_2 increased the surface area and pore volume, whereas these parameters were reduced as AuNPs were added, except for ST12Au, which had the greatest surface area and pore volume of all the materials under study. The different proportions of water in these materials can be responsible for this trend because the water/alkoxysilane ratio strongly affects the structure of gels [73]. Specifically, Yu and Wang [74] prepared TiO_2-SiO_2 materials with different water contents and the following behaviours were proposed according to the water/alkoxide ratio: (1) Low molar H_2O/alkoxysilane ratios, such as ST5Au, promote the partial hydrolysis of the precursor. Partially hydrolysed alkoxides condense, generating chain-like structures. The resulting cross-linked gel has a non-rigid structure, which can collapse easily during drying and ageing. Thus, the final structure has low pore volume and surface area; (2) High molar H_2O/alkoxysilane ratios,

such as ST25Au, promote the total hydrolysis of the precursor. In this case, the monomers condense to each other, creating a dense structure. This compact structure also has low pore volume and surface area; and, (3) Intermediate molar H_2O/alkoxysilane ratios, such as ST12Au, cause a partial hydrolysis of the precursor greater than (1) and thus, more hydrolysable groups are available for condensation, giving rise to a reticulated 3D-structure. This type of structure is less compact than (2) but it is rigid enough to not collapse during the drying and ageing process. As result, the structure has the highest pore volume and surface area.

STEM images of the synthesized AuNPs and their corresponding size distributions are shown in the supplementary information (Figures S2 and S3). They exhibited a significant anisotropy, with different shapes, and a particle size ranging from 1 to 30 nm with two maxima at 3 and 18 nm. The nanometric size of these particles is responsible of the LSPR effect observed by spectroscopy (see Figure 2).

HRTEM images of the Au-TiO_2/SiO_2 materials are shown in Figure 4. All of them were constituted by a silica matrix composed of amorphous silica particles, confirming the role played by n-octylamine [20]. However, the size of SiO_2 particles was significantly different for the materials under study, ranging from 15 to 25 nm for the silica matrix (S0Au). The particle size was reduced as TiO_2NPs were included in the formulation (10–15 nm for ST0Au) due to the nucleation promoted by TiO_2 [70]. Thus, in the absence of TiO_2 a larger SiO_2 particle size is required for the nucleation process to begin. In the case of the materials with AuNPs, the particle size ranged from 10–20 nm. The water increased the hydrolysis rate of the silica precursor and, consequently, the condensation was faster, promoting an increased growth of silica particles [75].

The TiO_2NPs were easily identified, because their crystalline structure was outlined against the amorphous silica matrix. The structure of the observed TiO_2NPs was anatase (Figure 4f). However, AuNPs were not visible during the HRTEM observation, due to their low load into the materials and their overlapping of the SiO_2 matrix.

The information obtained in physisorption experiments corroborated the obtained TEM images. Specifically, the packing of observed SiO_2 particles produce interstitial holes that would correspond with the maximum pore size distribution observed in N_2 physisorption (6 nm, see Figure 3). The TiO_2NPs, with a size of around 25–45 nm, were considerably larger than the particles of the silica matrix and thus, they increased the size of interstitial holes. For this reason, ST0Au had a pore size distribution wider than S0Au (without TiO_2). As AuNPs are integrated into the material, an open structure with greater pore size is observed (see Figure 3), as corroborated by N_2 physisorption. ST12Au was clearly the less compact structure as the greater surface area and porous volume confirmed.

In STEM-HAADF (Figure 5) mode, we identify the distribution of components in the materials. Specifically, in ST12Au (Figure 5a), TiO_2 was homogeneously dispersed throughout the matrix. However, in ST25Au (Figure 5b), TiO_2 produced agglomerates of around 200 nm with a poor dispersion in the silica matrix. These distributions confirm that the TiO_2 granulates (medium size of 20 μm) were disaggregated during the sol synthesis.

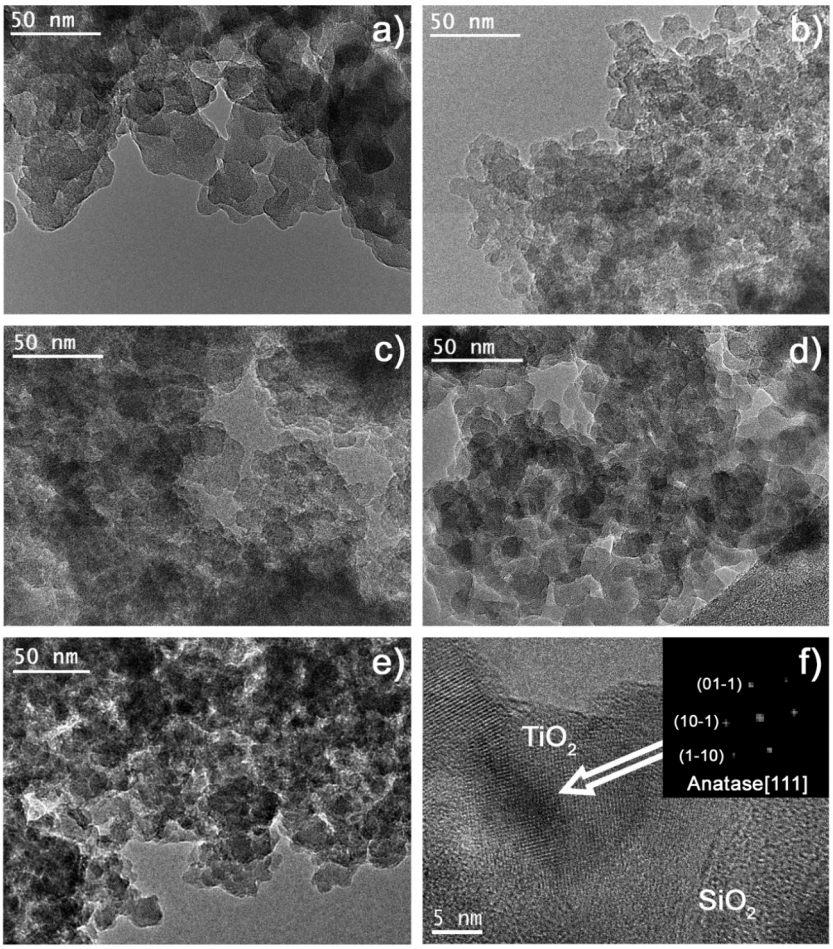

Figure 4. HRTEM images of photocatalysts (**a**) S0Au, (**b**) ST0Au, (**c**) ST5Au, (**d**) ST12Au, (**e**) ST25Au and (**f**) detail of a TiO_2NP and its digital diffraction pattern.

We also observe the AuNPs, because gold has a high contrast in this image mode. The size of these NPs (10–30 nm) matches the largest size (17.7 ± 4.4 nm) observed in the aqueous dispersion (see Figures S2 and S3). It was not possible to find the smallest AuNPs (3 ± 0.8) due to their reduced size, overlapping with silica matrix or aggregation. In addition, we observed that the AuNPs had a tendency to agglomerate as gold concentration is raised. Specifically, in ST12Au (Figure 5c), we found accumulations of around ten NPs disposed close to each other, whereas ST25Au (Figure 5d) presented accumulations of up to 50 NPs.

The XEDS point analysis over AuNPs (Figure 5e) confirmed their composition and, importantly, revealed the presence of titanium at the same area. Therefore, it can be concluded that AuNPs were located close to TiO_2NPs. This is fundamental for producing the energy transfers between AuNPs and TiO_2 by LSPR phenomena [76]. The charge injection mechanisms take place when the plasmonic nanoparticles and semiconductor are in direct contact with each other, allowing an effective transfer of electrons and holes [77]. On the other hand, when metal and semiconductor are nearby but they are separated by a non-conductive thin layer (silica in our case), energy transfers can take place through near-field electromagnetic and resonant photon-scattering mechanisms [78].

According to the information obtained by the TEM study, a nanostructural model of the Au-TiO_2/SiO_2 materials synthesized in this study was proposed (see Figure 6). We can conclude that AuNPs with completely different morphology and size, and sharp crystalline TiO_2 NPs with similar size are integrated in a mesostructured matrix composed of SiO_2 particles, produced by the action of n-octylamine.

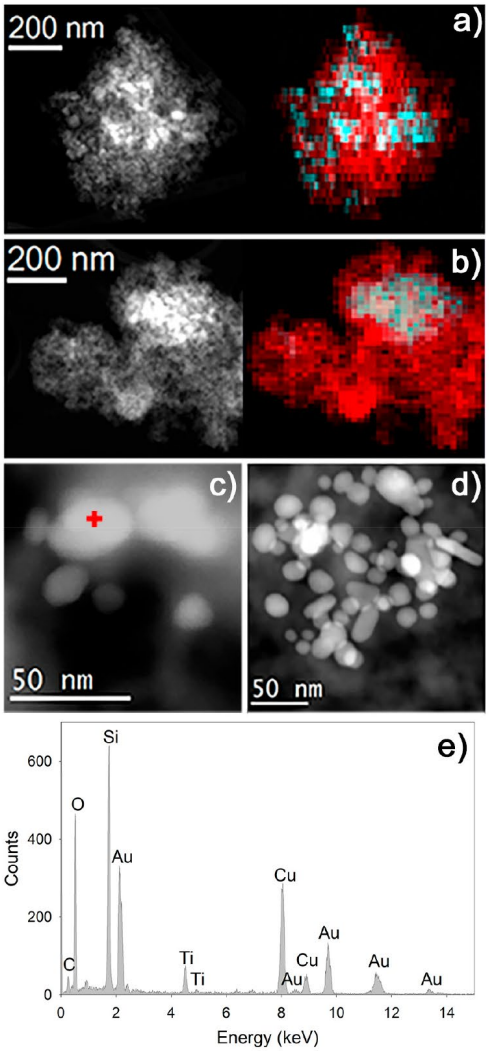

Figure 5. STEM-HAADF characterization of photocatalysts. (**a**) Image of ST12Au and its corresponding XEDS map for Si (red) and Ti (blue); (**b**) image of ST25Au and its corresponding XEDS map for Si (red) and Ti (blue); (**c**) AuNPs in ST12Au; (**d**) AuNPs in ST25Au and (**e**) example of XEDS point analysis acquired on the point marked in (**c**).

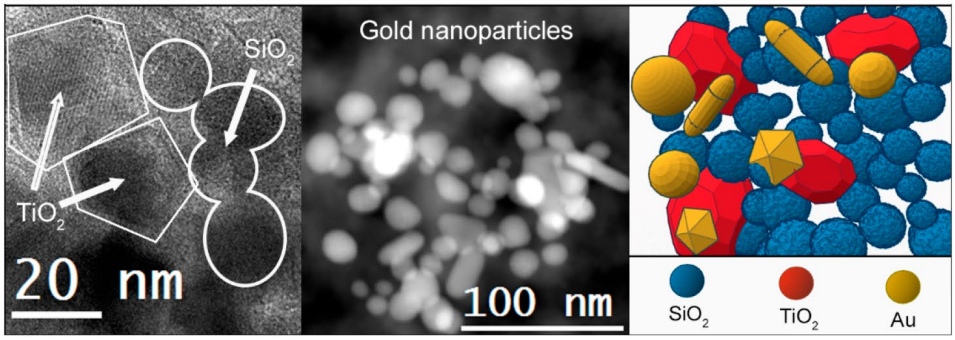

(**a**) (**b**) (**c**)

Figure 6. (**a**) HRTEM image of the xerogels under study; (**b**) HAADF image of detail of AuNPs into the xerogels and (**c**) model of nanostructure of photocatalyst built from these images.

3.2. Application on Stone and Characterization

The sols synthesized in this study were sprayed, under laboratory conditions, onto the building limestone samples in order to investigate its photocatalytic behaviour and other properties associated with the coatings.

Table 3 shows the uptake and dry matter values of the products. A clear relationship between the uptake and dry matter and the viscosity values (see Table 2) is observed. A lower viscosity allows a deeper penetration of the liquid product into the porous structure of the substrate and, consequently, produces higher uptake and dry matter.

Table 3. Averages values and standard deviations for properties of treated stones.

Sample	Uptake (g/m^2)	Dry Matter (g/m^2)	ΔE *	Peeling Test (mg/cm^2)
Untreated	-	-	-	0.079 ± 0.014
S0Au	480 ± 60	258 ± 40	5.2 ± 0.6	0.019 ± 0.016
ST0Au	428 ± 60	246 ± 40	5.0 ± 0.3	0.011 ± 0.015
ST5Au	381 ± 90	203 ± 60	3.5 ± 0.6	0.021 ± 0.015
ST12Au	302 ± 90	171 ± 60	3.4 ± 0.5	0.016 ± 0.018
ST25Au	281 ± 60	153 ± 40	3.5 ± 0.6	0.019 ± 0.013

One important limitation for practical application as building coatings would be changes in the colour of building materials. Therefore, total colour difference values (ΔE^*) of the stone induced by the photocatalysts were measured and these results are given in Table 3. All the photocatalysts produced colour changes close to the generally accepted threshold value ($\Delta E^* \leq 5$), even for the most restrictive applications such as ancient building restoration [79]. A digital reproduction of the stone colour, before and after the treatments, obtained from the CIEL*a*b* coordinates is shown in the supplementary information (see Figure S4). The most notable variation is observed for the products without AuNPs (S0Au and ST0Au). In order to analyse the contribution of each colour coordinate in ΔE^*, the changes of the coordinates were examined separately (see Figure 7). The greatest changes were observed for L and b coordinates, corresponding to luminosity and red-green shift, respectively. Comparing the products, the most significant variations were observed for the b coordinate. The purple-blue colour of products with AuNPs is different to the green change produced by the S0Au and ST0Au treatments (The highest values of b coordinate). For this reason, the products with AuNPs produced the lowest colour changes.

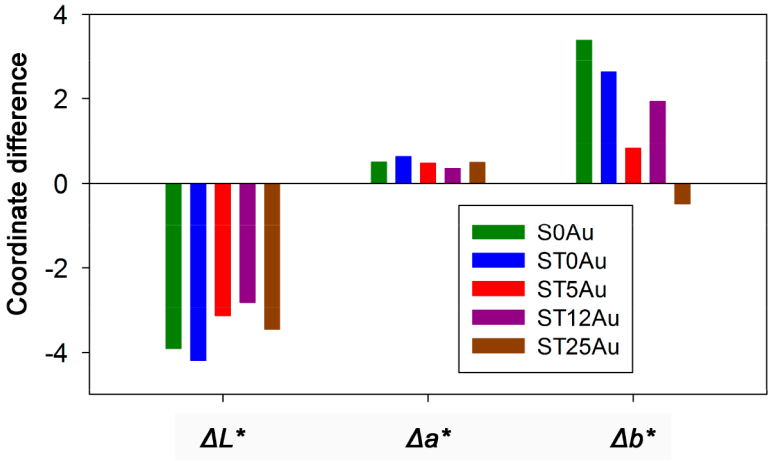

Figure 7. Changes in colour coordinates induced by the products under study.

The SEM images of the treated surfaces (Figure S5, in the supplementary information) show continuous and crack-free coatings. This confirms the role played by n-octylamine in preventing

cracking of the xerogels, as previously discussed [80]. Also, we have measured the thickness of coating, it ranged from 3 to 12 μm, with an average of 8 μm, for all the samples. As an example, a representative photograph of the transversal cutting of treated sample is showed in Figure S6.

The values corresponding to the material removed by the peeling test are shown in Table 3. It was significantly reduced for the treated stones, their values being practically zero for all the products applied. These results confirm that all the products under study present a suitable adhesion to the stone and they even produce an effective consolidation of the limestone surface (the material removed is lower than that corresponding to the untreated limestone).

Finally, and most importantly, we evaluated the self-cleaning effectiveness of the products under study by analysing the degradation of methylene blue (MB), deposited on the coated stone samples, under visible radiation. The evolution of dye degradation for the treated samples and their untreated counterparts is shown in Figure 8. In order to evaluate these differences, we recorded UV-visible absorbance spectra in the stained treated samples and their untreated counterpart (see Figure S7). In all the cases, we observe two maxima in the spectra at 660 and 600 nm that can be related to the presence of MB^+ and $(MB^+)_2$, respectively [81]. The peak associated to $(MB^+)_2$ is higher in the case of the untreated sample, whereas the opposite effect is observed in the treated samples. The shift of the absorbed maximum to a lower wavelength explains the observed violet hues of the untreated samples [82,83]. On the other hand, the slight differences observed between the treated samples can be associated with different MB penetration due to the different coating properties (textural properties, coating penetration, etc.) and irregularities of the stone samples.

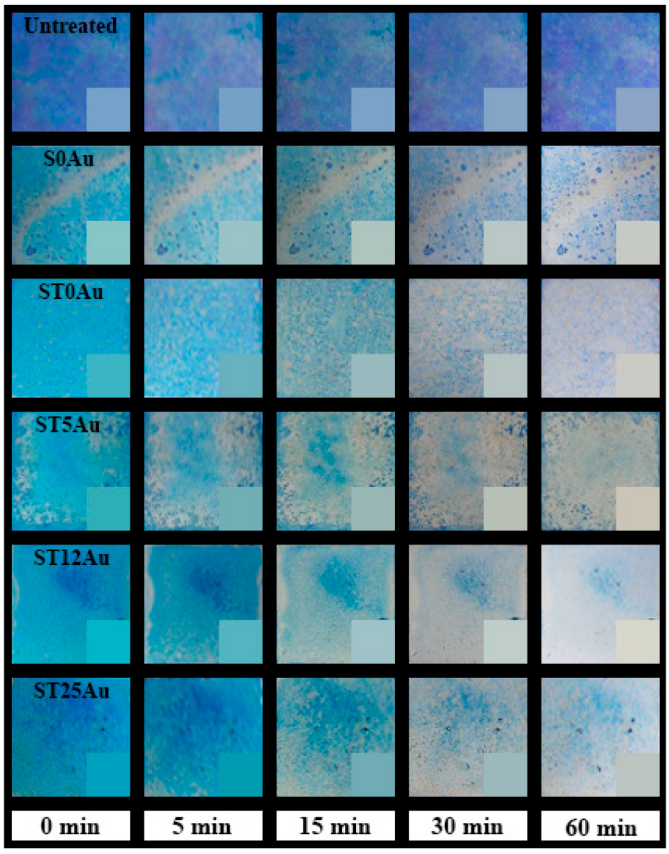

Figure 8. Photographs of evolution of decolourization of dye, deposited on the stone samples, during the first 60 min of the photodegradation test, the photographs correspond to the whole sample surfaces, 5 × 5 cm. The insets include the digital reproduction of the stone colour from the colour coordinates.

Nanomaterials **2018**, *8*, 177

In order to quantify the sample self-cleaning effectiveness, we use the total color difference, according the following equation:

$$\%\Delta E^* = \frac{\Delta E^*}{\Delta E_0^*} \quad (1)$$

where ΔE^* is the total color difference at a specific time with respect to the sample before staining, and ΔE_0^* is the total color difference of the sample prior to starting the decolorization process. These results are presented in Figure 9.

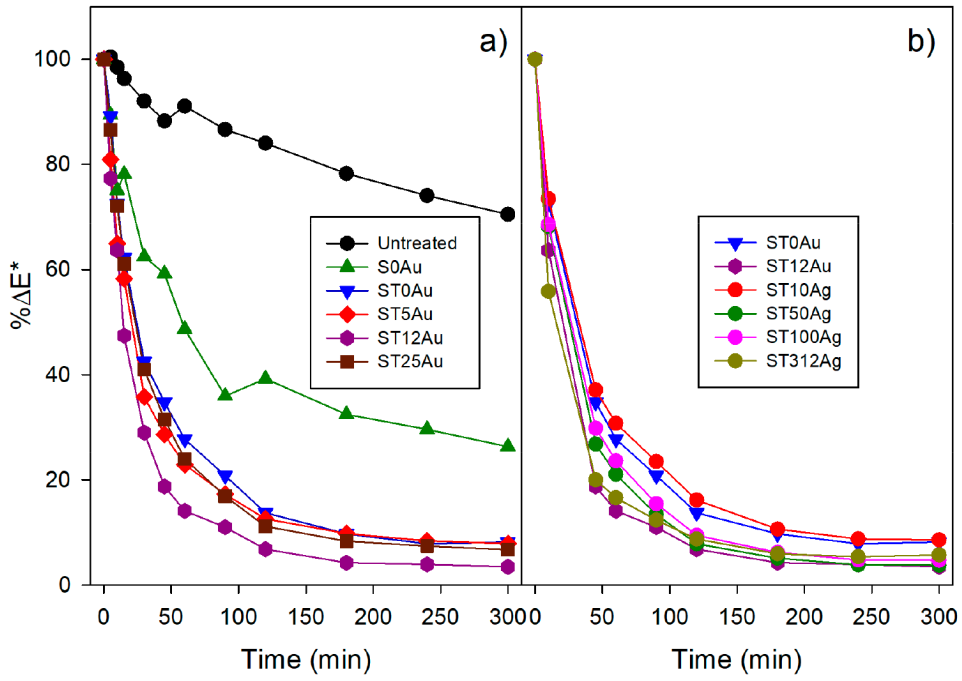

Figure 9. (**a**) Evolution of $\%\Delta E^*$ for the untreated and treated stone samples stained with methylene blue; (**b**) Comparison of results for ST and ST12Au, with the results obtained for the stones treated with different Ag-TiO_2/SiO_2 products.

The results included in Figure 9a show greater self-cleaning activity for the treated stone samples than the untreated stone. On the other hand, we want to comment that the MB degradation did not take place in dark conditions (see Figure S8). The untreated stone samples and their counterpart treated with the non-photoactive coating (S0Au) showed MB degradation. As reported in the literature [84], MB is degraded, under UV light, due to a purely photochemical mechanism associated with MB photolysis. In order to confirm MB photolysis, we have carried out a photodegradation test of MB deposited on quartz powder. Figure S9 in supplementary information shows the plot degradation and the evolution of methylene absorbance with the irradiation time.

The degradation rate of the sample treated with S0Au is significantly higher than that corresponding to the untreated sample due to the following issues:

- The degradation of the MB monomer (MB^+), which is mainly adsorbed in the treated sample, is faster than that of the dimer $(MB^+)_2$ [85,86].
- The coating restricts the MB penetration into the substrate and it has a large surface area compared with the stone. Therefore, MB is more exposed to light, oxygen and humidity.
- The stone has a greater absorption in the UV range than the silica coating (see Figure S10). This reduces the amount of high energy light available to produce the MB photolysis.

Comparing the products, the treatments including TiO_2 were more effective than those corresponding to S0Au, ST12Au being the most effective. This enhancement of self-cleaning activity is obviously due to the photocatalytic effect of TiO_2.

Moreover, since one of the first objectives of this work is to improve the photocatalysis of the materials by using Au instead of Ag, in Figure 9b, the Au-TiO_2/SiO_2 coating with the best performance (ST12Au) is compared with previously developed Ag-TiO_2/SiO_2 treatments [38]. The Ag-based coatings showed a poorer performance than that corresponding to the Au-TiO_2/SiO_2 based coating with the best performance, and only the product with the highest Ag content (3.2%) showed a similar degradation to the best-performing Au-TiO_2/SiO_2 coating (with an Au content of 0.12%). Additionally, it should be pointed out that the 3.2% Ag-TiO_2/SiO_2 coating showed an increase in ΔE^* for a degradation time above 180 min. This was due to the appearance of a brown colouration in the stone surface produced by the photochemical reaction of silver.

On the other hand, using the $\%\Delta E^*$ procedure, it was difficult to discern the activity sequence of the evaluated products because their degradation plots are overlapped. In spite of this methodology being commonly employed for evaluating the self-cleaning activity of building materials [10,11,18,46,50], their poor resolution led us to propose an alternative approach for self-cleaning testing on building materials.

Specifically, this approach is based on applying the Kubelka-Munk theory to the UV-Visible reflectance spectra. The Kubelka-Munk theory [87,88] is commonly used to explain the light absorption in a thin layer of dye deposited on a non or low-absorbent substrate [54], which can be considered to approximate the MB deposited on the stone samples under study. The following equation, specifically addressed for these systems is included in Equation (2):

$$f(R_\infty) = \frac{(1-R_\infty)^2}{2R_\infty} = \frac{k}{s} \quad (2)$$

where $f(R_\infty)$ (hereafter KM) is equivalent to absorbance, R_∞ is the diffuse reflectance, k is the dye molar absorption coefficient and s the surface scattering coefficient.

From this equation, the experimentally obtained diffuse reflectance spectra can be converted into the corresponding absorbance spectra, which is directly related to the quantity of MB. Specifically, we used the evolution of KM/KM_0, KM_0 as being the initial absorbance in the absorption maximum, to determinate the decay of concentration of the MB over time. This method should be more precise in determining the self-cleaning activities of the products under study, because the absorbance is directly related to the quantity of dye. The plots (Figure 10a) were similar to those obtained by the popular space color coordinates method, but the difference in activity between the coatings was easily discernible and thus, the following order in the self-cleaning activity can be established:

ST12Au > ST25Au > ST5Au > ST0Au > S0Au > Untreated.

This trend can be explained as follows: ST0Au activity was greater than that of S0Au, confirming the photocatalytic effect of TiO_2. All the products with AuNPs significantly increased the self-cleaning activity with respect to ST0Au. This demonstrates that the addition of AuNPs improves the photoactivity of TiO_2 in the photocatalysts under study.

In addition, the use of absorbance spectra allows a deeper study of methylene blue degradation. Specifically, a specific wavelength to discern between the degradation of MB monomer (660 nm) and dimer (600 nm) can be studied. The degradation profile of the monomer (Figure 9b) and the dimer (Figure 9c) show the same trend as the overall degradation plot (Figure 9a), but the monomer degradation is considerably faster than dimer degradation. As previously reported [85], this analysis is important because monomer and dimer degradation are not comparable due to their different degradation rates. In this study, the treated samples trend was similar for the three degradation profiles because MB is mainly adsorbed as a monomer. However, the difference between the untreated samples and their counterpart treated with S0Au is significantly different for overall and dimer

degradation profiles because MB, as previously discussed, corresponds to dimer and monomer species, respectively and thus, the degradation rate is different.

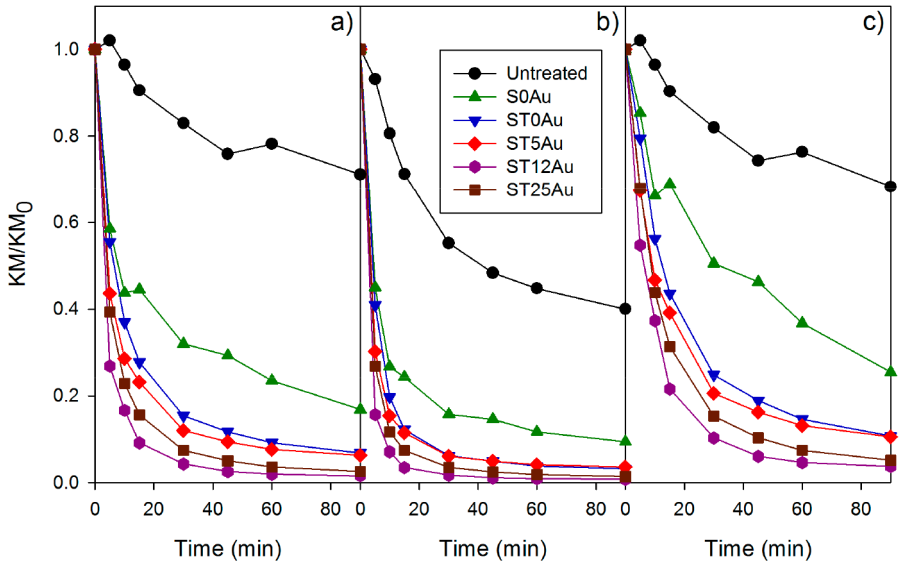

Figure 10. Evolution of KM/KM_0 for the untreated and treated stone samples stained with methylene blue, (**a**) overall degradation; (**b**) monomer degradation and (**c**) dimer degradation.

As MB absorbance is directly related to its concentration, we can use its evolution over time to fit the experimental data to a rate equation. The photodegradation of MB deposited on TiO_2 coated glass has been reported as a first order kinetic process [85]. However, our results were not well adjusted to a first order rate equation. This can be related to: (1) the coating thickness, 200 nm and 8 μm for the previous work and our study, respectively; (2) the porosity of the substrate, glass (non-porous substrate) and stone (porous substrate). In order to confirm this hypothesis, the ST0Au coating was deposited on glass by dip coating, and was subjected to a MB degradation experiment under the conditions described in the experimental section. The MB degradation was perfectly adjusted to a unique first order process (see Figure S11), confirming this study's hypothesis. A specific rate equation was obtained from the experimental results corresponding to the MB degradation plots, the initial and final values were independently fitted to two different first order equations. This can be associated with the existence of two processes with different rates, as previously proposed, for the degradation of dyes deposited on TiO_2 [89].

The assumption is an extreme simplification of the two kinetic models proposed in a previous paper [89]. One of them, named "unexposed portion model", assumes that only TiO_2 directly exposed to light can be degraded, and that the dye portion that penetrates into the TiO_2 layer (in the dark) cannot be degraded. Another alternative model, named "intensity influence model", considers that light intensity decreases through the thickness of TiO_2 and thus, the rate constant is dependent on the light intensity received. Both of these assumptions were combined and simplified to explain the two kinetics considered in the rate equation proposed in our work. Firstly, similar to the first model, the existence of two portions of MB was considered: (1) MB exposed on the sample surface, and, (2) MB into the substrate structure. Secondly, it was considered that the rate constant for MB inside the sample is reduced, due to its lower exposure to light. However, instead of considering a gradual rate constant decreasing through the penetration depth, a constant value is simplified which is lower than that corresponding to the surface degradation rate. Thus, the following equation combining two first-order processes was achieved:

$$\frac{KM}{KM_0} = (1-x)e^{-k_1 t} + xe^{-k_2 t} \quad (3)$$

where k_1 is the reaction rate of the fast degradation process (surface), k_2 is the degradation of the slow degradation process (inside) and x is the fraction of MB degraded by means of the slow process. These kinetic parameters and the coefficient of determination (R^2) are compiled in Table 4.

Table 4. Parameters of kinetic models calculated by the kinetic model proposed in this paper.

Sample	Degradation	k_1 (min^{-1})	k_2 (min^{-1})	x	R^2
Untreated	Overall	0.030	1.59×10^{-3}	0.812	0.964
	Monomer	0.039	1.33×10^{-16}	0.620	0.991
	Dimer	0.027	1.95×10^{-3}	0.798	0.966
S0Au	Overall	0.124	6.31×10^{-3}	0.345	0.959
	Monomer	0.185	9.85×10^{-3}	0.223	0.981
	Dimer	0.061	9.19×10^{-3}	0.613	0.993
ST0Au	Overall	0.163	1.67×10^{-2}	0.259	0.999
	Monomer	0.207	1.38×10^{-2}	0.095	0.999
	Dimer	0.071	5.72×10^{-3}	0.185	0.995
ST5Au	Overall	0.265	2.22×10^{-2}	0.282	0.996
	Monomer	0.309	1.95×10^{-2}	0.132	0.999
	Dimer	0.105	9.84×10^{-3}	0.244	0.998
ST12Au	Overall	0.437	5.54×10^{-2}	0.246	0.998
	Monomer	0.471	5.30×10^{-2}	0.094	0.999
	Dimer	0.136	1.87×10^{-2}	0.152	0.997
ST25Au	Overall	0.269	3.34×10^{-2}	0.234	0.999
	Monomer	0.322	3.16×10^{-2}	0.107	0.999
	Dimer	0.099	1.14×10^{-2}	0.148	0.999

These obtained parameters showed a good fit to the measured values (see Figure S12). Thus, we can use them to make quantitative comparisons. According to the previous consideration, the k_2 constants were effectively several orders of magnitude lower than k_1. Using the k_1 constants to compare the self-cleaning properties of the products under study, the activity sequence was in accordance with those obtained by the analysis of the evolution of KM/KM_0 (see Figure 10), k_2 also showed a similar trend. Comparing k_1 for the monomer and dimer degradation, we observe that k_1 is higher for the monomer, around three times that for treated stones, thus confirming the faster monomer degradation. Finally, we noticed differences in the x parameter values. S0Au treated stone presented a significant reduction of the x parameter with respect to untreated stone, as previously discussed; this is related to the presence of coatings preventing the MB penetration. The samples containing TiO_2-based coatings had similar x values and they were lower than S0Au (without TiO_2). This difference may be attributed to the different degradation processes that took place (photolysis and photodegradation).

We want to comment that the increase in photoactivity of the products did not present a direct relationship with the content of AuNPs, with ST12Au (intermediate content of AuNPs) being the most active product. We can explain this as a consequence of the influence of the structure and the texture of the coatings on their photoactivity. Photocatalyst structure is a relevant parameter, notably the Au and TiO_2 distribution in the silica matrix [49]. ST12Au, with the best photoactivity performance, showed a homogeneous distribution of the photoactive components in the matrix, as observed by TEM (see Figure 5a). In the case of ST25Au (Figure 5b,d), a poor dispersion of Au and TiO_2 into the silica matrix is observed.

Regarding the texture, since the dye degradation is a surface process, the contact between MB, TiO_2 and the parameters acting in the redox process (light, O_2 and H_2O) need to be maximized [90–93]. Thus, photocatalyst surface area plays a key role in the MB degradation [92,94–96]. Pore volume is also a relevant parameter because diffusion of substances (O_2, H_2O and dye) to active photocatalyst sites occurs through the pore structure [20,91,97,98]. Thus, although ST25Au had the highest content

of AuNPs, its low surface area and pore volume values (see Figure 3 and Table 2) resulted in its lower photoactivity. ST12Au with a medium content of AuNPs presented the highest surface area and pore volume in the products under study. Thus, ST12Au showed the highest photoactivity because it has the best compromise between (1) content of AuNPs, and consequent visible light absorption, (2) dispersion of TiO_2 and AuNPs in the silica matrix and (3) textural parameters.

Finally, we confirmed that under the conditions of our assay the MB photodegradation took place via oxidation. The mass spectroscopy experiments (Figure 11) showed an evident CO_2 and H_2O liberation during the light irradiation of the ST12Au sample. We selected this sample because it presented the highest photoactivity, and thus, it should release the highest amount of CO_2. When the illumination started, the CO_2 concentration in air quickly increased and reached a maximum level of around 340 ppm after approximately 30 min, then the CO_2 level slowly decreased. This behaviour is related to the faster MB degradation that we observed in the first min of the self-cleaning test. When the illumination was finished, the CO_2 concentration began to decrease abruptly, confirming that the CO_2 formation was interrupted. The water signal (m/c = 18) showed a similar behaviour, but its release profile was different, probably due to the water being adsorbed in the sample. The air mass spectrum during the illumination (see Figure S13) did not show signals in the range of mass/charge 50–185, corresponding to volatile organic compounds, which are intermediates of MB degradation. This evidence demonstrated that our photocatalysts have the capacity for oxidizing the MB completely to CO_2 and water, and intermediate volatile organic compound are not released.

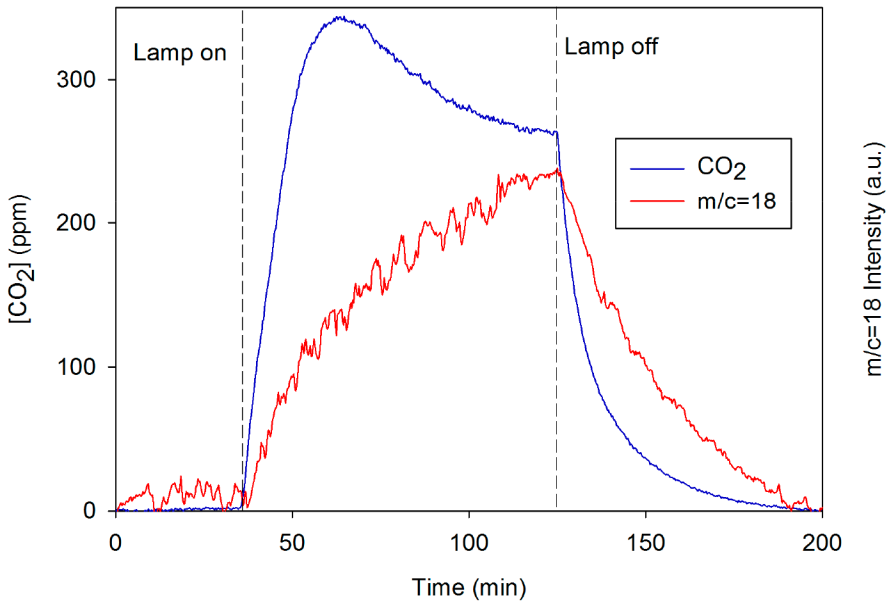

Figure 11. Evolution of CO_2 concentration and m/c = 18 signal (water) during the mass spectroscopy experiment.

In addition, we checked the degradation efficiency of the photocatalysts under study against a real staining agent for buildings. The self-cleaning test was carried out by using stone samples stained with soot. As a maximum absorbance in the visible spectrum is not observed for soot, we used the average KM values obtained in the spectral range of 420–440 nm to build the degradation plots. We chose these wavelengths because the maximum absorbance decrease took place in that zone of the spectrum (see Figure S14), and the average of several points corrects the noise of the measure. The soot decolourization trends (Figure 12) were similar to those obtained by MB: ST12Au > ST25Au ≈ ST5Au > ST0Au > S0Au > Untreated. By comparing soot and MB activity, we observed a significantly slower decolourization for soot. A fast soot decolourization was observed

in the first 6 h of the test, but it did not progress for longer times. This was probably related to the soot penetration into the pore structure of the stone and its strong adherence to the substrate.

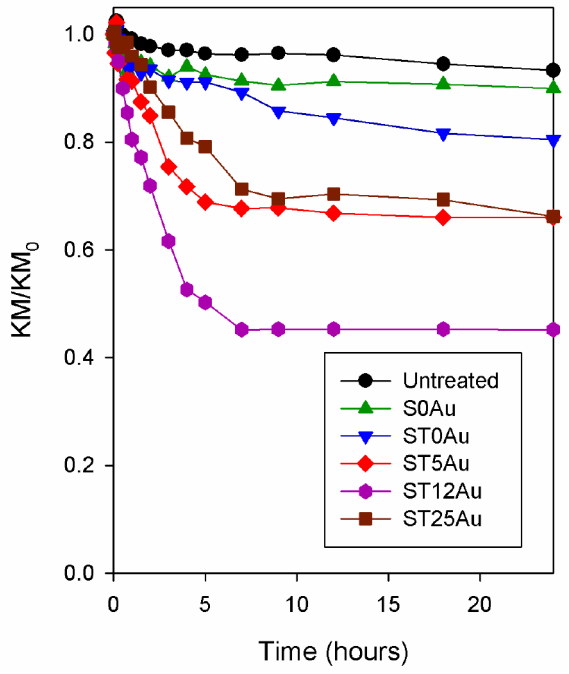

Figure 12. Evolution of KM/KM_0 for the untreated and treated stones stained with soot.

Finally, in order to evaluate the existence of photoinduced hydrophilicity on the samples under study, the water contact angle (CA) measurement was carried out on the surface of the samples, before and after light exposure. Before light exposure, all the treated surfaces showed hydrophilic properties, due to the hydrophilic nature of the silica matrix. Specifically, the untreated sample absorbed water and thus, the CA could not be measured. The CA values for the treated samples without TiO_2 (S0Au) showed a medium value of 71° ± 8°. The incorporation of TiO_2 into the coating increased the hydrophilic behaviour of the treated surface and thus, all samples containing TiO_2 showed contact angles with a medium value of 44° ± 9°. The test was repeated 24 h after light exposure, showing similar CA values, probably due to the low TiO_2 content in the coatings.

In spite of the absence of induced superhydrophilicity, all the TiO_2-based coatings showed an effective self-cleaning performance under water action, as shown in Figure 13, and in the video in the supplementary material. In the untreated sample, the water could not remove the stain droplet because it penetrated into the stone pores and thus, it was adhered. All the coatings prevented the stain penetration into the stone pores. In addition, the hydrophilic nature of the coatings promotes water spreading, favouring stain removal. Thus, the stain was only partially removed in the sample with the lowest hydrophilicity (S0Au), and it was completely removed in the other samples.

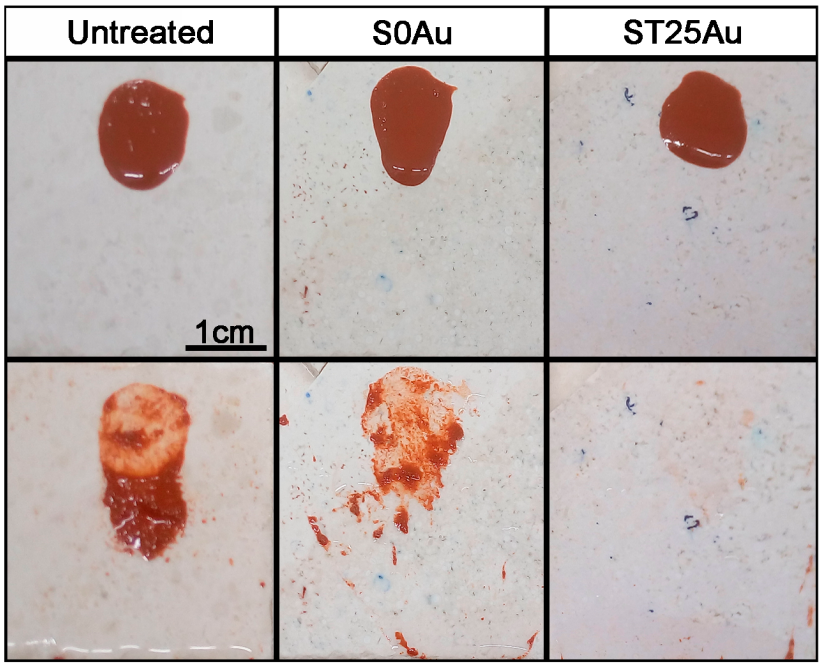

Figure 13. Photographs of the samples before and after the water streaming: untreated, S0Au and ST25Au. all photographs have the same scale.

4. Conclusions

We have designed a new and simple sol-gel route for producing Au-TiO_2/SiO_2 photocatalysts with application as self-cleaning coatings on building materials. The addition of a low content of AuNPs into the starting sol improves the TiO_2 photoactivity under solar radiation, because a significant absorption in the visible range (45% of solar radiation) is promoted. The sols obtained by this route were applied on a common building stone, producing coatings, which adhere firmly to the stone and preserve their aesthetic qualities.

We compared two different methodologies for evaluating self-cleaning on building materials. The commonly employed color method, based on the study of space color coordinates, and an alternative absorbance method, based on the Kubelka-Munk theory. This comparison demonstrated that the color methodology has a limited applicability whereas the absorbance method shows clear advantages: (1) it allows differences between coatings to be clearly discerned; (2) it allows degradation of different dye species in the system to be studied independently (in this case MB dimer and monomer); and, (3) it allows fitting the experimental data to a rate equation that allows dye degradation in a porous substrate to be explained.

Finally, we established that the self-cleaning effectiveness of the photocatalysts under study did not present a direct relationship with the content of AuNPs, an intermediate Au content being the optimal value. We can explain this as a consequence of the influence of the structure and the texture of the coatings on their photoactivity. Specifically, the product with intermediate Au content showed the highest pore volume, the highest surface area and the best dispersion of the photoactive components.

Supplementary Materials: The following are available online at http://www.mdpi.com/2079-4991/8/3/177/s1, Figure S1. Nitrogen physisorption isotherms and pore distribution of photocatalysts with 1% of TiO_2 prepared with different water content, Figure S2. HAADF-STEM image of AuNPs nanoparticles employed, Figure S3. Size distribution of AuNPs employed, Figure S4. Digital reproduction of stone color after and before treatments, Figure S5. SEM images of coated stones under study and their untreated counterpart, Figure S6. Optical Microscopy photograph of transversal cutting of treated stone. The coating was dyed with methylene blue for better observation, Figure S7. UV-visible absorbance spectra of MB deposited on untreated and on a treated stone, ST12Au treated sample was selected as representative example. The absorbance spectra were obtained from respective reflectance spectra, Figure S8. Evolution of %ΔE^* for a ST12Au treated stone sample stained with

methylene blue maintained in dark conditions, Figure S9. Degradation plot and absorbance evolution for MB with the irradiation time, Figure S10. UV-visible absorbance spectra of S0Au coating and the limestone employed in this work. The absorbance spectra were obtained from respective reflectance spectra, Figure S11. Left, evolution of MB degradation on ST0Au coating deposited on glass. Right, its corresponding fitting to first order rate equation. Figure S12. Fitting between the KM/KM_0 values measured (dots) and calculated by fitting to rate equation (lines) for the different degradations processes, overall (black), monomer (red) and dimer (blue), Figure S13. Mass spectrum of air from reactor obtained during the mass spectroscopy experiments when the sample was being irradiated with light, Figure S14. Example of soot absorbance spectra during soot self-cleaning test for ST12Au treated stone, Video 1. Self-cleaning test by water action.

Acknowledgments: This work has been supported by the Spanish Government (MINECO)/FEDER-EU (MAT2013-42934-R and MAT2017-84228-R). M.L. would also like to thank MINECO for his pre-doctoral grant (BES-2014-068031). J.J.D. is grateful to Ramon y Cajal program and the Ce-NanoSurPhases project grant from MINECO.

Author Contributions: M.L. and M.J.M. conceived and designed the experiments associated to the of the synthesis and characterization novel photoactive materials and they wrote the manuscript, excepting the experiments specified as follows: M.L.A.G. designed the AuNPs synthesis and J.J.D. conceived and performed the TEM, Mass Spectroscopy and Gas Chromatography experiments. He also contributed in the discussion associated to these experiments. Finally, M.L. performed the experimental work.

Conflicts of Interest: The authors declare no conflict of interest.

References

1. Peruchon, L.; Puzenat, E.; Girard-Egrot, A.; Blum, L.; Herrmann, J.M.; Guillard, C. Characterization of self-cleaning glasses using Langmuir–Blodgett technique to control thickness of stearic acid multilayers. *J. Photochem. Photobiol. A Chem.* **2008**, *197*, 170–176. [CrossRef]
2. Chen, J.; Poon, C.S. Photocatalytic construction and building materials: From fundamentals to applications. *Build. Environ.* **2009**, *44*, 1899–1906. [CrossRef]
3. Fujishima, A.; Honda, K. Electrochemical Photolysis of Water at a Semiconductor Electrode. *Nature* **1972**, *238*, 37–38. [CrossRef] [PubMed]
4. Fujishima, A.; Zhang, X.; Tryk, D.A. TiO_2 photocatalysis and related surface phenomena. *Surf. Sci. Rep.* **2008**, *63*, 515–582. [CrossRef]
5. Watanabe, T.; Nakajima, A.; Wang, R.; Minabe, M.; Koizumi, S.; Fujishima, A.; Hashimoto, K. Photocatalytic activity and photoinduced hydrophilicity of titanium dioxide coated glass. *Thin Solid Films* **1999**, *351*, 260–263. [CrossRef]
6. Xiaohong, W.; Zhaohua, J.; Huiling, L.; Xuandong, L.; Xinguo, H. TiO_2 ceramic films prepared by micro-plasma oxidation method for photodegradation of rhodamine B. *Mater. Chem. Phys.* **2003**, *80*, 39–43. [CrossRef]
7. Radeka, M.; Markov, S.; Lončar, E.; Rudić, O.; Vučetić, S.; Ranogajec, J. Photocatalytic effects of TiO_2 mesoporous coating immobilized on clay roofing tiles. *J. Eur. Ceram. Soc.* **2014**, *34*, 127–136. [CrossRef]
8. Gherardi, F.; Colombo, A.; D'Arienzo, M.; Di Credico, B.; Goidanich, S.; Morazzoni, F.; Simonutti, R.; Toniolo, L. Efficient self-cleaning treatments for built heritage based on highly photo-active and well-dispersible TiO_2 nanocrystals. *Microchem. J.* **2016**, *126*, 54–62. [CrossRef]
9. Liu, Q.; Liu, Q.; Zhu, Z.; Zhang, J.; Zhang, B. Application of TiO_2 photocatalyst to the stone conservation. *Mater. Res. Innov.* **2015**, *19*, S8. [CrossRef]
10. Bergamonti, L.; Alfieri, I.; Lorenzi, A.; Predieri, G.; Barone, G.; Gemelli, G.; Mazzoleni, P.; Raneri, S.; Bersani, D.; Lottici, P.P. Nanocrystalline TiO_2 coatings by sol–gel: Photocatalytic activity on Pietra di Noto biocalcarenite. *J. Sol-Gel Sci. Technol.* **2015**, *75*, 141–151. [CrossRef]
11. Licciulli, A.; Calia, A.; Lettieri, M.; Diso, D.; Masieri, M.; Franza, S.; Amadelli, R.; Casarano, G. Photocatalytic TiO_2 coatings on limestone. *J. Sol-Gel Sci. Technol.* **2011**, *60*, 437–444. [CrossRef]
12. Quagliarini, E.; Bondioli, F.; Goffredo, G.B.; Licciulli, A.; Munafò, P. Smart surfaces for architectural heritage: Preliminary results about the application of TiO_2-based coatings on travertine. *J. Cult. Herit.* **2012**, *13*, 204–209. [CrossRef]
13. Quagliarini, E.; Bondioli, F.; Goffredo, G.B.; Cordoni, C.; Munafò, P. Self-cleaning and de-polluting stone surfaces: TiO_2 nanoparticles for limestone. *Constr. Build. Mater.* **2012**, *37*, 51–57. [CrossRef]

14. Munafò, P.; Goffredo, G.B.; Quagliarini, E. TiO_2-based nanocoatings for preserving architectural stone surfaces: An overview. *Constr. Build. Mater.* **2015**, *84*, 201–218. [CrossRef]
15. Mendoza, C.; Valle, A.; Castellote, M.; Bahamonde, A.; Faraldos, M. TiO_2 and TiO_2–SiO_2 coated cement: Comparison of mechanic and photocatalytic properties. *Appl. Catal. B Environ.* **2015**, *178*, 155–164. [CrossRef]
16. Pinho, L.; Elhaddad, F.; Facio, D.S.; Mosquera, M.J. A novel TiO_2-SiO_2 nanocomposite converts a very friable stone into a self-cleaning building material. *Appl. Surf. Sci.* **2013**, *275*, 389–396. [CrossRef]
17. Rao, K.V.S.; Subrahmanyam, M.; Boule, P. Immobilized TiO_2 photocatalyst during long-term use: Decrease of its activity. *Appl. Catal. B Environ.* **2004**, *49*, 239–249. [CrossRef]
18. Calia, A.; Lettieri, M.; Masieri, M. Durability assessment of nanostructured TiO_2 coatings applied on limestones to enhance building surface with self-cleaning ability. *Build. Environ.* **2016**, *110*, 1–10. [CrossRef]
19. Poulios, I.; Spathis, P.; Grigoriadou, A.; Delidou, K.; Tsoumparis, P. Protection of marbles against corrosion and microbial corrosion with TiO_2 coatings. *J. Environ. Sci. Health Part A* **1999**, *34*, 1455–1471. [CrossRef]
20. Pinho, L.; Mosquera, M.J. Photocatalytic activity of TiO_2-SiO_2 nanocomposites applied to buildings: Influence of particle size and loading. *Appl. Catal. B Environ.* **2013**, *134–135*, 205–221. [CrossRef]
21. Pinho, L.; Mosquera, M.J. Titania-Silica Nanocomposite Photocatalysts with Application in Stone Self-Cleaning. *J. Phys. Chem. C* **2011**, *115*, 22851–22862. [CrossRef]
22. MacMullen, J.; Radulovic, J.; Zhang, Z.; Dhakal, H.N.; Daniels, L.; Elford, J.; Leost, M.A.; Bennett, N. Masonry remediation and protection by aqueous silane/siloxane macroemulsions incorporating colloidal titanium dioxide and zinc oxide nanoparticulates: Mechanisms, performance and benefits. *Constr. Build. Mater.* **2013**, *49*, 93–100. [CrossRef]
23. Sung-Suh, H.M.; Choi, J.R.; Hah, H.J.; Koo, S.M.; Bae, Y.C. Comparison of Ag deposition effects on the photocatalytic activity of nanoparticulate TiO_2 under visible and UV light irradiation. *J. Photochem. Photobiol. A Chem.* **2004**, *163*, 37–44. [CrossRef]
24. Murakami, N.; Ono, A.; Nakamura, M.; Tsubota, T.; Ohno, T. Development of a visible-light-responsive rutile rod by site-selective modification of iron(III) ion on {1 1 1} exposed crystal faces. *Appl. Catal. B Environ.* **2010**, *97*, 115–119. [CrossRef]
25. Sato, S.; Nakamura, R.; Abe, S. Visible-light sensitization of TiO_2 photocatalysts by wet-method N doping. *Appl. Catal. A Gen.* **2005**, *284*, 131–137. [CrossRef]
26. Cho, Y.; Choi, W.; Lee, C.H.; Hyeon, T.; Lee, H.I. Visible light-induced degradation of carbon tetrachloride on dye-sensitized TiO_2. *Environ. Sci. Technol.* **2001**, *35*, 966–970. [CrossRef] [PubMed]
27. Bera, S.; Lee, J.E.; Rawal, S.B.; Lee, W.I. Size-dependent plasmonic effects of Au and Au@SiO_2 nanoparticles in photocatalytic CO_2 conversion reaction of Pt/TiO_2. *Appl. Catal. B Environ.* **2016**, *199*, 55–63. [CrossRef]
28. Levchuk, I.; Sillanpää, M.; Guillard, C.; Gregori, D.; Chateau, D.; Parola, S. TiO_2 /SiO_2 porous composite thin films: Role of TiO_2 areal loading and modification with gold nanospheres on the photocatalytic activity. *Appl. Surf. Sci.* **2016**, *383*, 367–374. [CrossRef]
29. Lee, J.E.; Bera, S.; Choi, Y.S.; Lee, W.I. Size-dependent plasmonic effects of M and M@SiO_2 (M = Au or Ag) deposited on TiO_2 in photocatalytic oxidation reactions. *Appl. Catal. B Environ.* **2017**, *214*, 15–22. [CrossRef]
30. Liu, M.; Zhao, J.; Xiao, C.; Quan, Q.; Li, X. PPy-assisted fabrication of Ag/TiO_2 visible-light photocatalyst and its immobilization on PAN fiber. *Mater. Des.* **2016**, *104*, 428–435. [CrossRef]
31. Yu, J.; Dai, G.; Huang, B. Fabrication and Characterization of Visible-Light-Driven Plasmonic Photocatalyst Ag/AgCl/TiO_2 Nanotube Arrays. *J. Phys. Chem. C* **2009**, *113*, 16394–16401. [CrossRef]
32. Awazu, K.; Fujimaki, M.; Rockstuhl, C.; Tominaga, J.; Murakami, H.; Ohki, Y.; Yoshida, N.; Watanabe, T. A plasmonic photocatalyst consisting of silver nanoparticles embedded in titanium dioxide. *J. Am. Chem. Soc.* **2008**, *130*, 1676–1680. [CrossRef] [PubMed]
33. Kim, Y.-S.; Rai, P.; Yu, Y.-T. Microwave assisted hydrothermal synthesis of Au@TiO_2 core–shell nanoparticles for high temperature CO sensing applications. *Sens. Actuators B Chem.* **2013**, *186*, 633–639. [CrossRef]
34. Zhang, X.; Chen, Y.L.; Liu, R.-S.; Tsai, D.P. Plasmonic photocatalysis. *Rep. Prog. Phys.* **2013**, *76*, 46401. [CrossRef] [PubMed]
35. Tryba, B.; Piszcz, M.; Morawski, A.W. Photocatalytic and Self-Cleaning Properties of Ag-Doped TiO_2. *Open Mater. Sci. J.* **2010**, *4*, 5–8. [CrossRef]

36. Graziani, L.; Quagliarini, E.; D'Orazio, M. The role of roughness and porosity on the self-cleaning and anti-biofouling efficiency of TiO_2-Cu and TiO_2-Ag nanocoatings applied on fired bricks. *Constr. Build. Mater.* **2016**, *129*, 116–124. [CrossRef]
37. Goffredo, G.B.; Accoroni, S.; Totti, C.; Romagnoli, T.; Valentini, L.; Munafò, P. Titanium dioxide-based nanotreatments to inhibit microalgal fouling on building stone surfaces. *Build. Environ.* **2017**, *112*, 209–222. [CrossRef]
38. Pinho, L.; Rojas, M.; Mosquera, M.J. Ag–SiO_2–TiO_2 nanocomposite coatings with enhanced photoactivity for self-cleaning application on building materials. *Appl. Catal. B Environ.* **2015**, *178*, 144–154. [CrossRef]
39. Link, S.; El-Sayed, M.A. Spectral Properties and Relaxation Dynamics of Surface Plasmon Electronic Oscillations in Gold and Silver Nanodots and Nanorods. *J. Phys. Chem. B* **1999**, *103*, 8410–8426. [CrossRef]
40. Desireddy, A.; Conn, B.E.; Guo, J.; Yoon, B.; Barnett, R.N.; Monahan, B.M.; Kirschbaum, K.; Griffith, W.P.; Whetten, R.L.; Landman, U.; et al. Ultrastable silver nanoparticles. *Nature* **2013**, *501*, 399–402. [CrossRef] [PubMed]
41. Haruta, M. When gold is not noble: Catalysis by nanoparticles. *Chem. Rec.* **2003**, *3*, 75–87. [CrossRef] [PubMed]
42. Tian, B.; Li, C.; Gu, F.; Jiang, H. Synergetic effects of nitrogen doping and Au loading on enhancing the visible-light photocatalytic activity of nano-TiO_2. *Catal. Commun.* **2009**, *10*, 925–929. [CrossRef]
43. Ayati, A.; Ahmadpour, A.; Bamoharram, F.F.; Tanhaei, B.; Mänttäri, M.; Sillanpää, M. A review on catalytic applications of Au/TiO_2 nanoparticles in the removal of water pollutant. *Chemosphere* **2014**, *107*, 163–174. [CrossRef] [PubMed]
44. Subramanian, V.; Wolf, E.; Kamat, P.V. Semiconductor−Metal Composite Nanostructures. To What Extent Do Metal Nanoparticles Improve the Photocatalytic Activity of TiO_2 Films? *J. Phys. Chem. B* **2001**, *105*, 11439–11446. [CrossRef]
45. Primo, A.; Corma, A.; García, H. Titania supported gold nanoparticles as photocatalyst. *Phys. Chem. Chem. Phys.* **2011**, *13*, 886–910. [CrossRef] [PubMed]
46. Bergamonti, L.; Alfieri, I.; Franzò, M.; Lorenzi, A.; Montenero, A.; Predieri, G.; Raganato, M.; Calia, A.; Lazzarini, L.; Bersani, D.; Lottici, P.P. Synthesis and characterization of nanocrystalline TiO_2 with application as photoactive coating on stones. *Environ. Sci. Pollut. Res.* **2014**, *21*, 13264–13277. [CrossRef] [PubMed]
47. Mosquera, M.J.; De Los Santos, D.M.; Montes, A.; Valdez-Castro, L. New Nanomaterials for Consolidating Stone. *Langmuir* **2008**, *24*, 2772–2778. [CrossRef] [PubMed]
48. Illescas, J.F.; Mosquera, M.J. Producing Surfactant-Synthesized Nanomaterials In Situ on a Building Substrate, without Volatile Organic Compounds. *ACS Appl. Mater. Interfaces* **2012**, *4*, 4259–4269. [CrossRef] [PubMed]
49. Pinho, L.; Hernández-Garrido, J.C.; Calvino, J.J.; Mosquera, M.J. 2D and 3D characterization of a surfactant-synthesized TiO_2–SiO_2 mesoporous photocatalyst obtained at ambient temperature. *Phys. Chem. Chem. Phys.* **2013**, *15*, 2800–2808. [CrossRef] [PubMed]
50. Bergamonti, L.; Bondioli, F.; Alfieri, I.; Lorenzi, A.; Mattarozzi, M.; Predieri, G.; Lottici, P.P. Photocatalytic self-cleaning TiO_2 coatings on carbonatic stones. *Appl. Phys. A* **2016**, *122*, 124. [CrossRef]
51. Kapridaki, C.; Maravelaki, N.-P. TiO_2–SiO_2–PDMS nanocomposites with self-cleaning properties for stone protection and consolidation. *Geol. Soc. Lond. Spec. Publ.* **2016**, *416*, 285–292. [CrossRef]
52. Krantz, D.H. Color measurement and color theory: I. Representation theorem for Grassmann structures. *J. Math. Psychol.* **1975**, *12*, 283–303. [CrossRef]
53. Krantz, D.H. Color measurement and color theory: II. Opponent-colors theory. *J. Math. Psychol.* **1975**, *12*, 304–327. [CrossRef]
54. Fuller, M.P.; Griffiths, P.R. Diffuse reflectance measurements by infrared Fourier transform spectrometry. *Anal. Chem.* **1978**, *50*, 1906–1910. [CrossRef]
55. Gil, M.L.A.; Garrido, C.; Cantoral, J.M.; González-Rodríguez, V.E.; Carbu, M.; Cubillana-Aguilera, L.M.; Hidalgo-Hidalgo De Cisneros, J.L.; Naranjo-Rodríguez, I.; Luna, M.J.; Zarzuela, R.; et al. Synthesis of Gold Nanoparticles Using Aged Drago Leaf Extract (*Dracanea draco* L.): Manufacturing Process and Using. Spanish Patent ES 2580009 B2, 2015.

56. Cubillana-Aguilera, L.M.; Franco-Romano, M.; Gil, M.L.A.; Naranjo-Rodríguez, I.; Hidalgo-Hidalgo De Cisneros, J.L.; Palacios-Santander, J.M. New, fast and green procedure for the synthesis of gold nanoparticles based on sonocatalysis. *Ultrason. Sonochem.* **2011**, *18*, 789–794. [CrossRef] [PubMed]
57. Franco-Romano, M.; Gil, M.L.A.; Palacios-Santander, J.M.; Delgado-Jaén, J.J.; Naranjo-Rodríguez, I.; Hidalgo-Hidalgo De Cisneros, J.L.; Cubillana-Aguilera, L.M. Sonosynthesis of gold nanoparticles from a geranium leaf extract. *Ultrason. Sonochem.* **2014**, *21*, 1570–1577. [CrossRef] [PubMed]
58. Tauc, J. Optical properties and electronic structure of amorphous Ge and Si. *Mater. Res. Bull.* **1968**, *3*, 37–46. [CrossRef]
59. Tandon, S.P.; Gupta, J.P. Measurement of Forbidden Energy Gap of Semiconductors by Diffuse Reflectance Spectra. *Phys. Status Solidi B* **1970**, *38*, 363–367. [CrossRef]
60. Thommes, M.; Smarsly, B.; Groenewolt, M.; Ravikovitch, P.I.; Neimark, A.V. Adsorption Hysteresis of Nitrogen and Argon in Pore Networks and Characterization of Novel Micro- and Mesoporous Silicas. *Langmuir* **2006**, *22*, 756–764. [CrossRef] [PubMed]
61. Berns, R.S. *Billmeyer and Saltzman's Principles of Color Technology*; Wiley-Interscience: New York, NY, USA, 2000.
62. Drdácký, M.; Lesák, J.; Rescic, S.; Slížková, Z.; Tiano, P.; Valach, J. Standardization of peeling tests for assessing the cohesion and consolidation characteristics of historic stone surfaces. *Mater. Struct.* **2012**, *45*, 505–520. [CrossRef] [PubMed]
63. *Fine Ceramics (Advanced Ceramics, Advanced Technical Ceramics); Determination of Photocatalytic Activity of Surfaces in an Aqueous Medium by Degradation of Methylene Blue*; ISO 10678; International Organization for Standardization: Geneva, Switzerland, 2010.
64. Yan, X.; Ohno, T.; Nishijima, K.; Abe, R.; Ohtani, B. Is methylene blue an appropriate substrate for a photocatalytic activity test? A study with visible-light responsive titania. *Chem. Phys. Lett.* **2006**, *429*, 606–610. [CrossRef]
65. Rochkind, M.; Pasternak, S.; Paz, Y. Using dyes for evaluating photocatalytic properties: A critical review. *Molecules* **2015**, *20*, 88–110. [CrossRef] [PubMed]
66. Mills, A.; Wang, J.; Crow, M. Photocatalytic oxidation of soot by P25 TiO_2 films. *Chemosphere* **2006**, *64*, 1032–1035. [CrossRef] [PubMed]
67. Aelion, R.; Loebel, A.; Eirich, F. Hydrolisis of Ethyl Silicate. *J. Chem. Soc.* **1950**, *72*, 5705–5712. [CrossRef]
68. Widegren, J.; Bergström, L. Electrostatic Stabilization of Ultrafine Titania in Ethanol. *J. Am. Ceram. Soc.* **2002**, *85*, 523–528. [CrossRef]
69. Kosmulski, M.; Prochniak, P.; Rosenholm, J.B. Control of the Zeta Potential in Semiconcentrated Dispersions of Titania in Polar Organic Solvents. *J. Phys. Chem. C* **2009**, *113*, 12806–12810. [CrossRef]
70. Prabhu, A.; Gimel, J.-C.; Ayuela, A.; Dolado, J.S. Effect of Nano Seeds in C-S-H Gel Formation: Simulation Study from the Colloidal Point of View. In *CONCREEP 10*; American Society of Civil Engineers: Reston, VA, USA, 2015; pp. 877–886.
71. Thommes, M.; Kaneko, K.; Neimark, A.V.; Olivier, J.P.; Rodriguez-Reinoso, F.; Rouquerol, J.; Sing, K.S.W. Physisorption of gases, with special reference to the evaluation of surface area and pore size distribution (IUPAC Technical Report). *Pure Appl. Chem.* **2015**, *87*, 1051–1069. [CrossRef]
72. Kruk, M.; Jaroniec, M. Gas Adsorption Characterization of Ordered Organic—Inorganic Nanocomposite Materials. *Chem. Mater.* **2001**, *13*, 3169–3183. [CrossRef]
73. Brinker, C.J. Hydrolysis and condensation of silicates: Effects on structure. *J. Non-Cryst. Solids* **1988**, *100*, 31–50. [CrossRef]
74. Yu, H.; Wang, S. Effects of water content and pH on gel-derived TiO_2-SiO_2. *J. Non-Cryst. Solids* **2000**, *261*, 260–267. [CrossRef]
75. González-Álvarez, R.J.; Naranjo-Rodríguez, I.; Hernández-Artiga, M.P.; Palacios-Santander, J.M.; Cubillana-Aguilera, L.; Bellido-Milla, D. Experimental design applied to optimisation of silica nanoparticles size obtained by sonosynthesis. *J. Sol-Gel Sci. Technol.* **2016**, *80*, 378–388. [CrossRef]

76. Linic, S.; Christopher, P.; Ingram, D.B. Plasmonic-metal nanostructures for efficient conversion of solar to chemical energy. *Nat. Mater.* **2011**, *10*, 911–921. [CrossRef] [PubMed]
77. Primo, A.; Marino, T.; Corma, A.; Molinari, R.; García, H. Efficient visible-light photocatalytic water splitting by minute amounts of gold supported on nanoparticulate CeO_2 obtained by a biopolymer templating method. *J. Am. Chem. Soc.* **2011**, *133*, 6930–6933. [CrossRef] [PubMed]
78. Ingram, D.B.; Linic, S. Water Splitting on Composite Plasmonic-Metal/Semiconductor Photoelectrodes: Evidence for Selective Plasmon-Induced Formation of Charge Carriers near the Semiconductor Surface. *J. Am. Chem. Soc.* **2011**, *133*, 5202–5205. [CrossRef] [PubMed]
79. Miliani, C.; Velo-Simpson, M.L.; Scherer, G.W. Particle-modified consolidants: A study on the effect of particles on sol-gel properties and consolidation effectiveness. *J. Cult. Herit.* **2007**, *8*, 1–6. [CrossRef]
80. Illescas, J.F.; Mosquera, M.J. Surfactant-Synthesized PDMS/Silica Nanomaterials Improve Robustness and Stain Resistance of Carbonate Stone. *J. Phys. Chem. C* **2011**, *115*, 14624–14634. [CrossRef]
81. Umrao, S.; Sharma, P.; Bansal, A.; Sinha, R.; Singh, K. Multi-layered graphene quantum dots derived photodegradation mechanism of methylene blue. *RSC Adv.* **2015**, *5*, 51790–51798. [CrossRef]
82. Cenens, J.; Schoonheydt, R.A. Visible Spectroscopy of Methylene Blue on Hectorite, Laponite B, and Barasym in Aqueous Suspension. *Clays Clay Miner.* **1988**, *36*, 214–224. [CrossRef]
83. Dean, J.C.; Oblinsky, D.G.; Rafiq, S.; Scholes, G.D. Methylene Blue Exciton States Steer Nonradiative Relaxation: Ultrafast Spectroscopy of Methylene Blue Dimer. *J. Phys. Chem. B* **2016**, *120*, 440–454. [CrossRef] [PubMed]
84. Houas, A. Photocatalytic degradation pathway of methylene blue in water. *Appl. Catal. B Environ.* **2001**, *31*, 145–157. [CrossRef]
85. Murugan, K.; Rao, T.N.; Gandhi, A.S.; Murty, B.S. Effect of aggregation of methylene blue dye on TiO_2 surface in self-cleaning studies. *Catal. Commun.* **2010**, *11*, 518–521. [CrossRef]
86. Murugan, K.; Joardar, J.; Gandhi, A.S.; Murty, B.S.; Borse, P.H. Photo-induced monomer/dimer kinetics in methylene blue degradation over doped and phase controlled nano-TiO_2 films. *RSC Adv.* **2016**, *6*, 43563–43573. [CrossRef]
87. Kubelka, P.; Munk, F. Ein Beitrag zur Optik der Farbanstriche. *Z. Tech. Phys.* **1931**, *12*, 593–601.
88. Kubelka, P. New Contributions to the Optics of Intensely Light-Scattering Materials. Part I. *J. Opt. Soc. Am.* **1948**, *38*, 448–457. [CrossRef] [PubMed]
89. Julson, A.J.; Ollis, D.F. Kinetics of dye decolorization in an air–solid system. *Appl. Catal. B Environ.* **2006**, *65*, 315–325. [CrossRef]
90. Yamauchi, Y.; Takeuchi, F.; Todoroki, S.; Sakka, Y.; Inoue, S. Spherical Mesoporous Silica Particles with Titanium Dioxide Nanoparticles by an Aerosol-assisted Coassembly. *Chem. Lett.* **2008**, *37*, 72–73. [CrossRef]
91. Suzuki, N.; Jiang, X.; Radhakrishnan, L.; Takai, K.; Shimasaki, K.; Huang, Y.T.; Miyamoto, N.; Yamauchi, Y. Hybridization of Photoactive Titania Nanoparticles with Mesoporous Silica Nanoparticles and Investigation of Their Photocatalytic Activity. *Bull. Chem. Soc. Jpn.* **2011**, *84*, 812–817. [CrossRef]
92. Zhang, P.; Tian, J.; Xu, R.; Ma, G. Hydrophilicity, photocatalytic activity and stability of tetraethyl orthosilicate modified TiO_2 film on glazed ceramic surface. *Appl. Surf. Sci.* **2013**, *266*, 141–147. [CrossRef]
93. Ting, H.F.; Chen, C.M.; Lu, F.H.; Suen, S.Y. Adsorption and photodegradation of methylene blue using a bulk Ti material with porous titania layer prepared by chemical oxidation. *J. Taiwan Inst. Chem. Eng.* **2014**, *45*, 617–624. [CrossRef]
94. Jawad, A.H.; Mubarak, N.S.A.; Ishak, M.A.M.; Ismail, K.; Nawawi, W.I. Kinetics of photocatalytic decolourization of cationic dye using porous TiO_2 film. *J. Taibah Univ. Sci.* **2016**, *10*, 352–362. [CrossRef]
95. Zhang, J.; Grabstanowicz, L.R.; Gao, S.; Hosmane, N.S.; Huang, B.; Dai, Y.; Liu, D.; Xu, T. Visible-light photocatalytic $SiO_2/TiO_{2-x}C_x/C$ nanoporous composites using $TiCl_4$ as the precursor for TiO_2 and polyhydroxyl tannin as the carbon source. *Catal. Sci. Technol.* **2012**, *2*, 390–399. [CrossRef]
96. Sopyan, I.; Watanabe, M.; Murasawa, S.; Hashimoto, K.; Fujishima, A. A film-type photocatalyst incorporating highly active TiO_2 powder and fluororesin binder: Photocatalytic activity and long-term stability. *J. Electroanal. Chem.* **1996**, *415*, 183–186. [CrossRef]

97. Fattakhova-Rohlfing, D.; Szeifert, J.M.; Yu, Q.; Kalousek, V.; Rathouský, J.; Bein, T. Low-Temperature Synthesis of Mesoporous Titania−Silica Films with Pre-Formed Anatase Nanocrystals. *Chem. Mater.* **2009**, *21*, 2410–2417. [CrossRef]
98. Beyers, E.; Biermans, E.; Ribbens, S.; De Witte, K.; Mertens, M.; Meynen, V.; Bals, S.; Van Tendeloo, G.; Vansant, E.F.; Cool, P. Combined TiO_2/SiO_2 mesoporous photocatalysts with location and phase controllable TiO_2 nanoparticles. *Appl. Catal. B Environ.* **2009**, *88*, 515–524. [CrossRef]

Supplementary materials

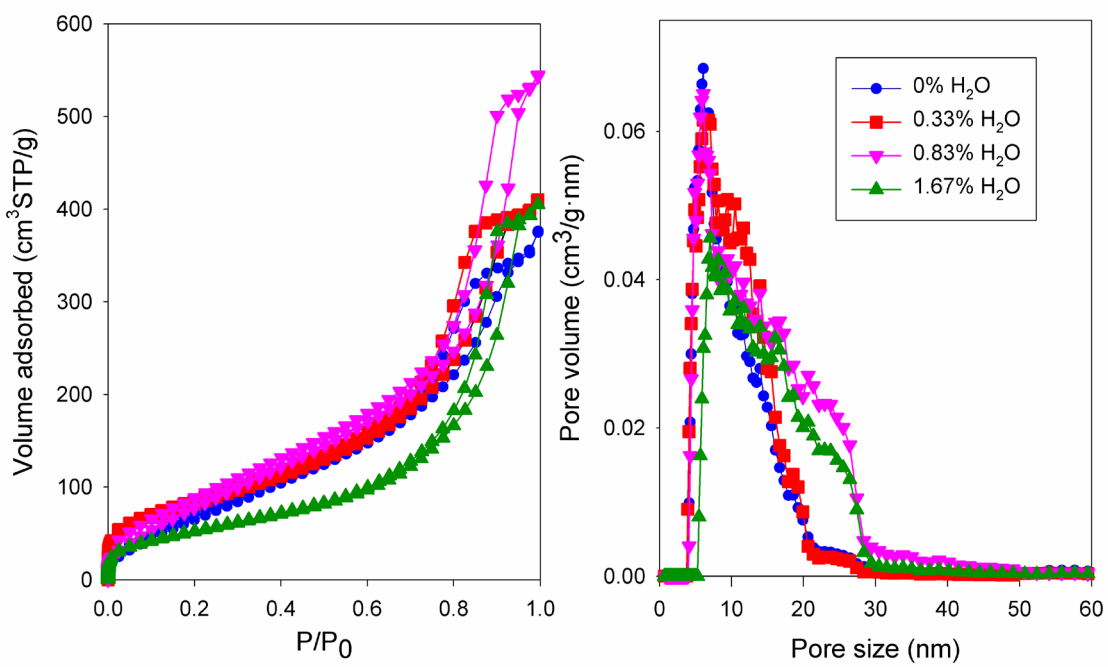

Figure S1. Nitrogen physisorption isotherms and pore distribution of photocatalysts with 1% of TiO_2 prepared with different water content.

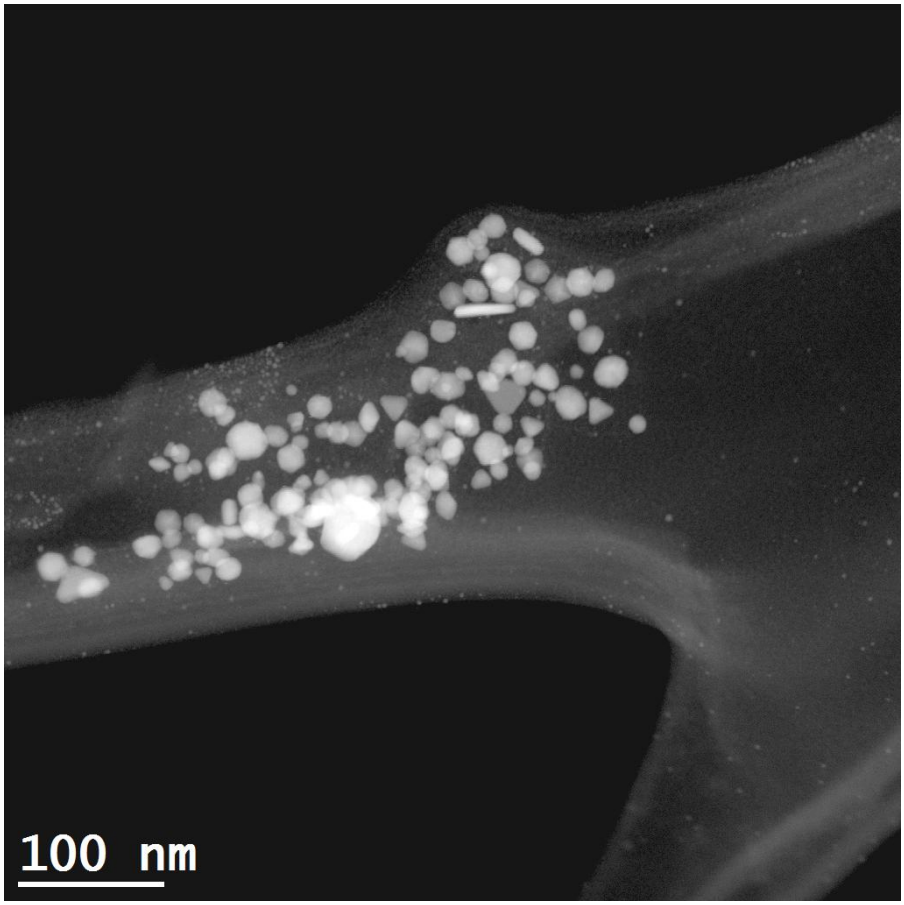

Figure S2. HAADF-STEM image of AuNPs nanoparticles employed.

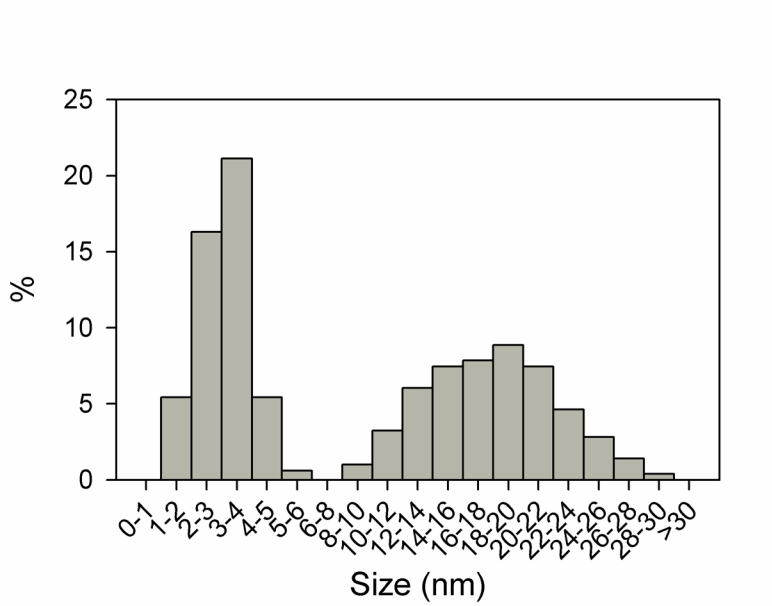

Figure S3. Size distribution of AuNPs employed.

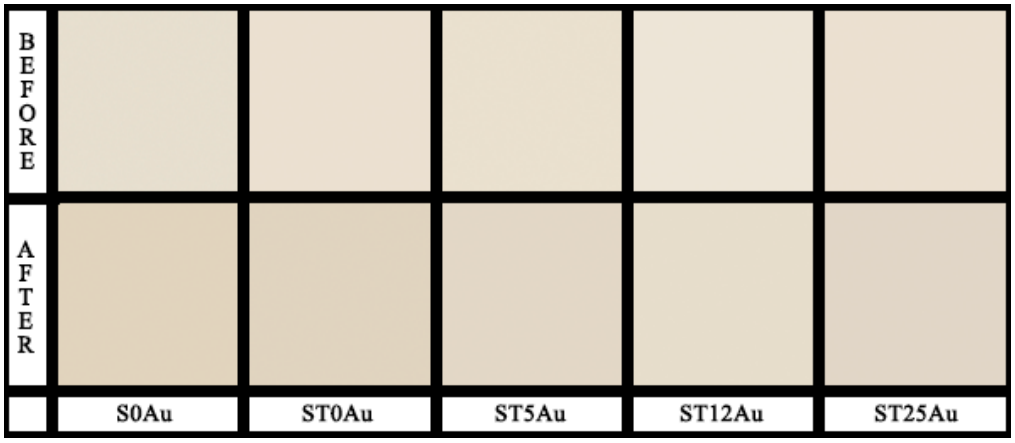

Figure S4. Digital reproduction of stone color after and before treatments.

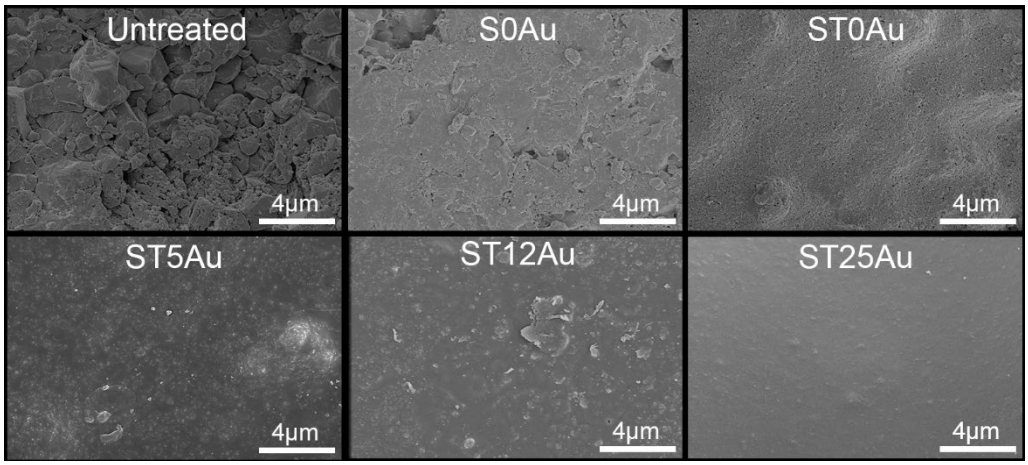

Figure S5. SEM images of coated stones under study and their untreated counterpart.

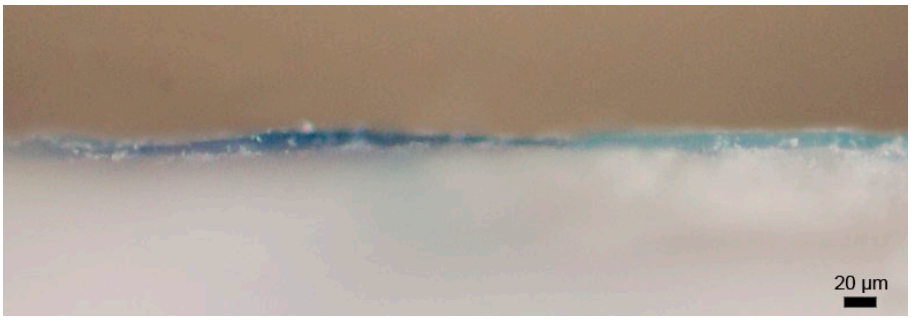

Figure S6. Optical Microscopy photograph of transversal cutting of treated stone. The coating was dyed with methylene blue for better observation.

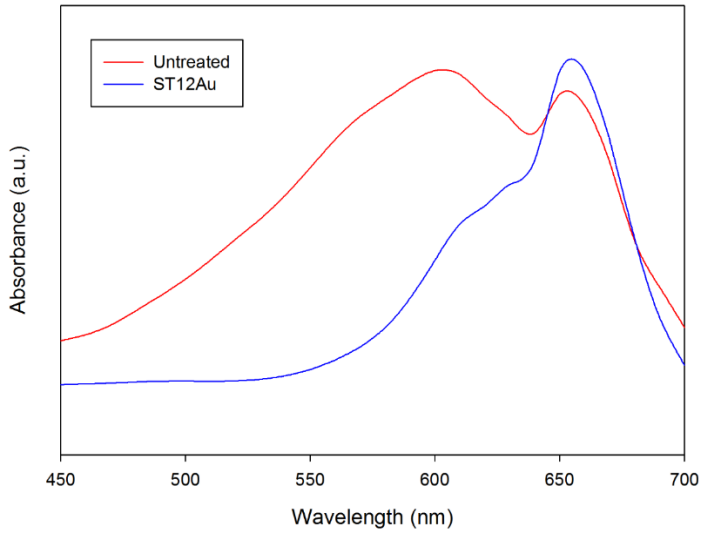

Figure S7. UV-visible absorbance spectra of MB deposited on untreated and on a treated stone, ST12Au treated sample was selected as representative example. The absorbance spectra were obtained from respective reflectance spectra.

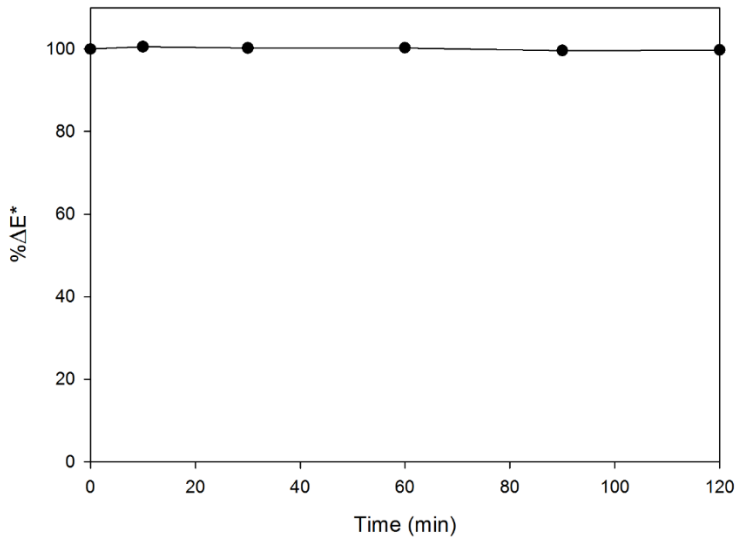

Figure S8. Evolution of %ΔE* for a ST12Au treated stone sample stained with methylene blue maintained in dark conditions.

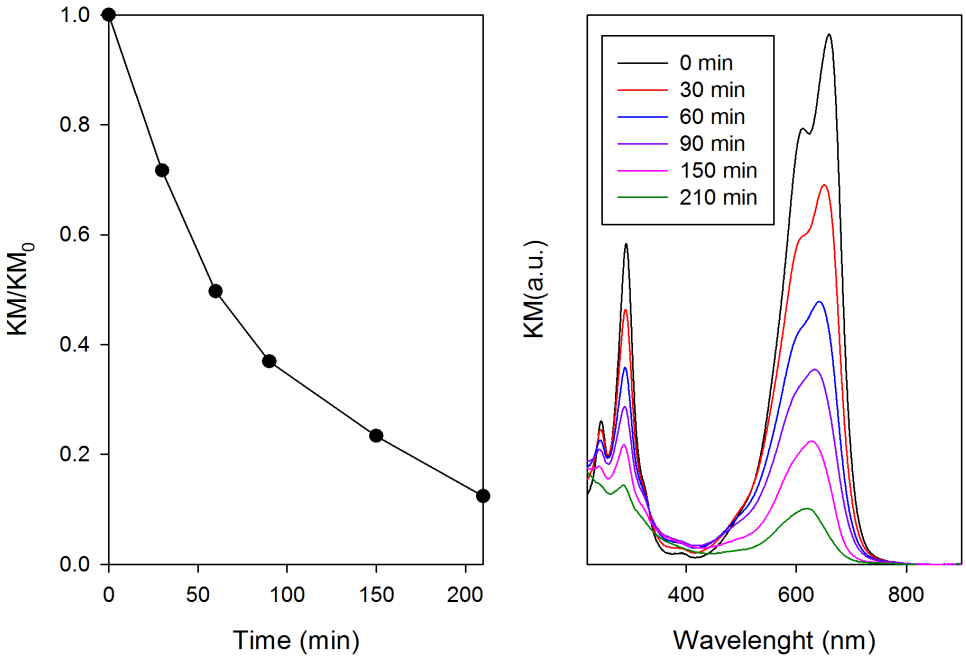

Figure S9. Degradation plot and absorbance evolution for MB with the irradiation time.

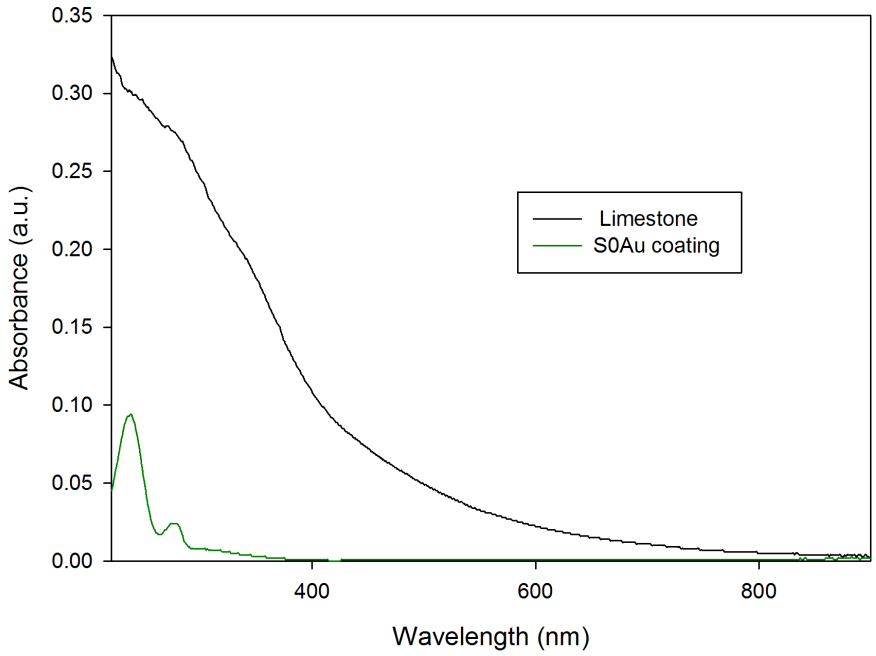

Figure S10. UV-visible absorbance spectra of S0Au coating and the limestone employed in this work. The absorbance spectra were obtained from respective reflectance spectra.

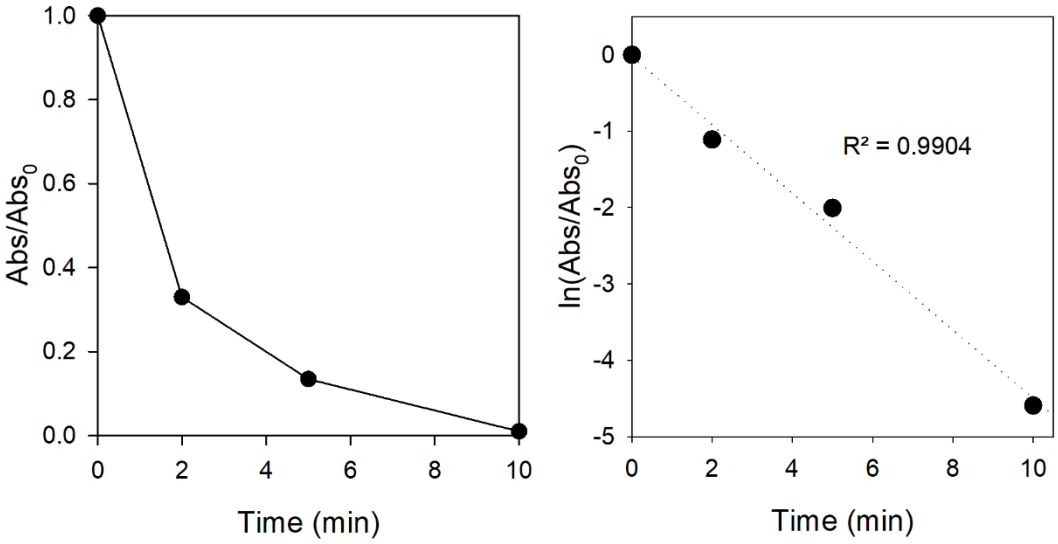

Figure S11. Left, evolution of MB degradation on ST0Au coating deposited on glass. Right, its corresponding fitting to first order rate equation.

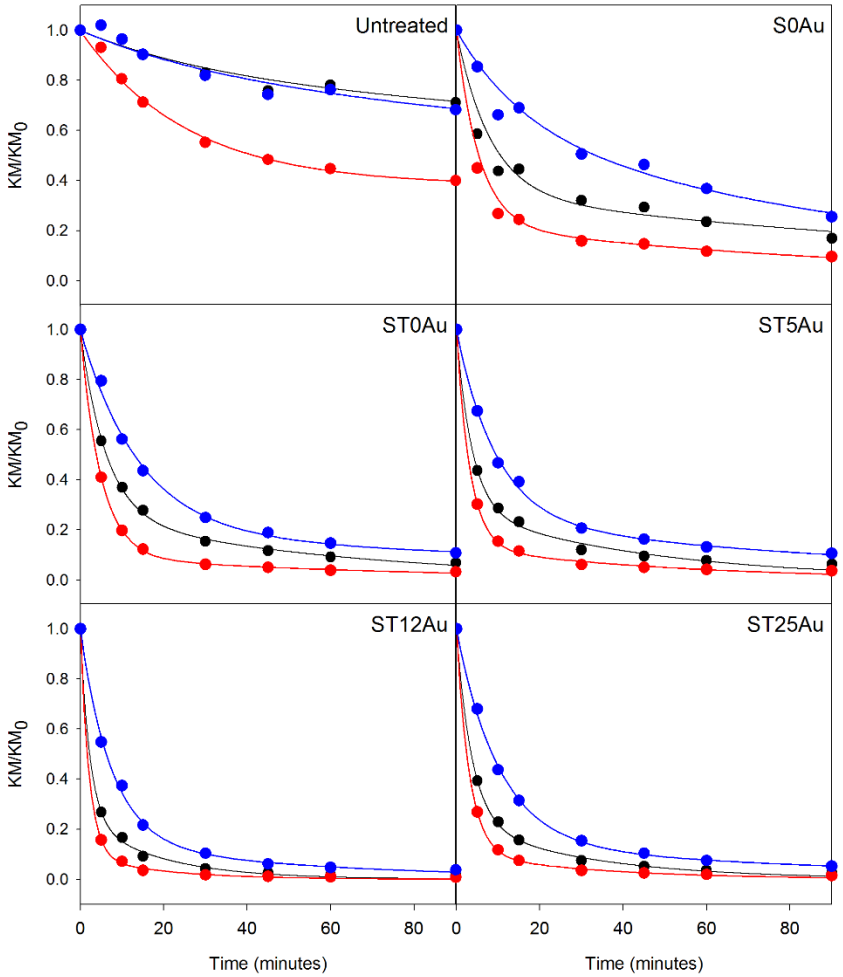

Figure S12. Fitting between the KM/KM_0 values measured (dots) and calculated by fitting to rate equation (lines) for the different degradations processes, overall (black), monomer (red) and dimer (blue).

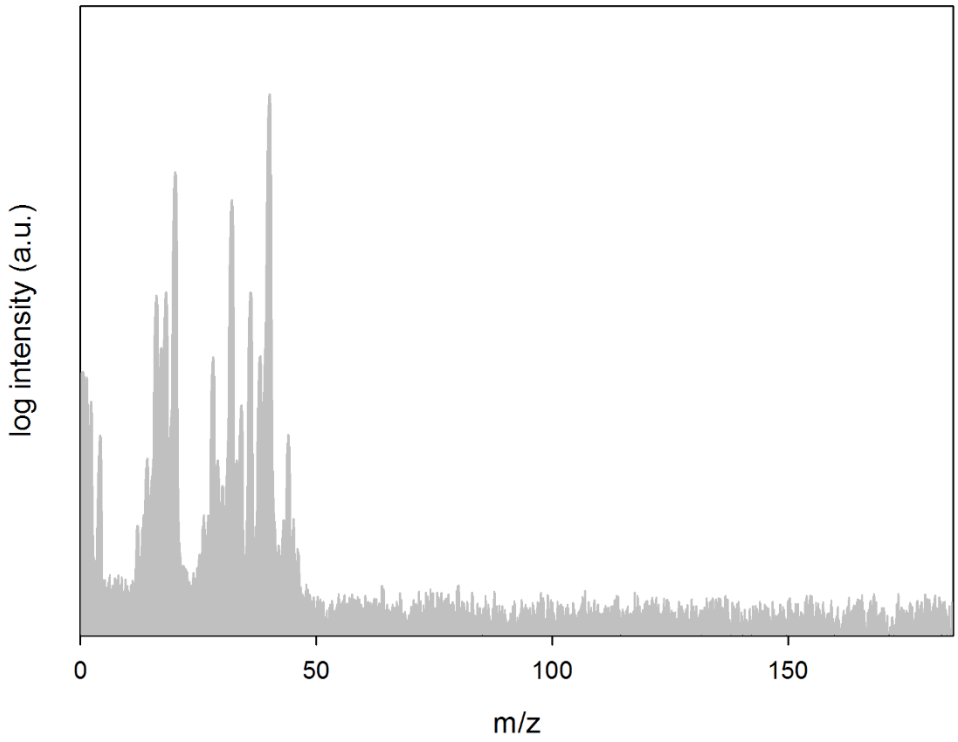

Figure S13. Mass spectrum of air from reactor obtained during the mass spectroscopy experiments when the sample was being irradiated with light.

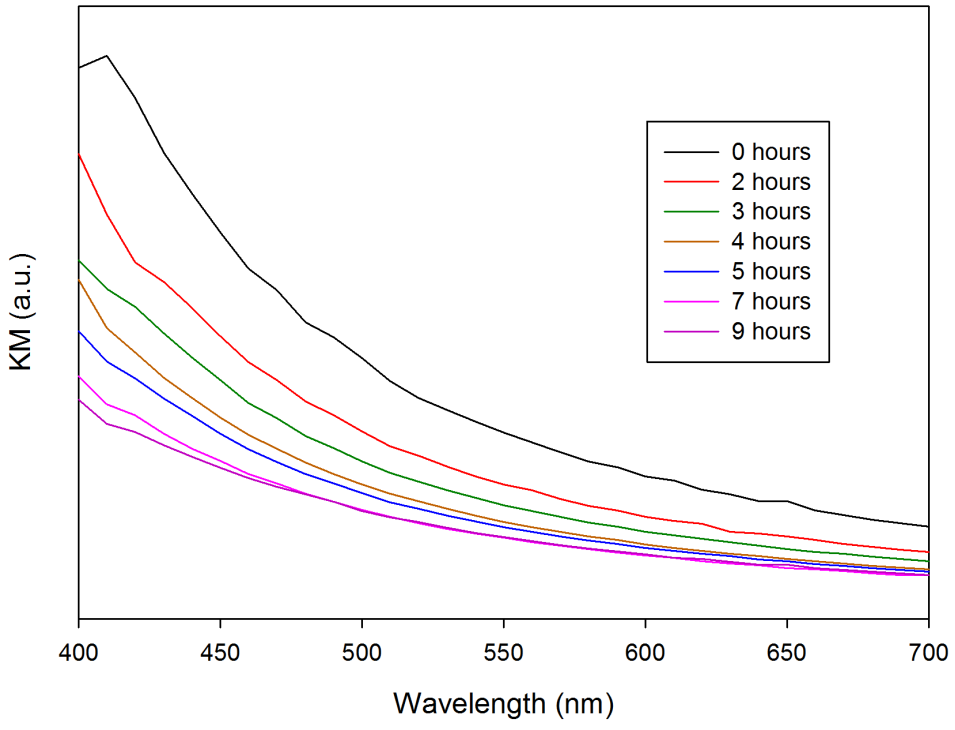

Figure S14. Example of soot absorbance spectra during soot self-cleaning test for ST12Au treated stone.

Video S1 showing the self-cleaning test by water action can be visualized in the following link: https://youtu.be/c9ahncU2Hvg

Chapter 4

Au-TiO_2/SiO_2 photocatalysts with NO_x depolluting activity: influence of gold particle size and loading

Chemical Engineering Journal 368 (2019) 417–427

Contents lists available at ScienceDirect

Chemical Engineering Journal

journal homepage: www.elsevier.com/locate/cej

Au-TiO_2/SiO_2 photocatalysts with NO_x depolluting activity: Influence of gold particle size and loading

Manuel Luna[a], José M. Gatica[b,*], Hilario Vidal[b], María J. Mosquera[a,*]

[a] Nanomaterials Group TEP243, Departamento de Química Física, Universidad de Cádiz, Puerto Real 11510, Spain
[b] Departamento C.M., I.M. y Química Inorgánica, Universidad de Cádiz, Puerto Real 11510, Spain

HIGHLIGHTS

- Au-TiO_2/SiO_2 photocatalysts with depolluting activity were developed.
- The relationship structure/performance of photocatalysts was discussed.
- The AuNPs produced an evident enhancement of TiO_2 photoactivity.
- The smaller AuNPs showed a better distribution on TiO_2 and they were more effective.
- The highest AuNPs loading promoted agglomeration and the subsequent worse performance.

GRAPHICAL ABSTRACT

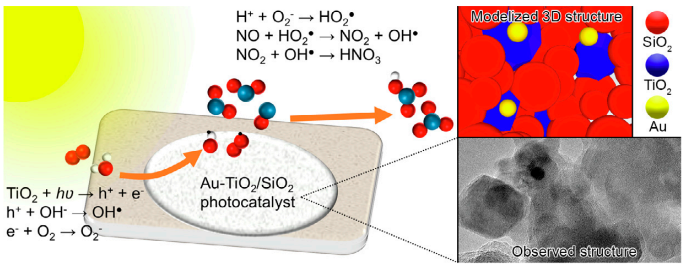

ARTICLE INFO

Keywords:
Photocatalyst
NOx depolluting
TiO_2
Au-TiO_2/SiO_2 composite
Buildings
Long-lasting coatings

ABSTRACT

The air pollution is becoming one of most important health problems around the world. Thus, the development of depolluting building materials is a crucial challenge. TiO_2 is a photocatalyst with demonstrated performance for degradation of NO_x and other typical pollutants. However, its limited absorption of solar light reduces its performance. In this study, Au-TiO_2NPs are integrated into a silica matrix in order to produce long-lasting coatings with de-pollutant performance and applicability in building. The interaction between Au and TiO_2 improves the photoactivity of TiO_2 and it promotes a considerably increase in visible light absorption. A significant role of the AuNPs size and their loading on the material photoactivity has been also demonstrated. The lowest AuNPs size enhances the activity due to their better dispersion and subsequently, the higher Au-TiO_2 interaction observed. Regarding the Au loading, the maximum photoactivity, in terms of NO conversion and dye degradation, was reached for the intermedium Au loading. It can be mainly associated to the abrupt increase of Au-TiO_2 agglomeration for the highest loading evaluated. Finally, it has been stablished that AuNPs also increased the selectivity of the NO oxidation to nitrates and nitrites, reducing the amount of NO_2 released.

1. Introduction

Nowadays, the atmospheric pollution continues being a serious issue due to the high amount of emissions of hazardous air pollutants, specifically more than 7000 tons of nitrogen oxides (NO_x) [1]. Emissions of NO_x to the atmosphere contribute with a volume of gases which is similar to that of CO, moreover, their toxicity is even four times higher. The problem is particularly worrying in urban areas mainly due to the intensification of industrial activity and the increasing number of motor vehicles in circulation [2]. As well known, NO_x not only affect human health but also are responsible for the increase off the greenhouse effect and, consequently, planetary climatic change.

* Corresponding authors.
E-mail addresses: josemanuel.gatica@uca.es (J.M. Gatica), mariajesus.mosquera@uca.es (M.J. Mosquera).

https://doi.org/10.1016/j.cej.2019.02.167
Received 9 January 2019; Received in revised form 14 February 2019; Accepted 23 February 2019
Available online 25 February 2019

Additionally, NO_x are one of the main responsible of acid rain. However, no matter the progress in energy and environmental efficiency of transport means, as well as the ever more restrictive limits to industrial discharges, our society is still far away from avoiding these hazardous emissions. Therefore, it is imperative to study actions that may favour their removal in urban centres.

One way to reduce the concentration of these pollutants in a urban atmosphere would be the creation of huge de-pollutant surfaces so allowing the environment "cleaning" or more specifically the direct use of buildings for such purpose [3,4]. In this sense, beyond NO_x photocatalytic decomposition [5–7] and their selective reduction [8,9], photocatalytic oxidation of NO_x using titanium dioxide as semiconductor photocatalyst incorporated to coatings has become over the last years the main competitive alternative, as confirmed by the growing number of commercial products so far available in the market and the increasing scientific focus on those products [10–14].

It is generally accepted that NO_x degradation by TiO_2 occurs through a mechanism [4,15], in which a fraction of the gases would be oxidized to NO_2 while the rest would be retained over the building material as nitrate species [16,17] which, being soluble, could be further eliminated from the surface by rain water in the form of nitric acid [18]. Moreover, this reaction might convert ozone into oxygen in parallel.

An important drawback of TiO_2 as for depolluting application under outdoor conditions is associated with its absorption capacity, localized in the ultraviolet range (< 400 nm), which only constitutes 3–5% of solar light. Therefore, the increase of TiO_2 photoactivity and the enhancement of its visible light (400–700 nm) absorption is desirable for improving the TiO_2 performance. Several methodologies have been described to reach this purpose, such as using noble metals [19], metal cations [20], non-metal [21] or organic compounds [22]. In the specific case of the visible light activation of TiO_2 in order to increase NO_x abatement, several papers using dopants such as Fe_2O_3 [23], carbon [24], nitrogen [25], zeolites [26], compounds like CaO and MgO [27] are found in the literature. It has also been reported that the TiO_2 doped with metal nanoparticles, for example PtO_x [28,29], displays spectral response in the visible area via plasma effect. However, as far as we know, very scarce studies using gold to modify TiO_2 in order to enhance NO oxidation [30] were reported [31,32]. Such deficit surprises considering this noble metal has been proven to further enhance functional performances of TiO_2 [18,33]. Additionally, it is important to remark that these approaches are tedious enough to prevent their application on facades and other buildings elements, which is a main target for depolluting materials.

We have recently studied the use of gold nanoparticles (AuNPs) to enhance the self-cleaning properties of TiO_2 integrated into a silica matrix [34]. The material is applied as a sol and it spontaneously gels inside the pore structure of different building materials, producing long-lasting self-cleaning coatings. As previously demonstrated materials [35–37], the use of a sol-gel route, permits an actual use of the obtained photocatalysts on facades and other building elements due to several reasons: (i) the low viscosities of the sols allow their application by using common and low cost methods, such as spraying or brushing, on numerous substrates; (ii) the sols penetrate in the porous structure of the substrate and xerogels coatings are spontaneously produced, favouring their application in situ. In addition, it has been demonstrated that the integration of TiO_2 into a SiO_2 matrix allows a better performance than a direct application of TiO_2 due to the improvement of substrate adhesion and the subsequent coating durability under outdoor exposure [34,38–40].

In this work, we optimize the Au-TiO_2/SiO_2 coatings synthesis in order to promote an effective depolluting performance. Accordingly, it is well established that the AuNPs catalytic activity has an inverse relationship with their size, and practically disappears for sizes above 20 nm [41]. However, in the case of Au-TiO_2 photocatalysis, the relationship between activity and the AuNPs size is not totally clear [42–44] because it can be a function of the different parameters (such as electronic factors, Au-TiO_2 interactions or plasmonic effects) altered as Au size is modified. Thus, the optimization of the Au size on the depolluting performance of the materials under study is the first challenge of this work.

On the other hand, the Au loading is also a relevant parameter in the optimization because their excess can produce: (i) their heterogeneous distribution in the TiO_2 [34]; (ii) recombination of photo induced electron-hole pairs [45,46]; (iii) their preferential light absorption instead of TiO_2 [42,47]. Thus, the second target of this work is to evaluate the role of the Au loading.

In order to conclude about the role played by these two parameters, we have deeply investigated structure, texture and chemical properties of the materials prepared with two different AuNPs size and three different Au/TiO_2 ratios under study, paying special attention to the existence of Au-TiO_2 interactions. The relationship between these properties and the photoactive and depolluting performances of the photocatalysts under study has been deeply discussed.

NO was chosen in the present study because it is considered in most studies dealing with pollution in outdoor conditions [30], it is also a typical indoor air pollutant that can be emitted from many sources [48]. The role of the Au in order to increase the selectivity of the NO oxidation to nitrate species instead of producing toxic NO_2 has been also investigated.

2. Experimental section

The AuNPs were prepared according to an adaptation of Turkevich synthesis [49], employing $KAuCl_4$ and trisodium citrate, both from Sigma Aldrich. $KAuCl_4$ solution was boiled for 10 min and sodium citrate solution (0.5 M) was added. The mixture was kept on heating until a complete change of colour was reached. Then, a 0.5% v/v of an aqueous solution of polyvinylpyrrolidone (PVP) 3% was added. Two Au dispersions with different particle size were prepared by modifying the citrate/Au proportion. Specifically, the $KAuCl_4$ contents were 0.5 and 1 mM, and the citrate/Au molar ratios were 5 and 1.25, respectively.

Next, the Au dispersions and the commercial TiO_2 particles were mixed in order to get slurries with three different Au/TiO_2 ratio: 0.25, 0.5 and 1% w/w. The TiO_2 employed was VP Aeroperl P25/20 particles from Evonik. These particles are microgranulates with an average particle size of 20 µm and 50 ± 15 m^2/g of surface area, produced by aggregation of P25 particles. The mixtures were dried in a vacuum oven at 60 °C overnight and the obtained solids were powdered. The characteristics of the prepared samples are compiled in Table 1.

Representative Au-TiO_2 samples were deposited onto lacey carbon coated copper grids for their Transmission Electron Microscopy characterization. A JEOL 2010F TEM/STEM microscope operated at 200 kV was employed. High Angle Annular Dark Field Scanning Transmission Electron Microscopy (HAADF-STEM) images were recorded using an electron probe of 0.5 nm and a camera length of 10 cm. The Au size was determined by measuring more than 100 particles from several images at the same magnification.

Fourier transform infrared (FTIR) spectra of the nanopowders were recorded using a FTIR-8400S from Shimadzu (8 cm^{-1} in resolution) in

Table 1
Nominal amount and average size of AuNPs employed for the photocatalysts preparation.

Sample	% Au/TiO_2	AuNPs size (nm)
T0.25Au38	0.25	38
T0.5Au38	0.5	38
T1Au38	1	38
T0.25Au13	0.25	13
T0.5Au13	0.5	13
T1Au3	1	13

the range from 4000 cm^{-1} to 700 cm^{-1} working in attenuated total reflection (ATR) mode.

Changes in the pH induced by aqueous dispersion of the Au-TiO_2 nanopowders (0.2% w/v) were measured.

The hydrodynamic sizes of nanopowders dispersions were studied by dynamic light scattering (DLS) using a Zetasizer Nano Z analyser from Malvern Instruments. For the sample preparation 2 mg of nanopowders were dispersed in 5 ml of water using an ultrasonic bath for 10 min.

The methylene blue (MB) solution decolouration under UV–Vis radiation was employed to study the photoactivity of Au-TiO_2 nanopowders. 10 mg of nanopowders were dispersed in 20 ml of water for 15 min using an ultrasonic cleaner and 200 µl of MB solution 1 mM was added in order to get a MB concentration nearly 10^{-5} M. The mixture was kept in the dark under vigorous stirring for 30 min to ensure the complete MB adsorption on TiO_2 before the test beginning. An Ultra Vitalux 300 W lamp from Osram was placed above the solution providing a total irradiance of 60 W/m^2, measured using a PM100D power meter equipped with a detector S302C from Thorlabs, and a UV irradiance of 4 W/m2, measured using a PCE-UV34 power meter from PCE Instruments. The UV–Visible spectra of the solution were recorded using a Shimadzu UV-2600 spectrophotometer at progressive irradiation times, after solid separation by centrifugation. The degradation plots were represented using the Abs/Abs_0 at 664 nm and the results were fitted to a first order rate equation, being the correlation coefficients higher than 0.99, obtaining the corresponding rate constants. The photocatalytic properties of selected samples were evaluated using a procedure similar to the previously described, replacing the MB solution by p-nitrophenol (p-NP) $5{\cdot}10^{-5}$ M. Finally the photocatalytic tests were repeated under exclusively visible light, 60 W/m^2 of filtered light from Ultra Vitalux lamp being employed.

The prepared Au-TiO_2 nanopowders were mixed with a silica precursor according to the synthesis previously described [34]. The silica precursor was TES40 WN (Wacker), an ethylsilicate oligomer that provides approximately 41% of silica upon complete hydrolysis. Then water and n-octylamine (Sigma Aldrich) were added and the mixture was stirred for 10 min under high-power ultrasound at 125 W, using a Sonopuls HD3200 ultrasonic homogenizer from Bandelin. The amounts of n-octylamine, water and Au-TiO_2 nanopowders with respect to the silica oligomer were 0.36% v/v, 0.83% v/v and 1% w/v, respectively. These samples were designated with an S preceding the name of the Au-TiO_2 photocatalyst that contained (see Table 1). In addition, for comparative purposes, the silica alone (S) and the TiO_2/SiO_2 (ST) sols were also prepared.

Next, 15 ml of sols were deposited on plastic Petri dishes with a diameter of 85 mm and maintained at room temperature. The spontaneous sol-gel transition took place and the gels were dried at laboratory conditions until constant weight. Powdered samples from the obtained xerogels were characterized according to the following procedure:

The UV–visible reflectance spectra were recorded on a UV-2600 spectrophotometer from Shimadzu equipped with an ISR-2600 integrating sphere, using $BaSO_4$ powder as white reference. The band-gap values were calculated by using the Kubelka-Munk function and the Tauc plot [50,51].

Textural characterization was performed by N_2 physisorption at −196 °C, using a Quantachrome Autosorb IQ. The adsorption data obtained from approximately 0.3 g of samples evacuated at 150 °C were analysed using a hybrid NLDFT (non-local density functional theory) approach [52] that allows quantification of both micro- and mesopores in order to obtain the pore size distribution of materials containing pores of different geometry.

The previously described TEM/STEM microscope was used to characterize the structure of the materials under study, HAADF-STEM images and high-resolution electron microscopy (HRTEM) images (the equipment has a spatial resolution of 0.19 nm in this mode) being recorded. The samples were prepared depositing the powdered xerogels onto lacey carbon coated copper grids.

The photocatalytic activity of the materials towards the oxidation of NO was studied using a protocol similar to the standardised test method developed for the characterisation of NO in air purification performance, ISO 22197-1 [53]. However, some of the specifications described in this standard were modified in order to study samples in the form of powders. In spite of this modification, under our experimental conditions a nearly equivalent pollutant load was preserved. The experimental setting was designed as follows: 5 glass rods (7 mm diameter) were placed into a tubular (2.2 cm inner diameter) quartz reactor, in order to reduce the void volume. 6 g of powdered samples were placed over the rods. Air was conveyed by a gas-washing bottle, filled with demineralised water in order to keep the absolute humidity of the supplied gas fixed at 25 ± 2 g/m^3. Air and NO gas streams were mixed to obtain the desired total flow (1000 cm^3/min) and concentration (3 ppm NO) and this stream flowed into the photocatalytic reactor. For illumination, two 15 W daylight fluorescent tubes were disposed parallel over the reactor, being the total irradiance 25 W/m^2 and the UV irradiance 1 W/m^2. The accurate measurement of the concentration of nitric oxide (NO), nitrogen dioxide (NO_2) and total oxide (NO_X) was performed by means of a chemiluminescence CLD NO/NOx analyser module (NGA 2000 model) from Emerson-Rosemount Analytical integrated in a gas conditioning unit. The methodology employed for the test was the following. The air/NO gas stream ran over the powdered xerogels in the dark for a period of 10 min without changes in the NO_X concentration profiles being observed, discarding significant adsorption on the sample surface or its direct photolysis. Subsequently, the photoreactor was irradiated for 8 min after which the lamp was turned off.

The NO conversion and selectivity towards other non-NO_2 products percentages were defined according to the following equations:

$$\%\text{NO conversion} = \frac{[NO]_{inlet} - [NO]_{outlet}}{[NO]_{inlet}} \times 100$$

$$\%\text{Selectivity} = 100 - \left(\frac{[NO_2]_{outlet}}{[NO]_{inlet} - [NO]_{outlet}} \times 100\right)$$

where $[NO]_{inlet}$ represents the concentration of NO in the feedstream and $[NO]_{outlet}$ and $[NO_2]_{outlet}$ are the concentration of NO or NO_2 in the outlet stream, respectively.

Fig. 1 shows a schematic representation of the homemade continuous flow gas setup including the design of the photocatalytic reactors employed and examples of the measurement methodologies.

3. Results and discussion

3.1. Au-TiO_2 nanopowders characterization

In order to obtain AuNPs with two different size, aqueous dispersions of Au with two different citrate/Au ratio were prepared. The colour of the Au dispersion prepared using the highest ratio was dark red, whereas the other one obtained was purple. These differences in colour are related to the different size of AuNPs [54], being smaller the ones prepared according to the highest citrate/Au ratio. After mixing with TiO_2, the obtained nanopowders showed the same colours than those corresponding to the two Au dispersions, being more intense as the Au content in the powder was raised.

The HAADF-STEM images of the nanopowders and the corresponding Au size distribution are shown in Fig. 2. The obtained results confirmed the smaller size of AuNPs prepared using the highest citrate amount, as extensively reported in previous papers [49,55]. For this sample (TxAu13), the AuNPs had spherical shape with an average diameter of 12.6 ± 1.9 nm and they were plentiful and dispersed homogeneously over the TiO_2. On the other hand, for the materials prepared with the AuNPs synthetized using the lowest citrate amount, the AuNPs had irregular shapes with an average size of 38.2 ± 11.6 nm and they were scarce and accumulated preferentially

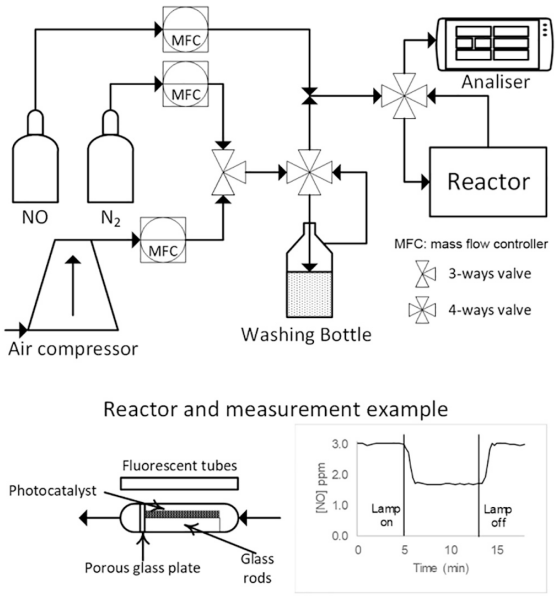

Fig. 1. Representation of the continuous flow gas setup, design of the photocatalytic reactors employed and examples of the measurements.

in certain areas of TiO_2.

The presence of the reagent remnants from the AuNPs synthesis (citrate and PVP) in the samples can promote TiO_2 agglomeration and it can also modify the xerogel structure, as discussed later. In order to elucidate the remnants presence, the Au-TiO_2 FTIR spectra were recorded (Fig. 3). For comparison, the spectrum corresponding to citrate, PVP and pure TiO_2NPs were also registered. In the 1000–2000 cm^{-1} region, where PVP and citrate have the stronger absorption bands, two main bands, around 1600 and 1400 cm^{-1}, were observed. These bands are related with the C-O stretching vibrations of citrate carboxylate groups (1582 and 1393 cm^{-1}) and PVP carbonyl groups (1582 cm^{-1}) [56,57] for the Au-TiO_2 nanopowders. The weak band at 1633 cm^{-1} present in pure VP TiO_2 particles, is characteristic of the TiO_2 and attributed to the H—O—H bending of water adsorbed in surface [58,59]. The intensity of the previously described bands is related with the amount of citrate and PVP employed in the AuNPs synthesis (see Table 2 showing the relative amount of the two compounds). These evidences allow concluding that citrate and PVP were present in the samples with the highest citrate amount (TxAu13 samples) whereas those with the lowest amount (TxAu38) contained mainly PVP, confirming that citrate was practically consumed in the synthesis.

Table 2 also shows the pH values obtained for the aqueous dispersions of the nanopowders under study. The obtained values highlight that the presence of PVP and citrate remnants changed their acid-base behaviour. The pH value was gradually increased as the Au content, and subsequently the amount of residual PVP and citrate, was raised. Concerning the comparison between the two types of materials, for the TxAu38 samples, containing mainly PVP, the pH was slightly increased. In the case of the TxAu13 samples, containing citrate and PVP, the pH

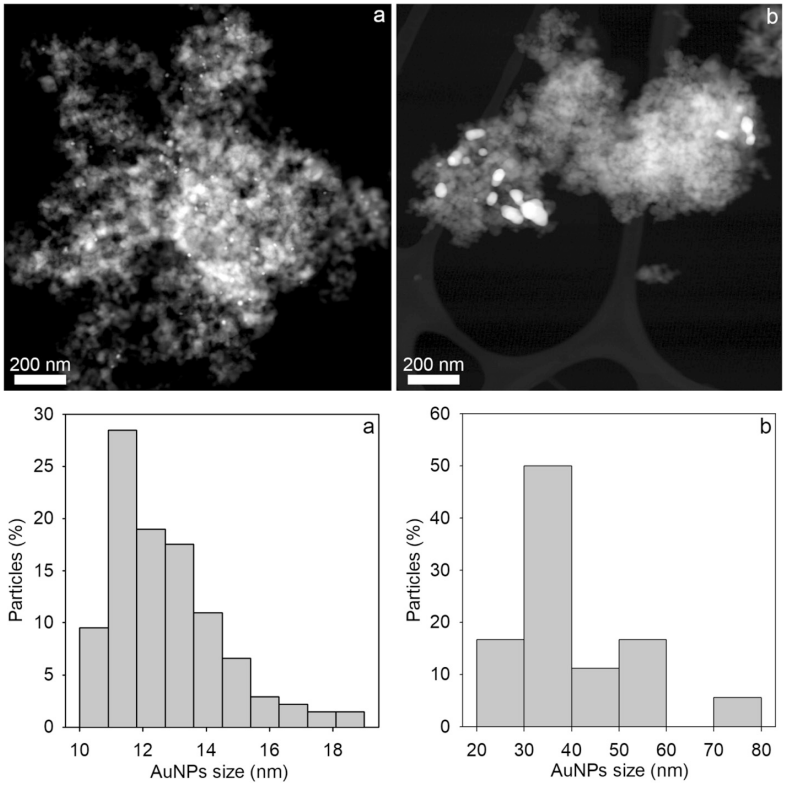

Fig. 2. HAADF-STEM image of two representative Au-TiO_2 nanopowders and respective AuNPs size distribution. a) T0.5Au13, containing the AuNPs prepared with the highest citrate/Au ratio; b) T0.5Au38, containing the AuNPs prepared with the lowest citrate/Au ratio.

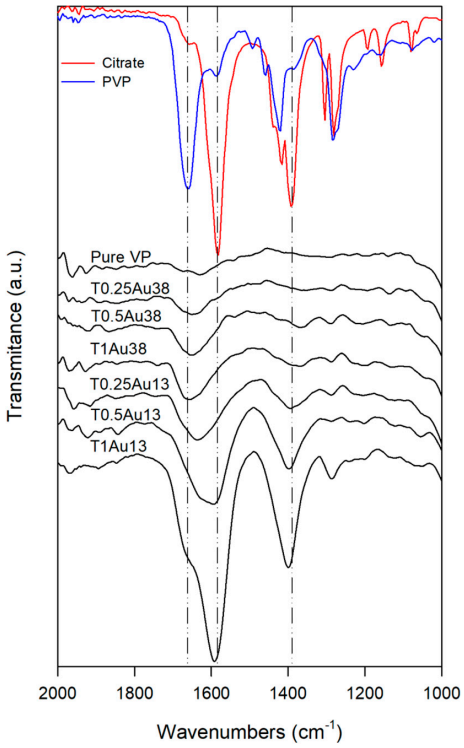

Fig. 3. FTIR spectra of sodium citrate, PVP, VP TiO_2 particles and the prepared nanopowders.

Table 2
Relative citrate and PVP amounts employed for preparation of the different nanopowders, pH values of their water dispersions and rate constants for the MB degradation tests.

Sample	Citrate*	PVP*	pH	Hydrodynamic sizes (nm)	Rate constant (h^{-1})
VP pure	0	0	5.22	55 and 201	0.86
T0.25Au38	1	1	5.36	54, 177 and 977	0.80
T0.5Au38	2	2	5.47	74, 219 and 1163	1.63
T1Au38	4	4	5.59	74, 215 and 2130	1.29
T0.25Au13	8	2	6.38	53, 185 and 828	1.75
T0.5Au13	16	4	6.45	62, 197 and 955	2.30
T1Au3	32	8	6.64	67, 190 and 1722	1.47

* Relative amounts with respect to those used in the T0.25Au38 sample preparation.

was significantly increased (by one unit).

The DLS technique was employed to study how the TiO_2 dispersion is affected by the Au incorporation. The obtained size distributions are included in Fig. S1 in the Supplementary information and their maximum values are compiled in Table 2. The VP particles showed a bimodal distribution with maxima at nearly 50 and 200 nm, corresponding to individual particles and small agglomerates composed by several particles. However, the Au-TiO_2 nanopowders dispersions showed a third peak in the micrometre scale, which indicates that they were worse dispersed than VP particles. Additionally, two trends were observed as Au content raised: (i) The average size of individual particles increased, which can be attributed to the presence of citrate and PVP adsorbed in the TiO_2 surface, producing an increase of their hydrodynamic size. (ii) The average size of bigger agglomerates increased, especially for the highest Au contents, whose sizes were nearly the

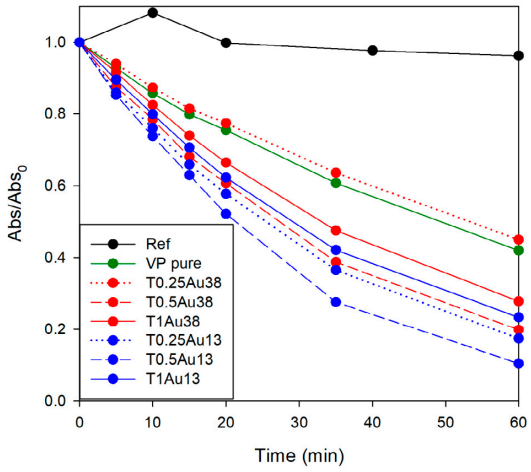

Fig. 4. Evolution of MB solution absorbance during the UV–Visible irradiation in the presence of TiO_2, the degradation curve for the MB solution without TiO_2 is also included as reference.

double that those corresponding to the lowest contents (see Table 2). These results highlight that the nanopowder dispersion was worse as the Au content was increased. The increasing amount of PVP in the Au-TiO_2 nanopowders could be responsible of this fact as the PVP chains can link the TiO_2 particles by hydrogen bonds [60], hindering their disaggregation during the ultrasonic stirring.

The influence of Au in TiO_2 photoactivity was studied by means of MB degradation tests, their results being shown in Fig. 4 and Table 2. In the absence of TiO_2 a slight absorbance decrease was observed for the longer times, which is due to the natural MB photolysis under UV irradiation [61]. By contrast, the fast drop in absorbance for the TiO_2 dispersions clearly demonstrated the photocatalytic effect of TiO_2. By comparing the Au-TiO_2 nanopowders under study, the following activity order can be stablished:

T0.5Au13 > T0.25Au13 > T0.5Au38 > T1Au13 > T1Au38 > VP > T0.25Au38

All samples (except T0.25Au38) showed higher MB degradation rates than the pristine VP particles, demonstrating the TiO_2 photoactivity enhancement produced by the Au. Two different trends concerning the size and loading of Au were observed for the Au-TiO_2 nanopowders. The samples containing the smaller AuNPs were more active than those containing the bigger ones, this higher activity can be explained by the following facts: (i) A lower size means a higher number of particles for the same Au weight (as revealed in Fig. 2), which increases the TiO_2-Au contact surface; (ii) As previously discussed in the HAADF-STEM characterization, the small particles presented a better dispersion onto TiO_2 support; (iii) Smaller particles shift the Fermi Level to more negative potentials, promoting a higher charge separation [62]. Regarding the Au content, the highest activity was reached for the samples with the intermediate Au loading for both Au-TiO_2 nanopowders series. The TiO_2 dispersion decline as Au content was raised, observed in the DLS characterization, can be responsible of this activity reduction. In addition, an excess of gold can promote adverse effects which reduce the TiO_2 photoactivity, such as the recombination of photo-induced electron-hole pairs [45,46] and the preferential light absorption by gold rather than TiO_2 [42,47].

The additional photocatalytic tests that were performed employing the sample that showed the highest MB degradation rate (T0.5Au13) allowed concluding that TiO_2 photoactivity enhancement induced by the Au took place. As well known, MB is a dye that absorbs in visible region and it can promote the visible light sensitization of TiO_2 [63].

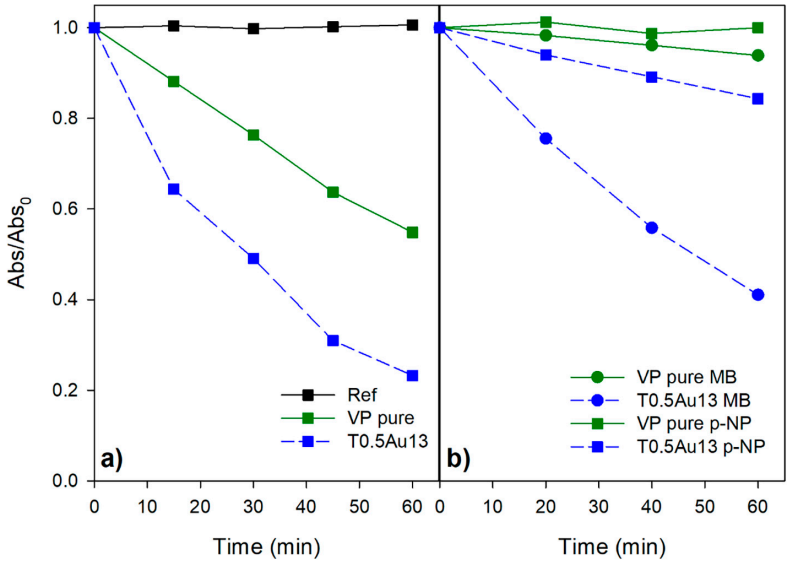

Fig. 5. Results of photocatalytic tests. a) p-NP degradation under UV–Visible irradiation. b) p-NP and MB degradation under visible irradiation.

For this reason, p-nitrophenol (p-NP), that does not present absorption in the visible region, was chosen for testing the photocatalytic properties of the samples (see Fig. 5a). In the absence of photocatalyst, no p-NP degradation was observed, demonstrating that the degradation observed was produced by the photocatalytic properties of TiO_2. In addition, the evident increase in the p-NP degradation rate proved the photocatalytic enhancement produced by gold. Finally, the photocatalytic behaviour under visible light was studied because the Au can promote the TiO_2 activation under these conditions. The evident TiO_2 photoactivity enhancement observed when gold is present (see Fig. 5b) confirmed the TiO_2 visible activation by gold. Additionally, it was observed a slight MB degradation while the p-NP degradation did not take place. This difference can be attributed to the MB, which can also promote the TiO_2 visible activation via dye sensitization mechanisms. However, the low degradation compared with Au/TiO_2 sample allows concluding that the MB sensitization effects are minor under the conditions employed.

3.2. Sol-gel characterization

The sol prepared without TiO_2 was uncoloured and transparent, whereas those with TiO_2 were opaque, being their colours: white for ST, purple for STxAu38 sols and pink for STxAu13 sols. In all the cases, the colour intensity was increased as the Au content was raised, highlighting the absorption of visible light, due to the localized surface plasmon resonance (LSPR) absorption of AuNPs [54]. TiO_2 was completely dispersed in the ST sol, but the sols containing Au showed a little amount of undispersed Au-TiO_2 nanopowders. This non-dispersed solid was increased with the gold content. This behaviour is explained in the further discussion of TEM results. The sols stored in closed vessels and dark conditions were stable for at least six months, which ensures their further commercial application.

The sol-gel transition of the sols deposited on Petri dishes spontaneously took place in less than 6 h, giving rise to crack-free and homogeneous gels with the same colours than the corresponding sols (see Fig. S2 in Supplementary information). The UV–Visible spectra of the powdered xerogels (see Fig. S3 in Supplementary information) clearly showed the absorption of TiO_2 in the UV zone and the absorption of AuNPs in the visible range. The intensity of LSPR absorption was higher as the Au content was raised, being always higher for STxAu13 photocatalysts (with the lowest AuNPs size) because the particle number is higher for the same Au amount. In addition, the LSPR band of STxAu38 photocatalysts was shifted to red and was wider than the STxAu13 ones. This is related to the higher size of the AuNPs and the wider particle size distribution as shown in Fig. 2 [54]. The intensity of TiO_2 absorption was lower for the photocatalysts containing Au probably due to fact they make difficult the TiO_2 dispersion during the sol synthesis and thus, the TiO_2 amount in the xerogel is lower, as previously discussed. Analogous spectra have been obtained after being stored for two years, confirming that AuNPs remains stable (see Fig. S4 in the Supplementary information).

We also calculated the band gap of the photocatalysts from the reflectance spectra and a band gap of around 3.25 eV for all the materials prepared, close to the TiO_2 anatase band gap (3.2 eV) was obtained. It confirms that the sol-gel process does not modify the TiO_2 structure [64].

N_2 physisorption measurements gave us a relevant information about the porous structure of the obtained xerogels. The adsorption–desorption isotherms and NLDFT pore size distributions, obtained from the adsorption branches for the materials under study, are shown in Fig. S4 in Supplementary material. The derived textural data are compiled in Table 3. The materials showed type IV(a) isotherms [65], characteristic of mesoporous materials due to the role played by n-octylamine [66], and they had a nearly H1 hysteresis loop, which is related to a compact structure of aggregated particles with uniform size

Table 3
Textural properties of the obtained xerogels.

Product	$S_{BET}(m^2/g)$	$V_{pore}(cm^3/g)^*$
S	325	0.572
ST	312	0.493
ST0.25Au38	313	0.551
ST0.5Au38	316	0.551
ST1Au38	310	0.554
ST0.25Au13	284	0.493
ST0.5Au13	282	0.437
ST1Au13	281	0.422

* Total pore volume determined by nitrogen adsorption volume at $P/P_0 = 0.985$.

and high connectivity between pores [67]. This structure is in accordance with the micelles inverse mechanism proposed for sols containinig n-octylamine [68]. The proposed model suggests that the water is encapsulated in the surfactant micelles that act as nanoreactors, producing silica particles with uniform size. The particles are packed, and mesopores are produced from the interparticle spaces.

The pore size distributions (Fig. S5 in Supplementary material) were also similar for the different photocatalysts under study, having a small fraction of microporosity with pore size below 1.7 nm and the main porosity in the mesoporous range of ≈3–21 nm with the maximum around 6 nm. The pore size distribution of S (without TiO_2) and STxAu38 (with the highest AuNPs size) products were nearly overlapped and they had the greatest ratio of bigger pores. On the other hand, the ST and ST0.25Au13 size distributions were also nearly overlapped. In addition, we remark that, for the STxAu13 materials, the increase of gold content reduced the bigger pores fraction.

As might be expected from the isotherms, minor differences in the textural properties were observed for the studied materials (see Table 3). Regarding their differences, STxAu13 materials showed lower surface area and pore volume values. Additionally, a reduction in the pore volume as Au content was raised was observed for STxAu13 series, which can be related with the reduction of big pores observed in the pore size distributions. The textural and pore size distribution changes can be explained as follows: (i) The incorporation of TiO_2 or Au-TiO_2 in the SiO_2 sol modifies the structure of the obtained xerogel [64]. Specifically, the addition of nanoparticles promotes the nucleation process [69], giving rise to a xerogel composed of smaller SiO_2 particles, as previously demonstrated [34,36], and subsequently the pore size distribution and pore volume are lower. (ii) The different texture observed for STxAu13 materials can be explained as a combination of the higher basicity of TiO_2 [70,71] and, especially, the change observed in the SiO_2 particle size, as below described in the discussion of the HRTEM results.

Representative HRTEM images are compiled in Fig. 6 in order to compare the nanostructure of the photocatalysts under study. All of them were composed by a silica matrix constituted by the aggregation of nearly spherical amorphous silica particles (Fig. 6 left), confirming the micelles inverse mechanism previously proposed [68]. The size of SiO_2 particles was around 15–25 nm, 10–23 nm and 8–18 nm for ST, ST0.5Au38 and ST0.5Au13, respectively. Similar structural characteristics were previously observed for other TiO_2/SiO_2 and Au-TiO_2/SiO_2 materials [34]. The pore size obtained by the physisorption technique can be associated to the created interstitial holes by a packing of spheres with sizes in the range that we observed for the silica particles forming the matrix of the photocatalysts. According to the mechanism proposed to explain the xerogel formation [68], the differences in SiO_2 particles size can be associated to the different amount of n-octylamine available for participating in the process. TiO_2 shows a strong affinity for amine moeties, promoting their absorption in its surface [72–74], but, the citrate and PVP remnants are also adsorbed on the TiO_2 surface [60,75], competing with n-octylamine adsorption and increasing the amount of free n-octylamine in the sol. This behaviour perfectly matches with the changes in SiO_2 size observed, decreasing progressively according to the amount of PVP and citrate present in the TiO_2.

Regarding the TiO_2 and Au distributions, they were integrated in the silica matrix (Fig. 6 centre). These particles were easily distinguished from the silica particles in the images. TiO_2 were identifiable because they had a higher size, a sharp shape and a clear crystalline structure. In the case of the Au, it was mainly recognizable because they had the darkest contrast. We want also to remark that Au and TiO_2 were in contact (see Fig. 6 right) which is essential to allow the LSPR-mediated charge injection from Au to TiO_2 [76].

The STEM-HAADF images together with the EDS maps provided us information about the distribution of TiO_2 and Au in the silica matrix. The images for the ST and STxAu13 xerogels are compiled in Fig. 7. The STxAu38 xerogels were not included in the Figure because they showed the same trends, except that in this case the AuNPs were hardly visible because of their lower loading due to their higher size. For the ST sample, TiO_2 was homogeneously dispersed in form of individual particles and agglomerates of 100–200 nm (Fig. 7a). On the other hand, in the photocatalysts prepared using Au-TiO_2 nanopowders the tendency to TiO_2 agglomeration was increased as the gold content was raised (Fig. 7b–d), revealing a worse TiO_2 dispersion as previously observed for the aqueous dispersions. The worse dispersion was observed in three ways: (i) decreasing of the number of individual TiO_2 particles; (ii) increasing of the size of TiO_2 agglomerates and (iii) increasing the proximity between the TiO_2 agglomerates. This poor dispersion can be directly related to the presence of undispersed Au/TiO_2 nanopowders after sol synthesis. The TiO_2 agglomeration was especially important for ST1Au13 (with the highest Au content), which presented agglomerates of micrometric size (Fig. 7e).

Regarding the AuNPs, they were dispersed in all the samples and located in the TiO_2 agglomerates. This confirms, as previously discussed, that Au kept in contact with TiO_2 during the sol-gel synthesis demonstrating that this method of incorporation of Au to TiO_2 is useful for this purpose. The size of AuNPs observed in the xerogels was similar to that observed previously in the original Au-TiO_2 nanopowders. Therefore, it confirms that the AuNPs remained unaltered and they were not aggregated.

3.3. NO degradation

Fig. 8 shows the NO, NO_2 and NO_X concentration profiles obtained during the NO oxidation tests under UV–Vis light irradiation. For the sake of clarity, the diagrams corresponding to the gold-containing samples have been plotted separately as function of the Au loading, and in each case compared to the unloaded S and ST samples. These profiles were characterized by three common stages: (i) In the absence of UV–Vis light irradiation, neither activation of the photocatalytic sites nor NO oxidation took place, consequently the concentration of NO was kept constant at 3 ppm; (ii) under UV–Vis light irradiation, the heterogeneous photocatalytic reaction occurred and the oxidation of the pollutant began. The decrease in NO concentration reached its maximum and became practically constant in this period of time, indicating complete activation of the photocatalytic sites. In parallel, NO_2 gas appeared in some extent as a product of the reaction, increasing the inlet NO_X concentration; (iii) when the irradiation was off, the NO concentration returned to its initial value.

The analysis of the second stage, related to the photoactivity region, leads to the NO conversion and selectivity towards other non-NO_2 products data which are summarized in Table 4. As expected inclusion of TiO_2 into the silica matrix converts into photocatalytic the inert starting material. On the other hand, the effect of including gold along with TiO_2 modifies the NO conversion in different ways as function of Au loading and size. Regarding the former there seems to be an optimum for the samples with intermediate content. This result resembles the behaviour observed in the MB degradation, offering another evidence of the negative effect of TiO_2 agglomeration that takes place in the samples with higher loading. Moreover, except for this intermediate content there is no a clear enhancement of the behaviour of the ST sample as consequence of gold doping. It is generally accepted that Au-TiO_2 exhibits higher activity than pure TiO_2 under both solar light and visible light irradiations due to the plasma effect from the Au quantum dots [18]. In this sense, a possible explanation for such observation could be a partial depletion of the amount of photoactive phase accessible due to the silica matrix, which might be compensated in ST0.5Au38 and ST0.5Au13.

In relation with the influence of the AuNPs size, it should be noticed that the comparison between samples with same loading makes clear the higher activity of those with smaller size. In order to rationalize these effects is convenient to consider the analysis performed in the scarce previous studies in which the role of Au in the photocatalytic

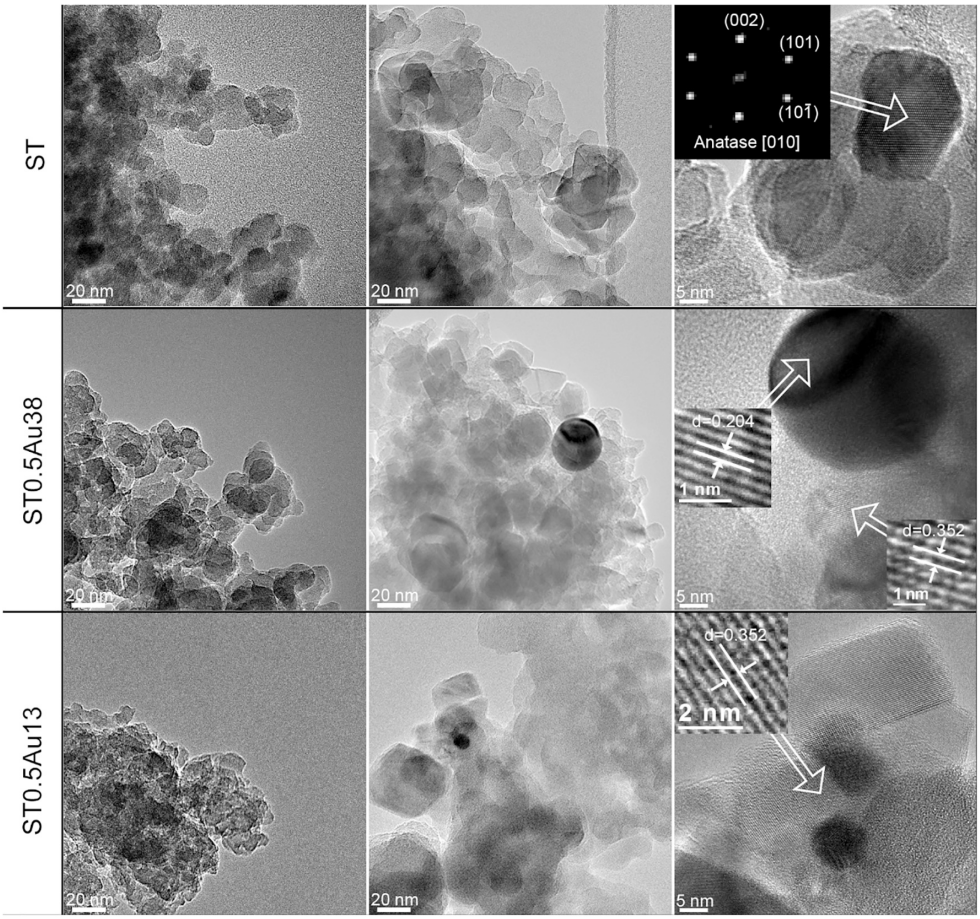

Fig. 6. Representative HRTEM images of the samples investigated. Left, silica matrix; centre, zone with TiO_2 and Au NPs; right, detail of crystalline structure of TiO_2 and Au NPs.

oxidation of NO has been reported. According to [32], the gold nanoparticles are very effective traps for electrons due to formation of a Schottky barrier at the metal-semiconductor contact. This effect prevents from fast recombination of photo-generated electrons and holes, so increasing the lifetime of these pairs. A requirement, however, is that Au is in contact with crystalline TiO_2. In this sense, the higher activity of our samples with smaller AuNPs size could be reasonably associated with a higher amount of gold atoms interacting with TiO_2 for the reaction [31]. On the other hand, our results suggest that only in the samples with intermediate Au loading the preparation leads to an optimum interaction capable of improving the photocatalytic behaviour of the TiO_2 alone.

The analysis of the selectivity to other products than NO_2 is also worthy of comment. All the samples containing gold exhibited similar selectivities, which were higher than that corresponding to the ST sample. The increase of selectivity when the photocatalyst includes Au has been previously reported [77]. This behaviour is not only attributed to the photoactivity enhancement induced by gold but also to its capacity to activate the O_2 and NO molecules via strong adsorption promoting the NO oxidation. The adsorbed O_2 in the photocatalysts is reduced by the photoinduced electrons yielding superoxide radicals that play a relevant role in the NO photooxidation [78]. The Au increases the oxygen absorption capacity of the photocatalysts enhancing the amount of O_2 available for reacting with the photogenerated electrons [33]. On the other hand, density functional theory (DFT) calculations have revealed that the NO adsorption on Au modifies the NO energy molecular levels in a way that its oxidation is favoured [31]. The results obtained in this study (Table 4) demonstrate that gold can also affect selectivity, increasing the fraction of adsorbed NO that ends up as innocuous adsorbed species rather than toxic nitrogen oxide. Aiming to obtain additional evidences of the formation of such species, FTIR spectra before and after the NO test onto the ST0.5Au13 sample were recorded (Fig. S6 in Supplementary material). As can be seen, before irradiation, no bands concerning N-O vibration modes were detected. Only those related to the silica were observed, in particular the intense band at 1090 cm^{-1} with its shoulder at 1190 cm^{-1}, and the small peak at 1650 cm^{-1} can be assigned to the stretching of ≡Si−O−Si≡ in the silica structure and the deformation of sorbed water, respectively. New bands in the 1300–1600 cm^{-1} range appear in the spectrum obtained after the NO test. In particular, according to [9] those located above 1500 cm^{-1} might correspond to monodentate and bidentate nitrates, while those between 1500 and 1300 cm^{-1} can be related to monodentate and bridging nitrites.

4. Conclusions

Photocatalysts with depolluting performance has been obtained by means of a simple sol-gel route. Specifically, Au-TiO_2NPs are integrated

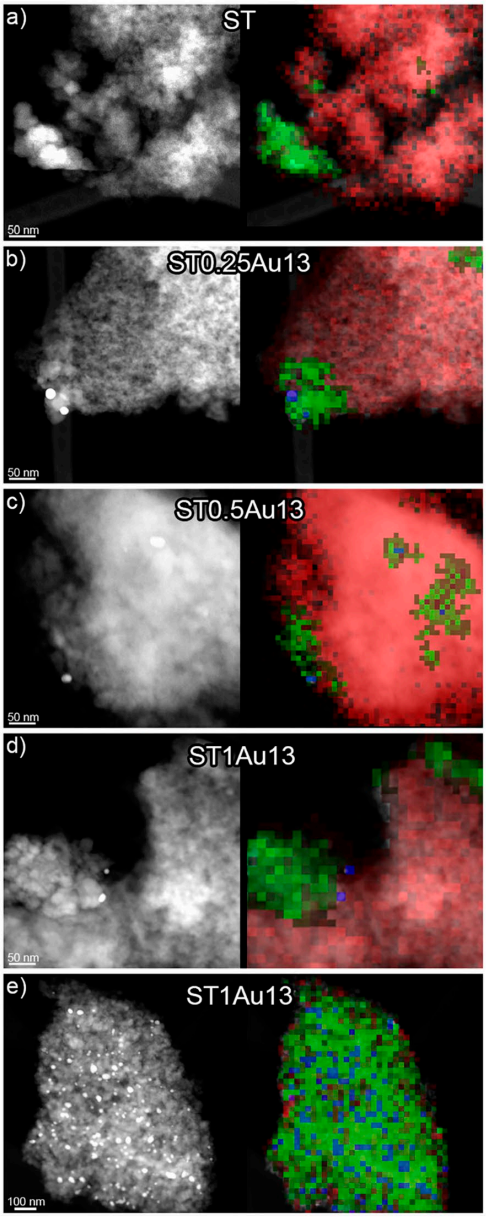

Fig. 7. Representative STEM-HAADF images of the photocatalysts and their corresponding EDS maps for Si (red), Ti (green) and Au (blue). (For interpretation of the references to colour in this figure legend, the reader is referred to the web version of this article.)

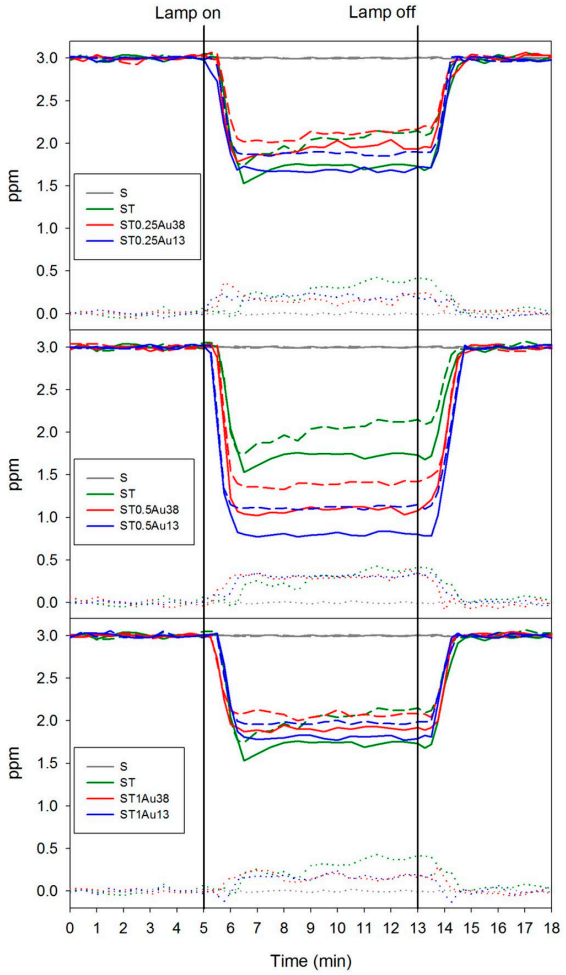

Fig. 8. Evolution of NO (continuous line), NOx (dashed line) and NO_2 (dotted line) during xerogel NO photodegradation test.

Table 4
Results of conversion and selectivity of xerogel NO photodegradation test.

	Conversion	Selectivity
S	0%	0%
ST	43%	77%
ST0.25Au38	36%	85%
ST0.5Au38	64%	84%
ST1Au38	37%	85%
ST0.25Au13	44%	85%
ST0.5Au13	73%	86%
ST1Au13	40%	86%

into a silica matrix in order to produce long-lasting coatings with applicability in building. The preparation method employed, consisting of a simple physical mixing between AuNPs and TiO_2, produces a Au-TiO_2 interaction, improving the nanopowder photoactivity. This activity is preserved as the nanopowder is integrated into the silica matrix. In addition, a considerably increase in visible light absorption is observed.

The role played by AuNPs size and their loading was investigated, giving rise to the following conclusions:

(1) The photoactivity is increased for the AuNPs with the lowest size due to their better dispersion and subsequently, their higher Au-TiO_2 interaction.
(2) The maximum photoactivity performance, in terms of conversion of NO and dye degradation, was reached for an intermedium Au loading, mainly, due to the abrupt increase of Au-TiO_2 agglomeration for the highest loading evaluated.

Finally, it has been stablished that AuNPs also increased the

selectivity of the NO oxidation to nitrates and nitrites, reducing the amount of NO_2 released.

Acknowledgments

This work has been supported by the Spanish Government/FEDER-EU (MAT2013-42934-R and MAT2017-84228-R). M. Luna would also like to thank the Spanish Government for his pre-doctoral grant (BES-2014-068031).

Appendix A. Supplementary data

Supplementary data to this article can be found online at https://doi.org/10.1016/j.cej.2019.02.167.

References

[1] European Environment Agency, European Union emission inventory report 1990–2014 under the UNECE Convention on Long-range Transboundary Air, Pollution (LRTAP) (2016), https://doi.org/10.2800/18374.
[2] J. Colls, A. Tiwary, Air Pollution, 3rd ed., CRC Press, London, 2010 https://www.taylorfrancis.com/books/9781351988926.
[3] L. Cassar, Photocatalysis of cementitious materials: clean buildings and clean air, MRS Bull. 29 (2004) 328–331, https://doi.org/10.1557/mrs2004.99.
[4] J. Chen, C.S. Poon, Photocatalytic construction and building materials: from fundamentals to applications, Build. Environ. 44 (2009) 1899–1906, https://doi.org/10.1016/j.buildenv.2009.01.002.
[5] M. Chen, J.W. Chu, NO_x photocatalytic degradation on active concrete road surface — from experiment to real-scale application, J. Clean. Prod. 19 (2011) 1266–1272, https://doi.org/10.1016/j.jclepro.2011.03.001.
[6] E. Quagliarini, F. Bondioli, G.B. Goffredo, A. Licciulli, P. Munafò, Smart surfaces for architectural heritage: Preliminary results about the application of TiO_2-based coatings on travertine, J. Cult. Herit. 13 (2012) 204–209, https://doi.org/10.1016/j.culher.2011.10.002.
[7] E. Quagliarini, F. Bondioli, G.B. Goffredo, C. Cordoni, P. Munafò, Self-cleaning and de-polluting stone surfaces: TiO_2 nanoparticles for limestone, Constr. Build. Mater. 37 (2012) 51–57, https://doi.org/10.1016/j.conbuildmat.2012.07.006.
[8] N. Bowering, G.S. Walker, P.G. Harrison, Photocatalytic decomposition and reduction reactions of nitric oxide over Degussa P25, Appl. Catal. B Environ. 62 (2006) 208–216, https://doi.org/10.1016/j.apcatb.2005.07.014.
[9] R.V. Mikhaylov, A.A. Lisachenko, B.N. Shelimov, V.B. Kazansky, G. Martra, G. Alberto, S. Coluccia, FTIR and TPD analysis of surface species on a TiO_2 photocatalyst exposed to NO, CO, and NO − CO mixtures: Effect of UV − Vis light irradiation, J. Phys. Chem. C. 113 (2009) 20381–20387, https://doi.org/10.1021/jp906176c.
[10] J. Kleffmann, et al., Discussion on “field study of air purification paving elements containing TiO2” by Folli, Atmos. Environ. 129 (2016) (2015) 95–97, https://doi.org/10.1016/j.atmosenv.2016.01.004.
[11] M. Faraldos, R. Kropp, M.A. Anderson, K. Sobolev, Photocatalytic hydrophobic concrete coatings to combat air pollution, Catal. Today 259 (2016) 228–236, https://doi.org/10.1016/j.cattod.2015.07.025.
[12] A. Mills, L. Burns, C. O'Rourke, S. Elouali, Kinetics of the photocatalysed oxidation of NO in the ISO 22197 reactor, J. Photochem. Photobiol. A Chem. 321 (2016) 137–142, https://doi.org/10.1016/j.jphotochem.2016.01.010.
[13] X. Li, Z. Le, X. Chen, Z. Li, W. Wang, X. Liu, A. Wu, P. Xu, D. Zhang, Graphene oxide enhanced amine-functionalized titanium metal organic framework for visible-light-driven photocatalytic oxidation of gaseous pollutants, Appl. Catal. B Environ. 236 (2018) 501–508, https://doi.org/10.1016/j.apcatb.2018.05.052.
[14] S. Xiao, W. Zhu, P. Liu, F. Liu, W. Dai, D. Zhang, W. Chen, H. Li, CNTs threaded (001) exposed TiO_2 with high activity in photocatalytic NO oxidation, Nanoscale 8 (2016) 2899–2907, https://doi.org/10.1039/C5NR07589K.
[15] S. Devahasdin, C. Fan, K. Li, D.H. Chen, TiO_2 photocatalytic oxidation of nitric oxide: transient behavior and reaction kinetics, J. Photochem. Photobiol. A Chem. 156 (2003) 161–170, https://doi.org/10.1016/S1010-6030(03)00005-4.
[16] J.S. Dalton, P.A. Janes, N.G. Jones, J.A. Nicholson, K.R. Hallam, G.C. Allen, Photocatalytic oxidation of NO_x gases using TiO_2: a surface spectroscopic approach, Environ. Pollut. 120 (2002) 415–422, https://doi.org/10.1016/S0269-7491(02)00107-0.
[17] Y. Komazaki, H. Shimizu, S. Tanaka, A new measurement method for nitrogen oxides in the air using an annular diffusion scrubber coated with titanium dioxide, Atmos. Environ. 33 (1999) 4363–4371, https://doi.org/10.1016/S1352-2310(99)00231-9.
[18] D. Barreca, G. Carraro, A. Gasparotto, C. Maccato, M.E.A. Warwick, E. Toniato, V. Gombac, C. Sada, S. Turner, G. Van Tendeloo, P. Fornasiero, Hydrogen production: Iron-titanium oxide nanocomposites functionalized with gold particles: From design to solar hydrogen production, Adv. Mater. Interfaces 3 (2016), https://doi.org/10.1002/admi.201670075.
[19] H.M. Sung-Suh, J.R. Choi, H.J. Hah, S.M. Koo, Y.C. Bae, Comparison of Ag deposition effects on the photocatalytic activity of nanoparticulate TiO_2 under visible and UV light irradiation, J. Photochem. Photobiol. A Chem. 163 (2004) 37–44, https://doi.org/10.1016/S1010-6030(03)00428-3.
[20] N. Murakami, A. Ono, M. Nakamura, T. Tsubota, T. Ohno, Development of a visible-light-responsive rutile rod by site-selective modification of iron(III) ion on {111} exposed crystal faces, Appl. Catal. B Environ. 97 (2010) 115–119, https://doi.org/10.1016/j.apcatb.2010.03.030.
[21] S. Sato, R. Nakamura, S. Abe, Visible-light sensitization of TiO_2 photocatalysts by wet-method N doping, Appl. Catal. A Gen. 284 (2005) 131–137, https://doi.org/10.1016/j.apcata.2005.01.028.
[22] Y. Cho, W. Choi, C.H. Lee, T. Hyeon, H.I. Lee, Visible light-induced degradation of carbon tetrachloride on dye-sensitized TiO_2, Environ. Sci. Technol. 35 (2001) 966–970, https://doi.org/10.1021/es001245e.
[23] R. Sugrañez, J. Balbuena, M. Cruz-Yusta, F. Martín, J. Morales, L. Sánchez, Efficient behaviour of hematite towards the photocatalytic degradation of NO_x gases, Appl. Catal. B Environ. 165 (2015) 529–536, https://doi.org/10.1016/j.apcatb.2014.10.025.
[24] L. Giraldo, J.C. Moreno-Pirajan, Activated carbon prepared from orange peels coated with titanium oxide nanoparticles: characterization and applications in the decomposition of NO_x, Orient. J. Chem. 30 (2014) 451–461 https://doi.org/10.13005/ojc/300207.
[25] R. Amadelli, L. Samiolo, M. Borsa, M. Bellardita, L. Palmisano, N-TiO_2 Photocatalysts highly active under visible irradiation for NO_X abatement and 2-propanol oxidation, Catal. Today. 206 (2013) 19–25, https://doi.org/10.1016/j.cattod.2011.11.031.
[26] K. Hashimoto, K. Wasada, M. Osaki, E. Shono, K. Adachi, N. Toukai, H. Kominami, Y. Kera, Photocatalytic oxidation of nitrogen oxide over titania–zeolite composite catalyst to remove nitrogen oxides in the atmosphere, Appl. Catal. B Environ. 30 (2001) 429–436, https://doi.org/10.1016/S0926-3373(00)00258-7.
[27] H. Ichiura, T. Kitaoka, H. Tanaka, Photocatalytic oxidation of NO_x using composite sheets containing TiO_2 and a metal compound, Chemosphere 51 (2003) 855–860, https://doi.org/10.1016/S0045-6535(03)00049-3.
[28] C.H. Huang, I.K. Wang, Y.M. Lin, Y.H. Tseng, C.M. Lu, Visible light photocatalytic degradation of nitric oxides on PtO_x-modified TiO_2 via sol–gel and impregnation method, J. Mol. Catal. A Chem. 316 (2010) 163–170, https://doi.org/10.1016/j.molcata.2009.10.015.
[29] Y.M. Lin, Y.H. Tseng, J.H. Huang, C.C. Chao, C.C. Chen, I. Wang, Photocatalytic activity for degradation of nitrogen oxides over visible light responsive titania-based photocatalysts, Environ. Sci. Technol. 40 (2006) 1616–1621, https://doi.org/10.1021/es051007p.
[30] Y. Boyjoo, H. Sun, J. Liu, V.K. Pareek, S. Wang, A review on photocatalysis for air treatment: From catalyst development to reactor design, Chem. Eng. J. 310 (2017) 537–559, https://doi.org/10.1016/j.cej.2016.06.090.
[31] D. Zhang, M. Wen, S. Zhang, P. Liu, W. Zhu, G. Li, H. Li, Au nanoparticles enhanced rutile TiO_2 nanorod bundles with high visible-light photocatalytic performance for NO oxidation, Appl. Catal. B Environ. 147 (2014) 610–616, https://doi.org/10.1016/j.apcatb.2013.09.042.
[32] I. Bannat, K. Wessels, T. Oekermann, J. Rathousky, D. Bahnemann, M. Wark, Improving the photocatalytic performance of mesoporous titania films by modification with gold nanostructures, Chem. Mater. 21 (2009) 1645–1653, https://doi.org/10.1021/cm803455k.
[33] W. Zhu, S. Xiao, D. Zhang, P. Liu, H. Zhou, W. Dai, F. Liu, H. Li, Highly efficient and stable Au/CeO_2–TiO_2 photocatalyst for nitric oxide abatement: Potential application in flue gas treatment, Langmuir 31 (2015) 10822–10830, https://doi.org/10.1021/acs.langmuir.5b02232.
[34] M. Luna, J. Delgado, M.L.A. Gil, M. Mosquera, TiO_2-SiO_2 coatings with a low content of AuNPs for producing self-cleaning building materials, Nanomaterials 8 (2018) 177, https://doi.org/10.3390/nano8030177.
[35] M.J. Mosquera, L.A.M. Carrascosa, N. Badreldin, Producing superhydrophobic/oleophobic coatings on Cultural Heritage building materials, Pure Appl. Chem. 90 (2018) 551–561, https://doi.org/10.1515/pac-2017-0404.
[36] R. Zarzuela, M. Carbú, M.L.A. Gil, J.M. Cantoral, M.J. Mosquera, CuO/SiO_2 nanocomposites: A multifunctional coating for application on building stone, Mater. Des. 114 (2017) 364–372, https://doi.org/10.1016/j.matdes.2016.11.009.
[37] L.A.M. Carrascosa, D.S. Facio, M.J. Mosquera, Producing superhydrophobic roof tiles, Nanotechnology 27 (2016) 095604, , https://doi.org/10.1088/0957-4484/27/9/095604.
[38] R.E. Ramírez-García, J.A. González-Rodríguez, M. Arroyo-Ortega, S.A. Pérez-García, L. Licea-Jiménez, Engineered TiO_2 and SiO_2-TiO_2 films on silica-coated glass for increased thin film durability under abrasive conditions, Int. J. Appl. Ceram. Technol. 14 (2017) 39–49, https://doi.org/10.1111/ijac.12614.
[39] V.B. Koli, S. Mavengere, J.-S. Kim, Photocatalytic properties of TiO_2-SiO_2-coated concrete on toluene gas, Mater. Res. Express. 5 (2018) 125006, , https://doi.org/10.1088/2053-1591/aae01c.
[40] A. Rosales, A. Maury Ramírez, R.M. De Gutiérrez, C. Guzmán, K. Esquivel, SiO_2@TiO_2 coating: Synthesis, physical characterization and photocatalytic evaluation, Coatings 8 (2018) 120, https://doi.org/10.3390/coatings8040120.
[41] M. Haruta, Size- and support-dependency in the catalysis of gold, Catal. Today 36 (1997) 153–166, https://doi.org/10.1016/S0920-5861(96)00208-8.
[42] A. Primo, A. Corma, H. García, Titania supported gold nanoparticles as photocatalyst, Phys. Chem. Chem. Phys. 13 (2011) 886–910, https://doi.org/10.1039/C0CP00917B.
[43] B. Cojocaru, Ş. Neaţu, E. Sacaliuc-Pârvulescu, F. Lévy, V.I. Pârvulescu, H. Garcia, Influence of gold particle size on the photocatalytic activity for acetone oxidation of Au/TiO_2 catalysts prepared by dc-magnetron sputtering, Appl. Catal. B Environ. 107 (2011) 140–149, https://doi.org/10.1016/j.apcatb.2011.07.007.
[44] B. Tian, J. Zhang, T. Tong, F. Chen, Preparation of Au/TiO_2 catalysts from Au(I)-thiosulfate complex and study of their photocatalytic activity for the degradation of

methyl orange, Appl. Catal. B Environ. 79 (2008) 394–401, https://doi.org/10.1016/j.apcatb.2007.11.001.
[45] B. Tian, C. Li, F. Gu, H. Jiang, Synergetic effects of nitrogen doping and Au loading on enhancing the visible-light photocatalytic activity of nano-TiO_2, Catal. Commun. 10 (2009) 925–929, https://doi.org/10.1016/j.catcom.2008.12.029.
[46] A. Ayati, A. Ahmadpour, F.F. Bamoharram, B. Tanhaei, M. Mänttäri, M. Sillanpää, A review on catalytic applications of Au/TiO_2 nanoparticles in the removal of water pollutant, Chemosphere 107 (2014) 163–174, https://doi.org/10.1016/j.chemosphere.2014.01.040.
[47] V. Subramanian, E. Wolf, P.V. Kamat, Semiconductor – Metal composite nanostructures. To what extent do metal nanoparticles improve the photocatalytic activity of TiO_2 films? J. Phys. Chem. B 105 (2001) 11439–11446, https://doi.org/10.1021/jp011118k.
[48] Q.L. Yu, H.J.H. Brouwers, Indoor air purification using heterogeneous photocatalytic oxidation. Part I: experimental study, Appl. Catal. B Environ. 92 (2009) 454–461, https://doi.org/10.1016/j.apcatb.2009.09.004.
[49] J. Turkevich, P.C. Stevenson, J. Hillier, A study of the nucleation and growth processes in the synthesis of colloidal gold, Discuss. Faraday Soc. 11 (1951) 55–75, https://doi.org/10.1039/df9511100055.
[50] J. Tauc, Optical properties and electronic structure of amorphous Ge and Si, Mater. Res. Bull. 3 (1968) 37–46, https://doi.org/10.1016/0025-5408(68)90023-8.
[51] S.P. Tandon, J.P. Gupta, Measurement of forbidden energy gap of semiconductors by diffuse reflectance technique, Phys. Status Solidi. 38 (1970) 363–367, https://doi.org/10.1002/pssb.19700380136.
[52] M. Thommes, B. Smarsly, M. Groenewolt, P.I. Ravikovitch, A.V. Neimark, Adsorption hysteresis of nitrogen and argon in pore networks and characterization of novel micro- and mesoporous silicas, Langmuir 22 (2006) 756–764, https://doi.org/10.1021/la051686h.
[53] ISO, 22197–1; Fine ceramics (advanced ceramics, advanced technical ceramics) – Test method for air purification performance of semiconducting photocatalytic materials – Part 1: Removal of nitric, oxide (2016).
[54] S. Link, M.A. El-Sayed, Spectral properties and relaxation dynamics of surface plasmon electronic oscillations in gold and silver nanodots and nanorods, J. Phys. Chem. B. 103 (1999) 8410–8426, https://doi.org/10.1021/jp9917648.
[55] N. Wangoo, K.K. Bhasin, S.K. Mehta, C.R. Suri, Synthesis and capping of water-dispersed gold nanoparticles by an amino acid: bioconjugation and binding studies, J. Colloid Interface Sci. 323 (2008) 247–254, https://doi.org/10.1016/j.jcis.2008.04.043.
[56] S.M. Tsimbler, L.L. Shevchenko, V.V. Grigor'eva, The IR absorption spectra of the tartrate and citrate complexes of nickel, cobalt, and iron, J. Appl. Spectrosc. 11 (1969) 1096–1101, https://doi.org/10.1007/BF00607851.
[57] J. Huang, H. Yang, M. Chen, T. Ji, Z. Hou, M. Wu, An infrared spectroscopy study of PES PVP blend and PES-g-PVP copolymer, Polym. Test. 59 (2017) 212–219, https://doi.org/10.1016/j.polymertesting.2017.02.005.
[58] P. Wang, M. Du, M. Zhang, H. Zhu, S. Bao, The preparation of tubular heterostructures based on titanium dioxide and silica nanotubes and their photocatalytic activity, Dalt. Trans. 43 (2014) 1846–1853, https://doi.org/10.1039/C3DT51959G.
[59] M. Kaur, N.K. Verma, $CaCO_3$/TiO_2 nanoparticles based dye sensitized solar cell, J. Mater. Sci. Technol. 30 (2014) 328–334, https://doi.org/10.1016/j.jmst.2013.10.016.
[60] G.S. Anjusree, A. Bhupathi, A. Balakrishnan, S. Vadukumpully, K.R.V. Subramanian, N. Sivakumar, S. Ramakrishna, S.V. Nair, A.S. Nair, Fabricating fiber, rice and leaf-shaped TiO_2 by tuning the chemistry between TiO_2 and the polymer during electrospinning, RSC Adv. 3 (2013) 16720–16727, https://doi.org/10.1039/c3ra42250j.
[61] A. Houas, Photocatalytic degradation pathway of methylene blue in water, Appl. Catal. B Environ. 31 (2001) 145–157, https://doi.org/10.1016/S0926-3373(00)00276-9.
[62] V. Subramanian, E.E. Wolf, P.V. Kamat, Catalysis with TiO_2/gold manocomposites. effect of metal particle size on the fermi level equilibration, J. Am. Chem. Soc. 126 (2004) 4943–4950, https://doi.org/10.1021/ja0315199.
[63] M. Rochkind, S. Pasternak, Y. Paz, Using dyes for evaluating photocatalytic properties: a critical review, Molecules. 20 (2015) 88–110, https://doi.org/10.3390/molecules20010088.
[64] L. Pinho, M.J. Mosquera, Photocatalytic activity of TiO_2-SiO_2 nanocomposites applied to buildings: influence of particle size and loading, Appl. Catal. B Environ. 134–135 (2013) 205–221, https://doi.org/10.1016/j.apcatb.2013.01.021.
[65] M. Thommes, K. Kaneko, A.V. Neimark, J.P. Olivier, F. Rodriguez-Reinoso, J. Rouquerol, K.S.W. Sing, Physisorption of gases, with special reference to the evaluation of surface area and pore size distribution (IUPAC Technical Report), Pure Appl. Chem. 87 (2015) 1051–1069, https://doi.org/10.1515/pac-2014-1117.
[66] J.F. Illescas, M.J. Mosquera, Producing surfactant-synthesized nanomaterials in situ on a building substrate, without volatile organic compounds, ACS Appl. Mater. Interfaces 4 (2012) 4259–4269, https://doi.org/10.1021/am300964q.
[67] M. Kruk, M. Jaroniec, Gas adsorption characterization of ordered organic-inorganic nanocomposite materials, Chem. Mater. 13 (2001) 3169–3183, https://doi.org/10.1021/cm0101069.
[68] D.S. Facio, M. Luna, M.J. Mosquera, Facile preparation of mesoporous silica monoliths by an inverse micelle mechanism, Microporous Mesoporous Mater. 247 (2017) 166–176, https://doi.org/10.1016/j.micromeso.2017.03.041.
[69] A. Prabhu, J.C. Gimel, A. Ayuela, J.S. Dolado, Effect of nano seeds in C-S-H gel formation: Simulation study from the colloidal point of view, CONCREEP 10, American Society of Civil Engineers, Reston, VA, 2015, pp. 877–886 https://doi.org/10.1061/9780784479346.104.
[70] C.J. Brinker, Hydrolysis and condensation of silicates: effects on structure, J. Non. Cryst. Solids 100 (1988) 31–50, https://doi.org/10.1016/0022-3093(88)90005-1.
[71] D. Balköse, Effect of preparation pH on pore structure of silica gels, J. Chem. Technol. Biotechnol. 49 (2007) 165–171 https://doi.org/doi.org/10.1007/BF00652834.
[72] T. Takeda, S. Okazaki, Adsorption of various amines on titanium(IV) oxide from aqueous solution, Chem. Soc. Jpn. 270 (1983) 608–611, https://doi.org/10.1246/nikkashi.1983.608.
[73] I.A. Polunina, A.A. Isirikyan, K.E. Polounine, S.S. Mikhailova, Water influence on the surfactant adsorption on TiO_2, Colloids Surfaces A Physicochem. Eng. Asp. 160 (1999) 141–146, https://doi.org/10.1016/S0927-7757(99)00360-X.
[74] L.F. Liao, W.C. Wu, C.C. Chuang, J.L. Lin, FTIR study of adsorption and reactions of methylamine on powdered TiO_2, J. Phys. Chem. B 105 (2001) 5928–5934, https://doi.org/10.1021/jp004285d.
[75] I.A. Mudunkotuwa, V.H. Grassian, Citric acid adsorption on TiO_2 nanoparticles in aqueous suspensions at acidic and circumneutral pH: surface coverage, surface speciation, and its impact on nanoparticle – nanoparticle interactions, J. Am. Chem. Soc. 132 (2010) 14986–14994, https://doi.org/10.1021/ja106091q.
[76] S. Linic, P. Christopher, D.B. Ingram, Plasmonic-metal nanostructures for efficient conversion of solar to chemical energy, Nat. Mater. 10 (2011) 911–921, https://doi.org/10.1038/nmat3151.
[77] M.J. Hernández Rodríguez, E. Pulido Melián, D. García Santiago, O. González Díaz, J.A. Navío, J.M. Doña Rodríguez, NO,, photooxidation with TiO_2 photocatalysts modified with gold and platinum, Appl. Catal. B Environ. 205 (2017) 148–157, https://doi.org/10.1016/j.apcatb.2016.12.006.
[78] Z. Wu, Z. Sheng, Y. Liu, H. Wang, N. Tang, J. Wang, Characterization and activity of Pd-modified TiO_2 catalysts for photocatalytic oxidation of NO in gas phase, J. Hazard. Mater. 164 (2009) 542–548, https://doi.org/10.1016/j.jhazmat.2008.08.028.

Supplementary materials

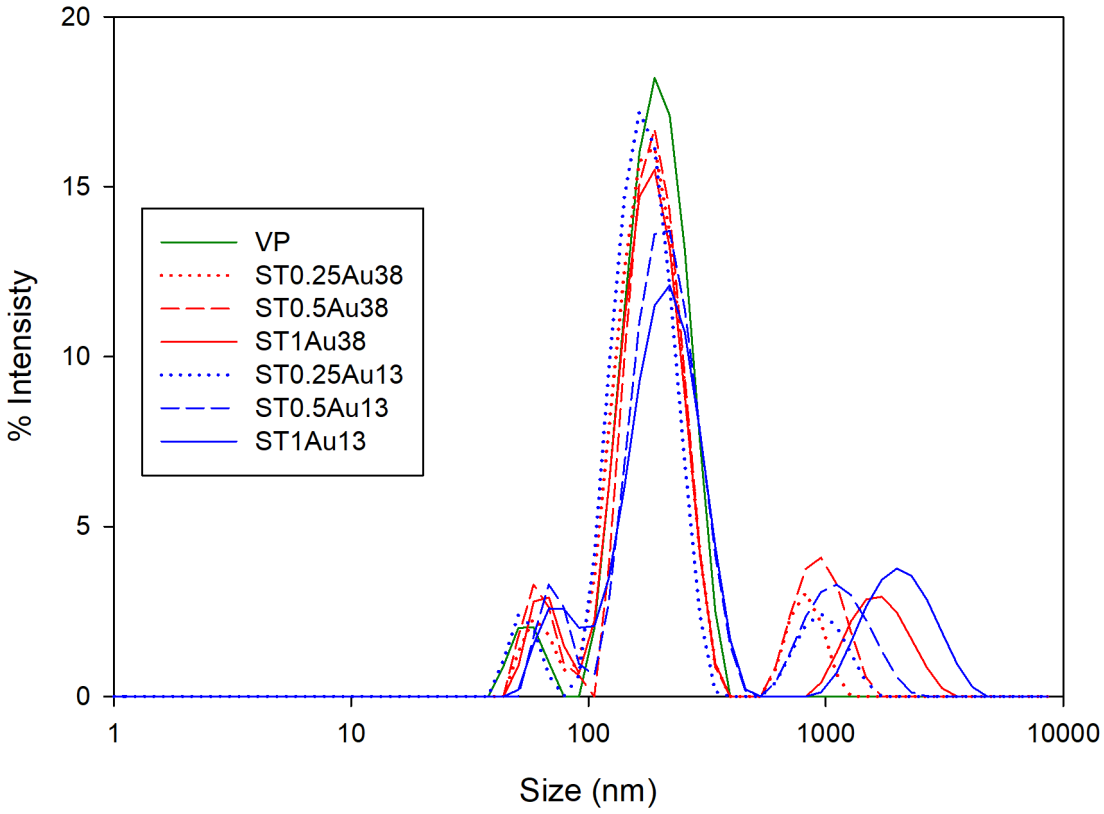

Figure S1. DLS size distributions of Au-TiO_2 nanopodwers dispersed in water.

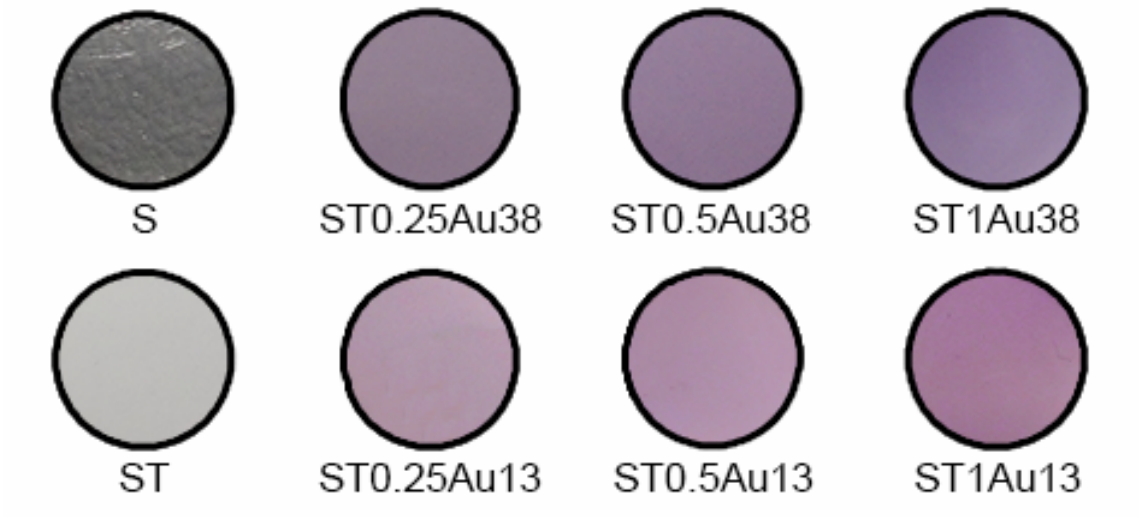

Figure S2. Photographs of obtained xerogels.

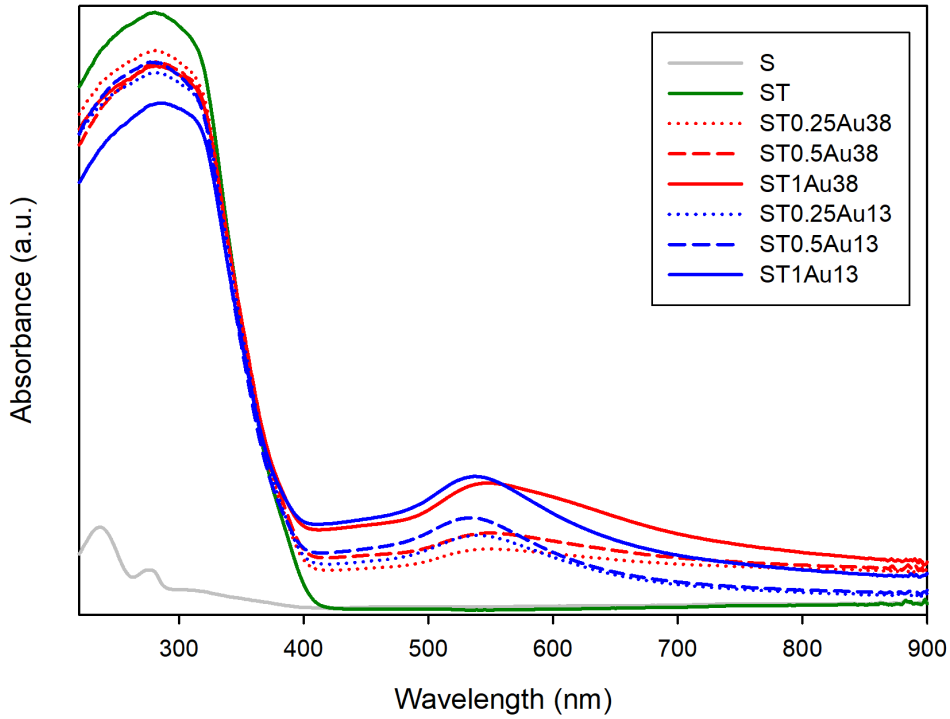

Figure S3. UV-Visible absorbance spectra of xerogels obtained from gelled sols. The absorbance spectra were obtained from respective reflectance spectra.

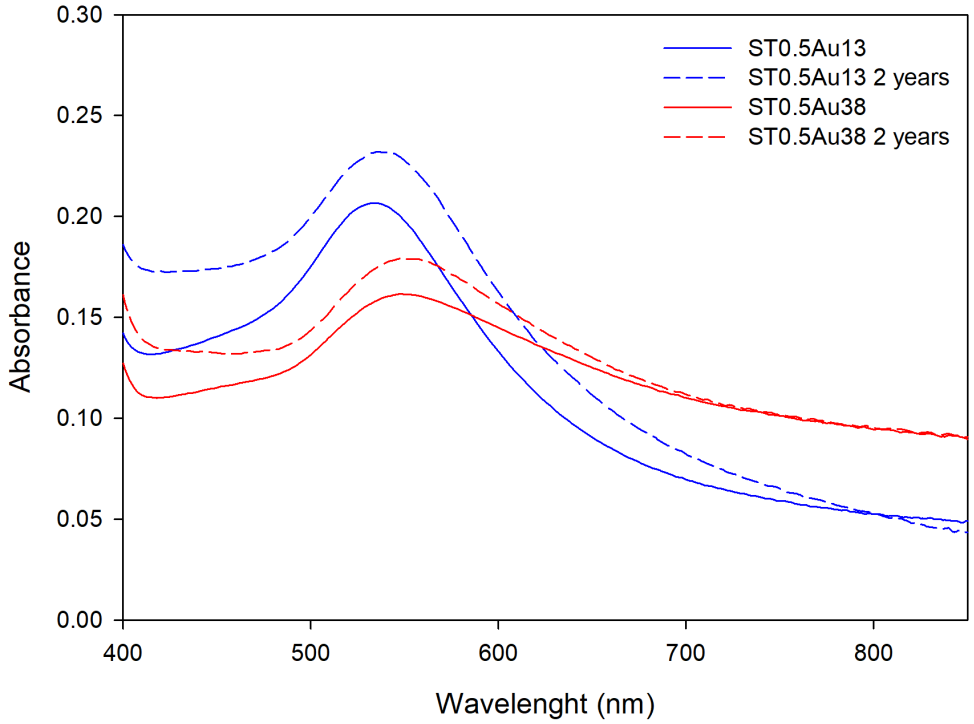

Figure S4. Comparison of the previous visible absorbance spectra with the spectra obtained two years after the photocatalysts synthesis for selected samples.

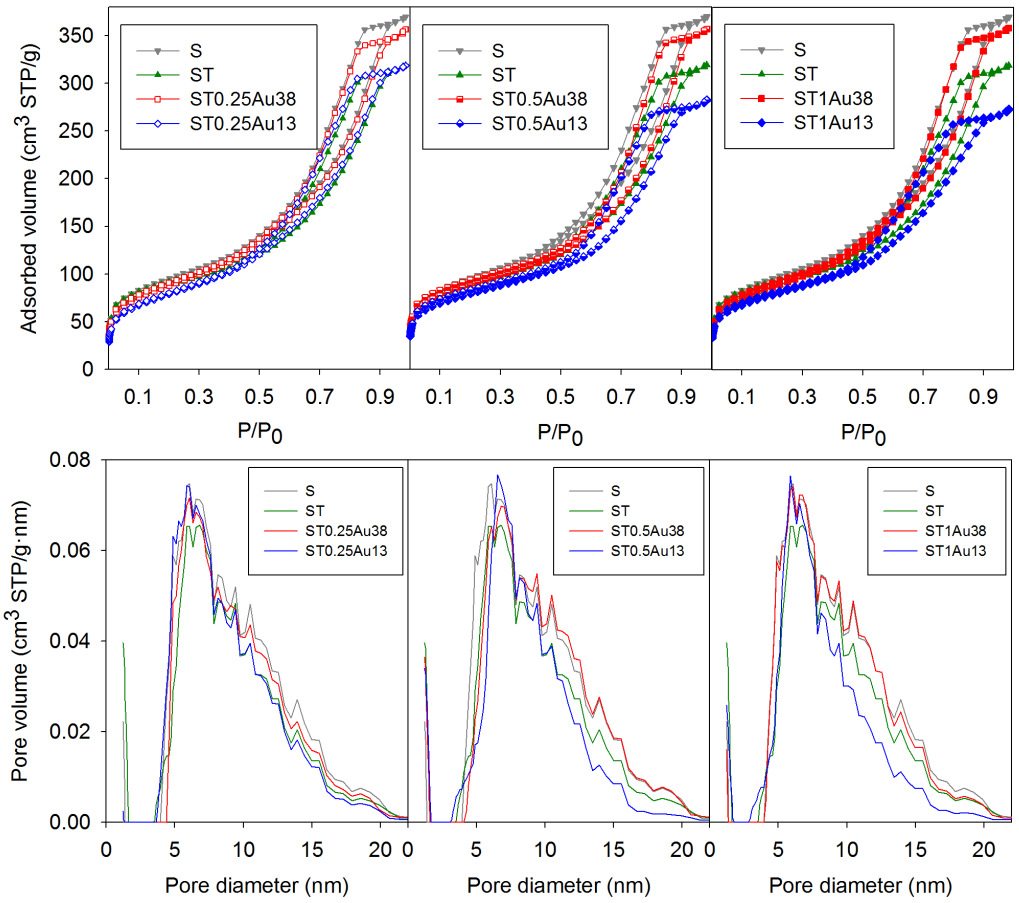

Figure S5. N_2 physisorption isotherms and NLDFT pore size distributions obtained for the photocatalysts under study.

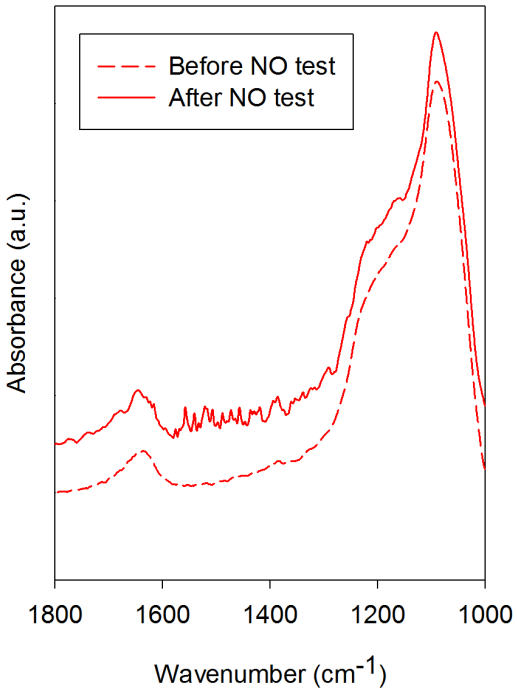

Figure S6. FTIR spectra of ST0.5Au13 before and after NO degradation test.

Chapter 5

Au-TiO_2/SiO_2 photocatalysts for building materials: self-cleaning and de-polluting performance

Au-TiO_2/SiO_2 photocatalysts for building materials: self-cleaning and de-polluting performance

Sent to Construction and Building Materials

Manuel Luna[a], María J. Mosquera[a*], Hilario Vidal[b], José M. Gatica[b**]

[a]Departamento de Química Física, Universidad de Cádiz, Puerto Real 11510, Spain

[b]Departamento C.M., I.M. y Química Inorgánica, Universidad de Cádiz, Puerto Real 11510, Spain

Corresponding authors: *; **josemanuel.gatica@uca.es

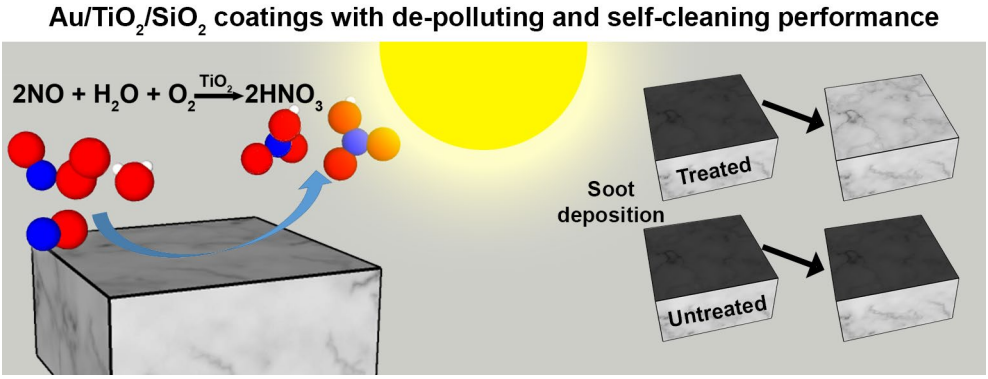

Highlights

Au-TiO_2/SiO_2 coating with self-cleaning and de-polluting activities were developed.

The Au-TiO_2/SiO_2 sols can be applied in situ on building materials by common methods.

The sols spontaneously gel in the substrate producing the photocatalytic coating.

The silica matrix promote the TiO_2 adherence to the substrate.

The AuNPs produced an evident enhancement of self-cleaning and depolluting activities

Abstract

Air pollution is one of the major problems of the current world, thus, there is an increasing focus on the development of technologies for its mitigation. TiO_2 is a photocatalytic that has been shown to have the capacity of produce self-cleaning and de-polluting building materials. However, the TiO_2 performance is limited in outdoor conditions due to its exclusive UV absorption. In this work, Au-TiO_2NPs are integrated into a sol-gel synthesis in order to produce long-lasting coatings with self-cleaning and de-polluting properties on building materials. This simple synthesis permits the application, in situ, on buildings. The enhancement of TiO_2 photoactivity by AuNPs is clearly demonstrated. The self-cleaning and de-polluting properties were evaluated using soot and NO, respectively, demonstrating that AuNPs also promote the TiO_2 performance. In addition, the role of AuNPs size and their loading on TiO_2 performance are investigated. It is demonstrated that the smaller AuNPs size and the intermedium gold content show the highest photoactivity.

Keywords: photocatalyst; de-polluting; self-cleaning; Au-TiO_2/SiO_2 composite; buildings materials; long-lasting coatings, NOx, soot.

1. Introduction

The air pollution is having a great impact on the quality of life in big cities and industrial areas around the world due to the high amount of hazardous substances emitted to the atmosphere, more than 7000 tons of NOx and 3000 kilotons of particulate matter (PM) are emitted yearly in Europe [1]. It is clearly proven that NOx promote the cancer mortality and other diseases [2]. NO_x are also a greenhouse gas and one of the main responsible of acid rain. Moreover, the combustion processes, specially, from vehicles and heating generate particulate matter constituted mainly by soot [3], which is deposited on the building facades deteriorating their

appearance [4] and, also, it promotes cardiovascular and respiratory diseases [5]. Considerable efforts are currently being made to reduce the concentration of these pollutants in urban areas [6], but these measures are not compatible with our current lifestyle and they have an important impact in the economy and the social life.

An alternative to reduce the concentration of these pollutants in the urban environment can be the employment of massive de-polluting surfaces, being the most attractive choice the use of photocatalytic building materials that can reach this goal by themselves under sunlight exposure [7,8]. The TiO_2 is the predominant photocatalyst chosen for this purposes [9] due to its excellent photocatalytic properties, stability, availability, low cost and lack of toxicity [10]. The TiO_2 mediates the photocatalytic removal of NO_x following three different mechanisms, the photo-oxidation, the photo-decomposition and the photo-selective catalytic reduction [11], being the first one the most common on building materials [12–17].

Regarding to the fouling associated to the pollution TiO_2 is also the main choice to produce a self-cleaning performance. The hydroxyl and oxygen radicals produced by the TiO_2 light activation are able to react with a wide carbon based compounds such as soot, which are degraded to CO_2 and water, producing the self-cleaning effect [18,19]. These self-cleaning properties have been widely studied by evaluating the photodegradation of organic dyes on building materials [20–29]. However, their study in more realistic scenarios, such as the soot photodegradation [30–35] has been hardly faced.

An important drawback of TiO_2 for outdoor application is related with its light absorption exclusively limited to UV region. The low fraction of UV radiation in the sunlight has promoted the development of modified TiO_2 photocatalyst in order to supply this deficiency [36]. The employment of metal nanoparticles is an effective method to enhance the TiO_2 photoactivity, because the metal-TiO_2 contact promotes the electron-hole pair separation and the charge

transfer phenomena and, additionally, the effects derived of the metal localized surface plasmon resonance improve the photoactivity under UV-Vis light [37]. The gold nanoparticles (AuNPs) show a high efficacy in the TiO_2 photoactivity enhancement [38,39], but the use of Au/TiO_2 photocatalyst for building materials has been scarcely studied [33,40,41].

Another drawback related to the use of TiO_2 photocatalysts on building is associated to their durability. The TiO_2NPs can be easily dispersed in water or organic solvents and applied in situ for producing TiO_2 coatings after solvent evaporation. Although these coatings shows a suitable performance, they are composed of an agglomeration of particles on the substrate surface that can be easily removed in outdoors conditions. The integration of TiO_2 into a SiO_2 matrix has been demonstrated to mitigate this problem due to the improvement of substrate adhesion [33,42–44]. Our research group has previously developed a sol-gel that has been reported to be an effective technique for the treatment of building materials [45–47] by several reasons: (i) The obtained sols have low viscosities that allow their in situ application by using common and low cost methods; (ii) they penetrate in the porous structure of the substrate and xerogels coatings with high adhesion to the substrate are spontaneously produced; (iii) the presence of n-octylamine in the synthesis promotes the formation of a crack-free mesoporous material.

In the present work, we evaluate the photocatalytic performance Au-TiO_2/SiO_2 on two different building stones. Two main parameters are studied, the AuNPs loading and their sizes. The loading is a key parameter because an excessive AuNPs loading can promote the electron-hole pairs recombination [38,48] and their preferential light absorption instead of TiO_2 [39,49]. The AuNPs size is also a relevant parameter to study, because the inverse correlation between catalytic activity and AuNPs [50] is not always met in photocatalysis [39,51,52]. The different phenomena involved in the Au/TiO_2 photocatalysts, such as electronic factors, Au-TiO_2 interactions or plasmonic effects, are differently altered when AuNPs size is modified.

For effectiveness evaluation, in this work the batch of Au-TiO_2/SiO_2 sols with three different AuNPs and two different sizes were applied on limestone samples and their photoactivity was evaluated by using methylene blue (MB) as a model dye. The Au-TiO_2/SiO_2 photocatalyst with the best performance was applied onto two different building stones (limestone and granite) in order to evaluate their NO de-polluting and soot self-cleaning properties.

2. Experimental

2.1. Materials

The AuNPs dipersions were prepared by an adaptation of Turkevich synthesis. A $KAuCl_4$ solution was boiled for 10 minutes and sodium citrate solution (0.5M) was added. Once the complete change of colour was reached, a small volume (0.5% v/v) of an aqueous solution of polyvinylpyrrolidone (PVP) 3% was added. The size of AuNPs obtained was controlled modifying the citrate/Au ratio in the synthesis. A red dispersion containing small AuNPs was prepared employing a citrate/Au ratio of 5 and a purple dispersion with bigger particles was obtained using a ratio of 1.25. Next, these AuNPs dispersions were mixed with TiO_2 particles in three different Au/TiO_2 proportions: 0.25, 0.5 and 1% w/w. The TiO_2 employed was VP Aeroperl P25/20 particles from Evonik, microgranulates with an average particle size of 20 μm and 50±15 m^2/g of surface area, produced by aggregation of P25 particles. The slurries obtained were dried in a vacuum oven at 60 °C overnight obtaining the final Au-TiO_2 nanopodwers. The size of AuNPs in the nanopodwers was determined by high angle annular dark field scanning transmission electron microscopy (HAADF-STEM) images acquired in a JEOL 2010F microscope, being the average sizes 12.6±1.9 nm and 38.2±11.6; see Figure S1 in supplementary material.

The Au-TiO_2/SiO_2 photocatalysts were prepared according to a synthesis previously described [33]. Specifically, the amount of components in respect to the silica oligomer were 0.36% v/v of n-octylamine, 0.83% v/v of water and 1% w/v of Au-TiO_2 nanopowders. In addition, for comparison purposes, sols without AuNPs containing pure VP particles and without any TiO_2 particles were prepared. The synthesized sols were named STxAuY, where S, T and Au indicate the presence of SiO_2, TiO_2 and Au, respectively, in the resultant coatings, x is the % w/w of Au/TiO_2 and Y refers to the average size, 13 or 38, of the AuNPs (in nm).

Two different building materials were employed for evaluating the photocatalysts under study. The first one was the Capri limestone, a stone quarried from Cabra (Spain) and commonly employed for facades facing. This stone presents a homogeneous structure, composed by calcite and has an open porosity of 12%. The white colour of this limestone is ideal for evaluating the degradation of stains deposited on its surface. The second one was the granite Grey Pearl which is quarried from Meis (Spain) and it has an open porosity lower than 1%. This granite is commonly employed for covering facades and other architectonic elements. The sols were directly applied (without dilution) on 4x4x2 cm stone samples by spraying onto one of the larger faces until its saturation. The surfaces were maintained wet during 1 minute and excess sols were removed by spraying air. Next, the samples were weighed to calculate the uptake of the products. Finally, the treated stones were dried under laboratory conditions until their weights were constant (approximately after two weeks) and their dry matters were calculated. These samples were named STxAuY/L or STxAuY/G, where L or G indicate that the corresponding photocatalyst was applied on a limestone or a granite sample, respectively.

2.2. Characterization

The rheological properties of the sols were studied immediately after their synthesis. A concentric cylinder viscometer (model DV-II+ with UL/Y adapter) from Brookfield operated

at 25 ºC was employed. The shear stress versus shear rate flow curves were generated and the viscosities were calculated as the slope of these curves in the Newtonian behaviour range evaluated.

15 ml of sols were placed in plastic Petri dishes and maintained at room temperature in order to study the sol-gel transition that took place spontaneously. The gels were dried at laboratory conditions until constant weight and the obtained xerogels were characterized using the following techniques. The visible reflectance spectra were recorded on a UV-2600 spectrophotometer from Shimadzu equipped with an ISR-2600 integrating sphere. Textural characterization was performed by N_2 physisorption at -196 ºC, using a Quantachrome Autosorb IQ. TEM and STEM images were recorded in the microscope previously described.

The changes in stone colour induced by the treatments were determined by using a solid reflection spectrophotometer, Colorflex model, from HunterLab. The conditions used were illuminant D65 and observer 10º. CIELa*b* colour space was used and variations in colour were evaluated using the total colour difference (ΔE*) parameter.

Scanning electron microscopy (SEM) images of the coatings were taken using a Nova NanoSEM model from the FEI Company, working at an acceleration voltage of 3 kV.

The TiO_2 particles adhesion to the substrate was evaluated subjecting a ST/L sample to aggressive conditions. The coated sample was immersed in 50 ml of water and was sonicated in an ultrasonic bath for 5 minutes. Next the sample was removed from the water, 200 mg of KBr were added and the mixture was dried at 120°C. The obtained solid was pressed into a pellet and its Fourier transform infrared (FTIR) spectra was recorded using an IRAffinity-1S from Shimadzu, in order to determine the composition of the matter leached by the sample. For comparative purposes, the process was repeated for other limestone samples coated with TiO_2,

employing a 1% VP water dispersion, named T/L sample. The amount of TiO_2 deposited was equivalent to those for ST and STXAu samples.

The self-cleaning properties of coated limestone samples were evaluated through a MB photodegradation test, adapted from a standard procedure [53]. It is well known that TiO_2 can degrade MB and other organic dyes by sensitization mechanisms [54,55]. Despite this, MB was chosen as a model substance because only a low portion of MB is degraded by sensitization mechanism and it is easy to determinate its discoloration in a short time, due to its fast degradation. Specifically, 320 μL of a 1 mM solution of methylene blue (MB) in ethanol was deposited, drop by drop, on the treated faces of the limestone samples and on their untreated counterparts. The samples were irradiated in a solar degradation chamber, Solarbox 3000eRH from CO.FO.ME.GRA., equipped with a 2500 W xenon arc lamp and an outdoor UV filter, monitoring the temperature, humidity and irradiance in the range 300-800 nm. The conditions in the chamber were 500 W/m^2 of irradiance, 60 ºC of temperature and 70±10 mg/m^3 of absolute humidity. The evolution of diffuse reflection spectra with time was followed by using the previously described spectrophotometer. The Kubelka-Munk function was used to obtain the equivalent MB absorbance to determine the MB degradation. As we previously demonstrated [33], this methodology provides better results than the evaluation of colour change, which is the methodology commonly employed to evaluate the self-cleaning in building materials.

Complementary, we analysed the gas released during the MB photodegradation, by using a Thermostar QMS 200 mass spectrometer from Pfeiffer, employing a 30 ml/min of O_2(5%)/Ar flow, over four samples of treated stone pieces, and their untreated counterpart, stained with methylene blue using the procedure previously described. The stained specimens were placed into a 81 mm x 81 mm × 25 mm homemade reactor built in poly(methyl methacrylate) (PMMA). Four samples were placed in each experiment in order to achieve a total surface area of 64 cm^2.

Evolution of CO_2 (m/c=44) and H_2O (m/c=18) traces in the gas phase versus time was monitored for the transient period induced by illumination of a 22W daylight fluorescent light bulb. The irradiation over the samples was 100W/m^2. The irradiance was measured using a PM100D power meter equipped with a detector S302C from Thorslabs. The same equipment was employed for the irradiance measurements described later in this work.

Finally, the photocatalyst that showed the best performance in the MB degradation test was evaluated against real staining and pollutant agents. Limestone and granite samples coated with this photocatalyst and with the material without AuNPs (ST), for comparative purposes, were subjected to the following procedures.

Soot, the most significant staining agent in building, was chosen to evaluate the self-cleaning activity of the treated stones. For soot deposition, we burnt 0.5 ml of hexane in a Ø6 cm petri dish and the treated faces of stones were exposed to this flame. Afterwards, we removed the excess and not adhered soot layer using compressed air. The stone samples were further irradiated in the solar degradation chamber and the evolution of diffuse reflection spectra were measured. The chamber operation conditions employed in these photocatalytic tests were identical to those used in the case of the previously described methylene blue degradation tests.

A de-pollutant test, based on NO degradation, was also carried out. The experimental conditions were designed, in order to achieve NO values detectable by the analyser, as follows. Four stone samples were placed inside the same homemade reactor employed for the previous mass spectrometry experiments. Air was conveyed by a gas-washing bottle, filled with demineralised water in order to keep the absolute humidity at 25 ± 2 g/m^3. Moist air and NO streams were mixed to obtain a total flow of 500 cm^3/min and a NO concentration of 20 ppm NO. This stream flowed through the reactor for 15 minutes to ensure it is filled with the gas mixture and the reactor was isolated from the rest of the system. Then, the samples were irradiated for 30

minutes using a 300W Ultra-Vitalux lamp from Osram, being the irradiance 500 W/m^2. Finally, the gas in the reactor was carried to a CLD NO/NOx analyser module (NGA 2000 model) from Emerson-Rosemount Analytical using a 1000 cm^3/min N_2 flow rate and the NO concentration over time was recorded.

The NO conversion was defined according to the following equation:

$$\text{NO conversion} = \frac{NO_{dark} - \text{NO}_{\text{light}}}{NO_{dark}} \times 100$$

where NO_{dark} and NO_{light} represent the area of NO concentration signal over time measured in dark conditions and after illumination, respectively.

The design of the reactor employed and an example of the measurement methodologies are included in Figure 1.

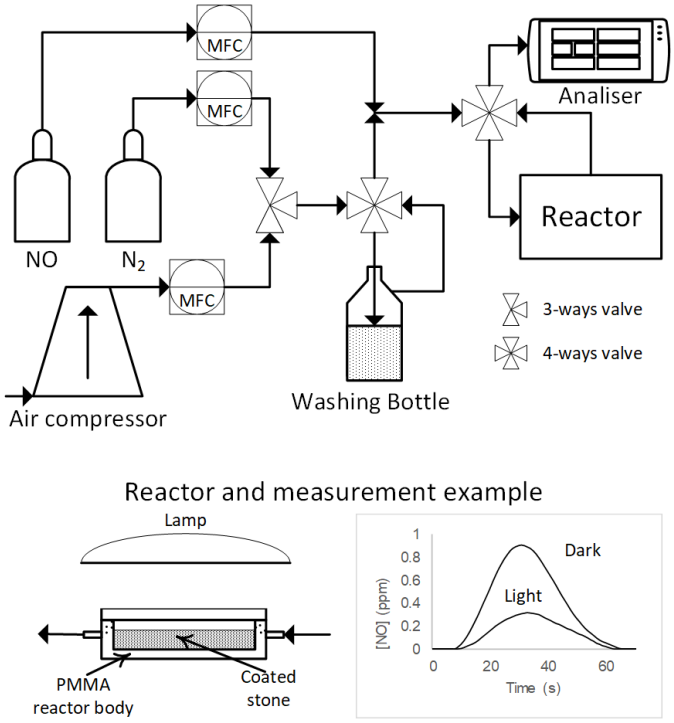

Figure 1. Representation of the flow gas setup, design of the photocatalytic reactor employed and an example of the measurements.

3. Results and discussion

3.1. Sol and gel characterization

The synthesized sols showed evident differences in appearance. The only silica sol (S) was uncoloured and transparent, whereas the inclusion of TiO_2 produced opaque sols. The AuNPs changed the white colour of ST sol to purple for STxAu38 sols and pink for STxAu13 sols, increasing the colour intensity with the Au loading. These colours highlighted the absorption in visible range, which is characteristic of the localized surface plasmon resonance (LSPR) of AuNPs [56]. Differences were also observed for the TiO_2 dispersion in the sols, as the TiO_2 was completely dispersed in the ST sol, but the STxAu sols included small amounts of undispersed Au-TiO_2 nanopowders, which was increased as Au loading was raised.

The silica sol (S) had a viscosity of 4.77 mPa·s whereas the other sols had higher viscosities with similar values, ranging from 4.99 to 5.07 mPa·s. As previously reported, this slight increasing of viscosity was due to the presence of TiO_2NPs [29,33]. These viscosities are even lower than those corresponding to commercial impregnation treatments (i.e. Tegovakon V100 shows a viscosity value of 5.25 mPa·s at 25ºC) [28]. These low viscosity values allow their application in situ in building materials by common procedures, such as spraying, brushing or using a roller. In addition, this low viscosity enhances sol penetration into the substrate, promoting a suitable adherence [29].

The sols deposited on Petri dishes spontaneously gelled in less than 6 hours, giving rise to homogeneous crack-free gels. The obtained xerogels showed the characteristic color produced by the LSRP absorption of AuNPs. This visible absorption was clearly visible in the recorded spectra (Figure 2a). The intensity of absorption was increased as the Au content was raised, being higher for STxAu13 photocatalysts. In addition, the LSPR bands for STxAu38

photocatalysts were shifted to red and were wider than the STxAu13 ones, which is related to the higher size of the AuNPs [56].

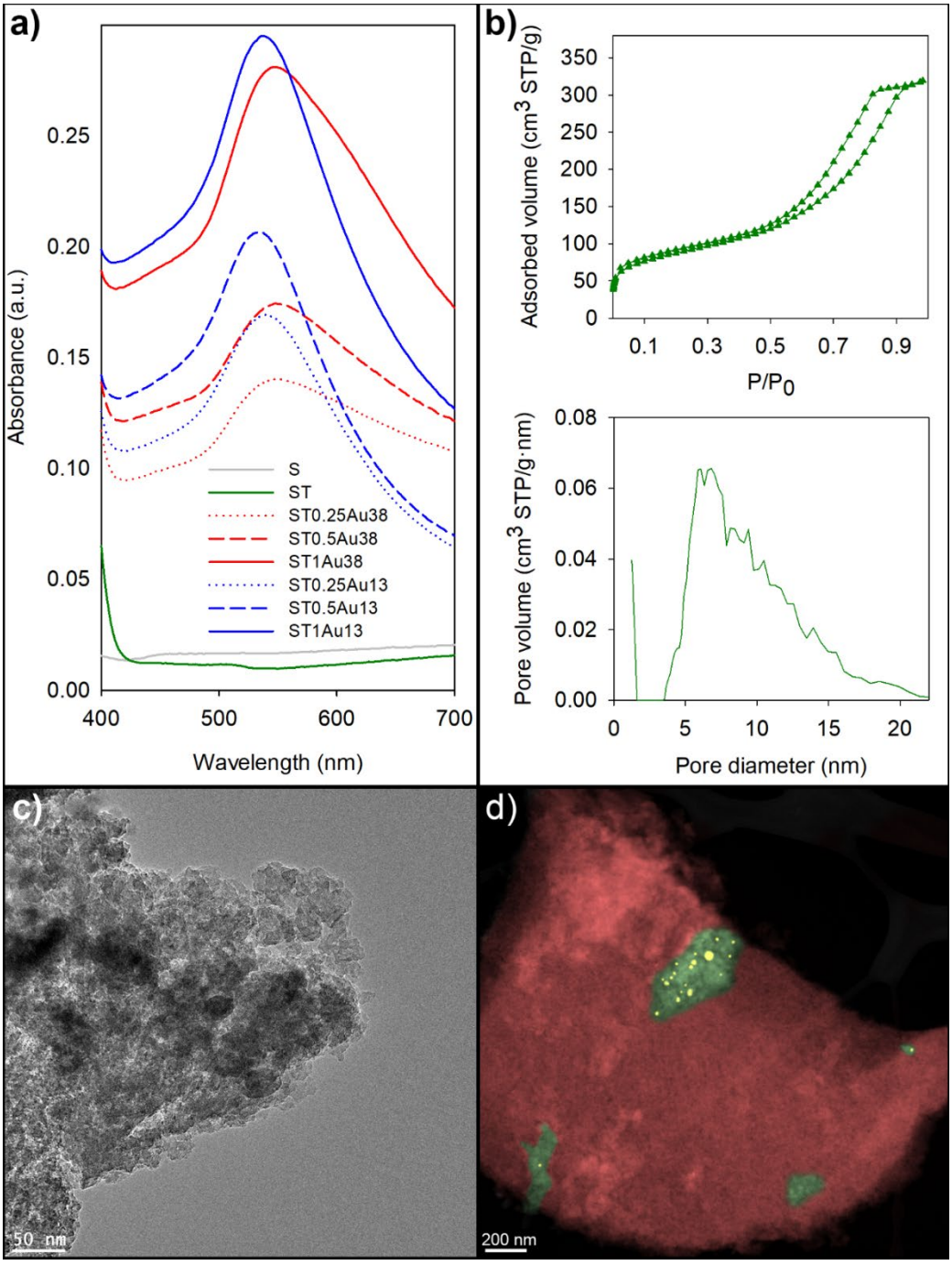

Figure 2. Representative results of xerogels characterization, a) visible spectra of xerogels, b) N_2 physisorption isotherm of ST xerogel and its corresponding pore size distribution, c) TEM image of ST xerogels and d) STEM image of ST1Au13 highlighting the components distribution, SiO_2 (red), TiO_2 (green) and Au (yellow).

All the xerogels showed similar type IV(a) N_2 isotherms Figure 2b with nearly H1 hysteresis loops, characteristics of mesoporous materials, as observed in their pore size distributions [57]. The N_2 adsorbed volume for the samples was in the range of 270-370 cm^3/g, providing large surface areas and pore volumes, 280-325 m^2/g and 0.42-0.57 cm^3/g respectively, which are fundamental for a good performance of the photocatalyst [58]. These isotherms are related to a structure composed by an aggregation of uniform particles and high pore connectivity [59], which is in accordance with the silica formation mechanism via micelles inverse proposed for sols containinig n-octylamine [60]. It has been suggested that the water is encapsulated in the surfactant micelles that act as nanoreactors giving rise to silica particles that are packed producing the interparticle spaces and the subsequent mesopores. The TEM charactetization (Figure 2c) showed that the xerogels under study were constituted by an aggregation of silica nanoparticles confirming the previous hypothesis. The STEM mode allowed identifying the distribution of TiO_2 and Au in the silica matrix. The TiO_2 was dispersed in the silica as individual particles or small agglomerates, on the other hand the AuNPs were always detected as disposed on the TiO_2. This behaviour confirmed that the AuNPs kept in contact with TiO_2 after the sol synthesis, which is fundamental to allow the Au-TiO_2 interactions, specially the SPR-mediated charge injection from gold to titania [61]. However, an important drawback was also found, the number and size of TiO_2 agglomerates was increased as AuNPs content was raised. This decrease of TiO_2 dispersion was slight for the 0.25 and 0.5% Au contents, but it was significant for 1% content showing Au-TiO_2 agglomerates of micrometric size (see Figure 2d).

3.2. Application of the photocatalysts on building materials

Table 1 shows the uptake, dry matter and ΔE^* values for the stone samples treated with the different sols under study.

Table 1. Uptake, dry matter and total colour difference (ΔE*) values of treated samples.

Treatment	Uptake (mg/cm^2)	Dry matter (mg/cm^2)	ΔE*
S/L	15.38	6.63	2.26
ST/L	12.75	6.25	1.90
ST0.25Au38/L	13.54	6.98	3.79
ST0.5Au38/L	12.92	5.94	5.37
ST1Au38/L	13.44	6.60	6.33
ST0.25Au13/L	15.52	7.60	3.50
ST0.5Au13/L	16.35	7.40	4.86
ST1Au13/L	14.79	7.08	5.97
ST/G	5.88	2.44	1.67
ST0.5Au13/G	5.62	2.50	3.58

The uptake and dry matter values were very similar for the same substrates because all the sols had similar viscosities and the slight differences were exclusively due to the intrinsic differences of the stone substrate. These values were considerably lower for granite samples, which are directly related to the porosity of the substrates, 9-12% for the limestone versus less than 1% for the granite. The average dry matter was near to the theoretical 41% of silica that the precursor provides upon complete hydrolysis, confirming that the sol-gel reaction took place once in the stone. The higher weights are due to non-hydrolysed ethoxy groups and/or ethanol occluded in the xerogel structure. Despite of the dry matter in granite was lower than that corresponding for the limestone, the amount of photocatalyst on the substrate surface was

higher for the granite as observed in Figure 3. The sol penetrated in the porous structure of limestone to a depth of 6 mm, whereas it remained in the surface of the non-porous granite (Figure 3a). This different behaviour resulted in an increase of the maximum coating thickness from 5 μm for limestone to 10 μm for the granite (Figure 3b).

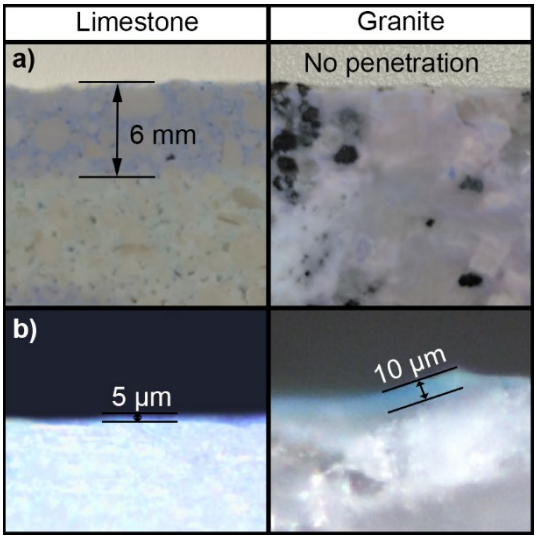

Figure 3. Images cross sections of ST13Au treated samples stained with MB aqueous solution, a) photographs showing the photocatalyst penetration in the substrates and b) optical microscope images showing coating thickness.

The change in colour induced by the treatments can be a relevant parameter in applications where the original material appearance should be preserved. The threshold value generally accepted for this type of restrictive applications is 5 [62]. In the case of the treatments under study, the colour changes produced were below the threshold excepting those corresponding to the highest Au content due to the pink/purple colour of the AuNPs. The ΔE^* values for granite samples were smaller than the corresponding for the limestone ones due to the lower amount of absorbed product.

The limestone samples observation by SEM confirmed that the treatments produced continuous and crack-free coatings, which covered the stone surface (Figure 4). This demonstrates the role played by n-octylamine to prevent the xerogel cracking [63] and therefore promoting the adhesion, and the subsequent durability, of the coatings [64,65]. The coating with 1% gold

content presented higher roughness than the coating with lower gold contents. The presence of big Au-TiO_2 agglomerates was responsible of this behaviour.

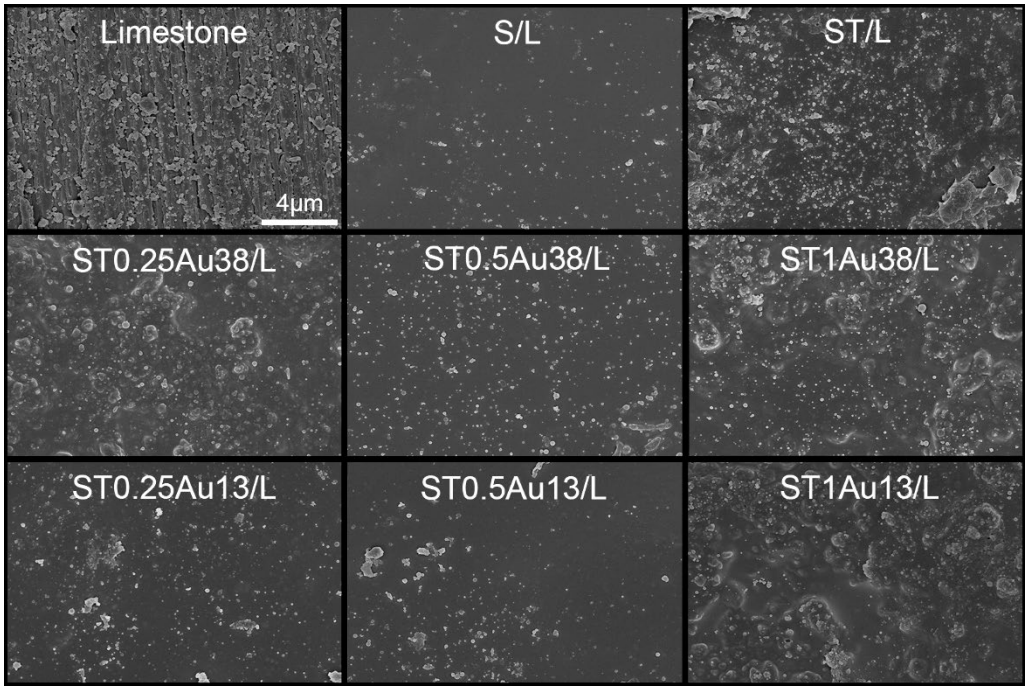

Figure 4. SEM images of treated stones and their untreated counterpart. All images have the same magnification.

The sonication of samples immersed on water was a simple method for evaluating the TiO_2 adhesion enhancement induced by the silica. First of all, a simple visual inspection of washing water allowed to conclude that the T/L sample produced higher turbidity than the ST/L (see Figure S2 in the supplementary material). The greater turbidity is related to the presence of TiO_2 particles which have an elevated refraction index. The composition of the material removed from the samples was determined by FTIR spectroscopy (Figure 5). The main bands observed for both samples mainly agree on the bands of the stone spectra, highlighting that the most of leached material correspond to calcite mineral grains disaggregated from the substrate. The ST/L sample only showed additional bands related to silica corresponding probably to xerogel removed together with the stone grains removed, but any TiO_2 signals were not observed. On the other hand, the T/L sample showed an evident absorption increase in the 400-800 cm^{-1} region that denote the presence of TiO_2NPs. These results demonstrate that the

employment of a silica matrix promote the TiO_2 adhesion to the building materials. Thus, these treatments should be more durable than a TiO_2 particles based-treatment under outdoor conditions.

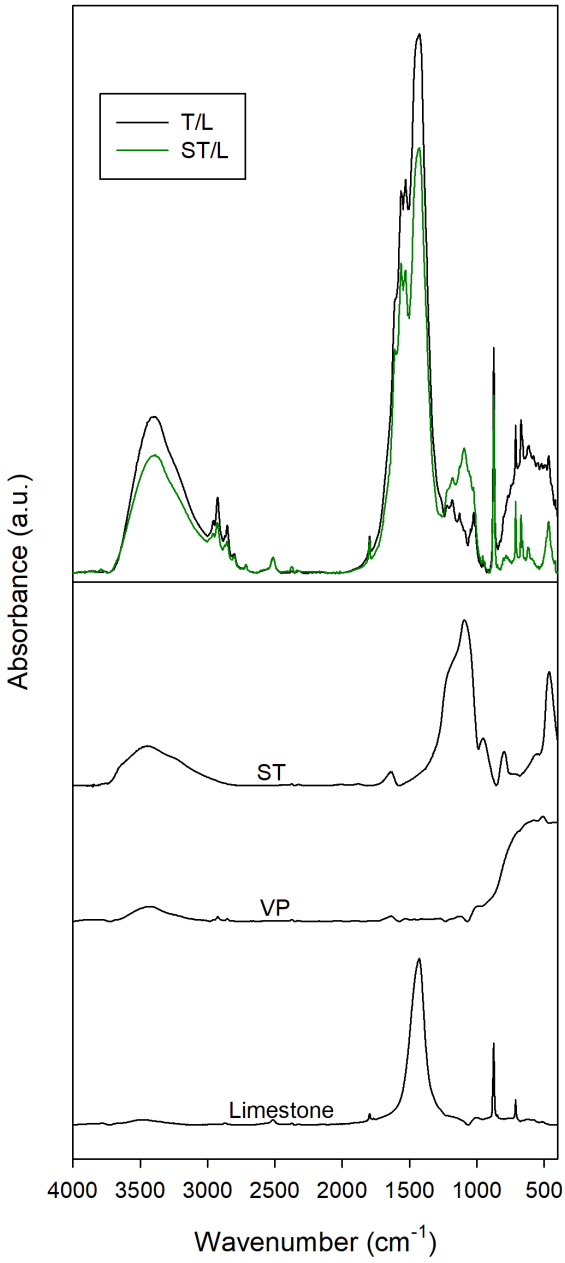

Figure 5. FTIR spectra of material removed from ST/L and T/L samples sonicated after immersion in water. For comparative purposes the spectra of limestone, ST xerogel and VP particles are also represented below.

3.3. Methylene blue degradation

The MB degradation profiles for the samples under study are compiled in Figure 6.

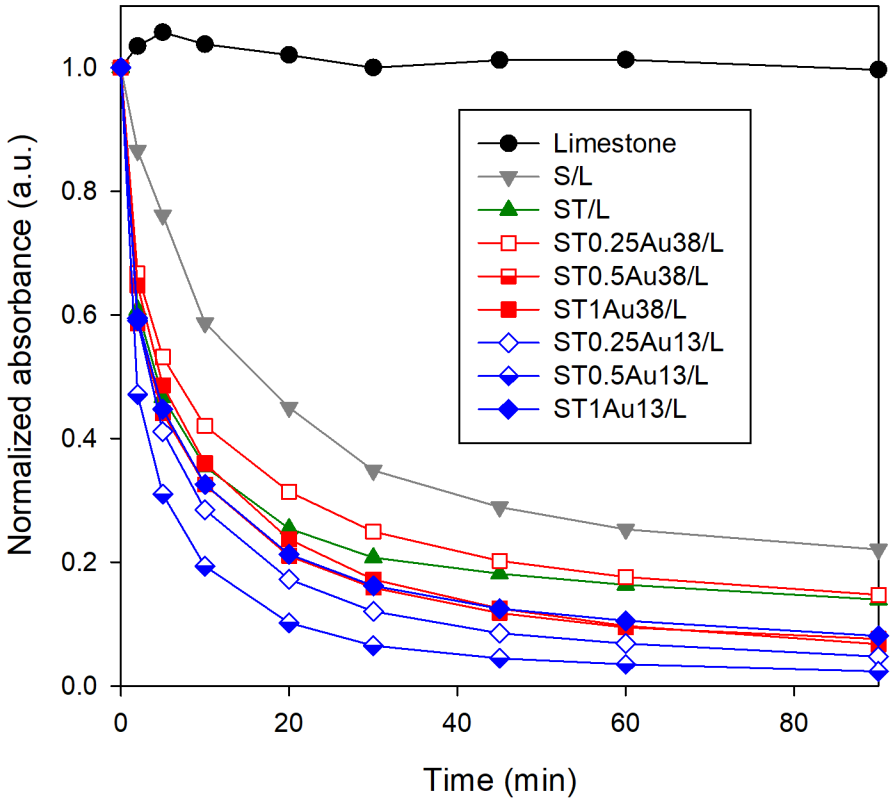

Figure 6. Evolution of methylene blue absorbance on the untreated and treated limestone samples.

The degradation profiles observed in Figure 6 allows stablishing the following sequence of MB degradation:

ST0.5Au13>ST0.25Au13>ST1Au13≈ST0.5Au38>ST1Au38>ST>ST0.25Au38>S>>Untreated

MB degradation on the untreated stone did not take place in the evaluated time range, but the S/L sample, which did not contain any photoactive component, considerably degraded the MB. This MB degradation is due to purely photochemical mechanisms associated to the MB photolysis, as previously discussed [66]. Degradation is not observed in the untreated samples because MB is absorbed into the pore structure and additionally, it is deposited as a dimer, which is not a favourable disposition for degradation, as previously discussed [33]. In the case

of the coated sample, the MB is more accessible to degradation because it is on the surface and additionally, MB monomers, the most effective form for degradation, are produced.

All the coatings including TiO_2 significantly increased the MB degradation, demonstrating that titania maintains its photocatalytic effect when it is integrated into a silica matrix [67]. Regarding to the AuNPs addition, all the coatings (except ST0.25Au38) showed a higher self-cleaning performance than those without gold. For these photocatalysts, we observed some trends concerning the AuNPs size and the AuNPs loading. The coatings with the smaller AuNPs were more effective than those containing the bigger AuNPs. It can be explained as a consequence of a lower size which implies a higher number of particles and a higher surface area for the same weight of bigger particles. This increases the LSPR effect and the probability of effective Ti-Au interactions.

Regarding to the Au loading effect, the maximum activity was reached for the coatings with the intermedium Au content in the two photocatalyst series. This behaviour can be attributable to the worst TiO_2 dispersion observed by STEM, especially for the photocatalysts with 1% of AuNPs. Additionally, a high gold content can reduce the TiO_2 photoactivity due to adverse effects, such as the recombination of photo-induced electron-hole pairs [38,48] and the preferential light absorption by gold rather than TiO_2 [39,49].

The MB degradation results were fitted to a kinetic equation where the MB degradation take place in two parallel first order process, being one significantly faster than the other, as previously reported [33]. The results of this fitting (see Table 2) show the goodness of fitting of the experimental results and they highlight a similar trend in MB degradation performance as visually observed.

Table 2. Parameters of fitting to the kinetic equation for methylene blue degradation test.

	k_1 (min^{-1})	k_2 (min^{-1})	x	R^2	$t_{75\%}$ (min)
S	0.096	0.007	0.390	0.997	67
ST	0.395	0.014	0.364	0.987	28
ST0.25Au38	0.370	0.016	0.449	0.989	38
ST0.5Au38	0.509	0.028	0.416	0.991	19
ST1Au38	0.412	0.028	0.451	0.994	21
ST0.25Au13	0.387	0.034	0.459	0.995	18
ST0.5Au13	0.716	0.057	0.363	0.997	7
ST1Au13	0.457	0.025	0.395	0.990	19

k_1: rate constant for the fast degradation process

k_2: rate constant for the slow degradation process

x: fraction of methylene blue degraded in the slow process

R^2: fitting correlation coefficient

$t_{75\%}$: time calculated using the equation for degrading the 75% of initial MB

Two types of photobleaching can take place in MB [68]: its simple decouloration by reduction towards the leuco form in the absence of oxygen, or its photooxidation producing total mineralization of the molecule to carbon dioxide and water in the presence of oxygen. Although under our experimental conditions, the mineralization should be favoured, mass spectroscopy was employed to study the gases released during this process for selected samples in order to confirm the total MB mineralization. Figure 7 shows the carbon dioxide evolution in the gas phase during the transient period induced by the illumination of the ST0.5Au13/L sample previously coated by MB exposed to an O_2(5%)/He flow. The sample illumination induces a gradual increase in the concentration of carbon dioxide and water (not shown) in the gas phase until reaching a maximum value. The effect must be associated with the photocatalytic process as far as after switching off the lamp, the CO_2 signal decreases to residual values. Moreover, in the case of this sample, which contains the gold nanoparticles, the effect is significantly more

intense than that occurring in untreated limestone or ST/L sample. These results confirm the efficiency of the proposed material and are of interest because the wide majority of experimental evidences regarding activity or mechanism of photobleaching of organic dyes have been obtained in aqueous medium and not in gas phase [69]. In the particular case of methylene blue, only Fujishima´s group [70] reported the remote elimination of this dye but studying two coated plates separated by microns.

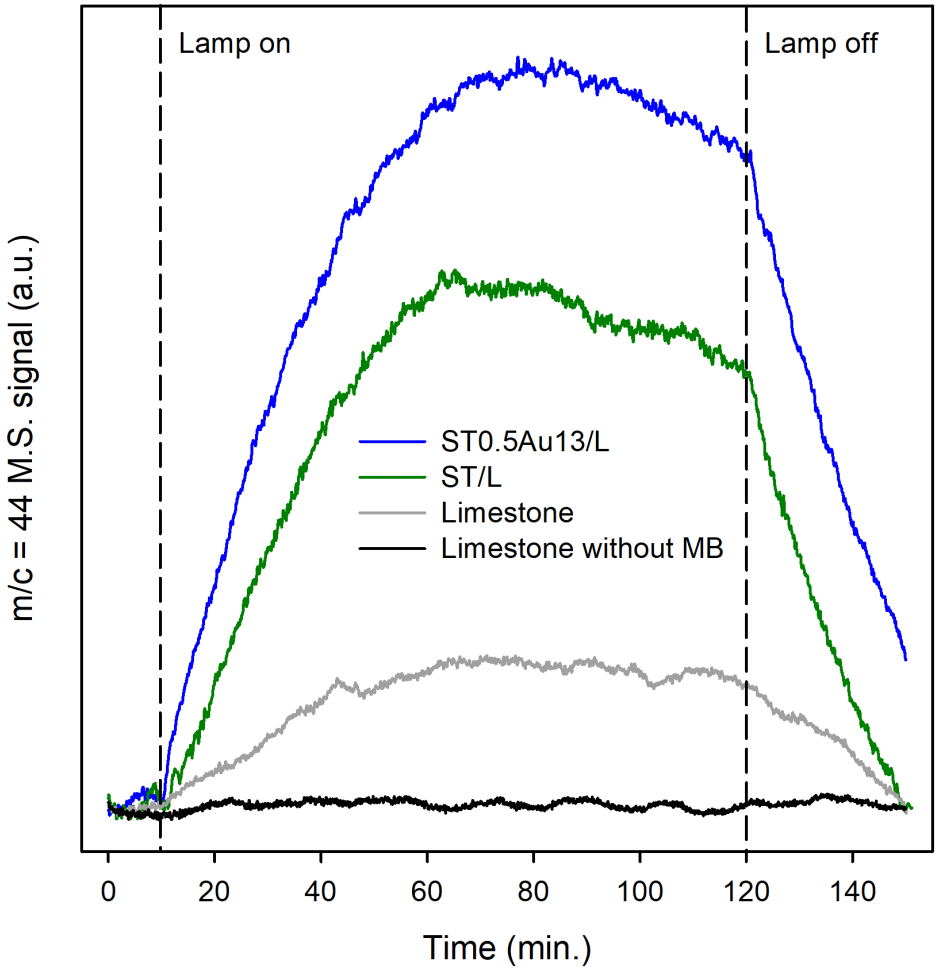

Figure 7. Carbon dioxide (m/c=44) evolution induced by the visible radiation illumination of limestones treated stained with methylene blue and their counterparts untreated with and without dye in a O_2(5%)/He flow as followed by means of mass spectrometry.

3.4. Self-cleaning and de-polluting performance on building stones

We evaluated the soot degradation using the average absorbance obtained in the spectral range of 420-440 nm for the stained stones, both limestone and granite. We selected this methodology because the soot does not have a maximum of absorption in the visible range [33]. The degradation plots are presented in Figure 8. We observed that the soot degradation was slower than the MB degradation (Figure 6) denoting the higher stability of soot. By comparing the coatings, we observed a higher self-cleaning performance for the stone samples coated with Au-TiO_2/SiO_2 photocatalysts. These results followed the same trend as that observed in the MB degradation test, and confirmed that the AuNPs promotes the self-cleaning effect. Additionally, we observed that the soot degradation was greater for the granite samples according to the higher amount of photocatalyst onto granite surface.

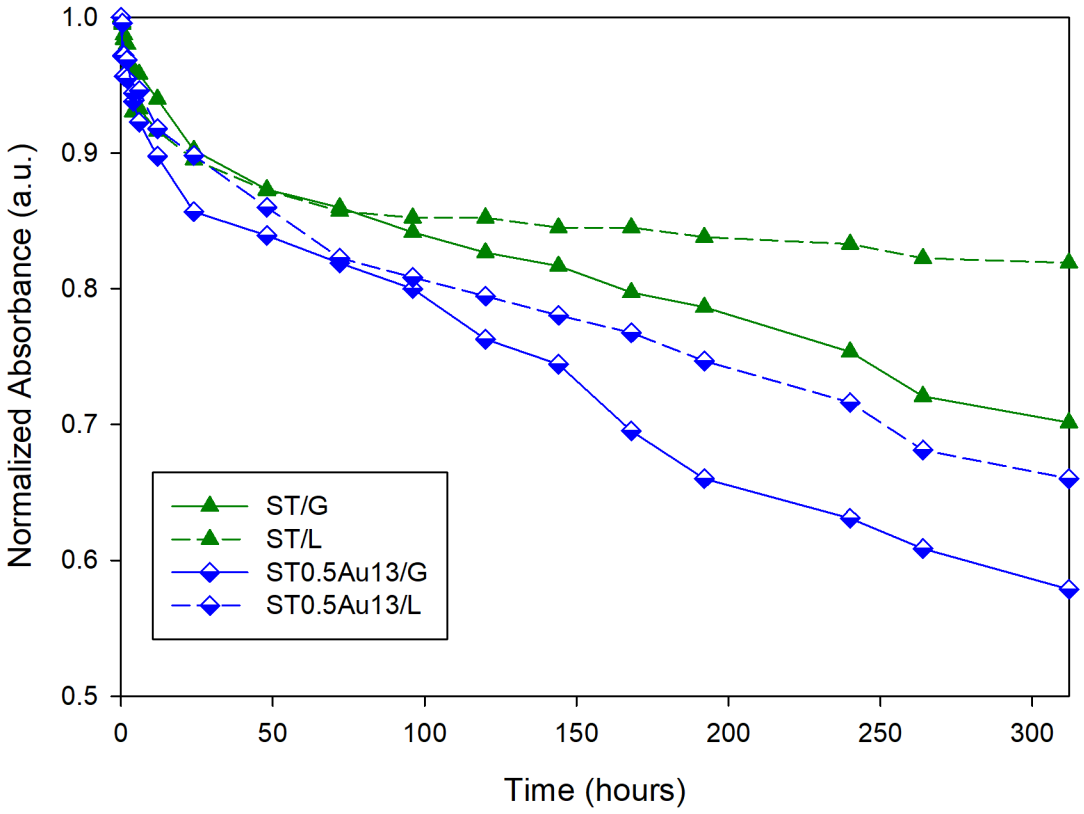

Figure 8. Evolution of soot absorbance on coated stone samples

Figure 9 compiles the results obtained for the NO de-polluting test. A NO degradation of 10-11% in presence of the untreated stones was measured, which is probably caused by chemical photoreactions with the water and oxygen in the sample or reactor walls under our experimental conditions. When the test took place using the TiO_2/SiO_2 coated samples, the NO degradation was noticeably increased demonstrating the photocatalytic oxidation produced by the coating. Regarding the Au-TiO_2/SiO_2 coated stones, the NO degradation was near the double of that corresponding to the TiO_2/SiO_2 coatings confirming that the photoactivity improvement induced by AuNPs doping remain in the coated materials. Finally, we also noted a greater de-polluting effect for the granite samples in connection with the lower granite porosity.

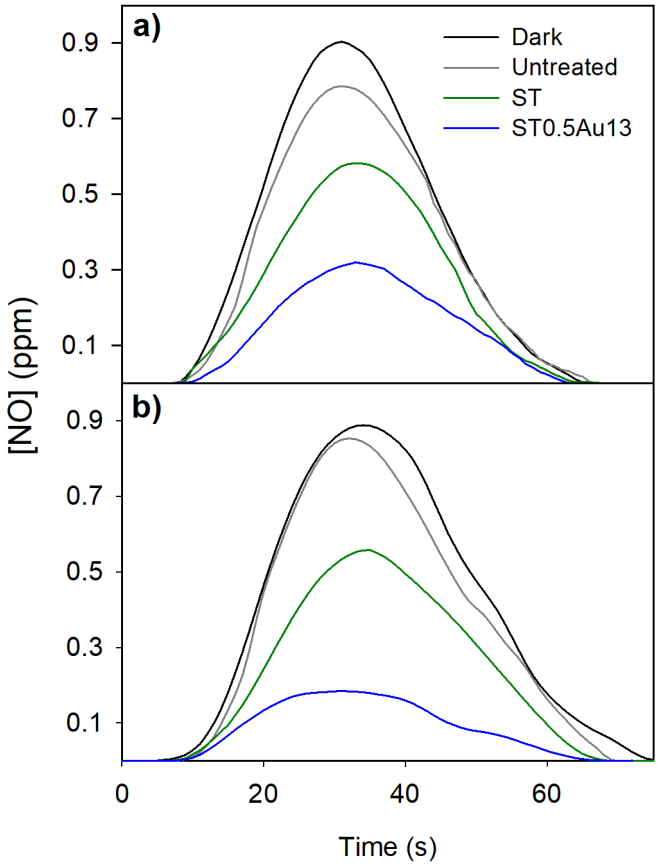

Figure 9. NO concentration curves obtained for the samples under dark conditions and after 30 minutes of UV-visible irradiation, a) limestone and b) granite

Table 3. Results of NO conversion of photodegradation test for stones.

Sample	% NO conversion
Untreated	11
ST/L	33
ST/G	42
ST0.5Au13/L	63
ST0.5Au13/G	79

4. Conclusions

Au-TiO_2/SiO_2 photocatalysts for building materials with self-cleaning and de-polluting performance has been obtained by using a sol-gel synthesis. Specifically, Au-TiO_2NPs were integrated into silica being applied by a simple procedure (spraying) on building materials. The sols spontaneously gel for producing long-lasting Au-TiO_2/SiO_2 coatings with photocatalytic properties. The TiO_2 integration in a silica matrix enhances its adherence to the substrate and the subsequent the coating durability. The AuNPs effectively increased the TiO_2 photoactivity and the self-cleaning and depolluting properties of the coated building materials.

A deeper analysis of the effect caused by the size and loading of AuNPs allows to optimize the formulation of the coating photocatalyst, in particular:

(1) The smallest AuNPs investigated (13 nm) produced a higher increase of TiO_2 photoactivity due to their better dispersion on TiO_2 and the higher Au-TiO_2 contact.

(2) The maximum photoactivity performance was reached for the intermedium AuNPs loading in the 0.25-1% range. The reduction of photoactivity for the highest AuNPs loading was

attributed to the formation of the big Au-TiO_2 agglomerates observed during the STEM characterization of the photocatalysts.

Conflict of interest

Authors declare that there are no conflicts of interest

Acknowledgments

This work has been supported by the Spanish Government/FEDER-EU (MAT2013-42934-R and MAT2017-84228-R). M. Luna would also like to thank the Spanish Government for his pre-doctoral grant (BES-2014-068031).

References

[1] European Environment Agency, European Union emission inventory report 1990–2014 under the UNECE Convention on Long-range Transboundary Air Pollution (LRTAP), 2016. https://doi.org/10.2800/18374.

[2] L. Bauleo, S. Bucci, C. Antonucci, R. Sozzi, M. Davoli, F. Forastiere, C. Ancona, Long-term exposure to air pollutants from multiple sources and mortality in an industrial area: a cohort study, Occup. Environ. Med. 76 (2019) 48–57. https://doi.org/10.1136/oemed-2018-105059.

[3] F.J. Kelly, J.C. Fussell, Size, source and chemical composition as determinants of toxicity attributable to ambient particulate matter, Atmos. Environ. 60 (2012) 504–526. https://doi.org/10.1016/j.atmosenv.2012.06.039.

[4] ICOMOS International Scientific Committe for Stone (ISCS), Illustrated Glossary on Stone Deterioration Patterns, 2010.

[5] World Health Organization, Health relevance of particulate matter from various sources, 2007. https://doi.org/5067587.

[6] F.M. Santos, Á. Gómez-Losada, J.C.M. Pires, Impact of the implementation of Lisbon low emission zone on air quality, J. Hazard. Mater. 365 (2019) 632–641. https://doi.org/10.1016/j.jhazmat.2018.11.061.

[7] L. Cassar, Photocatalysis of cementitious materials: Clean buildings and clean air, MRS Bull. 29 (2004) 328–331. https://doi.org/10.1557/mrs2004.99.

[8] J. Chen, C.S. Poon, Photocatalytic construction and building materials: From fundamentals to applications, Build. Environ. 44 (2009) 1899–1906. https://doi.org/10.1016/j.buildenv.2009.01.002.

[9] A. Di Paola, E. García-López, G. Marcì, L. Palmisano, A survey of photocatalytic materials for environmental remediation, J. Hazard. Mater. 211–212 (2012) 3–29. https://doi.org/10.1016/j.jhazmat.2011.11.050.

[10] A. Fujishima, X. Zhang, D.A. Tryk, TiO_2 photocatalysis and related surface phenomena, Surf. Sci. Rep. 63 (2008) 515–582. https://doi.org/10.1016/j.surfrep.2008.10.001.

[11] J. Lasek, Y.H. Yu, J.C.S. Wu, Removal of NOx by photocatalytic processes, J. Photochem. Photobiol. C Photochem. Rev. 14 (2013) 29–52. https://doi.org/10.1016/j.jphotochemrev.2012.08.002.

[12] T. Martinez, A. Bertron, E. Ringot, G. Escadeillas, Degradation of NO using photocatalytic coatings applied to different substrates, Build. Environ. 46 (2011) 1808–1816. https://doi.org/10.1016/j.buildenv.2011.03.001.

[13] M.Z. Guo, A. Maury-Ramirez, C.S. Poon, Photocatalytic activities of titanium dioxide

incorporated architectural mortars: Effects of weathering and activation light, Build. Environ. 94 (2015) 395–402. https://doi.org/10.1016/j.buildenv.2015.08.027.

[14] A. Folli, C. Pade, T.B. Hansen, T. De Marco, D.E. Macphee, TiO_2 photocatalysis in cementitious systems: Insights into self-cleaning and depollution chemistry, Cem. Concr. Res. 42 (2012) 539–548. https://doi.org/10.1016/j.cemconres.2011.12.001.

[15] R. Sugrañez, J.I. Álvarez, M. Cruz-Yusta, I. Mármol, J. Morales, J. Vila, L. Sánchez, Enhanced photocatalytic degradation of NO_x gases by regulating the microstructure of mortar cement modified with titanium dioxide, Build. Environ. 69 (2013) 55–63. https://doi.org/10.1016/j.buildenv.2013.07.014.

[16] R. Zouzelka, J. Rathousky, Photocatalytic abatement of NO_x pollutants in the air using commercial functional coating with porous morphology, Appl. Catal. B Environ. 217 (2017) 466–476. https://doi.org/10.1016/j.apcatb.2017.06.009.

[17] X.F. Chen, S.R. Lin, S.C. Kou, Effect of composite photo-catalysts prepared with recycled clay brick sands and nano-TiO_2 on methyl orange and NO_x removal, Constr. Build. Mater. 171 (2018) 152–160. https://doi.org/10.1016/j.conbuildmat.2018.03.099.

[18] P. Chin, G.W. Roberts, D.F. Ollis, Kinetic modeling of photocatalyzed soot oxidation on titanium dioxide thin films, Ind. Eng. Chem. Res. 46 (2007) 7598–7604. https://doi.org/10.1021/ie070083t.

[19] T. Ochiai, A. Fujishima, Photoelectrochemical properties of TiO_2 photocatalyst and its applications for environmental purification, J. Photochem. Photobiol. C Photochem. Rev. 13 (2012) 247–262. https://doi.org/10.1016/j.jphotochemrev.2012.07.001.

[20] A. Calia, M. Lettieri, M. Masieri, Durability assessment of nanostructured TiO_2 coatings applied on limestones to enhance building surface with self-cleaning ability, Build.

Environ. 110 (2016) 1–10. https://doi.org/10.1016/j.buildenv.2016.09.030.

[21] L. Bergamonti, G. Predieri, Y. Paz, L. Fornasini, P.P. Lottici, F. Bondioli, Enhanced self-cleaning properties of N-doped TiO_2 coating for Cultural Heritage, Microchem. J. 133 (2017) 1–12. https://doi.org/10.1016/j.microc.2017.03.003.

[22] L. Pinho, M. Rojas, M.J. Mosquera, Ag–SiO_2–TiO_2 nanocomposite coatings with enhanced photoactivity for self-cleaning application on building materials, Appl. Catal. B Environ. 178 (2015) 144–154. https://doi.org/10.1016/j.apcatb.2014.10.002.

[23] P. Munafò, E. Quagliarini, G.B. Goffredo, F. Bondioli, A. Licciulli, Durability of nano-engineered TiO_2 self-cleaning treatments on limestone, Constr. Build. Mater. 65 (2014) 218–231. https://doi.org/10.1016/j.conbuildmat.2014.04.112.

[24] M.Z. Guo, A. Maury-Ramirez, C.S. Poon, Self-cleaning ability of titanium dioxide clear paint coated architectural mortar and its potential in field application, J. Clean. Prod. 112 (2016) 3583–3588. https://doi.org/10.1016/j.jclepro.2015.10.079.

[25] F. Gherardi, A. Colombo, M. D'Arienzo, B. Di Credico, S. Goidanich, F. Morazzoni, R. Simonutti, L. Toniolo, Efficient self-cleaning treatments for built heritage based on highly photo-active and well-dispersible TiO_2 nanocrystals, Microchem. J. 126 (2016) 54–62. https://doi.org/10.1016/j.microc.2015.11.043.

[26] C. Kapridaki, N.-P. Maravelaki, TiO_2–SiO_2–PDMS nanocomposites with self-cleaning properties for stone protection and consolidation, Geol. Soc. London, Spec. Publ. 416 (2016) 285–292. https://doi.org/10.1144/SP416.6.

[27] L. Bergamonti, F. Bondioli, I. Alfieri, A. Lorenzi, M. Mattarozzi, G. Predieri, P.P. Lottici, Photocatalytic self-cleaning TiO_2 coatings on carbonatic stones, Appl. Phys. A. 122

(2016) 124. https://doi.org/10.1007/s00339-015-9560-y.

[28] L. Pinho, F. Elhaddad, D.S. Facio, M.J. Mosquera, A novel TiO_2–SiO_2 nanocomposite converts a very friable stone into a self-cleaning building material, Appl. Surf. Sci. 275 (2013) 389–396. https://doi.org/10.1016/j.apsusc.2012.10.142.

[29] L. Pinho, M.J. Mosquera, Photocatalytic activity of TiO_2-SiO_2 nanocomposites applied to buildings: Influence of particle size and loading, Appl. Catal. B Environ. 134–135 (2013) 205–221. https://doi.org/10.1016/j.apcatb.2013.01.021.

[30] J.M. De la Rosa, A.Z. Miller, J.S. Pozo-Antonio, J.A. González-Pérez, N.T. Jiménez-Morillo, A. Dionisio, Assessing the effects of UVA photocatalysis on soot-coated TiO_2-containing mortars, Sci. Total Environ. 605–606 (2017) 147–157. https://doi.org/10.1016/j.scitotenv.2017.06.127.

[31] M. Smits, C.K. Chan, T. Tytgat, B. Craeye, N. Costarramone, S. Lacombe, S. Lenaerts, Photocatalytic degradation of soot deposition: Self-cleaning effect on titanium dioxide coated cementitious materials, Chem. Eng. J. 222 (2013) 411–418. https://doi.org/10.1016/j.cej.2013.02.089.

[32] M. Smits, D. Huygh, B. Craeye, S. Lenaerts, Effect of process parameters on the photocatalytic soot degradation on self-cleaning cementitious materials, Catal. Today. 230 (2014) 250–255. https://doi.org/10.1016/j.cattod.2013.10.001.

[33] M. Luna, J. Delgado, M.L.A. Gil, M. Mosquera, TiO_2-SiO_2 coatings with a low content of AuNPs for producing self-cleaning building materials, Nanomaterials. 8 (2018) 177. https://doi.org/10.3390/nano8030177.

[34] P. Krishnan, M.H. Zhang, L.E. Yu, Removal of black carbon using photocatalytic silicate-based coating: Laboratory and field studies, J. Clean. Prod. 183 (2018) 436–448.

https://doi.org/10.1016/j.jclepro.2018.02.149.

[35] J.S. Pozo-Antonio, A. Dionísio, Self-cleaning property of mortars with TiO_2 addition using real diesel exhaust soot, J. Clean. Prod. 161 (2017) 850–859. https://doi.org/10.1016/j.jclepro.2017.05.202.

[36] S.G. Kumar, L.G. Devi, Review on modified TiO_2 photocatalysis under UV/visible light: Selected results and related mechanisms on interfacial charge carrier transfer dynamics, J. Phys. Chem. A. 115 (2011) 13211–13241. https://doi.org/10.1021/jp204364a.

[37] X. Zhang, Y.L. Chen, R.S. Liu, D.P. Tsai, Plasmonic photocatalysis., Rep. Prog. Phys. 76 (2013) 046401. https://doi.org/10.1088/0034-4885/76/4/046401.

[38] A. Ayati, A. Ahmadpour, F.F. Bamoharram, B. Tanhaei, M. Mänttäri, M. Sillanpää, A review on catalytic applications of Au/TiO_2 nanoparticles in the removal of water pollutant., Chemosphere. 107 (2014) 163–174. https://doi.org/10.1016/j.chemosphere.2014.01.040.

[39] A. Primo, A. Corma, H. García, Titania supported gold nanoparticles as photocatalyst, Phys. Chem. Chem. Phys. 13 (2011) 886–910. https://doi.org/10.1039/C0CP00917B.

[40] A. Truppi, M. Luna, F. Petronella, A. Falcicchio, C. Giannini, R. Comparelli, M. Mosquera, Photocatalytic activity of TiO_2/AuNRs–SiO_2 nanocomposites applied to building materials, Coatings. 8 (2018) 296. https://doi.org/10.3390/coatings8090296.

[41] L. Bergamonti, I. Alfieri, M. Franzò, A. Lorenzi, A. Montenero, G. Predieri, M. Raganato, A. Calia, L. Lazzarini, D. Bersani, P.P. Lottici, Synthesis and characterization of nanocrystalline TiO_2 with application as photoactive coating on stones, Environ. Sci. Pollut. Res. 21 (2014) 13264–13277. https://doi.org/10.1007/s11356-013-2136-5.

[42] R.E. Ramírez-García, J.A. González-Rodríguez, M. Arroyo-Ortega, S.A. Pérez-García, L. Licea-Jiménez, Engineered TiO_2 and SiO_2-TiO_2 films on silica-coated glass for increased thin film durability under abrasive conditions, Int. J. Appl. Ceram. Technol. 14 (2017) 39–49. https://doi.org/10.1111/ijac.12614.

[43] V.B. Koli, S. Mavengere, J.-S. Kim, Photocatalytic properties of TiO_2-SiO_2-coated concrete on toluene gas, Mater. Res. Express. 5 (2018) 125006. https://doi.org/10.1088/2053-1591/aae01c.

[44] A. Rosales, A. Maury-Ramírez, R.M.-D. Gutiérrez, C. Guzmán, K. Esquivel, SiO_2@TiO_2 Coating: Synthesis, Physical Characterization and Photocatalytic Evaluation, Coatings. 8 (2018) 120. https://doi.org/10.3390/coatings8040120.

[45] M.J. Mosquera, L.A.M. Carrascosa, N. Badreldin, Producing superhydrophobic/oleophobic coatings on Cultural Heritage building materials, Pure Appl. Chem. 90 (2018) 551–561. https://doi.org/10.1515/pac-2017-0404.

[46] R. Zarzuela, M. Carbú, M.L.A. Gil, J.M. Cantoral, M.J. Mosquera, CuO/SiO_2 nanocomposites: A multifunctional coating for application on building stone, Mater. Des. 114 (2017) 364–372. https://doi.org/10.1016/j.matdes.2016.11.009.

[47] L.A.M. Carrascosa, D.S. Facio, M.J. Mosquera, Producing superhydrophobic roof tiles, Nanotechnology. 27 (2016) 095604. https://doi.org/10.1088/0957-4484/27/9/095604.

[48] B. Tian, C. Li, F. Gu, H. Jiang, Synergetic effects of nitrogen doping and Au loading on enhancing the visible-light photocatalytic activity of nano-TiO_2, Catal. Commun. 10 (2009) 925–929. https://doi.org/10.1016/j.catcom.2008.12.029.

[49] V. Subramanian, E. Wolf, P. V. Kamat, Semiconductor−Metal composite nanostructures. To what extent do metal nanoparticles improve the photocatalytic activity of TiO_2 films?,

J. Phys. Chem. B. 105 (2001) 11439–11446. https://doi.org/10.1021/jp011118k.

[50] M. Haruta, Size- and support-dependency in the catalysis of gold, Catal. Today. 36 (1997) 153–166. https://doi.org/10.1016/S0920-5861(96)00208-8.

[51] B. Cojocaru, Ş. Neaţu, E. Sacaliuc-Pârvulescu, F. Lévy, V.I. Pârvulescu, H. Garcia, Influence of gold particle size on the photocatalytic activity for acetone oxidation of Au/TiO_2 catalysts prepared by dc-magnetron sputtering, Appl. Catal. B Environ. 107 (2011) 140–149. https://doi.org/10.1016/j.apcatb.2011.07.007.

[52] B. Tian, J. Zhang, T. Tong, F. Chen, Preparation of Au/TiO_2 catalysts from Au(I)-thiosulfate complex and study of their photocatalytic activity for the degradation of methyl orange, Appl. Catal. B Environ. 79 (2008) 394–401. https://doi.org/10.1016/j.apcatb.2007.11.001.

[53] ISO 10678; Fine ceramics (advanced ceramics, advanced technical ceramics); Determination of photocatalytic activity of surfaces in an aqueous medium by degradation of methylene blue, 2010.

[54] X. Yan, T. Ohno, K. Nishijima, R. Abe, B. Ohtani, Is methylene blue an appropriate substrate for a photocatalytic activity test? A study with visible-light responsive titania, Chem. Phys. Lett. 429 (2006) 606–610. https://doi.org/10.1016/j.cplett.2006.08.081.

[55] M. Rochkind, S. Pasternak, Y. Paz, Using dyes for evaluating photocatalytic properties: A critical review, Molecules. 20 (2015) 88–110. https://doi.org/10.3390/molecules20010088.

[56] S. Link, M.A. El-Sayed, Spectral properties and relaxation dynamics of surface plasmon electronic oscillations in gold and silver nanodots and nanorods, J. Phys. Chem. B. 103

(1999) 8410–8426. https://doi.org/10.1021/jp9917648.

[57] M. Thommes, K. Kaneko, A. V. Neimark, J.P. Olivier, F. Rodriguez-Reinoso, J. Rouquerol, K.S.W. Sing, Physisorption of gases, with special reference to the evaluation of surface area and pore size distribution (IUPAC Technical Report), Pure Appl. Chem. 87 (2015) 1051–1069. https://doi.org/10.1515/pac-2014-1117.

[58] L. Pinho, J.C. Hernández-Garrido, J.J. Calvino, M.J. Mosquera, 2D and 3D characterization of a surfactant-synthesized TiO_2–SiO_2 mesoporous photocatalyst obtained at ambient temperature, Phys. Chem. Chem. Phys. 15 (2013) 2800–2808. https://doi.org/10.1039/c2cp42606d.

[59] M. Kruk, M. Jaroniec, Gas adsorption characterization of ordered organic-inorganic nanocomposite materials, Chem. Mater. 13 (2001) 3169–3183. https://doi.org/10.1021/cm0101069.

[60] D.S. Facio, M. Luna, M.J. Mosquera, Facile preparation of mesoporous silica monoliths by an inverse micelle mechanism, Microporous Mesoporous Mater. 247 (2017) 166–176. https://doi.org/10.1016/j.micromeso.2017.03.041.

[61] S. Linic, P. Christopher, D.B. Ingram, Plasmonic-metal nanostructures for efficient conversion of solar to chemical energy, Nat. Mater. 10 (2011) 911–921. https://doi.org/10.1038/nmat3151.

[62] C. Miliani, M.L. Velo-Simpson, G.W. Scherer, Particle-modified consolidants: A study on the effect of particles on sol-gel properties and consolidation effectiveness, J. Cult. Herit. 8 (2007) 1–6. https://doi.org/10.1016/j.culher.2006.10.002.

[63] J.F. Illescas, M.J. Mosquera, Surfactant-Synthesized PDMS/Silica Nanomaterials Improve Robustness and Stain Resistance of Carbonate Stone, J. Phys. Chem. C. 115

(2011) 14624–14634. https://doi.org/10.1021/jp203524p.

[64] C. Mendoza, A. Valle, M. Castellote, A. Bahamonde, M. Faraldos, TiO_2 and TiO_2–SiO_2 coated cement: Comparison of mechanic and photocatalytic properties, Appl. Catal. B Environ. 178 (2015) 155–164. https://doi.org/10.1016/j.apcatb.2014.09.079.

[65] G. Borsoi, R. Veiga, A.S. Silva, Effect of nanostructured lime-based and silica-based products on the consolidation of historical renders, in: 3rd Hist. Mortars Conf., 2013: pp. 1–9. https://doi.org/10.13140/2.1.1988.9282.

[66] A. Houas, Photocatalytic degradation pathway of methylene blue in water, Appl. Catal. B Environ. 31 (2001) 145–157. https://doi.org/10.1016/S0926-3373(00)00276-9.

[67] L. Pinho, M.J. Mosquera, Titania-silica nanocomposite photocatalysts with application in stone self-cleaning, J. Phys. Chem. C. 115 (2011) 22851–22862. https://doi.org/10.1021/jp2074623.

[68] A. Mills, J. Wang, Photobleaching of methylene blue sensitised by TiO_2: an ambiguous system?, J. Photochem. Photobiol. A Chem. 127 (1999) 123–134. https://doi.org/10.1016/S1010-6030(99)00143-4.

[69] K. Rajeshwar, M.E. Osugi, W. Chanmanee, C.R. Chenthamarakshan, M.V.B. Zanoni, P. Kajitvichyanukul, R. Krishnan-Ayer, Heterogeneous photocatalytic treatment of organic dyes in air and aqueous media, J. Photochem. Photobiol. C Photochem. Rev. 9 (2008) 171–192. https://doi.org/10.1016/j.jphotochemrev.2008.09.001.

[70] T. Tatsuma, S. Tachibana, T. Miwa, D.A. Tryk, A. Fujishima, Remote bleaching of methylene blue by UV-irradiated TiO_2 in the gas phase, J. Phys. Chem. B. 103 (1999) 8033–8035. https://doi.org/10.1021/jp9918297.

Supplementary materials

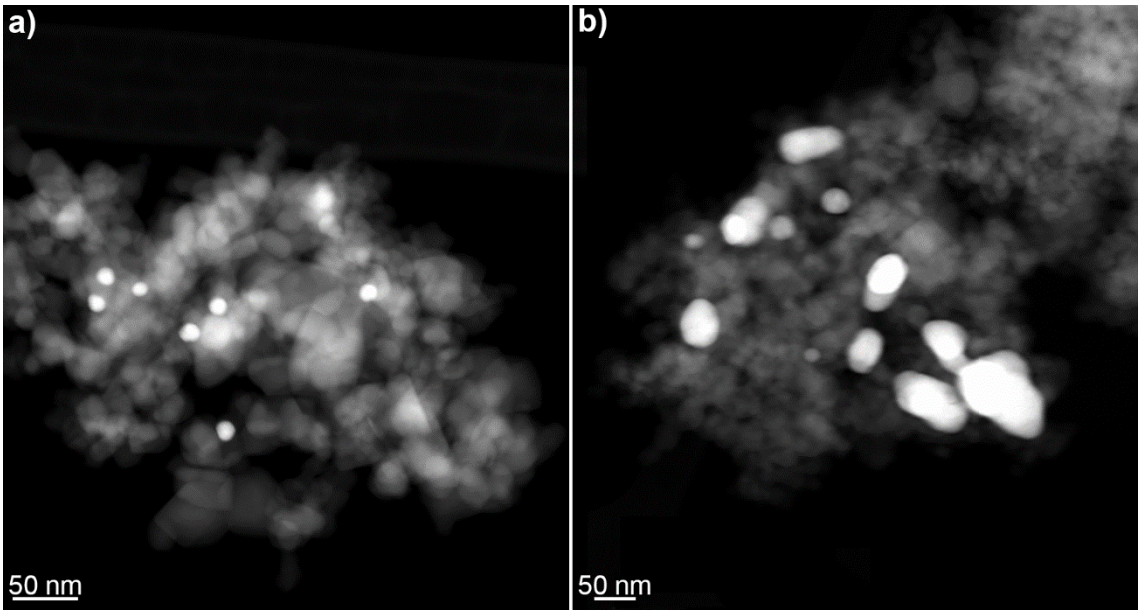

Figure S1. HAADF-STEM image of two representative Au-TiO_2 nanopowders with a Au/TiO_2 loading of 0.5%. a) containing the smaller AuNPs prepared with the highest citrate/Au ratio; b) containing the bigger AuNPs prepared with the lowest citrate/Au ratio. Gold nanoparticles can be displayed by their bright contrast

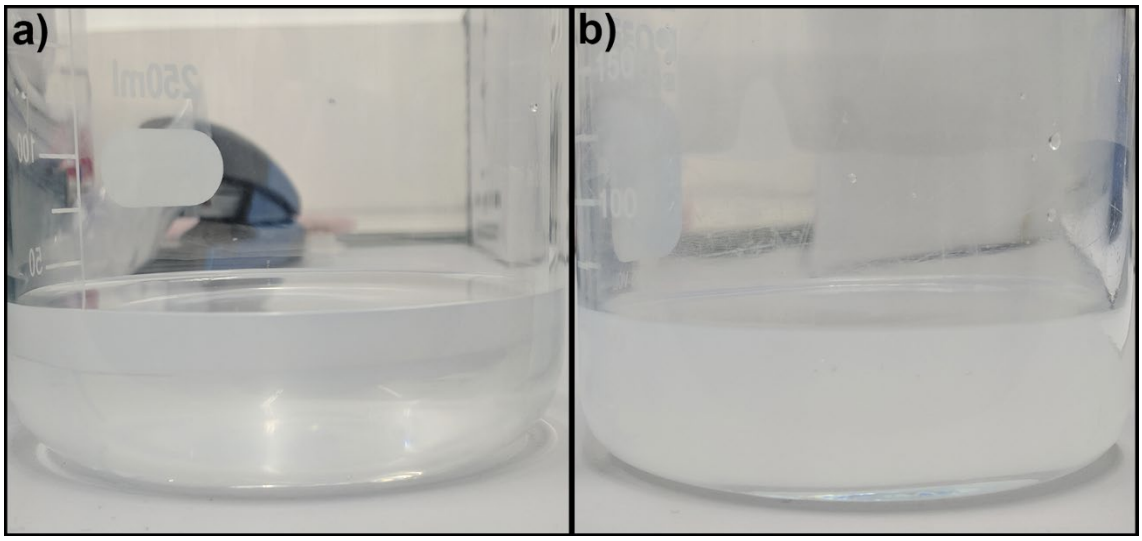

Figure S2. Washing water obtained after sonication of limestone coated samples immersed in water, a) ST/L and b) T/L.

Chapter 6

One-pot synthesis of Au/N-TiO_2 photocatalysts for environmental applications: enhancement of dyes and NO_x photodegradation

One-pot synthesis of Au/N-TiO_2 photocatalysts for environmental applications: enhancement of dyes and NO_x photodegradation

Sent to Powder Technology

Manuel Luna[a], José M. Gatica[b*], Hilario Vidal[b], María J. Mosquera[a**]

[a]Departamento de Química Física, Universidad de Cádiz, Puerto Real 11510, Spain

[b]Departamento C.M., I.M. y Química Inorgánica, Universidad de Cádiz, Puerto Real 11510, Spain

Corresponding authors: *josemanuel.gatica@uca.es; **mariajesus.mosquera@uca.es

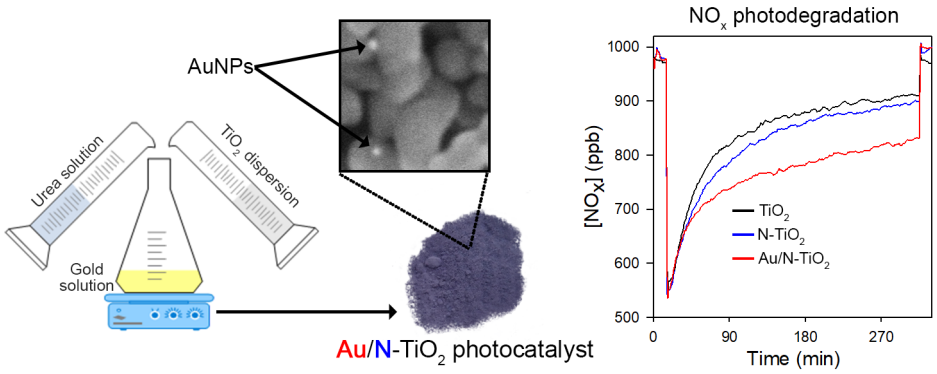

Highlights

Innovative one-pot synthesis of N and AuNPs doped TiO_2 environmental photocatalysts

Synergic action between Au and N-doping greatly enhanced TiO_2 activity and NO removal

Deposited AuNPs activated TiO_2 under visible radiation promoting NO photodegradation

Au/N-TiO_2 integration in a silica matrix favoured application preserving properties

Abstract

Au/N-TiO_2 photocatalysts with enhanced photoactivity thanks to nitrogen doping and gold nanoparticles (AuNPs) controlled deposition onto titania have been obtained by means of a simple and innovative one-pot synthesis promoting synergetic activity between these two approaches. The activity of the materials under study was evaluated by methylene blue and NO_x degradation tests as models of environmental remediation processes for water purification and air depollution. The use of a deposition-precipitation method employing urea allows obtaining Au/N-TiO_2 photocatalysts containing 0.3 at% of nitrogen and 0.5 wt% of gold. The results obtained confirmed that the presence of both, nitrogen and AuNPs, enhanced the TiO_2 photoactivity increasing the photodegradation of the dye and NO_x in a factor of 4.5 and 1.7, respectively. In particular, the AuNPs enabled the photoactivity under visible light and improved substantially the selectivity of the NO degradation process. The photocatalysts here proposed maintain their properties as they are integrated into a silica matrix producing a product with potential use for the coating of different substrates, such as building materials for application in urban areas and fabrics or foams for the photocatalytic filters production.

Keywords: photocatalyst; TiO_2; nitrogen doping; gold; Au/N-TiO_2; NO_x depolluting

1. Introduction

TiO_2 exhibits photoactivity in the presence of solar light and therefore it can show depolluting, self-cleaning and biocide activity. However, its performance is limited by its low absorption in the visible range, the most important component of solar radiation. This drawback can be overcome by titania doping with gold nanoparticles (AuNPs) [1,2]. According to the literature, the *in situ* Au deposition on the TiO_2 support instead of preformed AuNPs improves the Au-TiO_2 interaction and subsequently their photocatalytic enhancement [3]. The starting point of

this work is to adopt this strategy to produce Au-TiO_2 photocatalysts with improved properties with respect to those obtained by mixing of preformed Au and TiO_2 that we previously reported [1,2].

The simplest method for producing Au on TiO_2 is the wet impregnation, where the support is immersed in a gold salt solution and Au species are adsorbed on the titania surface by electrostatic interactions affected by the pH equilibriums [4,5], followed by separation and calcination steps. However, this procedure is unsuitable for gold because of: (i) its low yield, (ii) the AuNPs size is not under control and (iii) the resultant catalyst contains a considerable amount of impurities. Therefore other more tedious methods are preferred [6,7]. An easy modification of wet impregnation, providing an effective way to get well-dispersed supported catalysts, is the deposition-precipitation method (DP). In DP, an alkali is employed to favour the precipitation and adsorption of the gold salt as $Au(OH)_3$ on the support surface and the size of the AuNPs obtained can be controlled by adjusting the pH [8,9]. The drawback of DP in the specific case of Au-TiO_2 synthesis is associated to the compromise situation between the required AuNPs size and the gold deposition yield, because both parameters decrease for pH values above 5.5 [8,10,11]. In order to prevent this drawback, Geus [12] avoided the high local OH^- concentration, by using urea, which decomposes at temperatures higher than 60°C producing OH^- ions, which are consumed in the gold precipitation. The DP-urea method has been employed in the preparation of well dispersed gold supported catalysts with small particle size and a high yield [11,13]. Recently, it has been demonstrated that gold precipitation is not exactly promoted by the slow OH^- liberation, confirming that the mechanism involves the formation of gold intermediates with the products of urea decomposition [10].

According to the previous findings, the DP-urea method was chosen to prepare the photocatalysts of this study, because it allows getting AuNPs with size suitable for an effective

TiO_2 photoactivity enhancement. On the other hand, the urea is a nitrogen source widely employed for doping TiO_2 [14–16]. The nitrogen doping is another effective approach for the TiO_2 photoactivity enhancement [17] and it can be combined with the AuNPs in order to reach a synergetic effect on the TiO_2 photocatalytic activity, as demonstrated when gold was deposited on titania previously doped with nitrogen [18–20].

Considering all this background, the main target of this work is to prepare Au/N-TiO_2 photocatalysts with activity under visible light by using two different approaches creating synergies by a single one-pot procedure based on the DP-urea method: (i) nitrogen doping of TiO_2 and (ii) AuNPs deposition onto TiO_2. Specifically, the procedure was adapted to get a nearly 0.5 wt% Au gold content and the amount of urea employed was increased to ensure the nitrogen doping. In addition, three types of commercial TiO_2 particles with different size were employed in order to study the role played on the performance. This strategy simplifies the usual procedure for Au/N-TiO_2 synthesis where two steps are required: 1) the nitrogen doping of titania, and 2) the gold deposition in the previously prepared nitrogen-doped TiO_2. An in-depth characterization of the photocatalysts was carried out. The enhanced photoactivity caused by the synergy activity of nitrogen doping and gold AuNPs was investigated through methylene blue (MB) degradation test. Additionally, the NO_x depolluting effect of the photocatalysts under study, one of the most popular application purposes, was also studied.

In order to produce an effective photocatalytic material with potential applications in environmental remediation, the TiO_2 commonly requires its integration in a binder, such as silica. The binder promotes the photocatalyst separation from the liquid in water treatment application and enhances the adhesion to specific substrates in air purification or self-cleaning applications [21–24]. The choice as a binder of a porous silica matrix with large surface area that allows the diffusion of substances to the photoactive centres promoting the photoactivity

in comparison with a non-porous matrix is desirable [25]. According to these findings, the Au/N-TiO_2 particles were incorporated into a silica sol, following a method previously described [2] to produce Au/N-TiO_2/SiO_2 photocatalysts. In order to verify if the photoactivity is preserved once the Au/N-TiO_2 is integrated in the silica matrix, the photocatalytic performance and NO_x depolluting activity were also re-evaluated.

2. Experimental

2.1. Au/N-TiO_2 synthesis

6 g of TiO_2 were dispersed in 100 ml of water in an ultrasonic cleaner for 10 minutes, the TiO_2 dispersion being mixed under vigorous stirring with 100 ml of $KAuCl_4$ solution (1.9 mM) and 100 ml of urea solution (75% w/w urea/H_2O). The mixture was maintained under stirring and heated at 80°C for 2 hours. The TiO_2 was centrifuged, washed with water several times, dried at 100 °C overnight and, finally, calcined at 273 °C for 4 hours.

Three types of commercial TiO_2 particles from Evonik were employed for the photocatalysts preparation: Aeroxide P25, Aeroxide P90 and the granulated form of P25, VP Aeroperl P25/20. Some properties of these particles, provided by the manufacturer, are compiled in Table 1.

Table 1. Characteristics of TiO_2 particles employed

Particle	S_{BET} (m^2/g)	Anatase/Rutile Ratio	Particle size	Density (g/cm^3)
P25	50±15	80/20	21 nm[a]	0.13
P90	90±20	90/10	14 nm[a]	0.12
VP	50±15	80/20	20 μm[b]	0.70

[a] primary particle size

[b] particle granulate size

For comparative purposes, two alternative syntheses were also carried out as follows: (1) Au was removed by replacing the $KAuCl_4$ solution by water in order to get the corresponding nitrogen doped particles; (2) nitrogen was removed by replacing urea by water to obtain the TiO_2 particles subjected to the same thermal treatment.

2.2. Au/N-TiO_2 characterization

The tapped density of the powdered photocatalysts was determined using a procedure adapted from the standard ISO 787-11:1981 [26].

Inductively coupled plasma atomic emission spectroscopy (ICP-AES) analysis of gold content of the Au/N-TiO_2 materials was performed using an Iris Intrepid spectrophotometer from Thermo Scientific.

UV–visible reflectance spectra of particles were recorded on a UV-2600 spectrophotometer from Shimadzu equipped with an ISR-2600 integrating sphere, using $BaSO_4$ powder as reference. The band gap values were calculated by using the Kubelka-Munk function and the Tauc plot [27,28].

The X-ray diffraction (XRD) study was carried out with a X-ray powder D8 Advance diffractometer from Bruker, equipped with a secondary monochromator, Cu tube X-ray, using Cu K_α radiation. The phase composition was determined by means of a FullProf [29] based software that employs the Rietveld refinement [30], and the crystallite size was calculated using the Scherrer equation [31].

Textural characterization was performed by N_2 physisorption at -196 ºC, using an Autosorb IQ gas sorption analyser from Quantachrome. Analysis was performed using approximately 0.3 g of samples outgassed at 150 ºC under vacuum. The Brunauer-Emmett-Teller (BET) surface

area was determined using the multipoint BET method within the P/P_0 interval 0.025-0.30. The total pore volume was obtained at P/P_0=0.995. The Barrett-Joyner-Halenda (BJH) pore size distributions were calculated from the isotherm desorption branches.

X-ray Photoelectron Spectroscopy (XPS) measurements of the samples were acquired on an Axis Ultra DLD spectrometer from Kratos. The powder samples were analysed as pellets using Al K_α radiation (1486.6 eV) at a power of 150 W, and the binding energy (BE) scale was corrected using the C 1s core level from adventitious carbon at 284.8 eV.

The TiO_2 and Au particle size was studied using electron microscopy. Scanning Electron Microscopy (SEM) images were recorded in a Nova NanoSem microscope from FEI Company operating at 5kV in field immersion mode and using secondary electrons and a Through the Lens Detector (TLD). High Angle Annular Dark Field Scanning Transmission Electron Microscopy (HAADF-STEM) images were taken using a JEOL 2010F TEM/STEM microscope operated at 200 kV with an electron probe of 0.5 nm and a camera length of 10 cm.

2.3. Au/N-TiO_2 photocatalytic activity

First, the decolourization of methylene blue (MB) solution was employed to evaluate the photocatalytic activity of the different TiO_2 particles under study. 10 mg of TiO_2 particles were dispersed in 20 ml of water using an ultrasonic cleaner for 15 minutes and 200 µl of MB solution 1 mM was added in order to get a MB concentration nearly 10^{-5} M. The mixture was kept in the dark under vigorous stirring for 30 minutes to ensure the complete MB adsorption on TiO_2 before the test beginning. An Ultra Vitalux 300W lamp from Osram was placed above the solution providing an irradiance of 60 W/m^2, measured using a PM100D power meter equipped with a detector S302C from Thorslabs. The UV-Visible spectra of the solution were recorded using the UV-2600 spectrophotometer at progressive irradiation times, after solid separation by

centrifugation. The degradation plots were represented using the Abs/Abs_0 at 664 nm and the results were fitted to a first order rate equation, being the correlation coefficients higher than 0.96, obtaining the corresponding rate constants. Additional tests using different illumination were carried out in order to study the effect of the wavelength employed. Irradiation of 15W fluorescent blacklight bulb lamp at 15 W/m^2 and filtered irradiation of Ultra Vitalux lamp at 60 W/m^2 were employed.

Next, selected particles were deposited on 10x5x0.4 cm glass plates according to a method previously reported [32]. These TiO_2 coated glasses were employed for evaluating the NO photo-oxidation using the ISO 22197-1 standard [33], details of the system employed can be found in the literature [32,34]. The amount of NO and NO_x removed and the NO_2 generated were calculated employing the following expressions.

$$n_{NO} = \frac{f}{22.4}\int_{t_{on}}^{t_{off}} [NO]_{in} - [NO]_{out}\, dt$$

$$n_{NO_2} = \frac{f}{22.4}\int_{t_{on}}^{t_{off}} [NO_2]_{out}\; dt$$

$$n_{NO_x} = n_{NO} - n_{NO_2}$$

Where n_{xx} are the µmol of gas removed or generated, f is the normalized air flow in l/min (0ºC, 101.3 kPa), t_{off} and t_{on} are the times of lamp switch off and on respectively, $[NO]_{in}$ is the supply NO air concentration in ppm, $[NO]_{out}$ is the NO air concentration at the reactor exit in ppm and $[NO_2]_{out}$ is the NO_2 air concentration at the reactor exit in ppm.

Also, the selectivity to NO_2 of the process was calculated as follows:

$$\%\, NO_2\; selectivity = \; 100 \cdot \frac{n_{NO_2}}{n_{NO}}$$

In order to increase the amount of NO_x removed during the test, the TiO_2 coated glass samples previously tested were modified employing an alkali that promotes the elimination of HNO_3 in the form of nitrates. Firstly, the samples were consciously rinsed with water to remove the nitric acid produced, then 2 ml of a $Ca(OH)_2$ water dispersion (4 mg/ml) were deposited in each sample and finally, once dry, the NO photo-oxidation of samples was tested again.

An alternative preparation method of TiO_2 coated glass samples was employed to emphasize the photoactivity differences among the TiO_2 particles under study. A first TiO_2 layer was prepared on the glass surface according to the method previously employed, next 5 ml of a water dispersion containing 50 mg of $Ca(OH)_2$ and 50 mg of TiO_2 were deposited onto the first TiO_2 layer. The resultant samples were employed to perform the photo-oxidation NO_x tests.

2.4. Integration of Au/N-TiO_2 in a silica matrix, characterization and photocatalytic evaluation

The TiO_2 particles were mixed at 4% w/v with a silica precursor, TES40 WN (Wacker), an ethylsilicate oligomer that provides approximately 41% of silica upon complete hydrolysis, according to the procedure previously described [2]. The synthesized sols were designated preceding a letter S to the name of TiO_2 particles that they contain. Immediately after the synthesis 15 ml of sols were disposed on Ø85 mm plastic Petri dishes and maintained at 18±0.5 °C of temperature and 53±3 % of humidity. The spontaneous sol-gel transition took place overnight and the gels were dried at the same conditions until constant weight before their characterization and evaluation.

The UV-Visible spectra and nitrogen physisorption isotherms of the xerogels were obtained using the methodology previously described. In this case, the pore size distributions were calculated fitting the results of adsorption branches to a hybrid NLDFT (non-local density

functional theory) approach [35], a model considering that nitrogen adsorption on silica with cylindrical pores was employed.

The powdered xerogels were employed to perform the MB degradation test previously described. The following modifications were done: 50 mg of xerogel was employed, MB concentration was nearly $5 \cdot 10^{-5}$ M, the MB solution and xerogels were stirred during 1 hour before the irradiation, and 100 W/m^2 non-filtered irradiation of Ultra Vitalux lamp was employed.

For testing the xerogels, the NO degradation procedure was modified respect to that employed for particle evaluation. 2 g of powdered xerogel were disposed in a 15x1.8x0.2 cm cavity of an acrylic resin semi-cylinder and placed into a tubular (2.2 cm inner diameter) quartz reactor, (see diagram in Figure S1 in the supplementary information). The air was bubbled by a gas-washing bottle containing demineralised water in order to provide humidity to the air. The air was mixed with NO to obtain a 1000 ml/min flow with a 3 ppm NO concentration that was sent to the reactor. The sample was irradiated at 25 W/m^2 using two 15W daylight fluorescent light tubes. The NO and NOx concentrations were measured using a NGA 2000 model chemiluminescence CLD NO/NOx analyser module from Emerson-Rosemount Analytical. The sample was irradiated for a short period and the NO conversion and selectivity towards NO_2 were defined using the average concentrations according to the following equations:

$$\%\ \text{NO conversion} = 100 \cdot \frac{[\text{NO}]_{\text{in}} - [\text{NO}]_{\text{out}}}{[\text{NO}]_{\text{in}}}$$

$$\%\ \text{Selectivity} = 100 \cdot \frac{[\text{NO}_2]_{\text{out}}}{[\text{NO}]_{\text{in}} - [\text{NO}]_{\text{out}}}$$

where $[NO]_{inlet}$ represents the concentration of NO in the feedstream and $[NO]_{outlet}$ and $[NO_2]_{outlet}$ are the concentration of NO or NO_2 in the outlet stream, respectively.

3. Results and discussion

3.1. Au/N-TiO_2characterization

As well known, low amounts of P25 and P90 fill large volumes and they easily float in the air due to their low density. After the synthesis, the P25 and P90 particles showed a drastic compaction multiplying their density by 6.5 (Table 2) whereas the density of VP, initially compacted in a granulated form, was only increased by 25%. It should be highlighted that the primary particles (P25 and P90) are significantly agglomerated during the synthesis process.

Table 2. Properties of synthetized particles

Sample	Density (g/cm^3)	Au loading (wt%)	Band Gap (eV)	Phase content[a] (%)	Crystallite size[a] (nm)	S_{BET} (m^2/g)	V_{pore} (ml/g)
P25	0.12	n.a.	3.32	[82.8](17.2)	[21.3](31.2)	53	0.247
N-P25	0.79	n.a.	3.16	[83.4](16.6)	[22.0](32.7)	49	0.461
Au/N-P25	0.78	0.47±0.02	3.14	[82.5](17.5)	[21.7](32.7)	61	0.488
P90	0.13	n.a.	3.27	[88.1](11.9)	[13.8](21.3)	97	0.690
N-P90	0.83	n.a.	3.14	[88.9](11.1)	[12.5](18.7)	99	0.443
Au/N-P90	0.82	0.51±0.01	3.11	[88.6](11.4)	[12.4](21.2)	108	0.446
VP	0.67	n.a.	3.11	[81.1](18.9)	[21.3](31.8)	50	0.607
N-VP	0.85	n.a.	3.13	[82.6](17.4)	[21.1](32.2)	51	0.469
Au/N-VP	0.85	0.47±0.02	3.13	[80.9](19.1)	[21.5](31.3)	54	0.512

[a][Anatase](Rutile)

The ICP analysis revealed that the gold content was 0.47% for P25 and VP and 0.51% for P90, which represents a synthesis yield of 75 and 82 %, respectively. It is remarkable that P25 and VP, with the same surface area, showed the same gold content and P90, with higher surface

area, showed a slightly higher value. This confirms that the amount of gold deposited can be related with the TiO_2 surface area.

The TiO_2 colour was also modified after the synthesis. Specifically, the nitrogen doped particles showed a slightly yellowish colour whereas the particles containing gold had an intense purple-blue colour that confirmed the AuNPs presence (see Figure S2). The UV-Visible spectra of the particles under study (Figure 1) confirmed a slightly increase of visible absorption for N-TiO_2 particles. This low increase indicated that the amount of nitrogen incorporated to TiO_2 was below 1 % [36], but it has been demonstrated that a low nitrogen concentration can promote the trapping of photogenerated charge carriers [37], which is essential to enhance the TiO_2 photoactivity. On the other hand, the Au/N-TiO_2 particles had a considerable visible absorption with a band centred at 550-560 nm due to the localized surface plasmon resonance (LSPR) effect of AuNPs [38], this band being more intense for Au/N-P90 due to its higher gold content, as previously discussed. The band gap values calculated for P25 and P90 were around 3.3 eV (Table 2), which is close to the value for anatase (3.2) and also to those calculated by other authors [39–42]. The nitrogen doping produced a reduction of nearly 0.15 eV because the nitrogen introduces new energy levels in the TiO_2 at higher energy than the valence band [14]. The presence of AuNPs also produced a slightly decrease of the band gaps values. VP particles showed a lower band gap value than P25 and P90 but it was not modified after nitrogen doping or AuNPs addition.

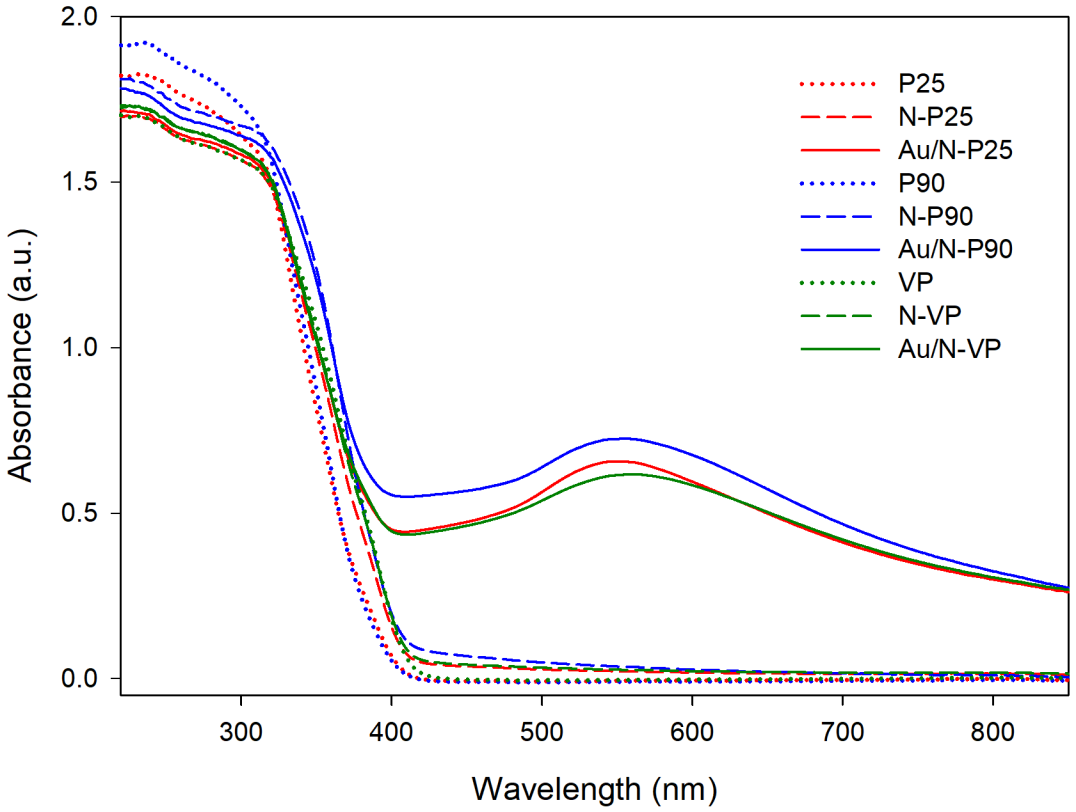

Figure 1. UV-Visible spectra of particles under study.

The XRD patterns (Figure S3 in the supplementary information) revealed that the starting titania samples are composed of anatase and rutile and no modification of the diagrams were observed after the synthesis performed. In particular, no gold peaks were observed due to the low size and concentration of AuNPs. Comparing the different particle series, the P25 and VP patterns were nearly identical, as a result of VP being an agglomerate of P25 primary particles. Regarding to P90, they showed wider peaks related to their lower particle size. The unchanged patterns after synthesis indicate that the low temperature calcination did not bring about the phase transformation from anatase to rutile nor induced the growth of the particles. The phase analysis reported anatase/rutile relations that nearly matched the values indicated by the manufacturer (see Table 2). The anatase crystallite sizes calculated for the different particles were nearly the same as those of the primary particles provided by the manufacturer (Table 2).

The rutile crystallite sizes were in all cases around 50% higher than the corresponding ones for anatase.

All samples showed nitrogen physisorption isotherms (Figure 2) of type IV(a), most of them with hysteresis H3-type, except N-P90 and Au/N-P90 with a nearly H1 hysteresis [43]. H3 hysteresis is characteristic of a mesoporous solid with a wide pore distribution containing macropores, whereas H1 is characteristic of mesoporous materials composed by a compact particle agglomeration [43,44]. These porous structures agreed with the pore size distributions obtained and illustrated in Figure 2. This different behaviour for P90 highlights a clear trend to agglomeration associated to their lower particle size. In addition, it is important to remark that P25 and P90 isotherms and their corresponding pore size distributions considerably changed after the synthesis. By the other hand, the isotherm profiles and pore size distributions for N-TiO_2 and Au/N-TiO_2 are practically identical for the three titania samples studied, confirming the absence of textural differences due to the gold inclusion.

Regarding their textural parameters (Table 2), the pore volume had the same trend than the isotherms and pore distributions and it was notably altered after the synthesis, but the surface area was not affected and it corresponded with the values determined by the manufacturer. These evidences indicate that the changes are not produced by the chemical modification of the particles; otherwise a physical alteration promoted by the particles agglomeration during the synthesis procedure is the probably responsible of the changes in the physisorption behaviour. The unaltered surface area indicates that the size of primary TiO_2 particle was not modified, as evidenced by XRD. The particle agglomeration was previously confirmed by the density measurements. The particles compaction reduced the interparticle size increasing the amount of mesopores, as it is observed in the pore size distribution. In fact, after the synthesis P25 particles showed isotherms and pore size distribution very similar to the corresponding ones for

VP, the commercial agglomerated form of P25. In the case of P90 the tendency toward the agglomeration was so intense that its isotherm became like the characteristic one for a particulate material showing a narrow mesoporous size distribution. On the other hand, the differences after the synthesis found in VP particles were not substantial, probably, due to fact that the particles were initially agglomerated.

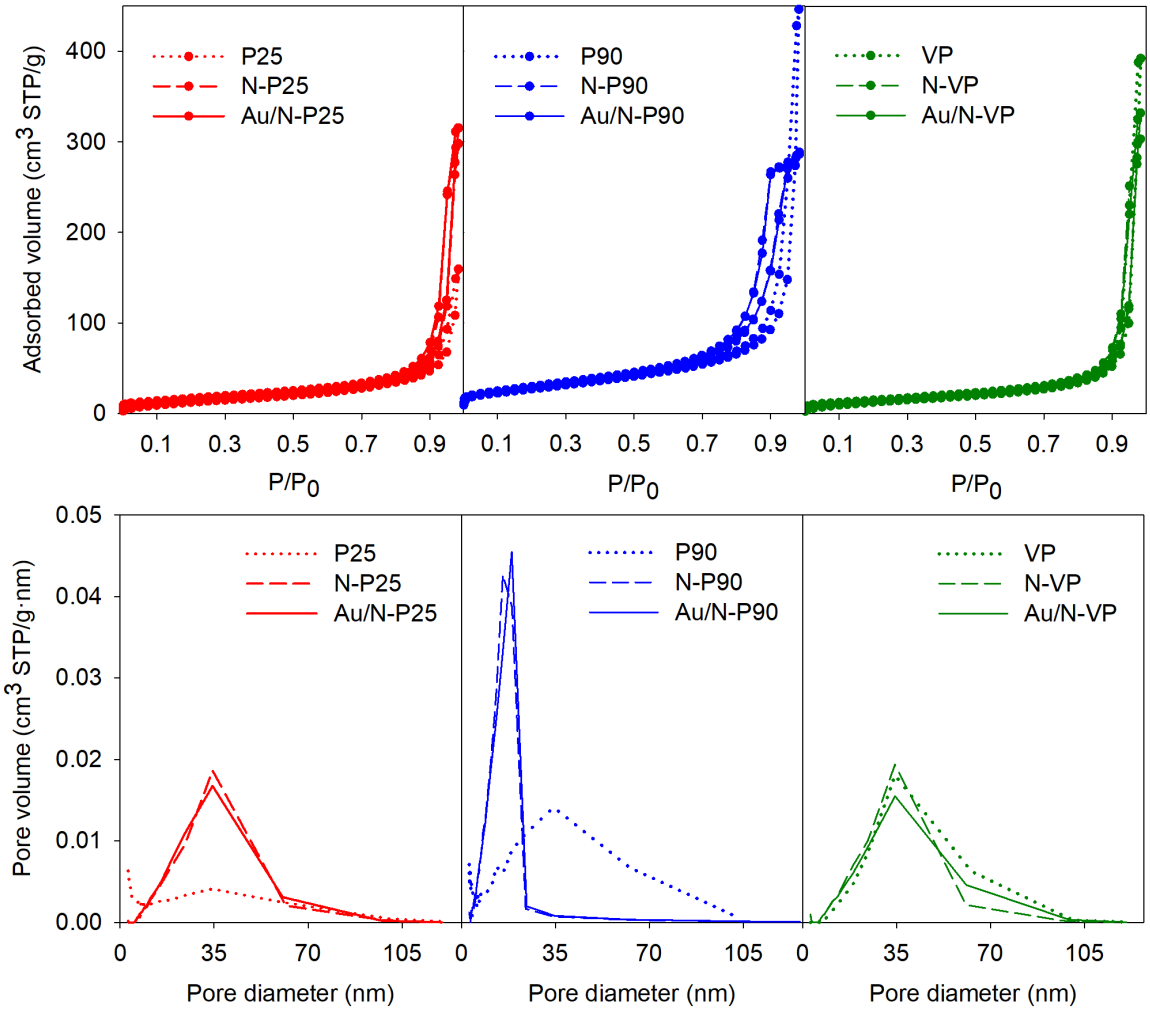

Figure 2. Nitrogen physisorption isotherms and BJH pore size distributions of the particles under study.

The P25 particles series was chosen to be characterized by XPS and the obtained results are plotted in Figure 3. All samples clearly showed the titanium and oxygen signals corresponding to TiO_2 and a carbon peak characteristic of adventitious carbon contamination. The N-P25 and Au/N-P25 samples had small peaks of nitrogen confirming their presence in the samples; finally,

the weak gold signal of AuNPs was present in Au/N-P25 sample. The atomic composition of the samples was determined from these spectra and it is listed in Figure 3. The Ti:O relation was nearly the theoretical 1:2 relation corresponding to the ideal TiO_2. The nitrogen content for N-P25 and Au/N-P25 was around 0.3 at%, confirming the UV-visible characterization results previously discussed Regarding the gold content, the 0.14 at% implies approximately a 1 wt% Au/TiO_2, which is more than the double the concentration determined by ICP. These discrepant results are related to the different nature of the techniques; ICP is a bulk analysis of the entire sample whereas the XPS information is received from the sample surface, where AuNPs are located.

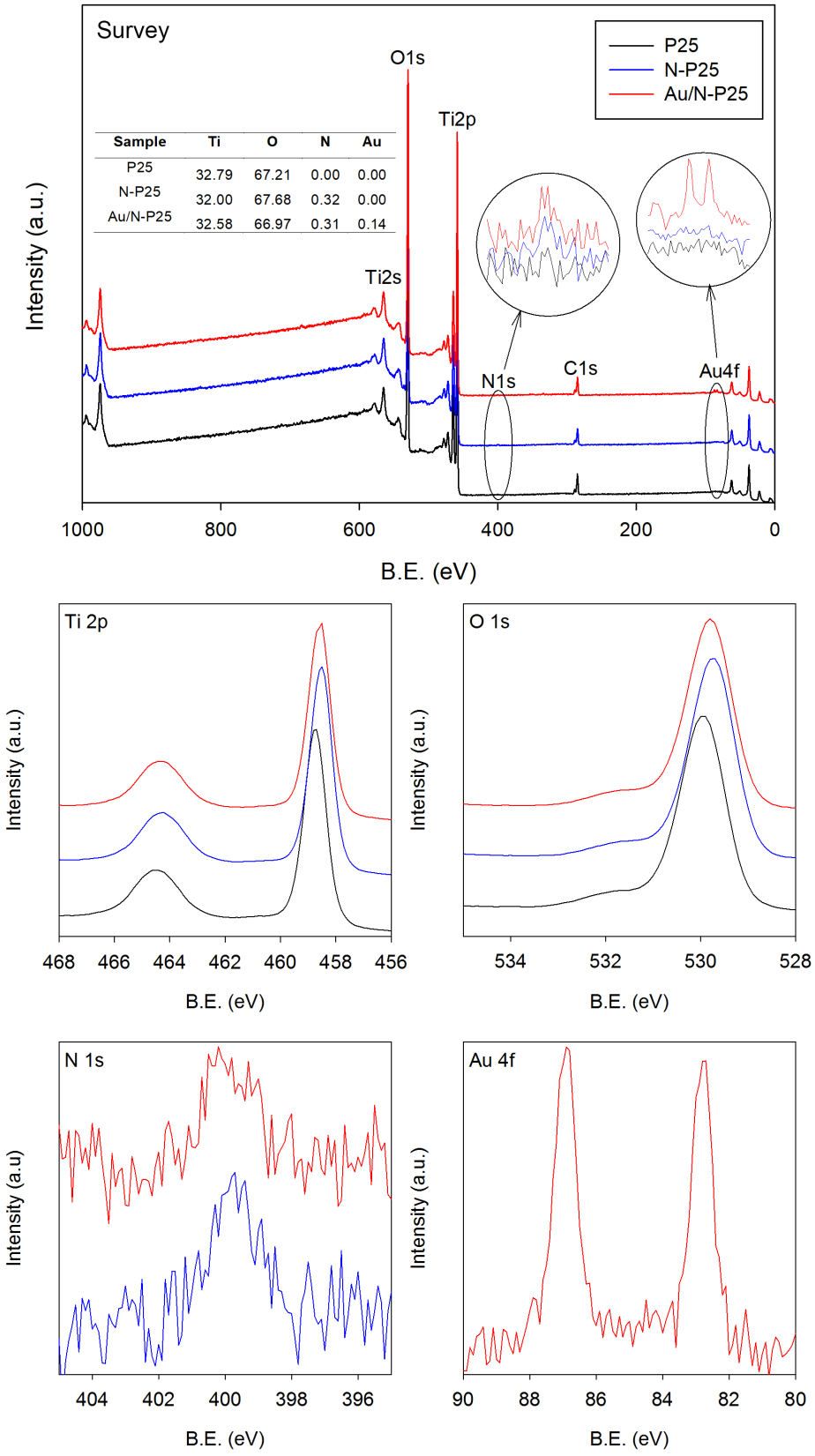

Sample	Ti	O	N	Au
P25	32.79	67.21	0.00	0.00
N-P25	32.00	67.68	0.32	0.00
Au/N-P25	32.58	66.97	0.31	0.14

Figure 3. Results of XPS characterization for P25 particle series. Survey spectra with the corresponding at% composition obtained and high resolution spectra of representative core levels.

The high resolution spectra show that Ti and O core level peaks were slightly shifted to lower binding energies. Ti $2p_{3/2}$ and $2p_{1/2}$ appeared at 458.7 and 464.6 eV, respectively, for P25 and at 458.5 and 464.2 for N-P25 and Au/N-P25, respectively; O 1s was shifted from 529.9 eV for P25 to 529.7 and 529.8 for N-P25 and Au/N-P25, respectively. These shifts take place when TiO_2 is doped with nitrogen [16,45–48], and, specifically a shift of 0.2 eV has been previously observed for 0.3% N doped TiO_2 [36]. Therefore, the observed shifts confirm that the detected nitrogen in our samples was integrated into the TiO_2 structure chemically bonded. The nitrogen has lower electronegativity than the oxygen and its insertion in the TiO_2 structure produces an electronic enrichment of titanium and oxygen. Next to the main oxygen peak, another weak signal appeared at around 532 eV like a shoulder in the tail of the main signal. The signals in this position are usually related to oxygen in organic matter contaminating the sample and the hydroxyl groups in the TiO_2 surface. N 1s peaks commonly only appear in two well-differenced areas, near 396 or 400 eV, depending on the type of N doping. In the studied samples, it is difficult to determine the exact position of N 1s peaks due to the strong noise, but they are clearly positioned close to 400 eV. The signals in this position have been widely described as a consequence of the presence of nitrogen in interstitial positions in the TiO_2 structure, specially oxidized nitrogen species [14,16,36,49–53]. Considering that the nitrogen compounds are easily oxidized and the samples were calcined in an oxidant ambient, it is reasonable that the samples incorporated oxidized nitrogen in interstitial position. Finally, the Au $4f_{7/2}$ peak is located at 82.7 eV that corresponds with Au^0 because cationic gold species appear at B.E. values higher than 84 eV, the reference for metallic gold. The value lower than 84 eV means that AuNPs possessed negative charge due to an electronic transfer from TiO_2 [6,54], confirming the electronic interaction between AuNPs and TiO_2. Additionally, a 0.2eV shift of valence band was observed for Au/N-P25 and N-P25 particles (see Figure S4 in the supplementary

information) which was nearly identical to the band gap reduction determined from UV-Vis spectra.

The images obtained from SEM are shown in Figure 4. All samples were composed by particles with polyhedral shapes. Regarding the size, most particles had a homogeneous size but some significantly bigger particles were observed. More precisely, the sizes of P25 and VP were commonly around 25 nm and 40-50 nm for the bigger ones. For P90, the medium size was 14 and bigger particles around 25-35 nm were also observed. The sizes of small particles were very similar to the size provided by the manufacturer and the size determined by XRD for anatase crystal. Therefore, we can conclude that the most abundant particles correspond to anatase crystals whereas the biggest and scarce particles correspond to rutile crystals. No significant difference in TiO_2 particle size or shape was observed after Au deposition, which agrees with the results above commented. Nevertheless, the SEM technique has allowed to detecting the presence of AuNPs in our samples (see insets in Figure 4).

The AuNPs were easily observable through HAADF-STEM characterization (see Figure 5), they were abundant and well dispersed on TiO_2. The AuNPs were small being the size mainly between 4 and 8 nm but slight differences in the size distributions were observed. The smallest AuNPs were present in Au/N-P25 with a size of 5.2±1.3 nm, whereas the size for Au/N-VP was 6.1±1.5 and Au/N-P90 had the widest distribution with a size of 6.2±2.1nm and a considerable amount of AuNPs bigger than 10 nm. However, it is difficult to discern whether these small differences were due to the support employed or they were due to the variability of the synthetic procedure. These results explain the lower visible absorption of Au/N-VP compared with Au/N-P25, the higher AuNPs size implies a lower number of AuNPs and the consequent reduction of the LRSP effect.

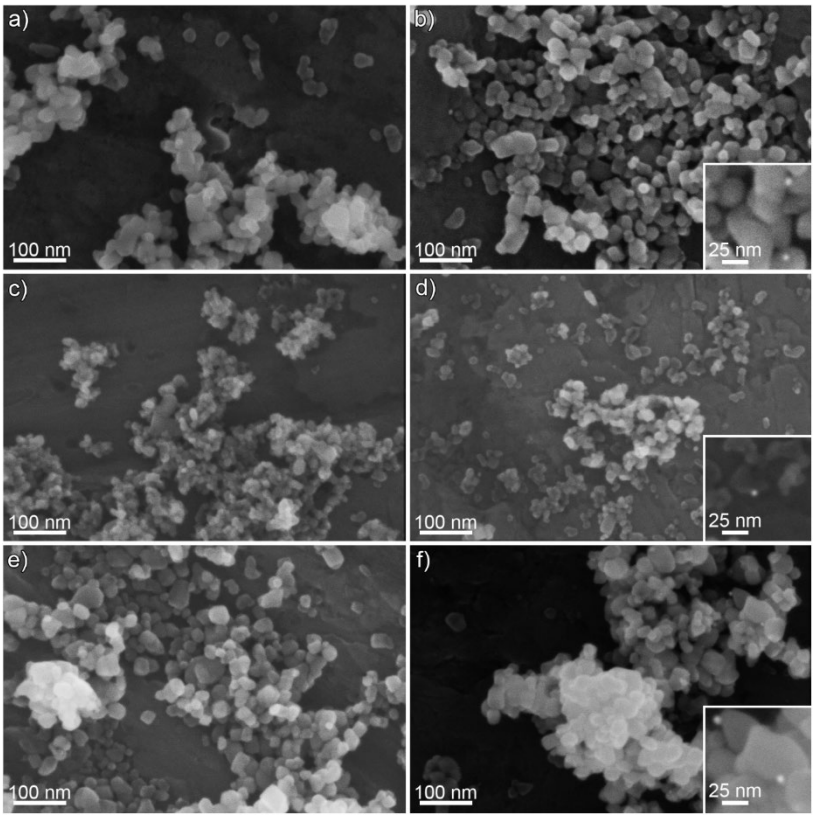

Figure 4. SEM images of commercial TiO_2 particles and the corresponding Au/N-TiO_2. The insets include the detail of a zone containing AuNPs (detected by its higher contrast). a) P25, b) Au/N-P25, c) P90, d) Au/N-P90, e) VP and f) Au/N-VP.

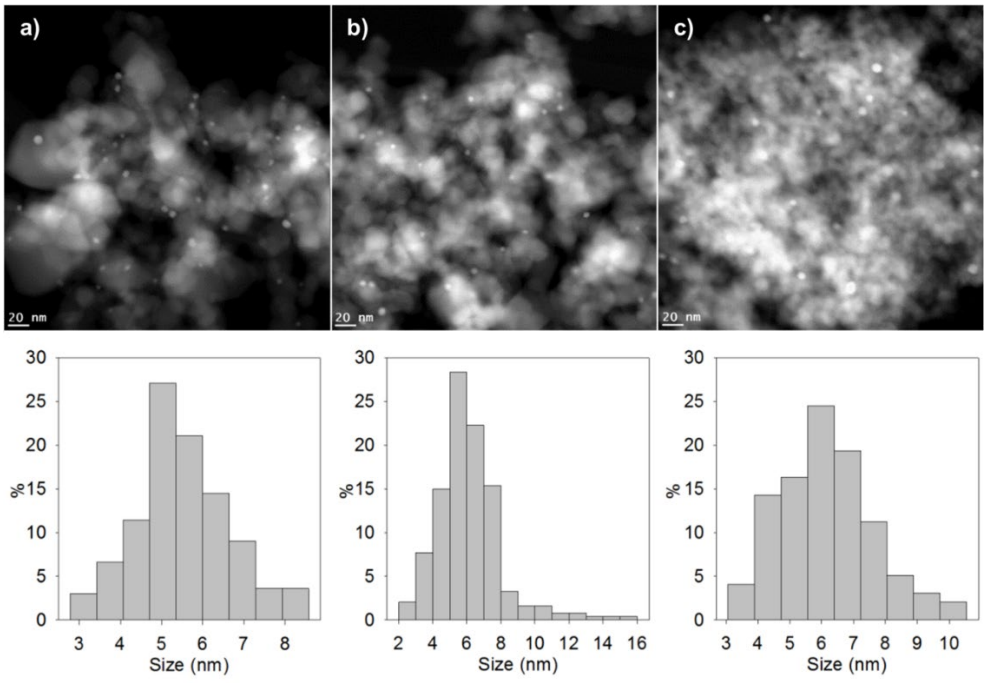

Figure 5. HAADF-STEM images of the Au/N-TiO_2 particles synthetized and their corresponding AuNPs size distributions. a) Au/N-P25, b) Au/N-P90 and c) Au/N-VP

3.2. Au/N-TiO_2 photocatalytic activity

In order to evaluate the photoactivity of the three photocatalysts series, MB degradation tests were performed. The results are plotted in Figure 6. For comparative purposes, the results for a blank test without any particle, P25 calcined at the same conditions employed in the synthesis and the Au/TiO_2 reference catalyst from the World Gold Council (Au/TiO_2WGC) were also included. This reference catalyst is prepared from P25 by DP method and it has a gold load of 1.4% and an average AuNPs size of 3.7±1.5 nm [55,56]. The tests were carried out in oxidant conditions where the MB photobleaching takes place via its mineralization by O_2 [57], thus the absorbance decrease was directly related to the photo-oxidation process. The results successfully fitted to a first order rate equation obtaining the rate constants compiled in Table 3.

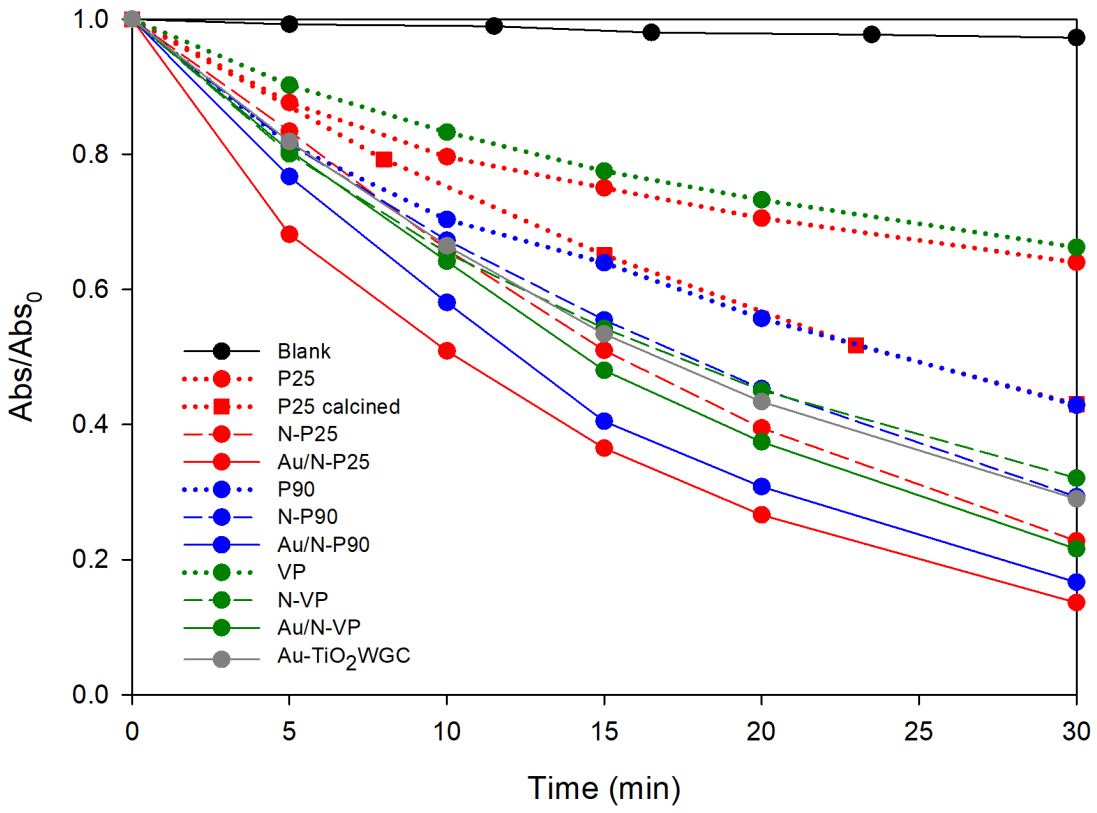

Figure 6. MB photodegradation in the presence of the studied TiO_2 particles under UV-Vis radiation.

Table 3. Rate constants obtained from the fitting of MB degradation results to a first order rate equation.

Sample	Rate Constant (h^{-1})		
	UV-Vis	UV	Vis
Blank	0.05	-	-
P25	0.86	2.70	0.03
P25 calcined	1.69	-	-
N-P25	2.99	4.32	0.04
Au/N-P25	3.94	6.12	0.24
P90	1.63	-	-
N-P90	2.44	-	-
Au/N-P90	3.62	-	-
VP	0.81	-	-
N-VP	2.27	-	-
Au/N-VP	3.09	-	-
Au/TiO_2WGC	2.81	-	-

In the absence of photocatalyst, a very small MB concentration decrease was observed, thus the MB photolysis contribution was negligible as compared with the MB photodegradation catalysed by TiO_2. The lowest photoactivity corresponded to the unmodified commercial particles, being the highest for P90 due to their smaller size and greater surface area. However, it was observed that the MB degradation for P90 was decelerated after some minutes, probably due to the particles agglomeration during the test that produced clusters of higher size reducing the TiO_2-solution contact. P25 and VP have the same surface area, but the MB degradation was slightly higher for P25. This difference is attributable to the granulated nature of VP that produced a worse dispersion in the solution.

It is well known that a heat treatment can modify the photocatalytic properties of TiO_2. For this reason, P25 particles were calcined under the same conditions employed in the synthesis in order to evaluate the effect of particle calcination in the MB photodegradation. The calcination produced an evident increase in the MB degradation rate of P25, the constant rate nearly

doubling that of the uncalcined particles. However, the previous particle characterization indicated that the soft heat treatment was not enough to produce changes in the morphology or phase composition of TiO_2 particles. This behaviour has been previously observed and attributed to the transformation of amorphous TiO_2 present in P25, which can reach the 13% of the sample [42,58,59], to anatase [39].

The nitrogen-doped particles showed a higher MB degradation rate than the undoped particles. The N-P25 degradation rate was also higher than that of the calcined P25, demonstrating that the nitrogen doping increases the particle photoactivity. The photocatalytic enhancement is due to two main factors: (i) the visible absorption increase, and the subsequent band gap decrease, as observed during the UV-Visible characterization, and (ii) the decrease of charge carriers recombination rate for the nitrogen-doped TiO_2 [60]. As for the undoped particles, the N-P25 rate was higher than the N-VP one, but the N-P90 rate was lower than that of N-P25 one. This decrease in N-P90 activity compared with the undoped particles is attributable to the particle agglomeration during the synthesis that made difficult its proper dispersion in the MB solution.

Finally, the particles containing the AuNPs showed the highest MB degradation rates, confirming the role of AuNPs in the improvement of the TiO_2 photocatalytic effect. The TiO_2-AuNPs contact modifies the energy levels and the charge transfer phenomena in TiO_2 surface. Specifically, the AuNPs act as reservoir of photogenerated charge carriers and they equilibrate the Fermi level, resulting in a diminution of electron-hole pair recombination and a promotion of electron transfer process with the reactant species [61–63]. Additionally, the LSPR effect of the AuNPs enhances the TiO_2 photoactivity under visible radiation [64]. The major mechanism taking place is the TiO_2 sensitization, the AuNPs electrons are excited when they receive visible radiation and they get enough energy to be injected in the TiO_2 conduction band triggering the

TiO_2 photocatalytic process [65]. In addition, other LSPR mediated processes that can enhance the TiO_2 photoactivity have been proposed:

(i) The excited AuNPs electrons colliding in the TiO_2-Au contact area can have enough kinetic energy for promoting the TiO_2 electrons to the valence band [66,67].

(ii) The LRSP excitation produces a local heating and the surrounding AuNPs can reach temperatures up to 100 °C favouring the photodegradation processes [68].

(iii) The LRSP increases the electric field around the AuNPs promoting the electron-hole pairs formation [69].

By comparing with Au/TiO_2WGC, it is observed that the Au/N-TiO_2 particles prepared according to our method were more active than the reference catalyst, even though the gold content of the prepared particles is nearly a third of that corresponding to the Au/TiO_2WGC. The lower photoactivity of the reference catalyst can be attributed to the following facts:

(i) The photoactivity enhancement produced by the nitrogen doping, which is not present in the reference catalyst.

(ii) The reference catalyst is optimized for conventional catalysis where a small AuNPs size is desired because the AuNPs size increasing drastically reduces the catalytic activity. However, for photocatalytic applications there is no clear relationship between AuNPs size and activity [3,70]. The low size of reference catalyst AuNPs can be inadequate to enhance the TiO_2 photoactivity due to the attenuation and disappearance of LSPR [71–73] or because the Au energy levels are unsuitable for producing the Au-TiO_2 energy transfer [6].

(iii) A higher gold content can be adverse favouring the electron-hole recombination [18,74] and, also, because the excess of gold can absorb the UV light reducing the amount available for the TiO_2 [3,75].

The activity order among the synthesised Au/N-TiO_2 particles was Au/N-P25>Au/N-P90>Au/N-VP. The highest degradation for Au/N-P25 is related to the better TiO_2 particle dispersion, which was previously mentioned, and its smaller and narrower AuNPs size distribution. Au/N-P90 showed a higher MB degradation rate than Au/N-VP due to its higher gold content.

The P25 particles series was chosen to carry out additional MB degradation experiments under only visible or only UV light in other to elucidate the nature of the mechanism that enhance the efficiency of TiO_2. The MB degradation curves are represented in Figure 7 and their corresponding constant rates are compiled in Table 3.

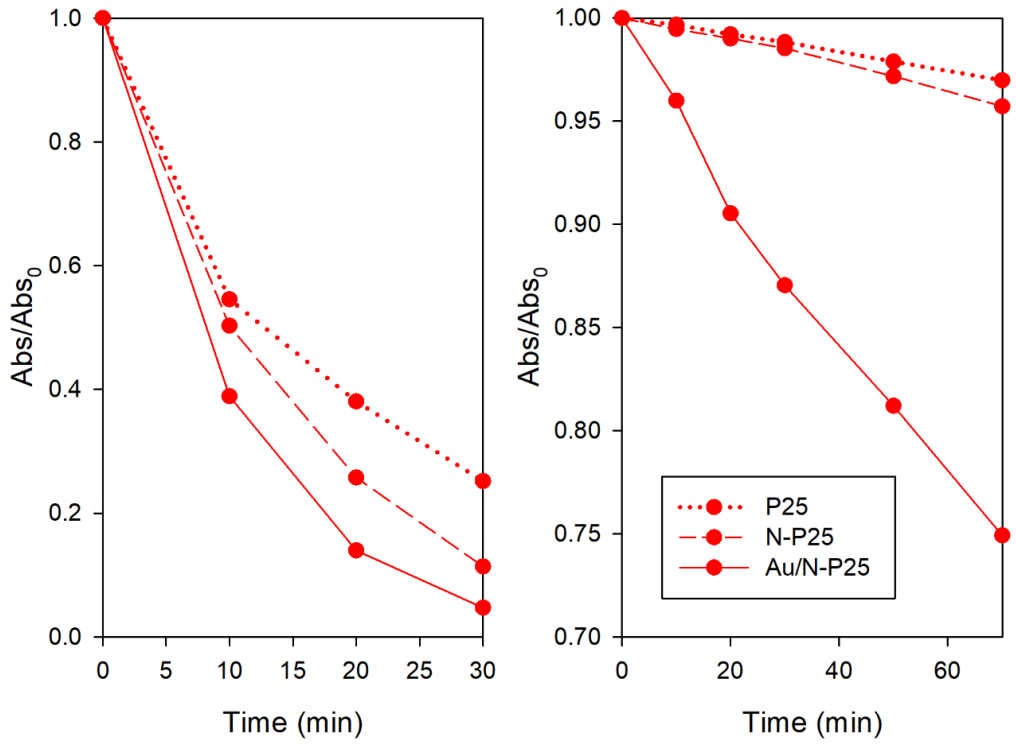

Figure 7. MB photodegradation in the presence of the studied TiO_2 particles under UV (left) and visible (right) radiation.

Under UV radiation, a progressive increase of MB degradation rate, in the order P25<N-P25<Au/N-P25, was observed. This radiation can effectively activate the TiO_2 but it is far away from the range of LSPR activation of AuNPs. Therefore, the TiO_2 photoactivity enhancement was due to the electronic phenomena previously described.

Under exclusively visible radiation, the MB degradation results were completely different, showing a considerable increase of MB degradation rate for the gold-containing sample. The filter cuts off the radiation with wavelength lower than 550 nm (see Figure S5 in the supplementary material), so the resultant visible light did not have enough energy to activate the TiO_2 but it corresponded to the range of AuNPs LSPR absorption. In the absence of TiO_2 activation the slightly MB degradation observed for P25 and N-P25 can be explained as a result of a sensitization effect produced by the MB [76,77]. However, the MB degradation rate was six-folded when the AuNPs are present demonstrating that the TiO_2 visible activation via AuNPs LSPR mechanisms took place in the Au/N-TiO_2 particles prepared. These results also confirm that the contribution to MB degradation due to TiO_2 visible sensitization by MB was negligible under UV and UV-visible radiation.

Since the Au/N-P25 particles showed the best MB degradation results, the P25 particle series was chosen for the NO photodegradation evaluation, the results being shown in Figure 8, and the corresponding amounts of NO and NO_x removed and NO_2 generated being presented in Table 4.

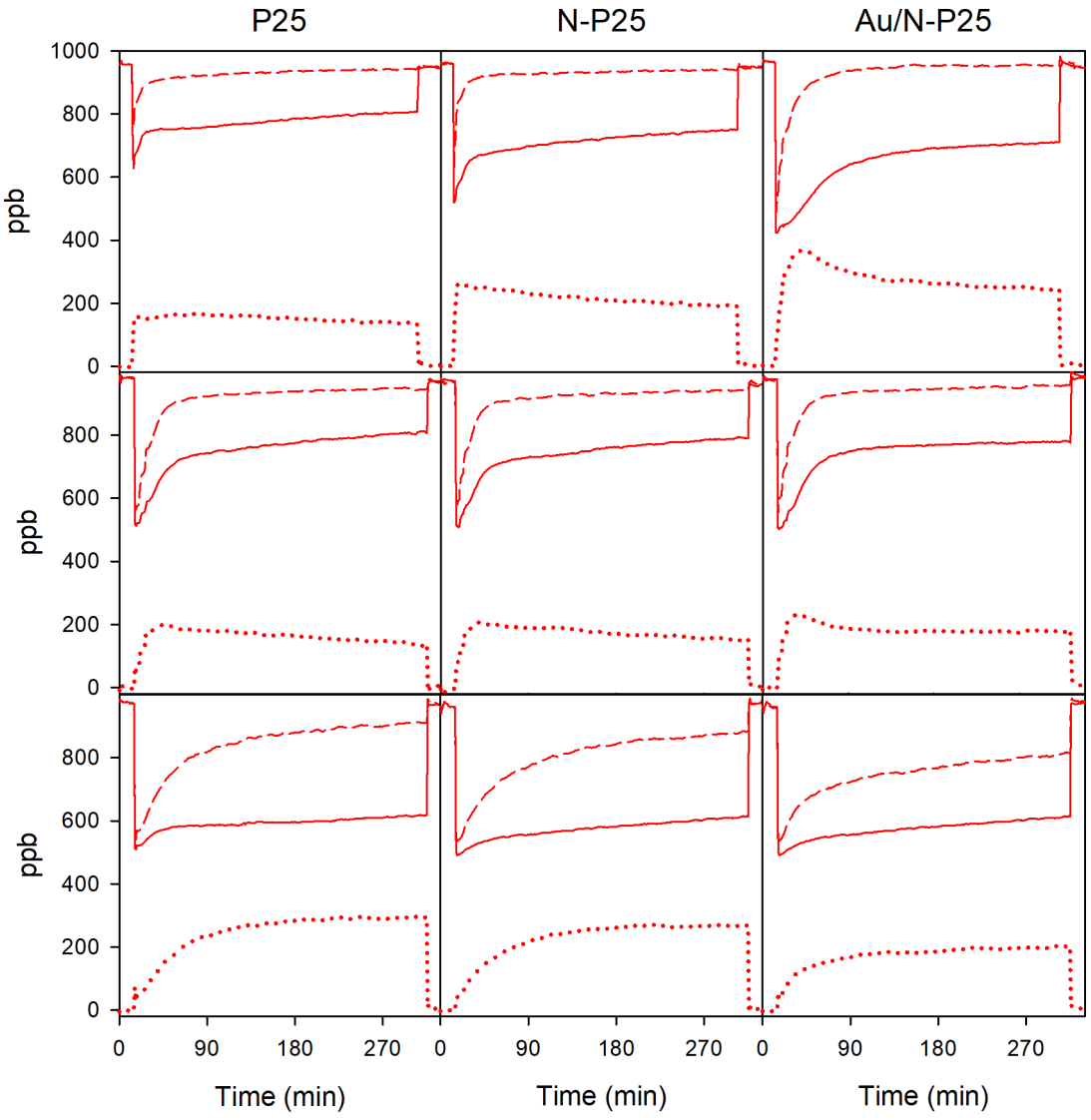

Figure 8. NO (continuous line), NO_2 (dotted line) and NO_x (dashed line) concentration profiles during the NO photodegradation test for the glass samples coated with (from top to bottom) only a first layer of TiO_2; first layer of TiO_2 and second one of $Ca(OH)_2$; and first layer of TiO_2 and second one of TiO_2+$Ca(OH)_2$.

Table 4. Results of the NO photodegradation test for the different TiO_2 coated glasses samples.

Sample	Particles	NO removed		NO_2 generated		NO_x removed		NO_2 selectivity
		µmol	%	µmol	%	µmol	%	
TiO_2	P25	6.5	18.5	5.5	15.7	1.0	2.9	84.6%
	N-P25	8.9	25.2	7.7	21.9	1.2	3.3	86.8%
	Au/N-P25	11.5	32.1	10.1	28.2	1.4	3.9	87.7%
TiO_2 + $Ca(OH)_2$	P25	8.1	23.0	5.9	16.8	2.2	6.2	72.8%
	N-P25	8.3	23.4	6.3	17.9	1.9	5.5	75.9%
	Au/N-P25	8.7	24.2	6.6	18.5	2.0	5.7	75.9%
TiO_2 + ($Ca(OH)_2$ and TiO_2)	P25	14.0	38.7	9.2	25.5	4.8	13.2	65.7%
	N-P25	14.5	39.2	8.6	23.4	5.8	15.8	59.3%
	Au/N-P25	14.6	40.5	6.5	17.9	8.2	22.6	44.5%

The NO photo-oxidation to HNO_3 in the presence of TiO_2 takes place following the consecutive reactions (1) to (3) [32].

$$4NO + O_2 + 2H_2O \xrightarrow{TiO_2} 4HNO_2 \quad (1)$$

$$4HNO_2 + O_2 \xrightarrow{TiO_2} 4NO_2 + 2H_2O \quad (2)$$

$$2H_2O + 4NO_2 + O_2 \xrightarrow{TiO_2} 4HNO_3 \quad (3)$$

Comparing with the initial results for the glass samples coated with a unique TiO_2 layer, an evident increase in the amount of NO removed for N-P25 and Au/N-P25 was observed, which demonstrated the TiO_2 photoactivity enhancement produced by the nitrogen doping and the AuNPs. However, although the NO conversion rise was reached, for depolluting purposes it is also relevant to study the amount of NO_2 generated during the process, as the NO_2 toxicity is

even higher than the NO one. NO_2 is not only generated as a reaction intermediate but its formation is promoted as the HNO_3 is accumulated in the TiO_2 surface according to reaction (4) [32,78]. Finally, once enough HNO_3 is produced, the process reaches an equilibrium condition where TiO_2 acts as NO to NO_2 converter as stated in equation (5)

$$2HNO_3 + NO \xrightarrow{TiO_2} 3NO_2 + H_2O \quad (4)$$

$$2NO + O_2 \xrightarrow{TiO_2} 2NO_2 \quad (5)$$

In this way, the samples started to release NO_2 reaching its maximum concentration after a few minutes of irradiation producing a drastic increase in the concentration of total nitrogen oxides (NO_x), resulting in a low net amount of NO_x removed in the test. All the samples suffered this "deactivation", because, although the amount of NO removed increased with the TiO_2 photoactivity enhancement, the amount of NO_2 generated was also proportionally increased. As a result, high selectivities to NO_2 and only slight increases in the percentages of NOx removed for N-P25 and Au/N-P25 were observed. This behaviour is frequently observed for TiO_2 particles deposited on glass. Specifically, it has been stablished that the HNO_3 produced is distributed homogeneously in the TiO_2 surface and the amount of HNO_3 to reach the saturation is proportional to the TiO_2 surface area, 0.04 μmol of HNO_3/mg or 0.5 molecules/nm^2 for P25 [78]. Based on these data, the amount of HNO_3 necessary for P25 sample saturation would be exactly the amount of NO_x removed in the test, 1 μmol. Thus, the nitrogen doping and AuNPs not only enhanced the TiO_2 photoactivity, but also increased the tolerance to HNO_3, 0.048 μmol/mg or 0.58 molecules/nm^2 for N-P25 and 0.056 μmol/mg or 0.67 molecules/nm^2 for Au/N-P25.

In order to make evident the differences in NO_x removal activity of the particles under study, $Ca(OH)_2$ was employed to produce alkaline conditions that promote the elimination of HNO_3

in the form of nitrates. A first attempt involved depositing a $Ca(OH)_2$ layer on the TiO_2 coated glass samples. The amount of NO_2 generated for these samples was lower than that corresponding to the first samples and subsequently the amount of NO_x removed was increased. However, the amount of NO removed for N-P25 and Au/N-P25 was also reduced, no differences in NO_x removal activity were observed between the samples, and the NO_x concentration continued increasing quickly after a few minutes of irradiation. The amount of $Ca(OH)_2$ added was enough to react with all the HNO_3 produced in a total NO conversion, so the HNO_3 was not effectively removed in these samples. Probably, the elimination of HNO_3 only took place in the zone of contact of TiO_2 and $Ca(OH)_2$ layers and the new top layer made difficult the NO diffusion to TiO_2, producing the decrease of NO conversion observed for N-P25 and Au/N-P25. In order to promote the TiO_2-$Ca(OH)_2$ contact, new samples were prepared depositing simultaneously TiO_2 and $Ca(OH)_2$ on the initial TiO_2 layer. These samples showed the highest NO removal activity but only slight increases in the amount of NO removed were observed for N-P25 and Au/N-P25 in comparison with P25. However, the amount of NO_2 generated was significantly reduced for N-P25 and especially for Au/N-P25, resulting in an increase in NO_x removal activity and a reduction of selectivity to NO_2. The nitrogen doping increased by 20% the amount of NO_x removed for P25 sample due to the photoactivity enhancement. On the other hand, Au/N-P25 increased it by 70%, which was not only due to the TiO_2 photoactivity enhancement caused by TiO_2 but also to the fact that the AuNPs participate in the process, adsorbing the NO on its surface and promoting its oxidation [2,79].

3.3. Integration of Au/N-TiO_2 in a silica matrix, characterization and photocatalytic evaluation

The xerogel containing the Au/N-TiO_2 particles showed an absorption in the visible range (Figure 9) shaped like the one previously observed for the isolated particles (Figure 1),

demonstrating that the AuNPs were not modified during the sol-gel synthesis process. Another relevant fact observed was the reduction of UV absorption associated to TiO_2 for the xerogels containing the N-TiO_2 and Au/N-TiO_2 particles. This reduction in the xerogel TiO_2 content was due to a small fraction of N-TiO_2 and Au/N-TiO_2 particles non-dispersed in the silica sol during the synthesis. The worse dispersion is related to the higher agglomeration of the synthetized particles as previous mentioned. Indeed N-P90 and Au/N-P90, that reported the highest agglomeration, presented the lowest UV absorption in the spectra.

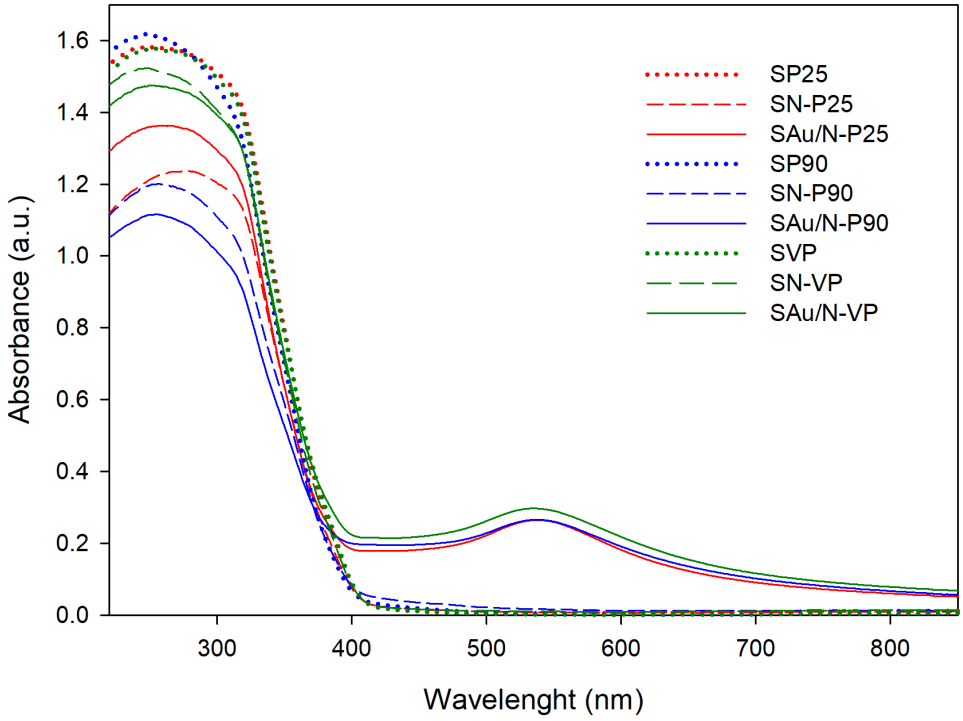

Figure 9. UV-Visible spectra of the xerogels under study.

Figure 10 compiles the nitrogen isotherms obtained for the xerogels. They were of type IV(a) with hysteresis that presented parallel branches almost vertical, classifiable as H1 [43]. This type of isotherm is characteristic of solids with cylindrical mesopores of uniform size, such us zeolites, ordered silicas or controlled porous glasses. The non-total verticality of hysteresis branches can be attributable to xerogels having wide pore size distributions (see Figure 10). Evident differences were observed for the P25 and P90 series between the xerogels containing

the pristine titania particles and those after the synthesis performed. By contrast, the isotherms of the materials prepared from VP particles series were practically overlapped. These differences can be attributed to the TiO_2 particle agglomeration that modifies how TiO_2 is distributed in the matrix. The same behaviour was observed for the pore size distribution. It should be emphasized that all xerogels containing the synthetized particles exhibited a similar double size distribution centred at 2.5 and 12 nm. Regarding the textural parameters (see Table 5), all xerogels prepared using the synthetized particles showed similar total pore volume values and the particles of P90 and VP series had specific surface areas significantly higher than P25 series, due to the presence of micropores.

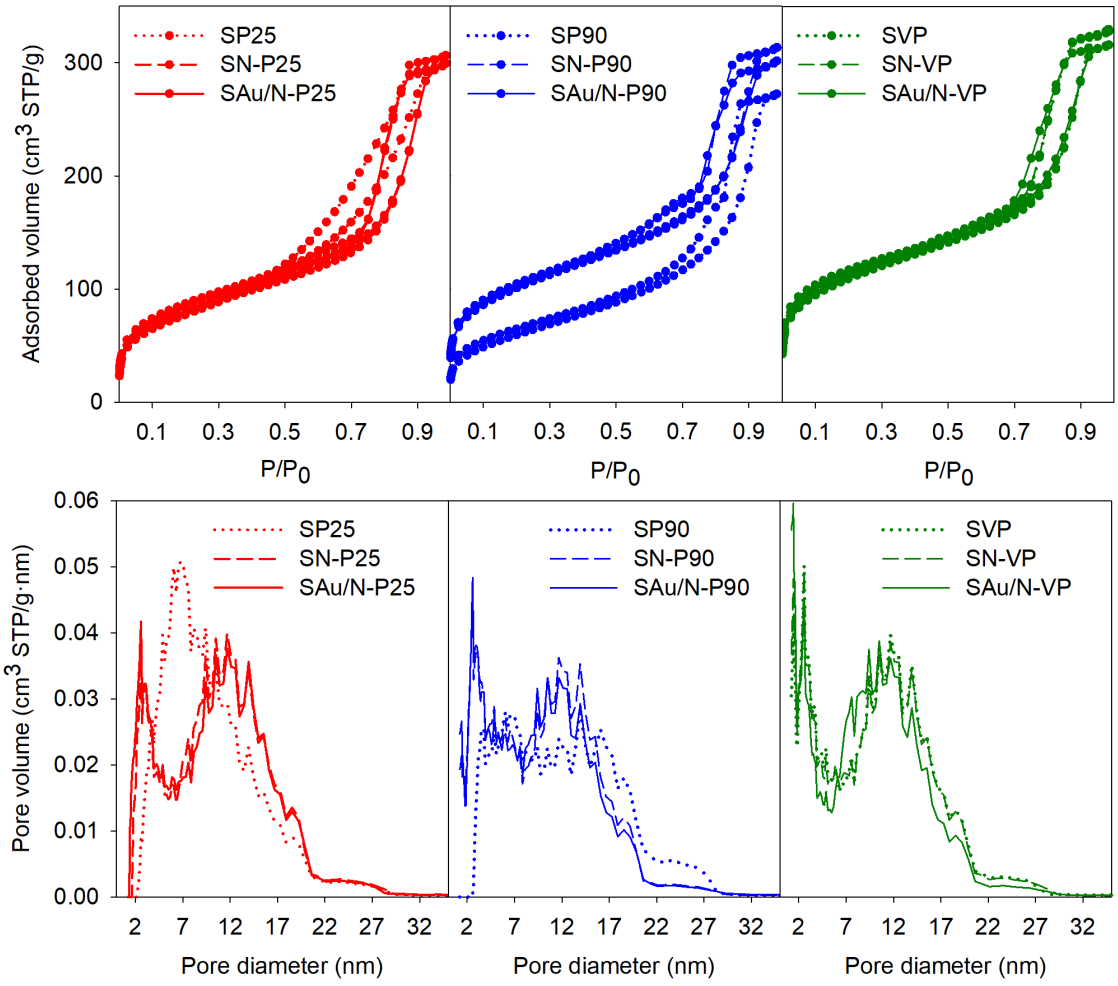

Figure 10. Nitrogen physisorption isotherms and NLDF pore size distributions of the xerogels under study.

Table 5. Textural properties and main results obtained in the MB and NO photodegradation tests using the prepared photocatalysts.

Sample	S_{BET} (m^2/g)	V_{pore} (cm^3/g)	Rate Constant (h^{-1})	% NO conversion	% NO_2 selectivity
SP25	278	0.473	0.75	32.3	18.6
SN-P25	289	0.463	1.07	43.3	16.2
SAu/N-P25	310	0.464	1.40	56.0	3.6
SP90	219	0.421	0.59	13.7	22.0
SN-P90	365	0.485	0.69	26.3	15.2
SAu/N-P90	365	0.466	0.87	37.7	4.4
SVP	394	0.510	0.68	22.3	19.6
SN-VP	403	0.508	0.99	36.7	16.4
SAu/N-VP	415	0.489	1.27	46.0	4.3

The MB photodegradation test in the presence of the powdered xerogels (see Figure 11 and Table 5) demonstrated that the TiO_2 photoactivity was preserved after its integration in the silica matrix. The obtained results were similar to the previous ones for the TiO_2 particles, observing the obvious photoactivity enhancement induced by the nitrogen doping and the AuNPs. Comparing the different starting TiO_2 particles, it was observed that P25 series showed the best results whereas P90 series showed the lowest MB degradation rates. These results contrast with the previous ones obtained for similar TiO_2/SiO_2 photocatalysts prepared with the same particles [80]. The highest activity of TiO_2/SiO_2 photocatalysts containing VP particles (named AP in the previous work) can be attributed to two main factors:

(i) The photocatalyst containing VP particles showed higher surface area and pore volume than that containing P25. Both parameters are factors that promote the photoactivity [81].

(ii) Not all P25 batches are equal, differences in phase composition and morphology of particles can be found between different batches of the manufacturer [82], thus, a more active batch can have been employed in the present work.

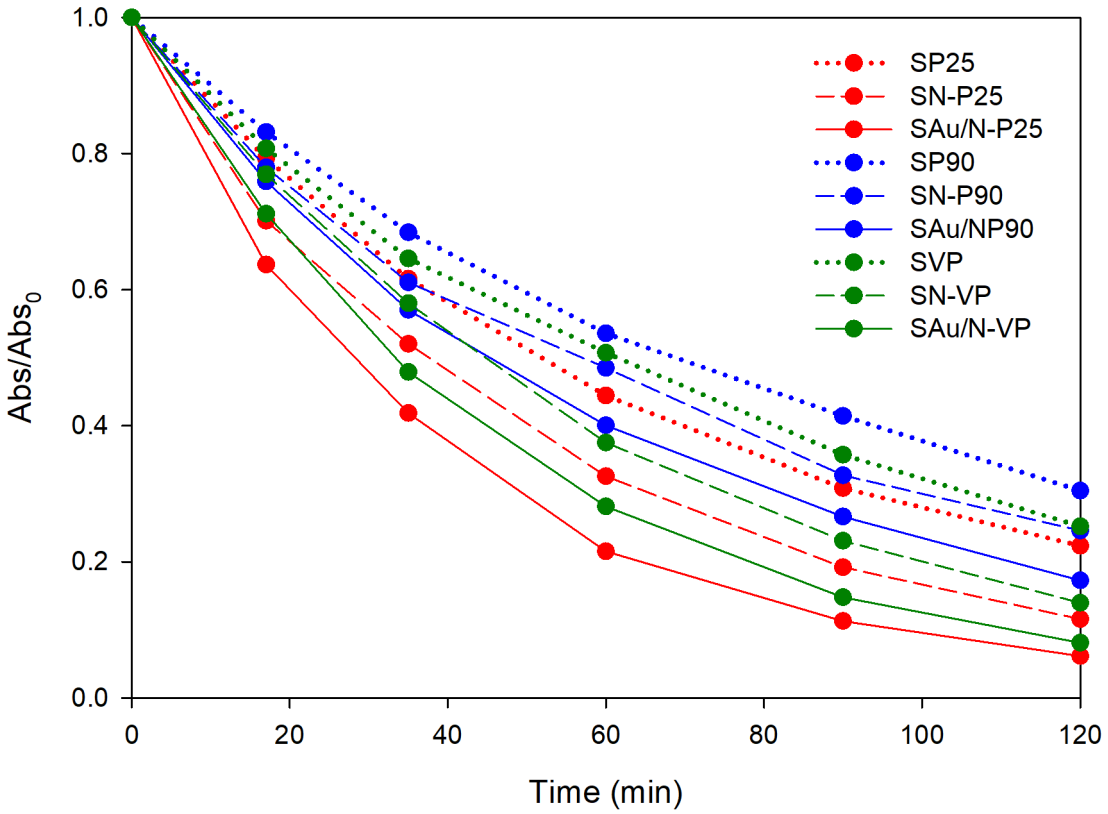

Figure 11. MB photodegradation in the presence of the TiO_2 particles integrated in a silica matrix under UV-Vis radiation.

Figure 12 shows a selection of the nitrogen oxides concentration profiles measured during the NO photodegradation tests. It was noticed that the "deactivation" observed for the TiO_2 coated glasses did not take place under the experimental conditions employed in this case. The short time of analysis and the high amount of photocatalyst employed ensured that the effect of the acid nitric produced in the process was negligible. In spite of the short times, the NO conversion values (see Table 5) showed the enhancement caused by the nitrogen doping and the AuNPs and differences between the different particles, as previously observed for the MB. Finally, an evident decrease in the NO_2 selectivity was observed when the AuNPs were included in the photocatalysts.

These results confirmed that once integrated in the silica matrix the Au/N-P25 particles preserved their better performance, demonstrating that P25 is the most suitable starting material for this synthesis.

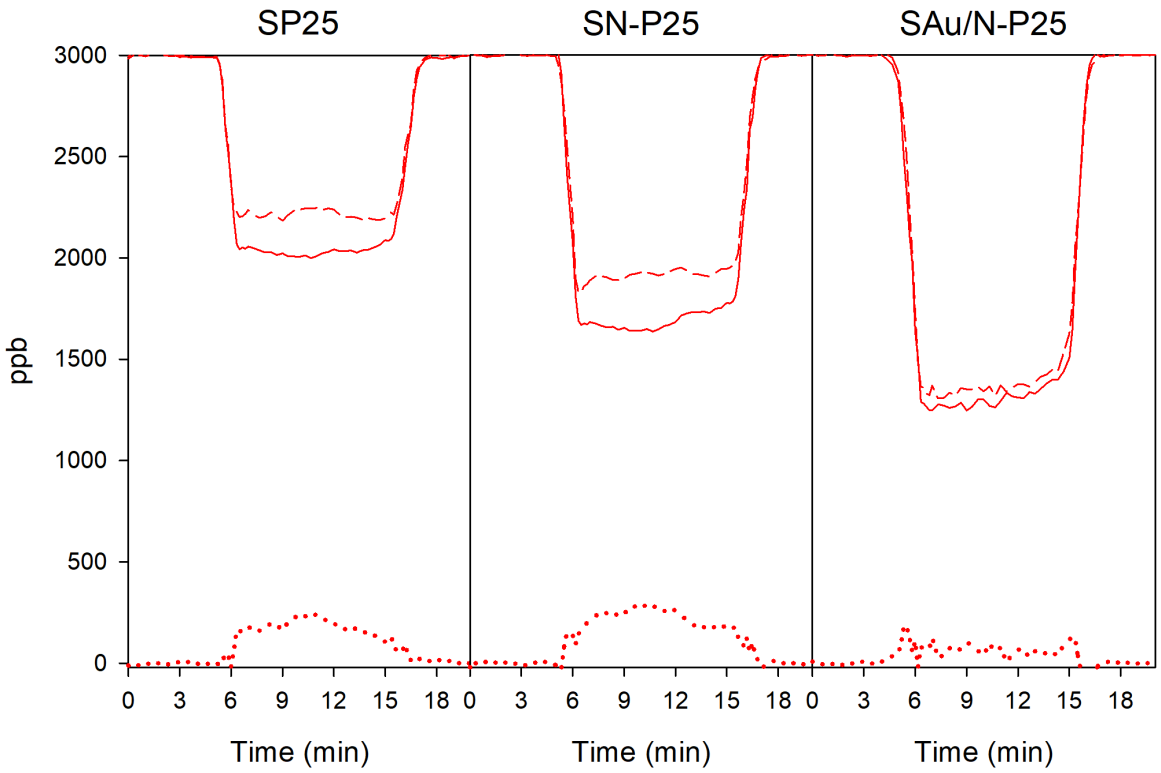

Figure 12. NO (continuous line), NO_2 (dotted line) and NO_x (dashed line) concentration profiles during the NO photodegradation test for the xerogels containing the P25 series particles.

4. Conclusions

Au/N-TiO_2 photocatalysts with enhanced photoactivity have been obtained by means of a simple and innovative one-pot synthesis based in the deposition-precipitation method using urea that allows to promote two synergic approaches: (i) nitrogen doping of TiO_2 and (ii) AuNPs deposition onto TiO_2. The obtained results confirmed that both nitrogen and AuNPs enhanced the TiO_2 photoactivity, but only AuNPs enabled the photoactivity under visible light. In addition, both components increased the NO photodegradation but only AuNPs improved the selectivity of the process.

The characterization studies demonstrated that the starting TiO_2 particle size and its phase composition are not altered by the preparation method, but the texture of the final product is substantially modified as far as the titania particles are agglomerated and compacted. This compaction was especially important for P90 particles and minor for VP particles due to their initial agglomerated state.

The Au/N-P25 particles showed the highest photoactivity because they had the lowest and narrowest AuNPs size distribution and they were less agglomerated than the other ones. P90 was the most active of the pristine TiO_2 particles but the photocatalysts prepared with them showed low activities due to their tendency to particles agglomeration.

The particles integrated into a silica matrix preserved their photocatalytic properties allowing their potential use in environmental remediation applications as demonstrated by the dye removal and NO depolluting tests.

Acknowledgments

This work has been supported by the Spanish Government/FEDER-EU (MAT2013-42934-R and MAT2017-84228-R). M. Luna would also like to thank the Spanish Government for his pre-doctoral grant (BES-2014-068031). We would also like to thank Prof. Andrew Mills and his group at the Queen's University of Belfast for allowing us to carry out the NO degradation measurements included in 3.2 section.

References

[1] M. Luna, J. Delgado, M.L.A. Gil, M. Mosquera, TiO_2-SiO_2 coatings with a low content of AuNPs for producing self-cleaning building materials, Nanomaterials. 8 (2018) 177. doi:10.3390/nano8030177.

[2] M. Luna, J.M. Gatica, H. Vidal, M.J. Mosquera, Au-TiO_2/SiO_2 photocatalysts with NO_x depolluting activity: Influence of gold particle size and loading, Chem. Eng. J. 368 (2019) 417–427. doi:10.1016/j.cej.2019.02.167.

[3] A. Primo, A. Corma, H. García, Titania supported gold nanoparticles as photocatalyst, Phys. Chem. Chem. Phys. 13 (2011) 886–910. doi:10.1039/C0CP00917B.

[4] G.C. Bond, D.T. Thompson, Catalysis by Gold, Catal. Rev. Sci. Eng. 41 (1999) 319–388. doi:10.1081/CR-100101171.

[5] A. Corma, H. Garcia, Supported gold nanoparticles as catalysts for organic reactions, Chem. Soc. Rev. 37 (2008) 2096–2126. doi:10.1039/b707314n.

[6] B. Tian, J. Zhang, T. Tong, F. Chen, Preparation of Au/TiO_2 catalysts from Au(I)-thiosulfate complex and study of their photocatalytic activity for the degradation of methyl orange, Appl. Catal. B Environ. 79 (2008) 394–401. doi:10.1016/j.apcatb.2007.11.001.

[7] P. Gunawan, R. Xu, Z. Zhong, Heterogeneous gold catalysts for selective oxidation reactions, in: Z. Ma, S. Dai (Eds.), Heterog. Gold Catal. Catal., Royal Society of Chemistry, Cambridge, 2014: pp. 288–400. doi:10.1039/9781782621645.

[8] S. Tsubota, D.A.H. Cunningham, Y. Bando, M. Haruta, Preparation of nanometer gold strongly interacted with TiO_2 and the structure sensitivity in low-temperature oxidation of CO, in: Stud. Surf. Sci. Catal., 1995: pp. 227–235. doi:10.1016/S0167-2991(06)81759-3.

[9] S. Tsubota, M. Haruta, T. Kobayashi, A. Ueda, Y. Nakahara, Preparation of Highly Dispersed Gold on Titanium and Magnesium Oxide, in: Stud. Surf. Sci. Catal., 1991: pp. 695–704. doi:10.1016/S0167-2991(08)64634-0.

[10] R. Zanella, L. Delannoy, C. Louis, Mechanism of deposition of gold precursors onto

TiO_2 during the preparation by cation adsorption and deposition–precipitation with NaOH and urea, Appl. Catal. A Gen. 291 (2005) 62–72. doi:10.1016/j.apcata.2005.02.045.

[11] R. Zanella, S. Giorgio, C.R. Henry, C. Louis, Alternative methods for the preparation of gold nanoparticles supported on TiO_2, J. Phys. Chem. B. 106 (2002) 7634–7642. doi:10.1021/jp0144810.

[12] J.W. Geus, Production and thermal pretreatment of supported catalysts, in: Stud. Surf. Sci. Catal., 1983: pp. 1–33. doi:10.1016/S0167-2991(09)60006-9.

[13] J.A. Reyes-Esqueda, A.B. Salvador, R. Zanella, Size control of Au nanoparticles on TiO_2 and Al_2O_3 by DP urea: Optical absorption and electron microscopy as control probes, J. Nanosci. Nanotechnol. 8 (2008) 3843–3850. doi:10.1166/jnn.2008.173.

[14] C.C. Hu, T.C. Hsu, L.H. Kao, One-step cohydrothermal synthesis of nitrogen-doped titanium oxide nanotubes with enhanced visible light photocatalytic activity, Int. J. Photoenergy. 2012 (2012) 1–9. doi:10.1155/2012/391958.

[15] Y. Ruzmanova, M. Stoller, M. Bravi, A. Chianese, A novel approach for the production of nitrogen doped TiO_2 nanoparticles, Chem. Eng. Trans. 43 (2015) 721–726. doi:10.3303/CET1543121.

[16] F. Peng, L. Cai, H. Yu, H. Wang, J. Yang, Synthesis and characterization of substitutional and interstitial nitrogen-doped titanium dioxides with visible light photocatalytic activity, J. Solid State Chem. 181 (2008) 130–136. doi:10.1016/j.jssc.2007.11.012.

[17] S.A. Ansari, M.M. Khan, M.O. Ansari, M.H. Cho, Nitrogen-doped titanium dioxide (N-doped TiO_2) for visible light photocatalysis, New J. Chem. 40 (2016) 3000–3009. doi:10.1039/C5NJ03478G.

[18] B. Tian, C. Li, F. Gu, H. Jiang, Synergetic effects of nitrogen doping and Au loading on enhancing the visible-light photocatalytic activity of nano-TiO_2, Catal. Commun. 10 (2009) 925–929. doi:10.1016/j.catcom.2008.12.029.

[19] I. Chiu, Z. Shen, R. Wu, Promotion Effect of Au on N/TiO_2 for Hydrogen Generation from Water Splitting, 14 (2014) 7125–7130. doi:10.1166/jnn.2014.8958.

[20] X. Li, T. Fan, H. Zhou, B. Zhu, J. Ding, D. Zhang, Microporous and Mesoporous Materials A facile way to synthesize biomorphic N-TiO_2 incorporated with Au nanoparticles with narrow size distribution and high stability, Microporous Mesoporous Mater. 116 (2008) 478–484. doi:10.1016/j.micromeso.2008.05.007.

[21] M. Bellardita, M. Addamo, A. Di Paola, G. Marcì, L. Palmisano, L. Cassar, M. Borsa, Photocatalytic activity of TiO_2/SiO_2 systems, J. Hazard. Mater. 174 (2010) 707–713. doi:10.1016/j.jhazmat.2009.09.108.

[22] V.B. Koli, S. Mavengere, J.-S. Kim, Photocatalytic properties of TiO_2-SiO_2-coated concrete on toluene gas, Mater. Res. Express. 5 (2018) 125006. doi:10.1088/2053-1591/aae01c.

[23] A. Rosales, A. Maury Ramírez, R.M. De Gutiérrez, C. Guzmán, K. Esquivel, SiO_2@TiO_2 coating: Synthesis, physical characterization and photocatalytic evaluation, Coatings. 8 (2018) 120. doi:10.3390/coatings8040120.

[24] R. Zouzelka, J. Rathousky, Photocatalytic abatement of NO_x pollutants in the air using commercial functional coating with porous morphology, Appl. Catal. B Environ. 217 (2017) 466–476. doi:10.1016/j.apcatb.2017.06.009.

[25] L. Pinho, M.J. Mosquera, Titania-silica nanocomposite photocatalysts with application in stone self-cleaning, J. Phys. Chem. C. 115 (2011) 22851–22862. doi:10.1021/jp2074623.

[26] ISO 787-11: General methods of test for pigments and extenders — Part 11: Determination of tamped volume and apparent density after tamping., (1981).

[27] J. Tauc, Optical properties and electronic structure of amorphous Ge and Si, Mater. Res. Bull. 3 (1968) 37–46. doi:10.1016/0025-5408(68)90023-8.

[28] S.P. Tandon, J.P. Gupta, Measurement of forbidden energy gap of semiconductors by diffuse reflectance technique, Phys. Status Solidi. 38 (1970) 363–367. doi:10.1002/pssb.19700380136.

[29] J. Rodríguez-Carvajal, Recent advances in magnetic structure determination by neutron powder diffraction, Phys. B Condens. Matter. 192 (1993) 55–69. doi:10.1016/0921-4526(93)90108-I.

[30] H.M. Rietveld, A profile refinement method for nuclear and magnetic structures, J. Appl. Crystallogr. 2 (1969) 65–71. doi:10.1107/S0021889869006558.

[31] P. Scherrer, Bestimmung der Größe und der inneren Struktur von Kolloidteilchen mittels Röntgenstrahlen, Nachrichten von Der Gesellschaft Der Wissenschaften Zu Göttingen, Math. Klasse. 2 (1918) 98–100. http://eudml.org/doc/59018.

[32] A. Mills, S. Elouali, The nitric oxide ISO photocatalytic reactor system: Measurement of NO_x removal activity and capacity, J. Photochem. Photobiol. A Chem. 305 (2015) 29–36. doi:10.1016/j.jphotochem.2015.03.002.

[33] ISO 22197-1; Fine ceramics (advanced ceramics, advanced technical ceramics) – Test method for air purification performance of semiconducting photocatalytic materials – Part 1: Removal of nitric oxide, 2016.

[34] A. Mills, L. Burns, C. O'Rourke, S. Elouali, Kinetics of the photocatalysed oxidation of NO in the ISO 22197 reactor, J. Photochem. Photobiol. A Chem. 321 (2016) 137–142. doi:10.1016/j.jphotochem.2016.01.010.

[35] J. Landers, G.Y. Gor, A. V. Neimark, Density functional theory methods for characterization of porous materials, Colloids Surfaces A Physicochem. Eng. Asp. 437 (2013) 3–32. doi:10.1016/j.colsurfa.2013.01.007.

[36] J. Wang, D.N. Tafen, J.P. Lewis, Z. Hong, A. Manivannan, M. Zhi, M. Li, N. Wu, Origin of Photocatalytic Activity of Nitrogen-Doped TiO_2 Nanobelts, J. Am. Chem. Soc. 131 (2009) 12290–12297. doi:10.1021/ja903781h.

[37] R. Katoh, A. Furube, K. Yamanaka, T. Morikawa, Charge Separation and Trapping in N-Doped TiO2 Photocatalysts: A Time-Resolved Microwave Conductivity Study, J. Phys. Chem. Lett. 1 (2010) 3261–3265. doi:10.1021/jz1011548.

[38] V. Amendola, R. Pilot, M. Frasconi, O.M. Maragò, M.A. Iatì, Surface plasmon resonance in gold nanoparticles: a review, J. Phys. Condens. Matter. 29 (2017) 203002. doi:10.1088/1361-648X/aa60f3.

[39] G. Wang, L. Xu, J. Zhang, T. Yin, D. Han, Enhanced photocatalytic activity of powders TiO_2 (P25) via Calcination Treatment, Int. J. Photoenergy. 2012 (2012) 1–9. doi:10.1155/2012/265760.

[40] R. López, R. Gómez, Band-gap energy estimation from diffuse reflectance measurements on sol–gel and commercial TiO_2: A comparative study, J. Sol-Gel Sci. Technol. 61 (2012) 1–7. doi:10.1007/s10971-011-2582-9.

[41] K. Doudrick, O. Monzón, A. Mangonon, K. Hristovski, P. Westerhoff, Nitrate reduction in water using commercial titanium dioxide photocatalysts (P25, P90, and Hombikat UV100), J. Environ. Eng. 138 (2012) 852–861. doi:10.1061/(ASCE)EE.1943-7870.0000529.

[42] M.E. Simonsen, H. Jensen, Z. Li, E.G. Søgaard, Surface properties and photocatalytic activity of nanocrystalline titania films, J. Photochem. Photobiol. A Chem. 200 (2008)

192–200. doi:10.1016/j.jphotochem.2008.07.013.

[43] M. Thommes, K. Kaneko, A. V. Neimark, J.P. Olivier, F. Rodriguez-Reinoso, J. Rouquerol, K.S.W. Sing, Physisorption of gases, with special reference to the evaluation of surface area and pore size distribution (IUPAC Technical Report), Pure Appl. Chem. 87 (2015) 1051–1069. doi:10.1515/pac-2014-1117.

[44] M. Kruk, M. Jaroniec, Gas adsorption characterization of ordered organic-inorganic nanocomposite materials, Chem. Mater. 13 (2001) 3169–3183. doi:10.1021/cm0101069.

[45] Y. Cong, J. Zhang, F. Chen, M. Anpo, Synthesis and characterization of nitrogen-doped TiO_2 nanophotocatalyst with high visible light activity, J. Phys. Chem. C. 111 (2007) 6976–6982. doi:10.1021/jp0685030.

[46] M. Sathish, B. Viswanathan, R.P. Viswanath, C.S. Gopinath, Synthesis, characterization, electronic structure, and photocatalytic activity of nitrogen-doped TiO_2 nanocatalyst, Chem. Mater. 17 (2005) 6349–6353. doi:10.1021/cm052047v.

[47] X. Chen, C. Burda, Photoelectron spectroscopic investigation of nitrogen-doped titania nanoparticles, J. Phys. Chem. B. 108 (2004) 15446–15449. doi:10.1021/jp0469160.

[48] H. Li, J. Li, Y. Huo, Highly active TiO_2N photocatalysts prepared by treating TiO_2 precursors in NH_3/ethanol fluid under supercritical conditions, J. Phys. Chem. B. 110 (2006) 1559–1565. doi:10.1021/jp055830j.

[49] Y.-C. Yen, S. Ou, K.-J. Lin, One-pot synthesis of nitrogen-doped TiO_2 nanowires with enhanced photocurrent generation, J. Chinese Chem. Soc. 64 (2017) 1392–1398. doi:10.1002/jccs.201700226.

[50] X. Wang, T.-T. Lim, Solvothermal synthesis of C–N codoped TiO_2 and photocatalytic evaluation for bisphenol A degradation using a visible-light irradiated LED photoreactor, Appl. Catal. B Environ. 100 (2010) 355–364. doi:10.1016/j.apcatb.2010.08.012.

[51] F. Peng, L. Cai, L. Huang, H. Yu, H. Wang, Preparation of nitrogen-doped titanium dioxide with visible-light photocatalytic activity using a facile hydrothermal method, J. Phys. Chem. Solids. 69 (2008) 1657–1664. doi:10.1016/j.jpcs.2007.12.003.

[52] H.U. Lee, S.C. Lee, S. Choi, B. Son, S.M. Lee, H.J. Kim, J. Lee, Efficient visible-light induced photocatalysis on nanoporous nitrogen-doped titanium dioxide catalysts, Chem. Eng. J. 228 (2013) 756–764. doi:10.1016/j.cej.2013.05.059.

[53] H. Kisch, S. Sakthivel, M. Janczarek, D. Mitoraj, A Low-Band gap, nitrogen-modified titania visible-light photocatalyst, J. Phys. Chem. C. 111 (2007) 11445–11449. doi:10.1021/jp066457y.

[54] S. Arrii, F. Morfin, A.J. Renouprez, J.L. Rousset, Oxidation of CO on gold supported catalysts prepared by laser vaporization: Direct evidence of support contribution, J. Am. Chem. Soc. 126 (2004) 1199–1205. doi:10.1021/ja036352y.

[55] Gold reference catalysts, Gold Bull. 36 (2003) 24–24. doi:10.1007/BF03214864.

[56] M. Azar, V. Caps, F. Morfin, J.L. Rousset, A. Piednoir, J.C. Bertolini, L. Piccolo, Insights into activation, deactivation and hydrogen-induced promotion of a Au/TiO_2 reference catalyst in CO oxidation, J. Catal. 239 (2006) 307–312. doi:10.1016/j.jcat.2006.02.012.

[57] A. Mills, J. Wang, Photobleaching of methylene blue sensitised by TiO_2: an ambiguous system?, J. Photochem. Photobiol. A Chem. 127 (1999) 123–134. doi:10.1016/S1010-6030(99)00143-4.

[58] H. Jensen, K.D. Joensen, J.E. Jørgensen, J.S. Pedersen, E.G. Søgaard, Characterization of nanosized partly crystalline photocatalysts, J. Nanoparticle Res. 6 (2004) 519–526. doi:10.1007/s11051-004-1714-3.

[59] B. Ohtani, O.O. Prieto-Mahaney, D. Li, R. Abe, What is Degussa (Evonic) P25?

Crystalline composition analysis, reconstruction from isolated pure particles and photocatalytic activity test, J. Photochem. Photobiol. A Chem. 216 (2010) 179–182. doi:10.1016/j.jphotochem.2010.07.024.

[60] K. Yamanaka, T. Morikawa, Charge-carrier dynamics in nitrogen-doped TiO_2 powder studied by femtosecond time-resolved diffuse reflectance spectroscopy, J. Phys. Chem. C. 116 (2012) 1286–1292. doi:10.1021/jp209210u.

[61] V. Subramanian, E.E. Wolf, P. V. Kamat, Catalysis with TiO_2/gold manocomposites. effect of metal particle size on the fermi level equilibration, J. Am. Chem. Soc. 126 (2004) 4943–4950. doi:10.1021/ja0315199.

[62] P. V Kamat, D. Meisel, Nanoparticles in advanced oxidation processes, Curr. Opin. Colloid Interface Sci. 7 (2002) 282–287. doi:10.1016/S1359-0294(02)00069-9.

[63] Y. Zhou, D.M. King, X. Liang, J. Li, A.W. Weimer, Optimal preparation of Pt/TiO_2 photocatalysts using atomic layer deposition, Appl. Catal. B Environ. 101 (2010) 54–60. doi:10.1016/j.apcatb.2010.09.005.

[64] X. Zhang, Y.L. Chen, R.S. Liu, D.P. Tsai, Plasmonic photocatalysis., Rep. Prog. Phys. 76 (2013) 046401. doi:10.1088/0034-4885/76/4/046401.

[65] S. Mubeen, G. Hernandez-Sosa, D. Moses, J. Lee, M. Moskovits, Plasmonic photosensitization of a wide band gap semiconductor: converting plasmons to charge carriers, Nano Lett. 11 (2011) 5548–5552. doi:10.1021/nl203457v.

[66] C. Langhammer, Z. Yuan, I. Zorić, B. Kasemo, Plasmonic properties of supported Pt and Pd nanostructures, Nano Lett. 6 (2006) 833–838. doi:10.1021/nl060219x.

[67] V.P. Zhdanov, C. Hägglund, B. Kasemo, Relaxation of plasmons in nm-sized metal particles located on or embedded in an amorphous semiconductor, Surf. Sci. 599 (2005) L372–L375. doi:10.1016/j.susc.2005.10.001.

[68] X. Chen, H. Zhu, J. Zhao, Z. Zheng, X. Gao, Visible-light-driven oxidation of organic contaminants in air with gold nanoparticle catalysts on oxide supports, Angew. Chemie Int. Ed. 47 (2008) 5353–5356. doi:10.1002/anie.200800602.

[69] J. Lee, T. Javed, T. Skeini, A.O. Govorov, G.W. Bryant, N.A. Kotov, Bioconjugated Ag Nanoparticles and CdTe Nanowires: Metamaterials with Field-Enhanced Light Absorption, Angew. Chemie Int. Ed. 45 (2006) 4819–4823. doi:10.1002/anie.200600356.

[70] B. Cojocaru, Ş. Neaţu, E. Sacaliuc-Pârvulescu, F. Lévy, V.I. Pârvulescu, H. Garcia, Influence of gold particle size on the photocatalytic activity for acetone oxidation of Au/TiO_2 catalysts prepared by dc-magnetron sputtering, Appl. Catal. B Environ. 107 (2011) 140–149. doi:10.1016/j.apcatb.2011.07.007.

[71] V. Amendola, M. Meneghetti, Size Evaluation of Gold Nanoparticles by UV−vis Spectroscopy, J. Phys. Chem. C. 113 (2009) 4277–4285. doi:10.1021/jp8082425.

[72] J.A. Scholl, A.L. Koh, J.A. Dionne, Quantum plasmon resonances of individual metallic nanoparticles, Nature. 483 (2012) 421–427. doi:10.1038/nature10904.

[73] S. Malola, L. Lehtovaara, J. Enkovaara, H. Häkkinen, Birth of the localized surface plasmon resonance in monolayer-protected gold nanoclusters, ACS Nano. 7 (2013) 10263–10270. doi:10.1021/nn4046634.

[74] A. Ayati, A. Ahmadpour, F.F. Bamoharram, B. Tanhaei, M. Mänttäri, M. Sillanpää, A review on catalytic applications of Au/TiO_2 nanoparticles in the removal of water pollutant., Chemosphere. 107 (2014) 163–174. doi:10.1016/j.chemosphere.2014.01.040.

[75] V. Subramanian, E. Wolf, P. V. Kamat, Semiconductor−Metal composite nanostructures. To what extent do metal nanoparticles improve the photocatalytic activity of TiO_2 films?, J. Phys. Chem. B. 105 (2001) 11439–11446. doi:10.1021/jp011118k.

[76] M. Rochkind, S. Pasternak, Y. Paz, Using dyes for evaluating photocatalytic properties: A critical review, Molecules. 20 (2015) 88–110. doi:10.3390/molecules20010088.

[77] N. Barbero, D. Vione, Why dyes should not be used to test the photocatalytic activity of semiconductor oxides, Environ. Sci. Technol. 50 (2016) 2130–2131. doi:10.1021/acs.est.6b00213.

[78] Y. Ohko, Y. Nakamura, N. Negishi, S. Matsuzawa, K. Takeuchi, Photocatalytic oxidation of nitrogen monoxide using TiO_2 thin films under continuous UV light illumination, J. Photochem. Photobiol. A Chem. 205 (2009) 28–33. doi:10.1016/j.jphotochem.2009.04.005.

[79] W. Zhu, S. Xiao, D. Zhang, P. Liu, H. Zhou, W. Dai, F. Liu, H. Li, Highly efficient and stable Au/CeO_2–TiO_2 photocatalyst for nitric oxide abatement: Potential application in flue gas treatment, Langmuir. 31 (2015) 10822–10830. doi:10.1021/acs.langmuir.5b02232.

[80] L. Pinho, M.J. Mosquera, Photocatalytic activity of TiO_2-SiO_2 nanocomposites applied to buildings: Influence of particle size and loading, Appl. Catal. B Environ. 134–135 (2013) 205–221. doi:10.1016/j.apcatb.2013.01.021.

[81] L. Pinho, J.C. Hernández-Garrido, J.J. Calvino, M.J. Mosquera, 2D and 3D characterization of a surfactant-synthesized TiO_2–SiO_2 mesoporous photocatalyst obtained at ambient temperature, Phys. Chem. Chem. Phys. 15 (2013) 2800–2808. doi:10.1039/c2cp42606d.

[82] N. Balázs, D.F. Srankó, A. Dombi, P. Sipos, K. Mogyorósi, The effect of particle shape on the activity of nanocrystalline TiO_2 photocatalysts in phenol decomposition. Part 2: The key synthesis parameters influencing the particle shape and activity, Appl. Catal. B Environ. 96 (2010) 569–576. doi:10.1016/j.apcatb.2010.03.006.

Supplementary materials

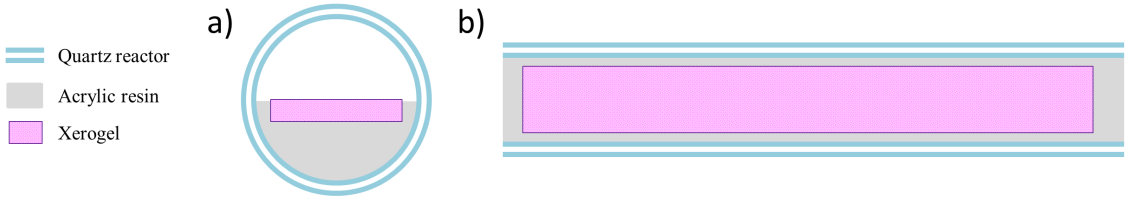

Figure S1. Diagram of xerogel samples disposition on quartz reactor, a) cross section, b) longitudinal section.

Figure S2. Photographs of P25 particle series.

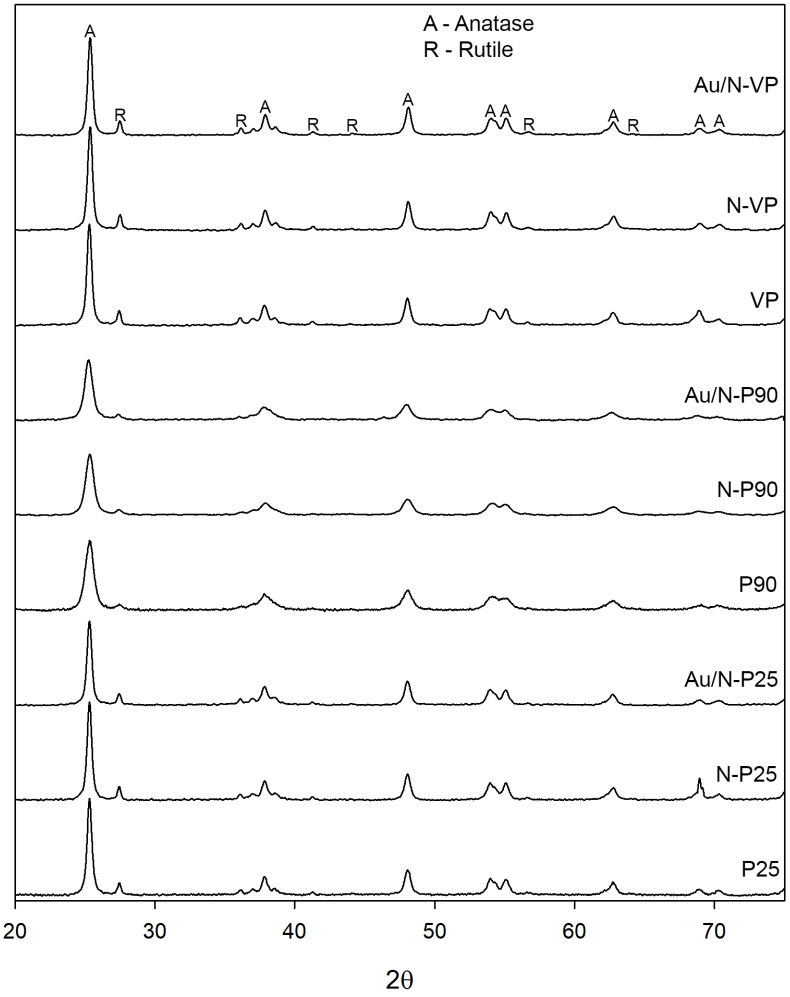

Figure S3. XRD patterns of the samples under study.

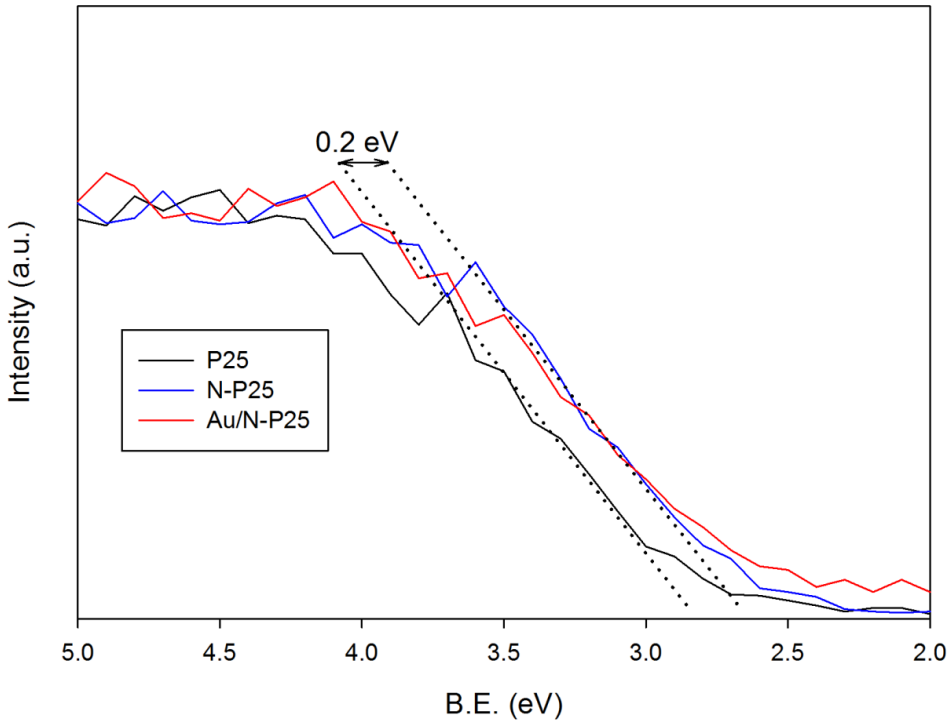

Figure S4. Detail of valence band in XPS spectra of P25 particle series.

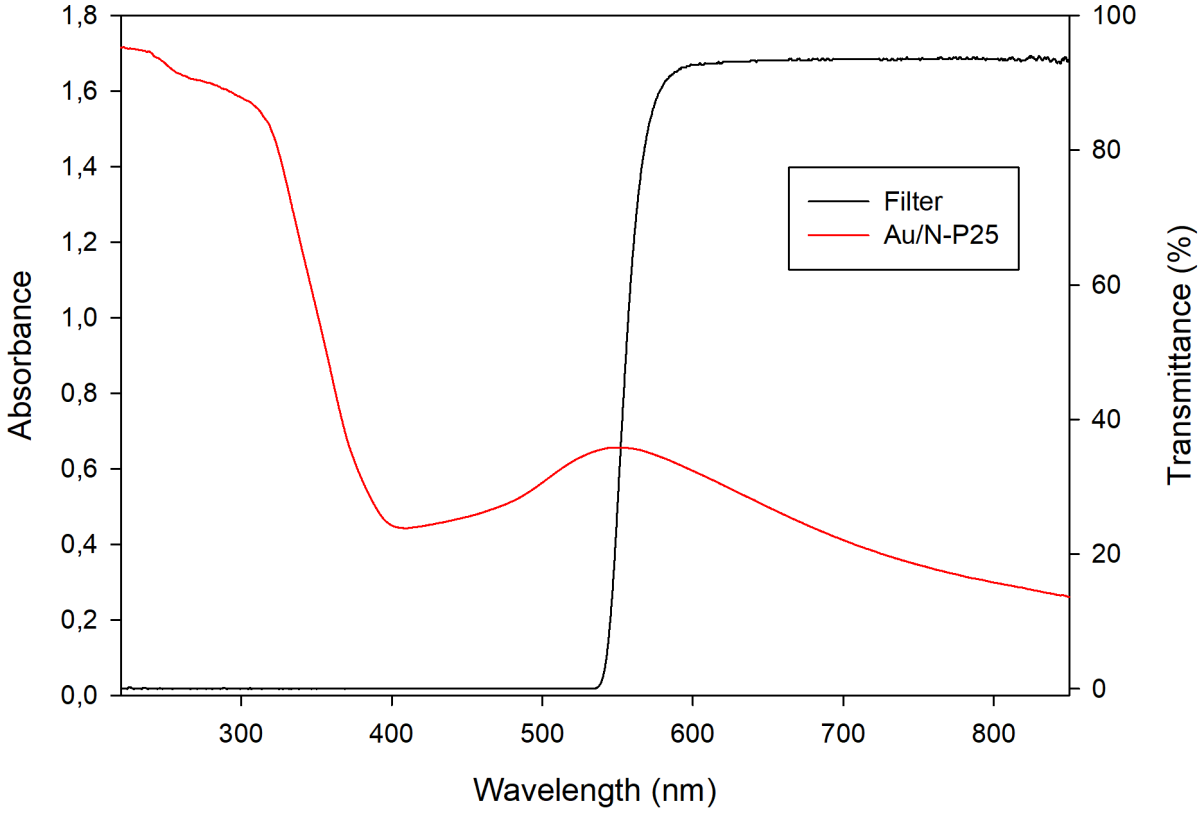

Figure S5. Transmittance spectrum of light filter employed for MB degradation test under visible light compared to the absorbance spectra of Au/N-P25 particles.

Chapter 7

Use of Au/N-TiO_2/SiO_2 photocatalysts in building materials with NO depolluting activity

Use of Au/N-TiO_2/SiO_2 photocatalysts in building materials with NO depolluting activity

Sent to Journal of Hazardous Materials

Manuel Luna[a], José M. Gatica[b*], Hilario Vidal[b], María J. Mosquera[a**]

[a]Departamento de Química Física, Universidad de Cádiz, Puerto Real 11510, Spain

[b]Departamento C.M., I.M. y Química Inorgánica, Universidad de Cádiz, Puerto Real 11510, Spain

Corresponding authors: *josemanuel.gatica@uca.es; **mariajesus.mosquera@uca.es

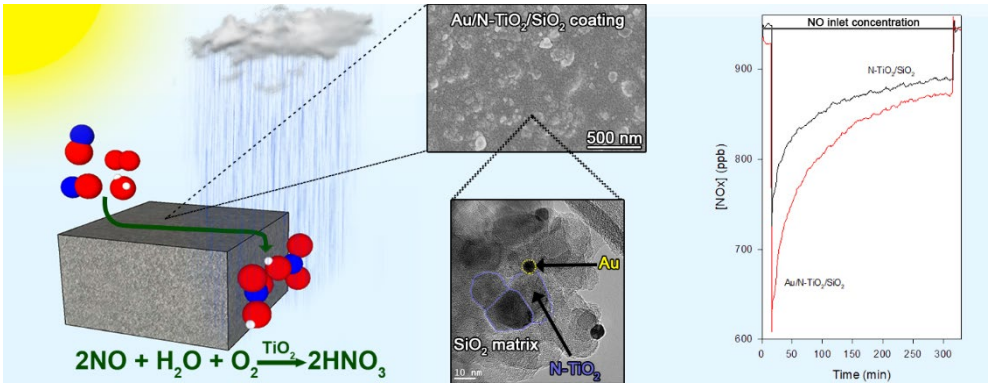

Highlights

New Au/N-TiO_2/SiO_2 photocatalysts for building materials with NO depolluting activity

The TiO_2/SiO_2 ratio of the coating is directly related with its photo-activity

The AuNPs considerably improve the performance of nitrogen-doped TiO_2

The substrate determines the photoactivity of the coated building material

Photoactivity, price and aesthetic impact can be balanced in the building material

Abstract

Two factors are key in the designing of a TiO_2 photocatalyst for building materials that meets the requirements for environmental applications: the TiO_2 light absorption restricted to UV and its poor adhesion to the substrates. In this work, two strategies of TiO_2 modification, nitrogen doping and AuNPs deposition, were combined in order to promote the TiO_2 photoactivity under solar radiation. By the other hand, the Au/N-TiO_2 photocatalysts were incorporated in a silica sol allowing their application by spray on three different building material substrates (limestone, granite and concrete), where the sol spontaneously produced Au/N-TiO_2/SiO_2 well-adhered coatings. The samples photoactivity was evaluated by dye degradation tests and NO depolluting measurements. The obtained results demonstrated that the AuNPs considerably enhanced the photoactivity of N-TiO_2, increasing the amount of NO_x removed by a factor of 1.5. In addition, the role of the substrate and the TiO_2/SiO_2 ratio of the coating were also investigated. The coatings practically triplicated their depolluting effectiveness on concrete in comparison with their application on limestone. A direct correlation between the TiO_2 loading and the photoactivity was observed, increasing NO_x abatement by a factor of 1.3 when the Au/N-TiO_2 loading of the coating was raised from 10 to 25%

Keywords: photocatalyst; NO de-pollution; Au-N-TiO2/SiO2; buildings materials

1. Introduction

TiO_2 is an efficient and polyvalent photocatalyst that has been implemented for a wide variety of applications related to energy and environment [1]. Specifically, the TiO_2 can be employed on building materials in order to get materials with self-cleaning, self-sterilizing or de-polluting properties [2], thanks to the same fundamental mechanism. Briefly, the TiO_2 light irradiation induces the formation of electron-hole pairs that can react with water or oxygen for producing

highly reactive radicals, which are able to degrade a wide range of organic and inorganic compounds [3]. However the TiO_2 effectiveness for building materials applications is restricted due to its absorption of light mainly located in the UV range which is scarce in both outdoor (solar light) and indoor (common visible lamps) conditions. Important efforts have been undertaken in order to resolve this drawback using different strategies of TiO_2 modification, such as metal deposition, doping or dye sensitization, among others [4]. Each TiO_2 modification causes specific changes in the TiO_2 but there are two main mechanisms responsible of TiO_2 photoactivity enhancement.

(1) The new elements incorporated to TiO_2 act as traps for the photogenerated charge carriers reducing the electron-hole pair recombination rate [5]. The higher lifetime electron-hole pairs increase the chance that they can react with the species involved in the process enhancing the photoprocess yield.

(2) The resultant photocatalysts have absorption in the visible range allowing the visible light activation of TiO_2. In the case of dopants, they are integrated in the TiO_2 modifying their composition and electronic structure, which induces a reduction of band-gap energy [6]. Other components, such as noble metal nanoparticles or organic dyes, absorb visible light by themselves and transfer their excited electron to the TiO_2 initiating the photoprocess [7,8].

In this sense, nitrogen has been proposed for its incorporation to the TiO_2 structure producing N-TiO_2 photocatalysts with enhanced photoactivity due to the reduction of electron-hole pairs recombination and the increase of visible light absorption [9]. By the other hand, the use of gold nano-particles (AuNPs) has been reported to significantly promote the TiO_2 performance, acting in several ways: (1) They also reduce electron-hole pairs recombination [10]; (2) Their localized surface plasmon resonance (LSPR) effect triggers different mechanisms that promote

the photoactivity under visible light, TiO_2 sensitization being the main mechanism [11]; (3) Gold also shows catalytic properties by itself that can promote certain photodegradation mechanism [12], as reported for NO_x photo-oxidation [13]. The combination of both, nitrogen and gold, produces Au/N-TiO_2 photocatalysts, whose activity is higher than that corresponding to N-TiO_2 or Au/TiO_2 photocatalysts alone [14–16].

Regarding the TiO_2 photocatalysts integration on building materials, they can be directly incorporated during their preparation, as in the case of tiles, mortars and concrete [17–20]. However, these methods are unsuitable for application on existing structures and thus, other strategies such as the photocatalyst dispersion in water or a solvent are commonly employed for in situ applications. The resultant coatings after the solvent evaporation show a suitable performance, but they are composed by an agglomeration of particles that can be easily detached by the weathering [21]. The use of a binder can mitigate this problem, being silica the ideal candidate because it has chemical affinity for the common building materials and has large surface areas for promoting the photocatalytic effect [22–25].

The photocatalysts developed in this work are based on the integration of a previously optimized Au/N-TiO_2 nano-material [26] in a sol-gel synthesis that has been recently reported to be effective for the treatment of building materials [27–29]. This method presents several advantages: (1) The obtained sols have low viscosities and consequently, they can be applied in situ on building by common and low cost application methods; (2) the sols penetrate in the porous structure of the substrate and spontaneously gel producing well-adhered coatings; (3) A surfactant, n-octylamine, integrated in the sol allows the formation of a crack-free mesoporous material by an inverse micelles mechanism [30]. As far as we know, there are no previous reports in the use of an advanced titania-based formulation employing both gold and nitrogen doping for application as an effective depolluting coating for building materials.

The Au/N-TiO_2/SiO_2 photocatalysts were here applied as sols on three different widespread used building substrates (limestone, granite and concrete) in order to evaluate their effectiveness in the degradation of deposited dyes and NO_x abatement. In parallel, a deep investigation of texture and structure of the developed photocatalysts and the coated substrates were carried out in order to stablish a relationship with their performance.

2. Experimental

2.1. Au/N-TiO_2/SiO_2 photocatalysts synthesis and application on building materials

Aeroxide P25 particles from Evonik were employed as TiO_2 starting material. 100 ml of P25 water dispersion (6 g/100 ml) were prepared in a ultrasonic cleaner for 10 minutes and they were mixed under vigorous stirring with 100 ml of $KAuCl_4$ solution (1.9 mM) and 100 ml of urea solution (75% w/w urea/H_2O). The slurry was maintained under stirring and heated at 80 °C for 2 hours, and after that it was centrifuged and washed with water several times. The obtained solid was dried at 100 °C overnight and, finally, calcined at 273 °C for 4 hours in order to obtain the Au/N-TiO_2 particles. The procedure was repeated replacing the $KAuCl_4$ solution by water in order to get the corresponding nitrogen doped TiO_2 particles named N-TiO_2. The synthesis of these materials was designed according to our previous optimization study [26].

The prepared Au/N-TiO_2 and N-TiO_2 particles were mixed with a silica precursor, TES40 WN (Wacker), an ethylsilicate oligomer that provides approximately 41% of silica upon complete hydrolysis, according to a procedure previously described [13]. The amount of Au/N-TiO_2 (or N-TiO_2) particles added to the synthesis was adjusted in order to obtain TiO_2/SiO_2 ratios in the final photocatalysts of 2.5, 10 and 25 wt.%. For the synthesis of the sol with the highest TiO_2 content, the silica oligomer was replaced by a TES40/isopropanol (2:1 v/v) mixture, in order to prevent an excessive sol viscosity. The sols were designated SXAu/N-TiO_2 or SXN-TiO_2,

where X refers to the TiO_2/SiO_2 ratio in the final photocatalyst. For comparative purposes, an additional photocatalyst without titania nitrogen-doping denominated as S10Au/TiO_2 was prepared, as previously described [13], using preformed AuNPs and P25 particles. After the synthesis 15 ml of sols were disposed on Ø85 mm plastic Petri dishes and maintained at 18±0.5 °C of temperature and 53±3 % of humidity. The spontaneous sol-gel transition took place overnight and the gels were dried at the same conditions until constant weight before their characterization.

Three different building materials, widely employed in construction for facade facing, pavements and wall covering, whether indoor or outdoor, were chosen as substrate for evaluating the photocatalysts under study: (1) Capri limestone, a stone quarried from Cabra (Spain) composed by calcite and with an open porosity of 9-12%; (2) Granite Grey Pearl, a stone quarried from Meis (Spain) that has an open porosity lower than 1%; and (3) HERPLAC® concrete, a glass fibre reinforced concrete (GFRC) board composed by an agglomerate of aggregates of dolomitic and limestone aggregates of 0.1 to 6 mm and Portland cement CEM I 52.5R, vibro-compacted and armed with alkali resistant fiberglass manufactured by HERMESA STONE, S.L. This concrete presents an open porosity of around 10%.

The sols were applied directly (without dilution) on 4x4x2 and 5x10x2 cm^3 pieces of the building materials by spraying onto one of the larger faces until its saturation. The surface was maintained wet for 1 minute, the sol excess was removed by spraying air and the samples were weighed to calculate the uptake of the products. Finally, the treated stones were dried at 18±0.5 °C and 53±3 % of humidity until constant weight (approximately after two weeks). These samples were named employing the name of the photocatalysts applied and a letter indicating the substrate, L (limestone), G (granite) or C (concrete). As an example S10Au/N-TiO_2/L indicates S10Au/N-TiO_2 photocatalysts deposited on limestone.

2.2. Characterization

The rheological properties of the sols were studied, immediately after the synthesis, using a viscometer (model DV-II+ with UL/Y adapter) from Brookfield operating at 25 ºC. The viscosities values were obtained as the slope of shear stress vs. shear rate curves in their ranges of Newtonian behaviour evaluated.

The obtained photocatalytic xerogels were characterized using the following techniques:

The UV–visible reflectance spectra were recorded on a UV-2600 spectrophotometer from Shimadzu equipped with an ISR-2600 integrating sphere, using $BaSO_4$ powder as white reference.

The N_2 physisorption isotherms at -196 ºC were obtained using a Quantachrome Autosorb IQ. Approximately 0.3 g of sample, previously calcined at 200 ºC overnight and evacuated at 150 ºC, were employed in the analysis. The corresponding pore size distributions were calculated using a hybrid NLDFT (non-local density functional theory) approach [31] considering the absorption of N_2 on silica containing cylindrical pores.

Scanning electron microscopy (SEM) images Au/N-TiO_2/SiO_2 photocatalysts were taken using a Nova NanoSEM model from the FEI Company, working at an acceleration voltage of 5 kV.

Transmission electron microscopy and high angle annular dark field scanning transmission electron microscopy (HAADF-STEM) images of the Au/N-TiO_2/SiO_2 photocatalysts were recorded using a JEOL 2010F TEM/STEM microscope operated at 200 kV.

The changes in stone colour induced by the treatments were determined by using a solid reflection spectrophotometer, Colorflex model, from HunterLab. The conditions used were

illuminant D65 and observer 10º. CIELa*b* colour space was used and variations in colour were evaluated using the total colour difference (ΔE*) parameter.

SEM images of building materials samples were taken using the previously described microscope.

2.3. Photocatalytic evaluation

The photocatalytic properties of the treated building materials samples were evaluated through a methylene blue (MB) photodegradation test, according to the methodology previously described [24]. Specifically, 320 µL of a 0.5 mM ethanolic MB were deposited on the samples and the conditions in the solar chamber were 250 W/m^2 of irradiance, 50 ºC of temperature and 45±5 % of relative humidity.

10x5x2 cm^3 coated samples were employed for evaluating the NO photo-oxidation using the ISO 22197-1 standard [32], details of the system employed can be found in the literature [33,34]. The amount of NO and NO_x removed and the NO_2 generated were calculated employing the following expressions.

$$n_{NO} = \frac{f}{22.4}\int_{t_{on}}^{t_{off}} ([NO]_{in} - [NO]_{out})\ dt$$

$$n_{NO_2} = \frac{f}{22.4}\int_{t_{on}}^{t_{off}} [NO_2]_{out}\ dt$$

$$n_{NO_x} = n_{NO} - n_{NO_2}$$

Where n_{xx} are the µmol of gas removed or generated, f is the normalized air flow in l/min (0ºC, 101.3 kPa), t_{off} and t_{on} are the times of lamp switch off and on respectively, $[NO]_{in}$ is the supply

NO air concentration in ppm, $[NO]_{out}$ is the NO air concentration at the reactor exit in ppm and $[NO_2]_{out}$ is the NO_2 air concentration at the reactor exit in ppm.

Also the selectivity to NO_2 of the process was calculated as follows:

$$\%\ NO_2\ selectivity = \ 100 \cdot \frac{n_{NO_2}}{n_{NO}}$$

3. Results and discussion

3.1. Photocatalysts characterization

A progressive increase of sol viscosity was observed as the TiO_2 content was raised and no differences were detected between Au/N-TiO_2/SiO_2 and N-TiO_2/SiO_2 sols (see Table 1) The sol with the lowest TiO_2 content had a viscosity value similar to that corresponding to commercial stone consolidant [35] Additionally, the use of isopropanol effectively reduced by a third the viscosity value of the sol containing the highest TiO_2 amount compared with the equivalent without it [36]. However, the TiO_2 sedimentation occurred faster for the sols containing the isopropanol.

Table 1. Sol viscosities and textural parameters of the photocatalysts under study.

Sample	Viscosity (mPa·s)	S_{BET} (m^2/g)	V_{pore} (cm^3/g)*
S2.5N-TiO_2	5.5	389	0.294
S2.5Au/N-TiO_2	5.7	384	0.275
S10N-TiO_2	7.3	250	0.241
S10Au/N-TiO_2	7.0	260	0.251
S25N-TiO_2	17.2	226	0.307
S25Au/N-TiO_2	15.8	244	0.292

* total pore volume determined by nitrogen adsorption volume at $P/P_0 = 0.995$

The first indication of the presence of AuNPs was the intense pink-purple colour of the Au/N-TiO_2/SiO_2 photocatalysts that contrasted with the white colour of the N-TiO_2/SiO_2. This visible absorption revealed the localized surface resonance plasmon (LSRP) effect of the AuNPs whose absorption band is clearly visible in the UV-Vis spectra of the xerogels (Figure 1). The intensity of the LSRP band and the xerogels colour were increased as the amount of Au/N-TiO_2 particles in the xerogel was raised. The strong absorption of TiO_2 was localized in the UV region of spectra. The intensity of TiO_2 absorption was significantly increased from the TiO_2/SiO_2 ratio of 2.5% to that of 10% but no differences were observed between 10% and 25% due to the spectra saturation.

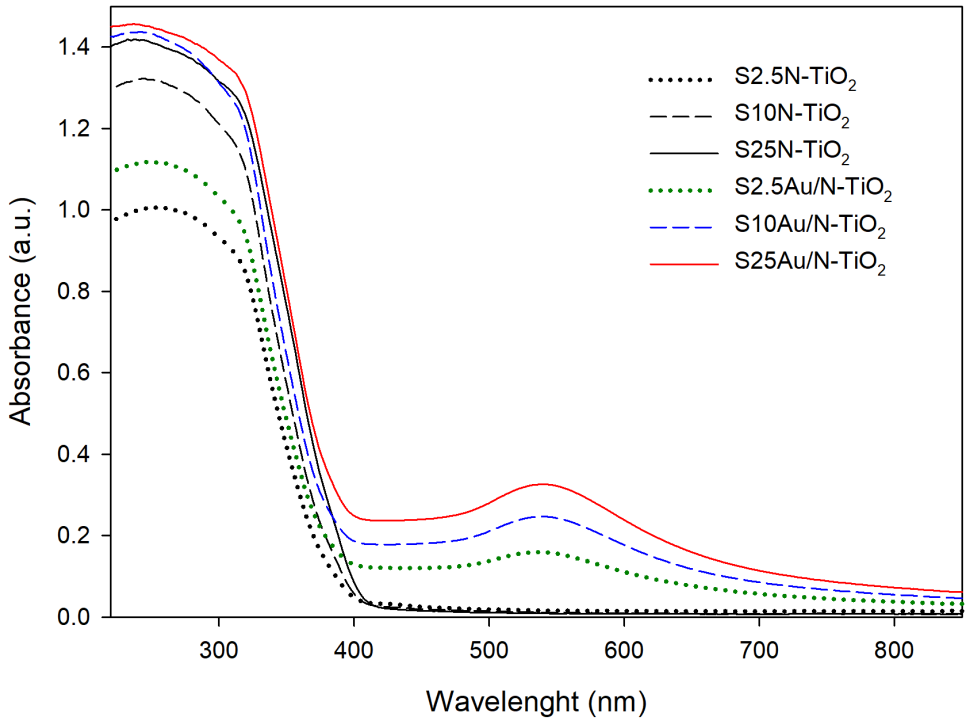

Figure 1. UV-Visible absorbance spectra of the photocatalysts under study. The absorbance spectra were obtained from the respective reflectance spectra.

The porous structure of the photocatalysts was studied by means of N_2 physisorption, obtaining the isotherms and corresponding pore size distributions shown in Figure 2. The plots for N-TiO_2/SiO_2 are not represented because they practically overlap with those of the equivalent

Au/N-TiO_2/SiO_2 photocatalysts. All the samples showed type IV(a) isotherms with H2 hysteresis loops, which are characteristic of mesoporous materials where there is pore blocking [37]. Comparing the isotherms, there was a gradual hysteresis transformation from H2(a) to H2(b) as the TiO_2 content was raised, being both characteristic of ink-bottle pores. However, H2(a) hysteresis is observed when the desorption occurs via cavitation, suggesting that necks of the pores are much narrower than their bodies [38]. Therefore, the observed transition must be a consequence of the introduction of bigger TiO_2 particles in the xerogels structure promoting the formation of bigger pores. This fact was effectively observed in the pore size distribution curves where there was a progressive disappearance of the micropores and small mesopores with a corresponding increase in the amount of bigger mesopores. The most remarkable difference in the textural parameters (see Table 1) was the higher surface area for the photocatalysts with the lowest TiO_2 content, which is related with their higher mesopore fraction.

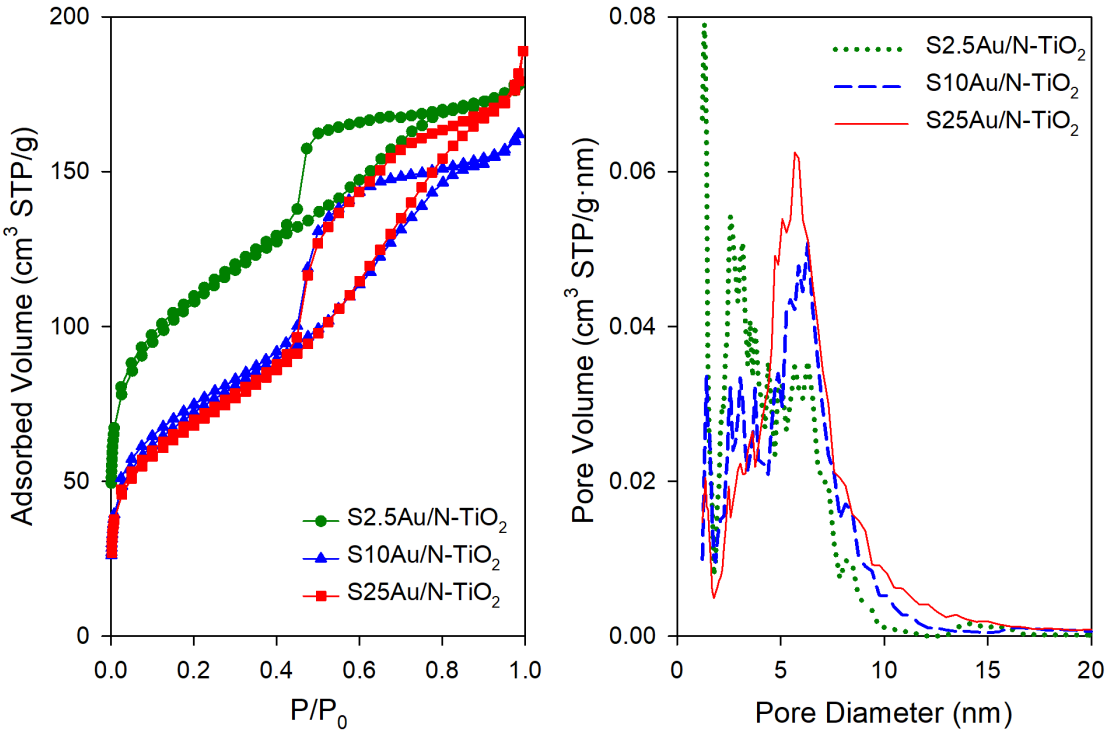

Figure 2. N_2 physisorption isotherms and NLDFT pore size distributions obtained for the Au/N-TiO_2/SiO_2 photocatalysts under study.

The SEM images (Figure 3.a-c) showed that the photocatalysts had rough and porous surfaces that contain particles corresponding to the TiO_2. In the specific case of photocatalysts with the highest TiO_2 content, large TiO_2 particles agglomerates emerging on the surface were observed (Figure S1 in the supplementary material). The TEM images (Figure 3.d-f) revealed fine details about the photocatalysts nano-structure showing polyhedral crystalline TiO_2 particles and smaller AuNPs, with the darkest contrast, that are integrated in an amorphous silica matrix composed by a compaction of poor-defined particles. The formation of SiO_2 particles is a consequence of the role played by n-octylamine, promoting an inverse micelle mechanism [30]. This structure looked less compact as the TiO_2 content was raised, which is related with the increase of bigger pores revealed by the N_2 physisorption study. The Au phase was also detected being in contact with the TiO_2 particles (Figure 3.g), which is fundamental to get an effective Au-TiO_2 interaction via LSPR-mediated charge injection [39]. Finally, the STEM-HAADF images and their corresponding XEDS maps allowed studying the TiO_2 distribution in the matrix (see Figure 3.j-o). First, as might be expected, the amount of TiO_2 was higher as the TiO_2/SiO_2 ratio of the photocatalyst was raised. Regarding the TiO_2 dispersion, it was homogeneous for the 2.5 and 10% TiO_2/SiO_2 ratios. On the contrary, the TiO_2 was evidently agglomerated in the photocatalyst with the highest TiO_2/SiO_2, confirming the results previously observed by SEM. This TiO_2 agglomeration can be a consequence of the isopropanol introduction in the sol, reducing the colloidal stability of TiO_2 (as observed by the higher tendency to sedimentation).

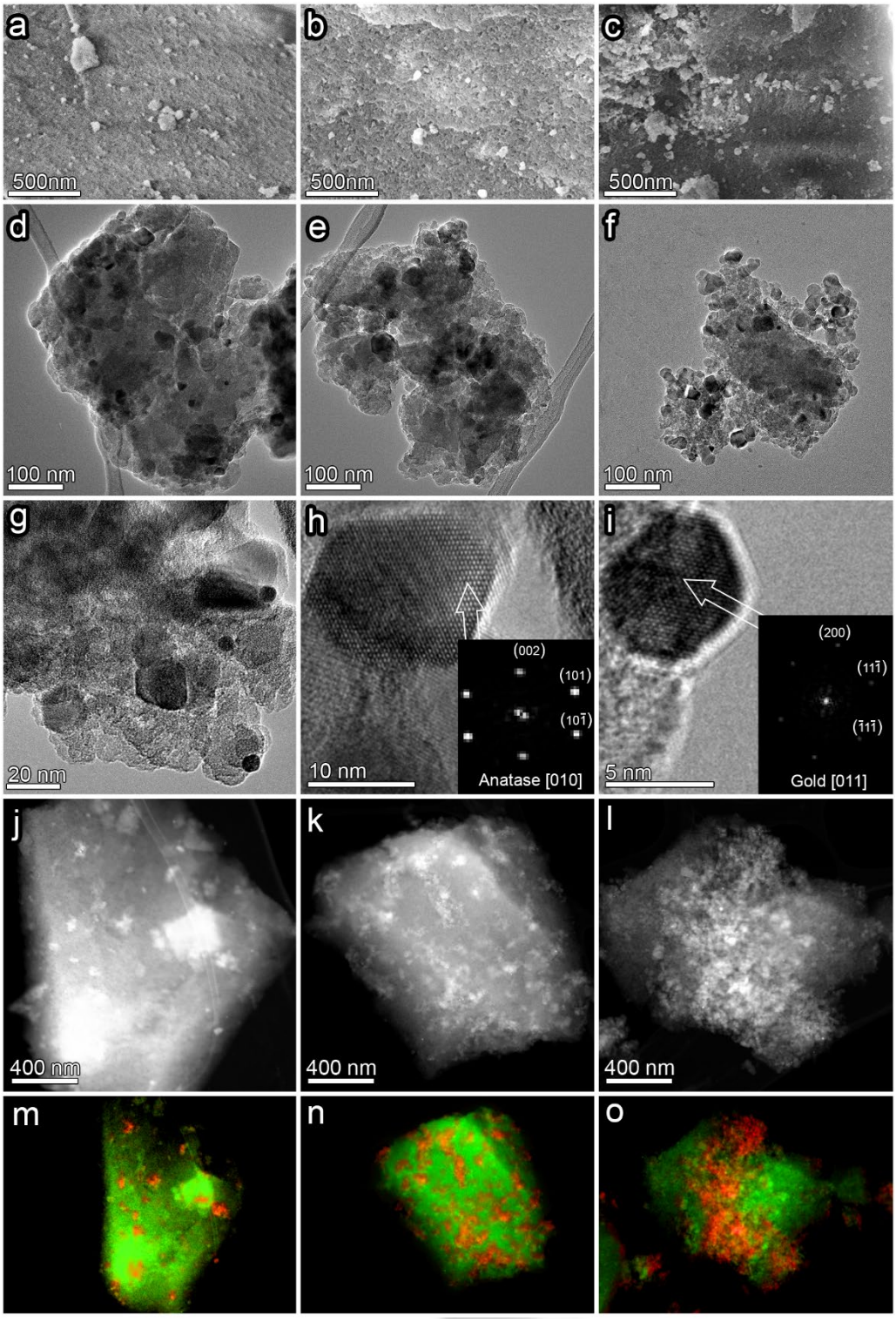

Figure 3. Electron microscopy images of the Au/N-TiO_2/SiO_2 photocatalysts under study. SEM images of a) S2.5Au/N-TiO_2/SiO_2, b) S10Au/N-TiO_2/SiO_2 and c) S25Au/N-TiO_2/SiO_2. TEM images of d) S2.5Au/N-TiO_2/SiO_2, e) S10Au/N-TiO_2/SiO_2, f) S25Au/N-TiO_2/SiO_2, detail of g) Au and TiO_2 particles, h) TiO_2 and i) Au structure. STEM-HAADF images of j) S2.5Au/N-TiO_2/SiO_2, k) S10Au/N-TiO_2/SiO_2, l) S25Au/N-TiO_2/SiO_2 and m), n), l) their corresponding XEDS maps showing the TiO_2 (red) and SiO_2 (green) distribution.

3.2. Building materials samples characterization

The sol uptake values (Table 2) were dependent on the substrate and sol viscosity, but not affected by the presence of gold. The uptake values for the granite samples were lower than the sensitivity of the balance because the sol could not penetrate in the non-porous structure and produced a thin layer on the polished surface. By contrast, the sol penetrated inside the porous substrates, limestone and concrete, producing higher uptakes. Regarding the effect of the sol viscosity, the uptake was reduced as viscosity was raised because the higher viscosity makes difficult the penetration inside the substrate porous structure. This photocatalysts penetration in the substrate was confirmed by observation of the cross section of the samples (Figure S2), being the penetration depth values compiled in Table 2. The lower penetration for concrete samples contrasts with their higher sol absorption. This anomalous behaviour can be related to the presence of big holes in the concrete, produced by air bubbles trapped into the cement paste during manufacturing process, which can accumulate large amounts of sol.

Table 2. Uptake values, photocatalysts penetration and total colour difference (ΔE*) for the treated building materials samples.

Sample	**Uptake (mg/cm^2)**	**Penetration (mm)**	**ΔE***
S2.5Au/N-TiO_2/G	<0.6	-	1.4
S10Au/N-TiO_2/G	<0.6	-	2.5
S25Au/N-TiO_2/G	<0.6	-	3.6
S2.5Au/N-TiO_2/L	11.4	7.2	2.4
S10Au/N-TiO_2/L	7.5	5.5	6.9
S25Au/N-TiO_2/L	6.0	5.0	13.5
S2.5Au/N-TiO_2/C	17.0	2.5	2.6
S10Au/N-TiO_2/C	14.4	2.0	7.1
S25Au/N-TiO_2/C	12.5	1.7	17.7

The SEM images of the building materials samples (Figure 4) showed that the photocatalyst produced a continuous and homogeneous coating that covered the original substrate surface. The absence of fractures in the coating demonstrates the role played by the n-octylamine to prevent the xerogel cracking [40] which promotes the adhesion, and the subsequent durability, of the coatings [41,42]. The higher magnification allows confirming that the coatings were constituted by an agglomeration of small particles corresponding to the silica particles produced via micelles inverse mechanism proposed for sols containing n-octylamine [30]. The TiO_2 particles of bigger size were especially present in the surface of the coatings with the highest TiO_2 content.

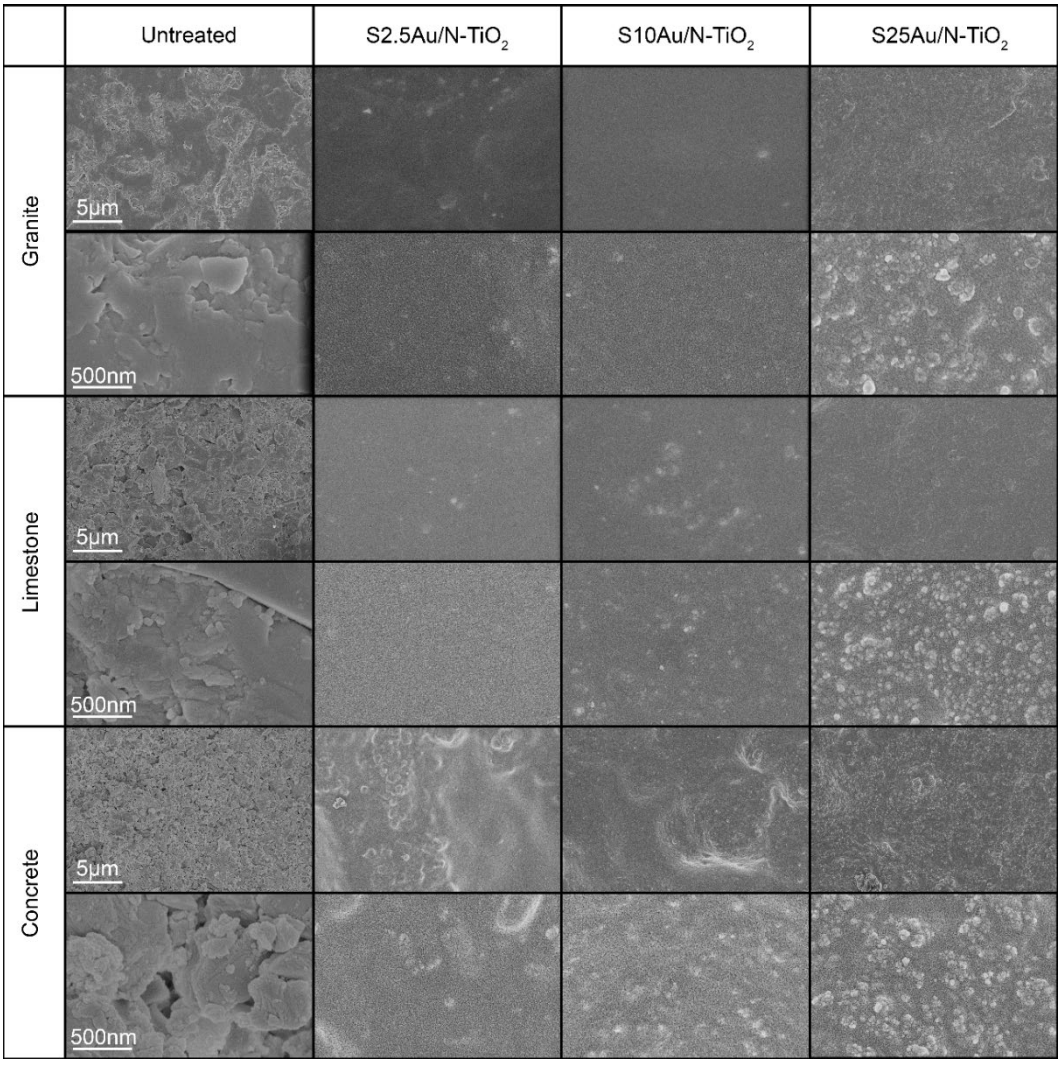

Figure 4. SEM images of the building materials samples, the images in the same row has the same magnification.

As might be expected, the colour changes of the substrates induced by the treatments (Table 2) were determined by two factors, the sol absorption of the substrate and the gold amount in the photocatalyst. In this way, the ΔE* values for the S25Au/N-TiO_2/L and S25Au/N-TiO_2/C samples were excessive, since this parameter can be relevant in certain applications where the material appearance should be preserved, being 5 the value generally accepted [43]. By comparison, the ΔE* values for the N-TiO_2/SiO_2 photocatalyst were in the range 1-2, being the characteristic colour of the AuNPs, which was completely different from the substrate colours, the responsible of this behaviour. In fact, the case of concrete and limestone samples was extreme due to their quasi-white colours being possible to restrict the colour change in substrates with other colours. For example, the application of the S10Au/N-TiO_2 photocatalyst on grey concrete instead of white reduced the ΔE* value from 8.2 to 4.3.

On the other hand, since the high price of gold, its impact on the cost of the catalysts was also evaluated. This cost associated to gold is directly related with the uptake values and the Au content in the sol, being in the range 0.01-0.07 €/m^2 for the granite, 0.19-0.70 €/m^2 for the limestone and 0.28-1.47 €/m^2 for the concrete (estimate from the current market value of gold 37 €/g). For comparison, the photocatalytic paint KEIM Soldalit®-ME [44] has a treatment cost of approximately 10 €/m^2 considering its price and its typical consumption. Therefore, the developed treatments can be commercially viable, especially for low absorbent substrates and low TiO_2/SiO_2 ratios. In addition this cost can be further decreased reducing the sol uptake. Therefore, the amount of photocatalyst applied on the substrate can be reduced applying an only silica sol as a primer before the Au/N-TiO_2/SiO_2 sol application, this strategy can also help to mitigate the problems associated to the substrate colour changes.

3.3. Photocatalytic evaluation

MB was employed for evaluating the photocatalytic properties of treated building material samples, being the results compiled in Figure 5. The MB deposited on untreated stones was degraded due to its own photolysis under UV radiation, as previously reported [45]. All treatments accelerated the MB degradation rate confirming that the TiO_2 contained in the coatings provided photocatalytic properties to the substrates. In addition, the increase of TiO_2 content increased the coating performance. This behaviour was the expected since the TiO_2 is the photoactive component of the nanocomposite. However, other photocatalysts parameters, such as their textural properties, also affect their photoactivity, as previously reported for TiO_2/SiO_2 coatings prepared using the same TiO_2 ratios [36]. Therefore, the synthesis modification incorporating isopropanol allowed increasing the TiO_2/SiO_2 ratio of coating, which promoted its photoactivity. In the specific case of the limestone substrate the coatings with 25% TiO_2/SiO_2 ratio showed practically the same performance as the coatings with 10%. This anomaly is due to the fraction of MB dimer, which is slowerly degraded [24], being higher for the 25% TiO_2/SiO_2 coating (see Figure S3). Regarding the AuNPs inclusion, all the Au/N-TiO_2/SiO_2 photocatalysts showed higher activities than the corresponding N-TiO_2/SiO_2 ones. This photoactivity enhancement was especially significant for S2.5Au/N-TiO_2 that reached an activity comparable to the N-TiO_2/SiO_2 coating with a 10% TiO_2/SiO_2 ratio, and even a 25% ratio for the granite. These results confirmed the effectiveness of AuNPs for enhancing the TiO_2 photoactivity, allowing a good performance in spite of the reduction of the TiO_2 loading. The AuNPs on the TiO_2 surface act as reservoir of photogenerated electron-hole pairs, reducing their recombination and promoting their transference to the species involved in the photocatalytic process [46–48]. Additionally, the AuNPs LSPR can also enhance the TiO_2 photoactivity under visible radiation [11], being the TiO_2 sensitization mechanism the most important one [49]. Finally, all the Au/N-TiO_2/SiO_2 coatings showed higher activity than the

Au/TiO_2/SiO_2 previously developed [13], being this fact related to: (1) the preparation method; the catalyst prepared using preformed AuNPs generally gives lower activities than those prepared from gold deposition methods [10]; (2) the AuNPs size, the small size implies a higher number of particles increasing the TiO_2-Au contact and smaller particles shift the fermi level promoting the charge separation [46]; (3) the nitrogen doping promotes the TiO_2 photoactivity for reducing the charge carriers recombination rate [50], producing a synergic effect with gold [16].

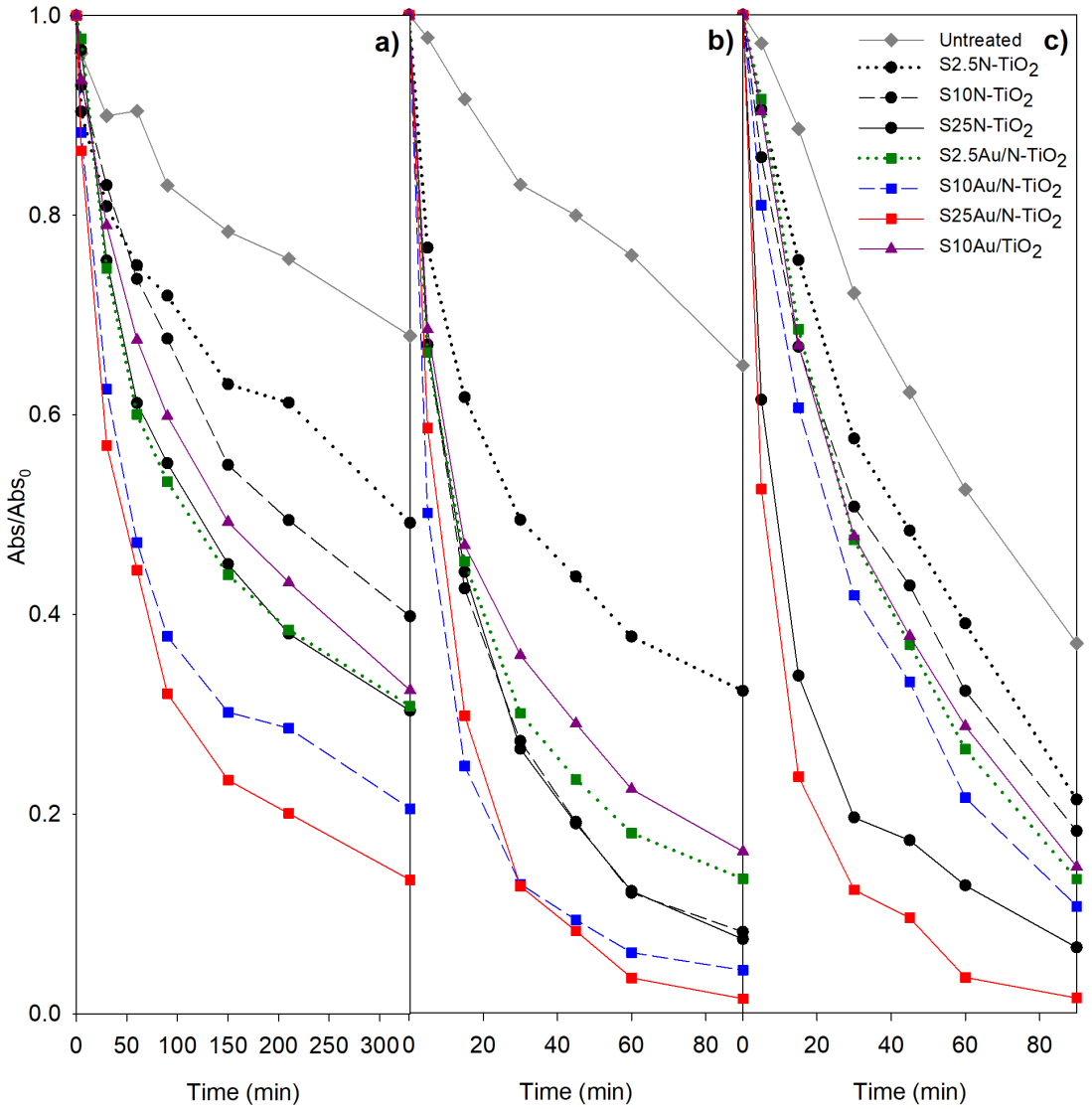

Figure 5. Evolution of methylene blue absorbance on the building materials samples.

According to the MB degradation tests, selected samples were employed for testing their NO de-polluting properties, the obtained results being compiled in Figure 6 and Table 3. The photoactivity of the samples was evidenced by the immediate and sharp decrease in NO concentration, continuing with a slight increase during the test. Simultaneously, NO_2 was generated causing that the NO_x concentration maintains higher than the NO one. This apparently activity reduction is frequently observed for long duration tests [34], due to the HNO_3 accumulation in the photocatalysts that promote the NO to NO_2 conversion [51]. According to the measured NO_x elimination percentages, two clear trends (which were in accordance with those resulting from the above commented MB degradation study) were observed. Thus, the amount of NO_x removed was increased as (1) the TiO_2/SiO_2 ratio was raised and (2) the AuNPs were included in the coating. This effect of AuNPs is not only a matter of the enhancement in TiO_2 photoactivity induced by doping with AuNPs, but the gold can also activate the O_2 and NO via adsorption mechanisms promoting the NO oxidation. Regarding the different substrates, the low activity of granite samples was related to the relatively low amount of photocatalyst deposited. On the other hand, the concrete samples showed the highest activity being the amount of NO_x removed by them nearly 3 times that of the limestone samples. In addition to the higher amount of photocatalyst deposited in this substrate, this fact is attributable to its different acid-base behaviour. Both, limestone and concrete, have an alkaline nature but concrete basicity is higher and even the treated surfaces showed a pronounced basic behaviour, as demonstrated by a simple phenolphthalein test (see Figure S4 in supplementary material). The basic medium can promote the HNO_3 elimination in the form of nitrates enhancing the amount of NO_x removed. In this sense, the addition of an alkali, such as CaO, can be a viable strategy to optimize this type of photocatalysts for NO_x removal applications. Finally, to put the obtained results in perspective, a previous study of Zouzelka and Rathousky [52] was employed for comparison. In that work the NOx photodegradation of concrete samples coated

with a P25-based photocatalytic paint was tested under the same conditions employed in the present work. Specifically, the samples had a TiO_2 loading of 5 mg/cm^2 and showed an initial NO_x photodegradation rate of 176 µmol·m^{-2}·h^{-1}. By contrast, the initial degradation rate for the S25Au/N-TiO_2/C sample, calculated from the first 30 minutes of test, was 344 µmol·m^{-2}·h^{-1} and its TiO_2 loading was only 1 mg/cm^2. Therefore, the developed Au/N-TiO_2/SiO_2 coatings practically duplicate the NO_x depolluting performance of a common TiO_2 coating reducing by a fifth the amount of TiO_2 necessary, which demonstrates the potential of these photocatalysts for depolluting purposes.

Table 3 Results of the NO photodegradation tests.

Sample	NO removed		NO_x removed		% NO_2 selectivity
	µmol	%	µmol	%	
S25N-TiO_2/G	0.5	1.5	0.2	0.6	60.0
S25Au/N-TiO_2/G	1.7	6.0	0.6	1.9	70.6
S10N-TiO_2/L	2.4	6.4	0.9	2.3	62.5
S10Au/N-TiO_2/L	2.8	7.6	1.3	3.6	53.6
S25N-TiO_2/L	3.5	9.4	1.0	2.8	71.4
S25Au/N-TiO_2/L	5.3	14.3	1.7	4.5	67.9
S10N-TiO_2/C	3.8	11	2.0	5.9	51.4
S10Au/N-TiO_2/C	5.2	15.1	3.2	9.3	38.5
S25N-TiO_2/C	6.8	19.6	3.2	9.2	52.9
S25Au/N-TiO_2/C	8.5	24.5	4.2	12	51.7

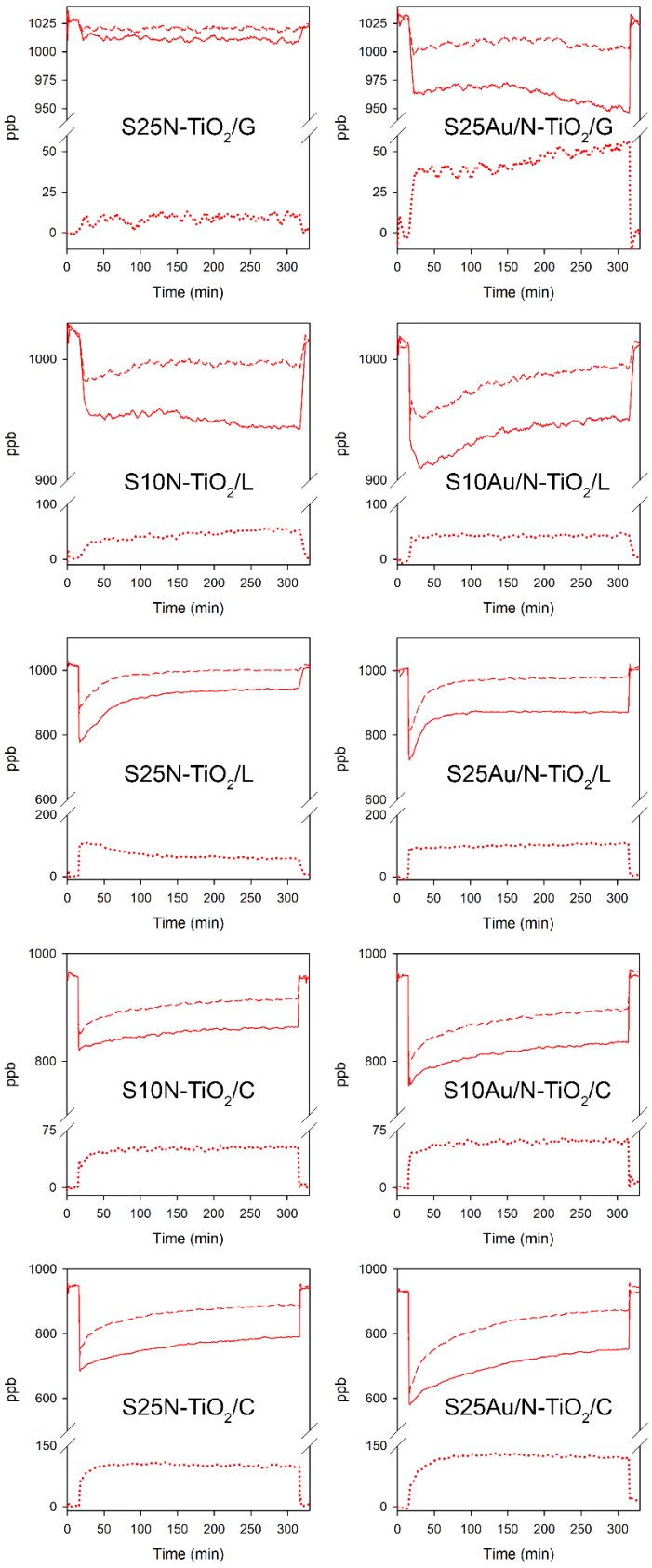

Figure 6. Evolution of NO (continuous line), NO_2 (dotted line) and NO_x (dashed line) concentration profiles during the NO photodegradation tests.

4. Conclusions

Au/N-TiO_2/SiO_2 photocatalysts with potential use for building materials showing de-polluting performance have been obtained by using a sol-gel synthesis. Specifically, TiO_2 particles doped with nitrogen and AuNPs were integrated in the synthesis, obtaining sols that can be applied on building materials by common procedures. The sols spontaneously gel on the building materials producing the Au/N-TiO_2/SiO_2 photocatalysts that cover the substrate surface, creating a photocatalytic coating. Three parameters that affect the coating performance were studied, obtaining the following conclusions.

(1) The substrate in which the sols are applied determines the final characteristics of the treated materials. The substrate porosity affects strongly the sol absorption, higher amounts of photocatalyst enhance the photoactivity but also induce higher color variations of the substrates. The chemical composition of the substrate can also modify the sample activity. In this work it has been demonstrated that a substrate with a higher alkaline behavior like concrete promotes the NO_x photodegradation.

(2) The promoted-TiO_2/SiO_2 ratio of the coating is directly related to its activity. On the other hand, the sol viscosity is increased as the TiO_2 loading is raised reducing the absorption and penetration in the substrate. In addition, a high TiO_2/SiO_2 ratio, as the highest one evaluated in this work (25 % wt.), can cause drastic color variations.

(3) The AuNPs considerably promote the activity of nitrogen-doped TiO_2. Specifically, the Au/N-TiO_2/SiO_2 coatings show activities comparable to those corresponding to the N-TiO_2/SiO_2 coatings with higher TiO_2/SiO_2 ratios. Additionally, it has been demonstrated that the combined titania modification with nitrogen and AuNPs employed produces photocatalysts which are considerably more active than those prepared from preformed

AuNPs and non-doped TiO_2. However, the AuNPs inclusion has the disadvantage of inducing strong color variations.

Therefore, these three parameters can be adjusted in other to get a photocatalytic building material with the desired compromise between activity, aesthetic characteristics and treatment cost.

Acknowledgments

This work has been supported by the Spanish Government/FEDER-EU (MAT2013-42934-R and MAT2017-84228-R). M. Luna would also like to thank the Spanish Government for his pre-doctoral grant (BES-2014-068031). We would also like to thank Prof. Andrew Mills and his group at the Queen's University of Belfast for allowing us to carry out the NO degradation measurements.

References

[1] M.T. Noman, M.A. Ashraf, A. Ali, Synthesis and applications of nano-TiO_2: a review, Environ. Sci. Pollut. Res. 26 (2019) 3262–3291. doi:10.1007/s11356-018-3884-z.

[2] J. Chen, C.S. Poon, Photocatalytic construction and building materials: From fundamentals to applications, Build. Environ. 44 (2009) 1899–1906. doi:10.1016/j.buildenv.2009.01.002.

[3] T. Ochiai, A. Fujishima, Photoelectrochemical properties of TiO_2 photocatalyst and its applications for environmental purification, J. Photochem. Photobiol. C Photochem. Rev. 13 (2012) 247–262. doi:10.1016/j.jphotochemrev.2012.07.001.

[4] H. Park, Y. Park, W. Kim, W. Choi, Surface modification of TiO_2 photocatalyst for environmental applications, J. Photochem. Photobiol. C Photochem. Rev. 15 (2013) 1–20. doi:10.1016/j.jphotochemrev.2012.10.001.

[5] R. Katoh, A. Furube, K. Yamanaka, T. Morikawa, Charge separation and trapping in N-Doped TiO_2 photocatalysts: A time-resolved microwave conductivity study, J. Phys. Chem. Lett. 1 (2010) 3261–3265. doi:10.1021/jz1011548.

[6] R. Asahi, T. Morikawa, T. Ohwaki, K. Aoki, Y. Taga, Visible-light photocatalysis in nitrogen-doped titanium oxides, Science (80-.). 293 (2001) 269–271. doi:10.1126/science.1061051.

[7] Y. Xu, C.H. Langford, UV- or visible-light-induced degradation of X3B on TiO_2 nanoparticles: The influence of adsorption, Langmuir. 17 (2001) 897–902. doi:10.1021/la001110m.

[8] N.T. Nolan, M.K. Seery, S.J. Hinder, L.F. Healy, S.C. Pillai, A Systematic Study of the Effect of Silver on the Chelation of Formic Acid to a Titanium Precursor and the Resulting Effect on the Anatase to Rutile Transformation of TiO_2, J. Phys. Chem. C. 114 (2010) 13026–13034. doi:10.1021/jp1016054.

[9] S.A. Ansari, M.M. Khan, M.O. Ansari, M.H. Cho, Nitrogen-doped titanium dioxide (N-doped TiO_2) for visible light photocatalysis, New J. Chem. 40 (2016) 3000–3009. doi:10.1039/C5NJ03478G.

[10] A. Primo, A. Corma, H. García, Titania supported gold nanoparticles as photocatalyst, Phys. Chem. Chem. Phys. 13 (2011) 886–910. doi:10.1039/C0CP00917B.

[11] X. Zhang, Y.L. Chen, R.S. Liu, D.P. Tsai, Plasmonic photocatalysis., Rep. Prog. Phys. 76 (2013) 046401. doi:10.1088/0034-4885/76/4/046401.

[12] M. Haruta, When gold is not noble: Catalysis by nanoparticles, Chem. Rec. 3 (2003) 75–87. doi:10.1002/tcr.10053.

[13] M. Luna, J.M. Gatica, H. Vidal, M.J. Mosquera, Au-TiO_2/SiO_2 photocatalysts with NO_x depolluting activity: Influence of gold particle size and loading, Chem. Eng. J. 368 (2019) 417–427. doi:10.1016/j.cej.2019.02.167.

[14] I. Chiu, Z. Shen, R. Wu, Promotion Effect of Au on N/TiO_2 for Hydrogen Generation from Water Splitting, 14 (2014) 7125–7130. doi:10.1166/jnn.2014.8958.

[15] X. Li, T. Fan, H. Zhou, B. Zhu, J. Ding, D. Zhang, Microporous and Mesoporous Materials A facile way to synthesize biomorphic N-TiO_2 incorporated with Au nanoparticles with narrow size distribution and high stability, Microporous Mesoporous Mater. 116 (2008) 478–484. doi:10.1016/j.micromeso.2008.05.007.

[16] B. Tian, C. Li, F. Gu, H. Jiang, Synergetic effects of nitrogen doping and Au loading on enhancing the visible-light photocatalytic activity of nano-TiO_2, Catal. Commun. 10 (2009) 925–929. doi:10.1016/j.catcom.2008.12.029.

[17] V. Vaiano, G. Sarno, P. Ciambelli, D. Sannino, Functionalization of ceramic tiles with N-doped TiO_2 and their photocatalytic function under UV or visible light irradiation, J. Adv. Oxid. Technol. 17 (2014) 193–201.

[18] M. Radeka, S. Markov, E. Lončar, O. Rudić, S. Vučetić, J. Ranogajec, Photocatalytic effects of TiO_2 mesoporous coating immobilized on clay roofing tiles, J. Eur. Ceram. Soc. 34 (2014) 127–136. doi:10.1016/j.jeurceramsoc.2013.07.010.

[19] J.S. Pozo-Antonio, A. Dionísio, Self-cleaning property of mortars with TiO_2 addition using real diesel exhaust soot, J. Clean. Prod. 161 (2017) 850–859. doi:10.1016/j.jclepro.2017.05.202.

[20] M.M. Hassan, H. Dylla, L.N. Mohammad, T. Rupnow, Evaluation of the durability of titanium dioxide photocatalyst coating for concrete pavement, Constr. Build. Mater. 24 (2010) 1456–1461. doi:10.1016/j.conbuildmat.2010.01.009.

[21] L. Pinho, M.J. Mosquera, Titania-silica nanocomposite photocatalysts with application in stone self-cleaning, J. Phys. Chem. C. 115 (2011) 22851–22862. doi:10.1021/jp2074623.

[22] R.E. Ramírez-García, J.A. González-Rodríguez, M. Arroyo-Ortega, S.A. Pérez-García, L. Licea-Jiménez, Engineered TiO_2 and SiO_2-TiO_2 films on silica-coated glass for increased thin film durability under abrasive conditions, Int. J. Appl. Ceram. Technol. 14 (2017) 39–49. doi:10.1111/ijac.12614.

[23] V.B. Koli, S. Mavengere, J.-S. Kim, Photocatalytic properties of TiO_2-SiO_2-coated concrete on toluene gas, Mater. Res. Express. 5 (2018) 125006. doi:10.1088/2053-1591/aae01c.

[24] M. Luna, J. Delgado, M.L.A. Gil, M. Mosquera, TiO_2-SiO_2 coatings with a low content of AuNPs for producing self-cleaning building materials, Nanomaterials. 8 (2018) 177. doi:10.3390/nano8030177.

[25] A. Rosales, A. Maury Ramírez, R.M. De Gutiérrez, C. Guzmán, K. Esquivel, SiO_2@TiO_2 coating: Synthesis, physical characterization and photocatalytic evaluation, Coatings. 8 (2018) 120. doi:10.3390/coatings8040120.

[26] M. Luna, J.M. Gatica, H. Vidal, M.J. Mosquera, One-pot synthesis of Au/N-TiO_2 photocatalysts for environmental applications: enhancement of dyes and NO_x photodegradation, manuscript submitted to Powder Technol. (2019).

[27] M.J. Mosquera, L.A.M. Carrascosa, N. Badreldin, Producing superhydrophobic/oleophobic coatings on Cultural Heritage building materials, Pure Appl. Chem. 90 (2018) 551–561. doi:10.1515/pac-2017-0404.

[28] R. Zarzuela, M. Carbú, M.L.A. Gil, J.M. Cantoral, M.J. Mosquera, CuO/SiO_2 nanocomposites: A multifunctional coating for application on building stone, Mater. Des. 114 (2017) 364–372. doi:10.1016/j.matdes.2016.11.009.

[29] L.A.M. Carrascosa, D.S. Facio, M.J. Mosquera, Producing superhydrophobic roof tiles, Nanotechnology. 27 (2016) 095604. doi:10.1088/0957-4484/27/9/095604.

[30] D.S.D.S. Facio, M. Luna, M.J.M.J. Mosquera, Facile preparation of mesoporous silica monoliths by an inverse micelle mechanism, Microporous Mesoporous Mater. 247 (2017) 166–176. doi:10.1016/j.micromeso.2017.03.041.

[31] M. Thommes, B. Smarsly, M. Groenewolt, P.I. Ravikovitch, A. V. Neimark, Adsorption hysteresis of nitrogen and argon in pore networks and characterization of novel micro- and mesoporous silicas, Langmuir. 22 (2006) 756–764. doi:10.1021/la051686h.

[32] ISO 22197-1; Fine ceramics (advanced ceramics, advanced technical ceramics) – Test method for air purification performance of semiconducting photocatalytic materials – Part 1: Removal of nitric oxide, 2016.

[33] A. Mills, L. Burns, C. O'Rourke, S. Elouali, Kinetics of the photocatalysed oxidation of NO in the ISO 22197 reactor, J. Photochem. Photobiol. A Chem. 321 (2016) 137–142. doi:10.1016/j.jphotochem.2016.01.010.

[34] A. Mills, S. Elouali, The nitric oxide ISO photocatalytic reactor system: Measurement of NO_x removal activity and capacity, J. Photochem. Photobiol. A Chem. 305 (2015) 29–36. doi:10.1016/j.jphotochem.2015.03.002.

[35] L. Pinho, F. Elhaddad, D.S. Facio, M.J. Mosquera, A novel TiO_2–SiO_2 nanocomposite converts a very friable stone into a self-cleaning building material, Appl. Surf. Sci. 275 (2013) 389–396. doi:10.1016/j.apsusc.2012.10.142.

[36] L. Pinho, M.J. Mosquera, Photocatalytic activity of TiO_2-SiO_2 nanocomposites applied to buildings: Influence of particle size and loading, Appl. Catal. B Environ. 134–135 (2013) 205–221. doi:10.1016/j.apcatb.2013.01.021.

[37] M. Thommes, K. Kaneko, A. V. Neimark, J.P. Olivier, F. Rodriguez-Reinoso, J. Rouquerol, K.S.W. Sing, Physisorption of gases, with special reference to the evaluation of surface area and pore size distribution (IUPAC Technical Report), Pure Appl. Chem. 87 (2015) 1051–1069. doi:10.1515/pac-2014-1117.

[38] K.A. Cychosz, R. Guillet-Nicolas, J. García-Martínez, M. Thommes, Recent advances in the textural characterization of hierarchically structured nanoporous materials, Chem. Soc. Rev. 46 (2017) 389–414. doi:10.1039/c6cs00391e.

[39] S. Linic, P. Christopher, D.B. Ingram, Plasmonic-metal nanostructures for efficient conversion of solar to chemical energy, Nat. Mater. 10 (2011) 911–921. doi:10.1038/nmat3151.

[40] J.F. Illescas, M.J. Mosquera, Surfactant-Synthesized PDMS/Silica Nanomaterials Improve Robustness and Stain Resistance of Carbonate Stone, J. Phys. Chem. C. 115 (2011) 14624–14634. doi:10.1021/jp203524p.

[41] C. Mendoza, A. Valle, M. Castellote, A. Bahamonde, M. Faraldos, TiO_2 and TiO_2–SiO_2 coated cement: Comparison of mechanic and photocatalytic properties, Appl. Catal. B Environ. 178 (2015) 155–164. doi:10.1016/j.apcatb.2014.09.079.

[42] G. Borsoi, R. Veiga, A.S. Silva, Effect of nanostructured lime-based and silica-based products on the consolidation of historical renders, in: 3rd Hist. Mortars Conf., 2013: pp. 1–9. doi:10.13140/2.1.1988.9282.

[43] C. Miliani, M.L. Velo-Simpson, G.W. Scherer, Particle-modified consolidants: A study on the effect of particles on sol-gel properties and consolidation effectiveness, J. Cult. Herit. 8 (2007) 1–6. doi:10.1016/j.culher.2006.10.002.

[44] KEIM Soldalit®-ME, https://www.keimpaintshop.co.uk/shop/view/9-Soldalit-ME-/405-White (accessed March 14, 2019).

[45] A. Houas, Photocatalytic degradation pathway of methylene blue in water, Appl. Catal. B Environ. 31 (2001) 145–157. doi:10.1016/S0926-3373(00)00276-9.

[46] V. Subramanian, E.E. Wolf, P. V. Kamat, Catalysis with TiO_2/gold manocomposites. effect of metal particle size on the fermi level equilibration, J. Am. Chem. Soc. 126 (2004) 4943–4950. doi:10.1021/ja0315199.

[47] P. V Kamat, D. Meisel, Nanoparticles in advanced oxidation processes, Curr. Opin. Colloid Interface Sci. 7 (2002) 282–287. doi:10.1016/S1359-0294(02)00069-9.

[48] Y. Zhou, D.M. King, X. Liang, J. Li, A.W. Weimer, Optimal preparation of Pt/TiO_2 photocatalysts using atomic layer deposition, Appl. Catal. B Environ. 101 (2010) 54–60. doi:10.1016/j.apcatb.2010.09.005.

[49] S. Mubeen, G. Hernandez-Sosa, D. Moses, J. Lee, M. Moskovits, Plasmonic photosensitization of a wide band gap semiconductor: converting plasmons to charge carriers, Nano Lett. 11 (2011) 5548–5552. doi:10.1021/nl203457v.

[50] K. Yamanaka, T. Morikawa, Charge-carrier dynamics in nitrogen-doped TiO_2 powder studied by femtosecond time-resolved diffuse reflectance spectroscopy, J. Phys. Chem. C. 116 (2012) 1286–1292. doi:10.1021/jp209210u.

[51] Y. Ohko, Y. Nakamura, N. Negishi, S. Matsuzawa, K. Takeuchi, Photocatalytic oxidation of nitrogen monoxide using TiO_2 thin films under continuous UV light illumination, J. Photochem. Photobiol. A Chem. 205 (2009) 28–33. doi:10.1016/j.jphotochem.2009.04.005.

[52] R. Zouzelka, J. Rathousky, Photocatalytic abatement of NO_x pollutants in the air using commercial functional coating with porous morphology, Appl. Catal. B Environ. 217 (2017) 466–476. doi:10.1016/j.apcatb.2017.06.009.

Supplementary materials

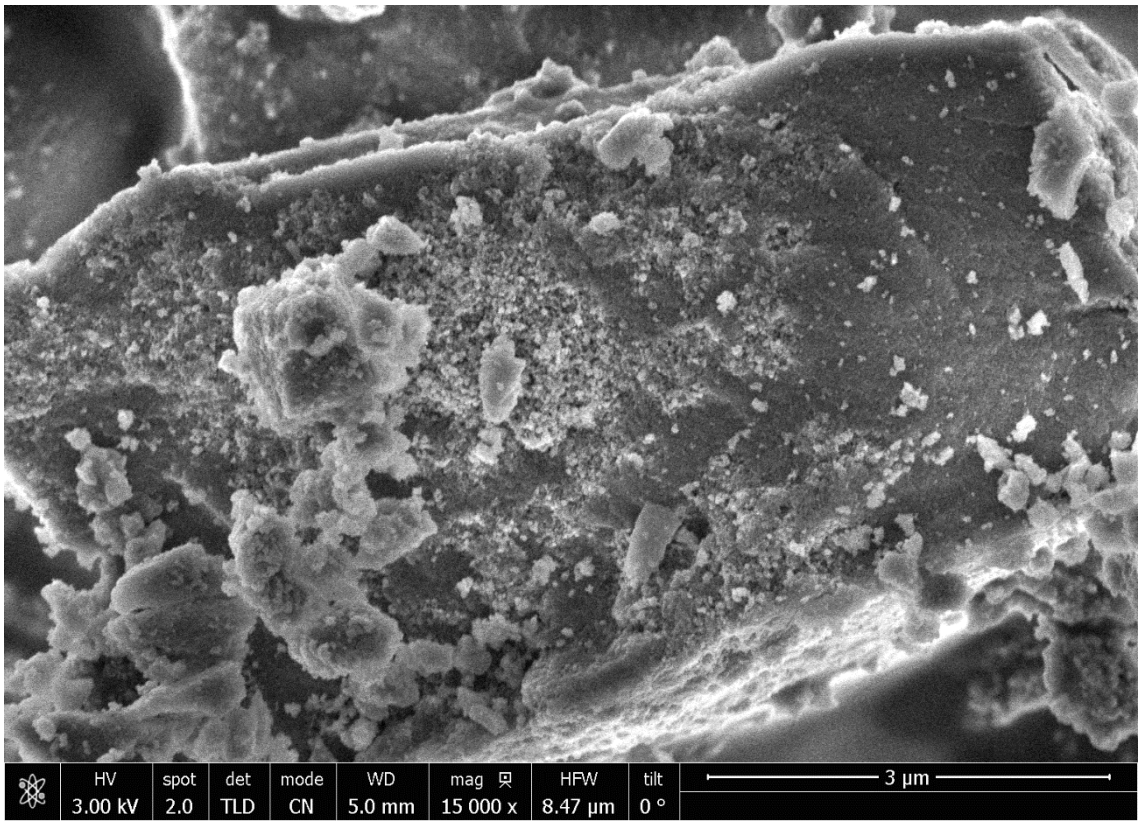

Figure S1. SEM image showing a general view of the Au/N-TiO_2/SiO_2 photocatalyst.

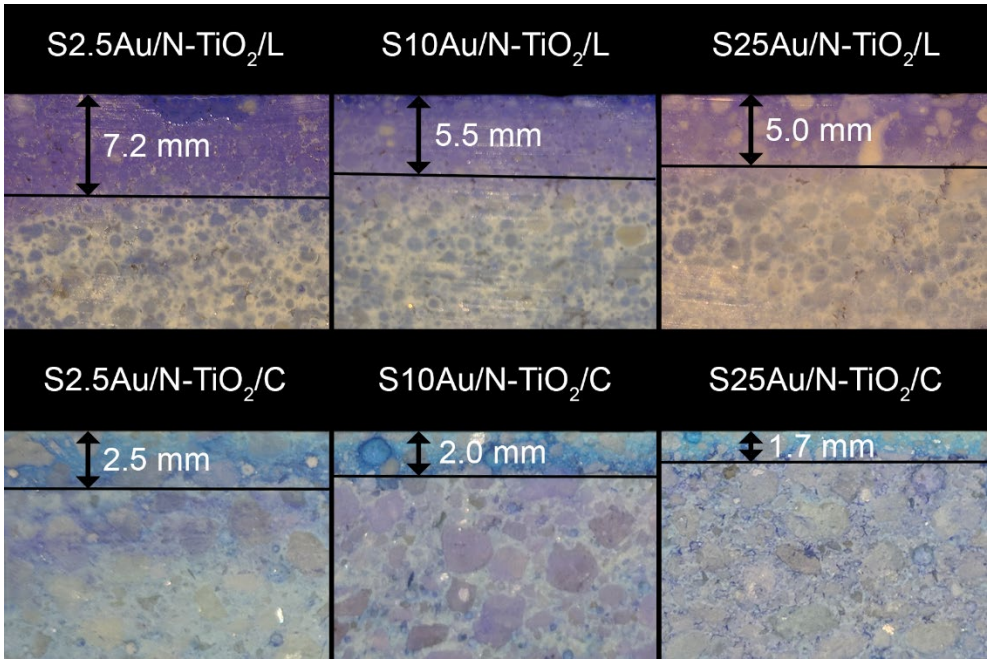

Figure S2. Cross section photographs of treated building material samples stained with methylene blue in order to highlight the photocatalyst penetration in the substrate.

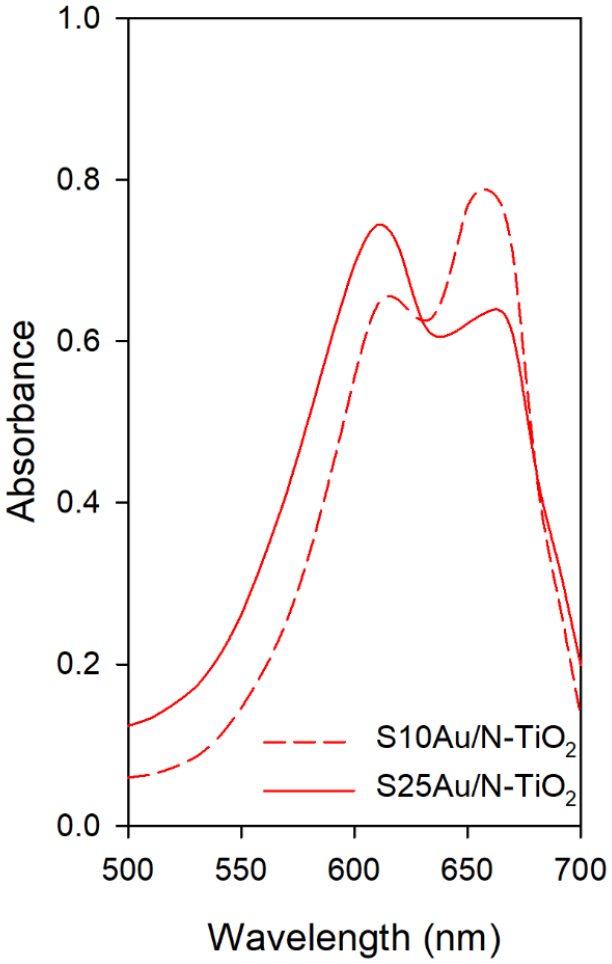

Figure S3. Absorbance spectra of MB deposited on treated limestone samples.

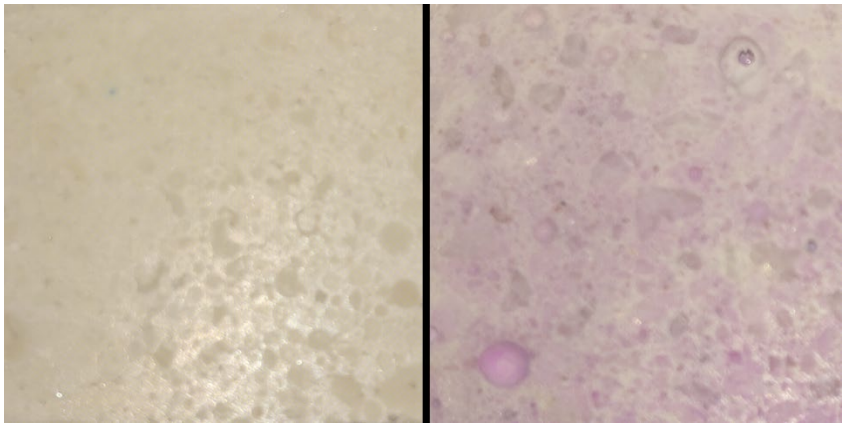

Figure S4. Photographs of samples treated with S2.5Au/N-TiO_2 photocatalysts after phenolphthalein tests. Left, limestone and right, concrete.

Chapter 8

General discussion

This Doctoral Thesis is focused on the development of new $Au/TiO_2/SiO_2$ photocatalysts for self-cleaning and depolluting applications on building materials. Firstly, we made a preliminary study incorporating AuNPs into a TiO_2/SiO_2 sol-gel synthesis previously developed by our research group. The AuNPs induced an enhancement of the self-cleaning properties of the TiO_2/SiO_2 coating, demonstrating that gold could be a good candidate for promoting the coating photoactivity. Secondly, a new method of AuNPs incorporation to the photocatalyst was employed in order to prevent the disadvantages associated to the previous methodology. Additionally, the role of AuNPs size and their loading were investigated. Finally, in order to increase the Au-TiO_2 interaction and further enhanced the activity of our materials, we employed a direct method of gold deposition on TiO_2 instead of the use of preformed AuNPs.

According to the sequential methodology employed for the obtaining of the photocatalytic building materials, three different types of samples can be distinguished: (1) the Au and Au/TiO_2 nanoparticles incorporated to the silica sol; (2) the obtained $Au/TiO_2/SiO_2$ photocatalysts; and (3) the building materials samples coated with the $Au/TiO_2/SiO_2$ photocatalysts. Thus, the following discussion has been structured in three blocks where the characterization and evaluation results obtained for each type of samples are discussed.

8.1. Au and Au/TiO_2 nanoparticles

8.1.1. Methodology of AuNPs incorporation to the photocatalysts

The first AuNPs evaluated for promoting the TiO_2 photoactivity were prepared from $KAuCl_4$ employing a Dracaena Draco leaves extract as reducing and stabilizing agent. These AuNPs were selected because their well-stablished synthesis had been developed by our group at the time that the Thesis work started [1]. The AuNPs presented a wide variety of shapes and a broad range of sizes from 1 to 30 nm (Chapter 3, Figure S2), specifically, a clear bimodal distribution was observed (Chapter 3, Figure S3) composed by small spherical particles of 3±0.8 nm diameter and big anisotropic particles of 17.7±4.4 nm in size. Different volumes of a concentrated AuNPs dispersion were directly added to the sol-gel synthesis in order to get Au/TiO_2 loadings in the range 0-0.5% wt. for the final photocatalysts. As will be discussed later, this first approach had several drawbacks and, consequently, we implemented a new method for the AuNPs incorporation.

The second method of gold incorporation consisted of depositing preformed AuNPs on TiO_2 to produce Au/TiO_2 particles that would be integrated in the sol-gel synthesis. Because the relationship between activity and Au size is not totally clear in literature for Au/TiO_2 photocatalysis [2–4], we opted for using AuNPs with two different sizes. For this purpose, an adaptation of Turkevich synthesis [5] (synthesis details can be found in Chapter 4.2) was chosen for several reasons: (1) the AuNPs size can be modulated varying the citrate/Au ratio employed in the synthesis; (2) the AuNPs obtained with this synthesis showed good stability; and (3) it is a “cleaner” synthesis as far as only citrate and PVP are employed whereas the leave extract is a complex mixture of organic compounds [6]. The Au/TiO_2 photocatalysts were prepared by

simply mixing the obtained AuNPs dispersions with TiO_2 particles, according to Au/TiO_2 proportions in the range 0.25-1%, these particles will be referred to as AuCit/TiO_2.

Finally, we decided to optimize the Au/TiO_2 photocatalysts synthesis employing a method of direct gold deposition on TiO_2 in order to promote the Au-TiO_2 interaction. In this sense, the deposition-precipitation method employing urea was chosen, because it allows getting AuNPs with suitable size for an effective TiO_2 photoactivity enhancement [7]. In addition, the urea is a nitrogen source widely employed for doping TiO_2 [8–10], which is another effective approach for the TiO_2 photoactivity enhancement [11]. Therefore by using this method it can be possible to combine both strategies (AuNPs deposition and nitrogen doping) in order to reach a synergetic effect on the TiO_2 photocatalytic activity, as demonstrated when gold was deposited on titania previously doped with nitrogen [12–14]. Specifically, the procedure was adapted to get a nearly 0.5 wt% Au gold content and the amount of urea employed was increased to ensure the nitrogen doping, as described in detail in Chapter 6. Another important issue was the study of the effect of the properties of titania in the photocatalyst activity, and we opted for employing three different types of commercial TiO_2 particles, P25, P90 and VP (Chapter 6, Table 1). We employed VP TiO_2 particles in the previous photocatalysts preparations of this Thesis because our group found that they were the best suited for TiO_2/SiO_2 photocatalysts preparation [15]. However, now we were studying a new photocatalytic system where a higher Au-TiO_2 interaction takes place and the use of different TiO_2 particles must be re-evaluated for optimizing the photocatalyst. These photocatalysts will be referred to as Au/N-TiO_2 or N-TiO_2, and therefore for referring to a specific type of TiO_2 particles we will employ its commercial denomination, such as Au/N-P25 and N-P25 for the catalysts prepared from P25.

8.1.2. Au/TiO_2 photocatalysts characterization

The AuCit/TiO_2 photocatalysts prepared employing the AuNPs synthetized with the highest Au/Citrate ratio showed spherical AuNPs with an average diameter of 12.6±1.9 nm homogeneously dispersed over the TiO_2 (see Chapter 4, Figure 2a). On the other hand, for the materials prepared with the AuNPs synthetized using the lowest citrate amount, the AuNPs had irregular shapes with an average size of 38.2±11.6 nm and they were heterogeneously dispersed being accumulated in certain areas of TiO_2 (see Chapter 4, Figure 2b). The FTIR analysis of these photocatalysts evidenced the presence of citrate and PVP remnants from the AuNPs synthesis (see Chapter 4, Figure 3). These species adsorbed in the TiO_2 surface modified the pH behaviour of the TiO_2 and promoted the particle agglomeration (Chapter 4, Table 2). Specifically, it has been reported that the PVP chains can link the TiO_2 particles by hydrogen bonds [16], which hinders their disaggregation during the ultrasonic stirring.

The Au/N-TiO_2 photocatalysts were in-depth characterized in order to correlate their compositional, textural and structural properties, with their photocatalytic performance. The UV-Vis characterization (Chapter 6, Figure 1) demonstrated that the nitrogen doping produced a slightly increase in the photocatalyst visible absorption and it induced a reduction of the band gap value of 0.15 eV, which is because nitrogen introduces new energy levels in the TiO_2 at higher energy than the valence band [10]. On the other hand, the AuNPs deposition notably increased the visible light absorption showing a band centred at 550-560 nm characteristic of the localized surface plasmon resonance (LSPR) effect of AuNPs [17]. The textural study by means of nitrogen physisorption analysis (Chapter 6, Figure 2 and Table 2) showed that the specific surface area of the photocatalyst was not altered by the nitrogen doping or gold deposition, but the pore volume and pore size distribution were substantially modified. This behaviour was explained as the TiO_2 primary particle size was not modified but the particles

were compacted, which was confirmed by SEM (Chapter 6, Figure 4), XRD (Chapter 6, Figure S3 and Table 2) and the increase of photocatalyst density (Chapter 6, Table 2). The XPS (Chapter 6, Figure 3) provided information about the atomic energy levels, observing peak positions and shifts that confirmed the nitrogen doping of the titania and the Au-TiO_2 interaction. Finally, the TEM observation (Chapter 6, Figure 5) revealed small AuNPs homogenously dispersed on the TiO_2, whose sizes were 5.2±1.3 nm for Au/N-P25, 6.2±2.1nm for Au/N-P90 and 6.1±1.5 for Au/N-VP.

8.1.3. Au/TiO_2 photocatalysts evaluation

The photoactivity of the Au/TiO_2 photocatalysts was evaluated by degradation tests using methylene blue (MB) as a probe (Chapter 4, Figure 4 and Chapter 6, Figure 6), this dye has been widely employed for the photocatalytic evaluation of Au/TiO_2 photocatalysts [18]. The tests were carried out in oxidant conditions where the MB photobleaching takes place via mineralization [19], thus the absorbance decrease was directly related to the organic dye concentration reduction due to the photo-oxidation process. In the absence of photocatalyst, a very small MB concentration decrease was observed due to the natural MB photolysis under UV irradiation [20]. By contrast, the fast absorbance reduction in the presence of photocatalyst clearly demonstrated the photocatalytic effect of TiO_2.

In general, the AuNPs accelerated the MB degradation rate confirming their role in the TiO_2 photoactivity enhancement. The TiO_2-AuNPs contact modifies the energy levels and the charge transfer phenomena in the TiO_2 surface. Specifically, the AuNPs act as reservoir of photogenerated charge carriers and they equilibrate the Fermi level, resulting in a diminution of the electron-hole pair recombination and a promotion of the electron transfer process with the reactant species [21–23]. Additionally, the LSPR effect of the AuNPs enhances the TiO_2 photoactivity under visible radiation [24]. The major mechanism taking place is the TiO_2

sensitization, the AuNPs electrons are excited when they receive visible radiation and they get enough energy to be injected in the TiO_2 conduction band triggering the TiO_2 photocatalytic process [25]. In addition, other LSPR mediated processes that can enhance the TiO_2 photoactivity have been proposed: (1) the excited AuNPs electrons colliding in the TiO_2-Au contact area can have enough kinetic energy for promoting the TiO_2 electrons to the valence band [26,27]; (2) the LRSP excitation produces a local heating and the surrounding AuNPs can reach temperatures up to 100 °C favouring the photodegradation processes [28]; and (3) the LRSP increases the electric field around the AuNPs promoting the electron-hole pairs formation [29].

The examination of MB degradation results for the AuCit/TiO_2 photocatalysts allows us concluding that there are two important trends related to the Au size and loading. The samples containing the smaller AuNPs were more active, which can be explained by (1) their higher number (see Chapter 4, Figure 2) that increases the TiO_2-Au contact surface; (2) their better dispersion onto TiO_2 support; and (3) the Fermi Level shift to more negative potentials, promoting a higher charge separation [21]. Regarding the Au content, it was found that the optimum was the intermediate content evaluated, 0.5 %, for both average size of particles, lower and higher. This behaviour is attributed to the tendency to TiO_2 agglomeration increased as gold content was raised, as confirmed by DLS. In addition, a high gold loading can reduce the TiO_2 photoactivity by promoting the recombination of electron-hole pairs [12,18] or due to the preferential light absorption by gold rather than TiO_2 [2,30].

The Au/N-TiO_2 photocatalysts showed the relatively highest MB degradation rates confirming the already mentioned synergetic effect of nitrogen doping and AuNPs combination. In addition to the advantages induced by gold, the nitrogen doping reduced the photocatalysts band gap increasing the visible absorption, as previously discussed, and decreased the charge carriers

recombination rate of TiO_2 [31]. Comparing the obtained kinetic constants data (Chapter 4, Table 2 and Chapter 6, Table 3), we can see that the best AuCit/TiO_2 photocatalyst increased the MB degradation rate of TiO_2 by a factor of 2.7 whereas the Au/N-VP (prepared using the same type of TiO_2 particles) showed an increase of 3.6 times. This definitively confirmed the best suitability of the corresponding of this methodology for preparing Au/TiO_2 photocatalysts. The better performance is a consequence of three factors: (1) the nitrogen doping that is only present in the Au/N-TiO_2 photocalysts, (2) the relatively lower AuNPs size that favours the Au-TiO_2 interactions, as previously discussed; and (3) the preparation method employed because the catalysts prepared from preformed AuNPs are generally less active [2]. Comparing the three Au/N-TiO_2 photocatalysts prepared, Au/N-P25 showed the highest MB degradation performance, which was attributed to less agglomerated particles and to its smaller and narrower AuNPs size distribution.

Additional MB degradation experiments under only visible light were carried out (Chapter 4, Figure 5b and Chapter 6, Figure 7) in order to elucidate if the AuNPs can trigger the TiO_2 photoprocess under this part of the electromagnetic spectra. The utilization of this radiation is particularly important for environmental applications where the sun is the light source. In the absence of AuNPs the TiO_2 activation did not take place and a slightly MB degradation, which can be explained as a result of a sensitization effect produced by the MB [32,33], was observed. However, the MB degradation rate was considerably higher when the AuNPs were present demonstrating that the TiO_2 visible activation via AuNPs LSPR mechanisms took place in the Au/TiO_2 materials prepared. These results also confirm that the contribution to MB degradation due to TiO_2 visible sensitization by MB was negligible for the previous tests.

The degradation of p-nitrophenol, that does not present absorption in the visible region, was also evaluated (Chapter 4 Figure 5). The purpose of this test was demonstrating the

photoactivity enhancement induced by gold, because there is controversy about the use of dyes for photocatalysts evaluation when visible light is present [32]. In the absence of photocatalyst, no degradation was observed, whereas the photocatalysts produced evident degradations, being higher for the AuCit/TiO_2. These results demonstrated that the photocatalysts could degrade different types of organic compounds and not only dyes that could promote sensitization mechanisms under visible light.

Finally, the NO photodegradation of the optimized Au/N-TiO_2 photocatalyst was also evaluated (Chapter 6 Figure 8 and Table 4). The NO abatement is one of the major interest focus of TiO_2 photocatalysis, due to the high concentration of nitrogen oxides in the air our cities that can exceed the safety levels [34]. The initial results showed an evident increase in the amount of NO removed for N-P25 and Au/N-P25, which demonstrated the TiO_2 photoactivity enhancement produced by the nitrogen doping and the AuNPs. In this process, NO is oxidized to HNO_3 being the NO_2 produced as a reaction intermediate [35]. Therefore, it is also relevant to study the amount of NO_2 generated during the process, as the NO_2 toxicity is even higher than the NO one. In addition, the HNO_3 accumulation on the TiO_2 surface promotes the direct NO to NO_2 conversion [35,36]. In this way, the NO_2 concentration quickly increased producing that the total amount of nitrogen oxides (NO_x) removed was low. As a result, high selectivities to NO_2 and only slight increases in the percentages of NO_x removed for N-P25 and Au/N-P25 were observed.

In order to make evident the differences in NO_x removal activity of the particles under study, $Ca(OH)_2$ was employed to produce alkaline conditions that promote the elimination of HNO_3 in the form of nitrates. Specifically, the simultaneous deposition of TiO_2 photocatalysts and $Ca(OH)_2$ demonstrated to be an effective approach to promote the NO_x removal. Specifically, the amount of removed NO_x was considerably increased and the selectivity to NO_2 reduced.

The nitrogen doping increased by 20% the amount of removed NO_x for P25 sample due to the photoactivity enhancement. On the other hand, Au/N-P25 increased it by 70%. This behaviour is not only attributed to the photoactivity enhancement induced by gold but also to its capacity to activate the O_2 and NO molecules via strong adsorption promoting the NO oxidation. The adsorbed O_2 in the photocatalysts is reduced by the photoinduced electrons yielding superoxide radicals that play a relevant role in the NO photooxidation [37]. The Au increases the oxygen absorption capacity of the photocatalysts enhancing the amount of O_2 available for reacting with the photogenerated electrons [38]. On the other hand, density functional theory (DFT) calculations have revealed that the NO adsorption on Au modifies the NO energy molecular levels in a way that its oxidation is favoured [39].

8.2. Au/TiO_2/SiO_2 photocatalysts

As a consequence of the three methodologies of gold incorporation described in the previous section, three different Au/TiO_2/SiO_2 photocatalysts were developed. The first type consisted of the photocatalysts prepared by including in the sol-gel synthesis the AuNPs prepared using the leaves extract (preparation details can be found in Chapter 3), they will be named as AuD/TiO_2/SiO_2 for easy identification. The second type correspond to those prepared by including the AuCit/TiO_2 photocatalysts (preparation details can be found in Chapter 4), named as AuCit/TiO_2/SiO_2. The Au/N-TiO_2 photocatalysts (specifically the Au/N-P25 particles) were employed for preparing the last type of photocatalyst evaluated (preparation details can be found in Chapter 7), named as Au/N-TiO_2/SiO_2.

8.2.1. Characterization

8.2.1.1. Sol rheology and sol-gel transition

The studied sols showed a nearly Newtonian behaviour at the shear range evaluated and sol viscosity values were calculated as the slope of shear rate *vs* shear stress curves, with a goodness of fit higher than 0.99 (see results in Chapter 3, Table 2, Chapter 5 and Chapter 7, Table 1).

As AuNPs were integrated in the AuD/TiO_2/SiO_2 photocatalysts synthesis dispersed in water, the increase of Au loading also involved the increase in the amount of water content in the synthesis media (Chapter 3 Table 1). It is well known that water has an important impact in the hydrolysis rate of the sol-gel reaction [40]. Indeed, a clear correlation between viscosity (Chapter 3, Table 2) and the sol water content was observed, which can be explained taking into account that the higher hydrolysis rate promotes the progress of the sol-gel process and therefore increasing the viscosity.

The TiO_2 incorporation in the sol also affected the viscosity, observing its progressive increase as the TiO_2 content in the sol was raised. This trend was previously reported by our group [15], where a viscosity of 45 mPa·s was measured for a TiO_2/silica oligomer ratio of 10%. However, we have prepared Au/N-TiO_2/SiO_2 photocatalysts employing the same TiO_2/silica oligomer relation incorporating isopropanol to the mixture and we achieve to reduce the viscosity to 16 mPa·s.

The viscosity values of the developed sols ranged from 4.5 to 17 mPa·s, the viscosities near to the lower threshold are similar to those corresponding to commercial silica sols employed for protecting building materials. Tegovakon V100 from Evonik, one of the most popular commercial stone consolidants, has a viscosity of 5.25 mPa·s at 25 °C [41]. Although we have obtained products that triplicate the viscosity of the cited consolidants, this value is still far

away of the 100 mPa·s, viscosity value considered acceptable in the paint industry [42]. Therefore, the low viscosities allow their application by common procedures, such as spraying, brushing, as coatings of building materials, even under outdoor conditions, and promote the sol penetration into the substrate porous structure improving the adherence of the resultant coatings.

The obtained sols stored in closed vessels and dark conditions were stable for at least six months, which ensures an enough time frame since the photocatalysts preparation until their *in situ* application on a building. By the contrary, the sols place in open reservoirs spontaneously gel and dry giving rise to crack-free and homogeneous xerogels, confirming the role of the n-octylamine catalyzing the process and preventing the fractures [43].

The duration of sol-gel transition was strongly affected by the water content in the sol, as demonstrated in the study of AuD/TiO_2/SiO_2 photocatalysts that contained different water amounts (Chapter 3, Table 2). The gelification time decreased as water content was raised producing quasi-instantaneous gelation for water contents greater than or equal to 2.5%, setting the limit for the sol applicability. This fact is also a consequence of the hydrolysis rate promotion by water. For the other sols (AuCit/TiO_2/SiO_2 and Au/N-TiO_2/SiO_2) with the same water amount (0.83%), the sol-gel transition took place overnight.

8.2.1.2 Nitrogen Physisorption

The nitrogen physisorption was a useful technique to study the photocatalysts texture and correlate the obtained results with the material performance. All the developed photocatalysts presented type IV(a) isotherms (Chapter 3, Figure 3; Chapter 4, Figure S5; Chapter 6, Figure 10; and Chapter 7, Figure 2), which are characteristic of mesoporous materials [44]. The observed hysteresis loops can be classified as H1, H2(a), H2(b) or intermediate situations, which are characteristic of porous silicas [44,45]. H1 is found in materials with narrow and

homogeneous size distributions, whereas H2 corresponds to materials with more complex pore structure where there is pore blocking due to ink-bottle pore geometry. Specifically, H2(a) hysteresis is observed when the desorption occurs via cavitation, suggesting that necks of the pores are much narrower than their bodies. Indeed, we can observe a clear correlation between the isotherm hysteresis and the corresponding pore size distributions. H2(a) hysteresis was observed for the materials with small pore size mainly located below 5 nm, whereas materials with maximum pore size around 6 nm showed H2(b) hysteresis that became H1 as the fraction of bigger pores was raised.

Significant differences in isotherms were observed for the AuD/TiO_2/SiO_2 photocatalysts with different Au loading (Chapter 3, Figure 3), finding the highest surface area and pore volume for the material with intermedium Au content. Again, this was a consequence of the different amount of water incorporated to the sol-gel synthesis, as demonstrated by preparing photocatalysts without gold but varying the water content (Chapter 3, Figure S1).

By the other hand, the AuCit/TiO_2/SiO_2 photocatalysts containing citrate and PVP remnants showed less accused differences (Chapter 4, Figure S5. These species adsorbed on the TiO_2 surface changed its pH behaviour (Chapter 4 Table 2) which is a key factor in the sol-gel process [46,47]. Additionally, TiO_2 shows a strong affinity for amine moeties, promoting their absorption on its surface [48–50] , but, the citrate and PVP remnants are also adsorbed on the TiO_2 surface [16,51], competing with n-octylamine adsorption and modifying the amount of free catalyst in the sol.

The study of Au/N-TiO_2/SiO_2 (Chapter 7 Figure 2) allowed to concluding that the increase of theTiO_2 content in the photocatalysts promotes the formation of bigger pores and confirmed that the AuNPs did not modify the xerogel structure.

The textural parameters calculated from the isotherms reflected the differences previously discussed (Chapter 3, Table 2; Chapter 4, Table 3; Chapter 6, Table 5; and Chapter 7, Table 1). We found that the surface area of the developed photocatalysts ranged from 150 to 400 m^2/g and their pore volume was in the range 0.30-0.75 cm^3/g. Since the photodegradation reactions are surface processes, the contact between TiO_2 and the agents acting in the redox process (light, O_2 and H_2O) needs to be maximized [52–55]. Thus, the photocatalyst surface area and pore volume play a key role in the photocatalyst performance, promoting the exposed photocatalyst surface and the diffusion of substances to the active photocatalyst sites through the pore structure [15,53,54,56–60].

8.2.1.3 Electron Microscopy

TEM images of the $Au/TiO_2/SiO_2$ photocatalysts (Chapter 3, Figure 4; Chapter 4, Figure 6; and Chapter 7, Figure 3) highlight that they were composed by a matrix of aggregated amorphous silica particles where the TiO_2 particles are embedded. This structure is in accordance with the results to which leads the micelles inverse mechanism proposed for sols containing n-octylamine [61], which suggests that the water is encapsulated in the surfactant micelles that act as nanoreactors, producing silica particles with uniform size. The porous structure observed by nitrogen physisorption correspond to the interstitial holes produced by the SiO_2 and TiO_2 nanoparticles packing.

STEM-HAADF images and their corresponding XEDS maps (Chapter 3, Figure 5; Chapter 4 Figure 7; and Chapter 7, Figure 3) gave us information about the TiO_2 distribution in the photocatalysts. In general, TiO_2 was distributed in the whole SiO_2 matrix in the form of individual particles and small agglomerates. However, some synthesis parameters favours the TiO_2 agglomeration reducing their dispersion along the matrix. For $AuD/TiO_2/SiO_2$ photocatalysts it was observed that a high water content in the synthesis promotes the formation

of larger TiO_2 agglomerates (Chapter 3, Figure 5). The AuCit/TiO_2/SiO_2 photocatalysts showed tendency to TiO_2 agglomeration as the gold content was raised (Chapter 4, Figure 7), revealing even massive agglomerates of micrometric size for the highest Au Loading. As previously discussed, the PVP linked the TiO_2 particles and hindered their dispersion during the sol-gel synthesis. Finally, the Au/N-TiO_2/SiO_2 photocatalysts (Chapter 7, Figure 3) with TiO_2/SiO_2 ratios of 2.5 and 10 % showed a good TiO_2 dispersion demonstrating that the optimized Au/N-TiO_2 particles can be easily dispersed. On the other hand, for the highest TiO_2 loading (25 %) the titania agglomeration effect was significant, showing areas without TiO_2 and domains were the presence of titania is predominant. This was a consequence of isopropanol addition to the sol, this solvent could modify the electrostatic interactions in the sol promoting the attraction forces between the TiO_2 particles.

Regarding the AuNPs distribution in the photocatalysts, it was demonstrated that the method of gold incorporation used is a key factor in the Au/TiO_2/SiO_2 photocatalysts preparation. The AuNPs in the AuD/TiO_2/SiO_2 photocatalysts were detected forming accumulations of AuNPs whose size was increased as gold content was raised (Chapter 3, Figures 5,c and d). This poor dispersion can be explained as the AuNPs were not freely dispersed in the sol but they remained dispersed in the water encapsulated in the n-octylamine micelles. However, the AuNPs distribution was completely different for the other photocatalysts that wre prepared incorporating the AuNPs previously deposited on the TiO_2. Both, AuCit/TiO_2/SiO_2 and Au/N-TiO_2/SiO_2, showed their particles individually dispersed and unequivocally located in contact with TiO_2 (Chapter 4, Figure 6 and Chapter 7, Figure 3), confirming that the Au and TiO_2 particles were not separated during the sol-gel synthesis process. This Au-TiO_2 contact is necessary to achieve the enhancement of the TiO_2 photoactivity because it is necessary for the LSPR-mediated charge injection mechanisms to take place [62].

8.2.2. Photocatalytic evaluation

8.2.2.1 Methylene blue degradation

The MB degradation tests were employed for evaluate the Au/N-TiO_2/SiO_2 photocatalysts performance and determine which are the most appropriate Au/N-TiO_2 particles for their integration in the silica matrix. The obtained results (Chapter 6, Figure 11) were similar to the previous ones for the Au/N-TiO_2 photocatalysts before their integration in the silica matrix (Chapter 6, Figure 6), observing the obvious photoactivity enhancement induced by the nitrogen doping and the AuNPs. These results confirmed that the photocatalysts activity was preserved after their integration in the silica matrix. Comparing the different starting TiO_2 particles, it was observed that P25 series showed the best results whereas P90 series showed the lowest MB degradation rates. As previously discussed, this behaviour can be related to the different agglomeration that suffered the particles. Finally, our results contrast with the previous ones obtained for similar TiO_2/SiO_2 photocatalysts prepared with the same particles [15]. The highest activity of the TiO_2/SiO_2 photocatalysts containing VP particles (named AP in the previous work) can be attributed to two main factors: (1) the photocatalyst containing VP particles showed higher surface area and pore volume than that containing P25, both parameters being factors that promote the photoactivity [63]; and (2) not all P25 batches are equal, differences in phase composition and morphology of particles can be found between different batches of the manufacturer [64], thus, a more active batch can have been employed in the present work.

8.2.2.2 NO degradation

The use of the developed photocatalysts for producing depolluting building materials is one of their desired applications, thus NO, a typical gas pollutant in urban environments in areas of

high motor vehicle traffic, was chosen to evaluate the photocatalysts performance. The specifications described in the ISO standard were modified in order to study samples in the form of powders. In spite of this modification, under our experimental conditions a nearly equivalent pollutant load was preserved.

Three common stages were observed in the NO profiles for the evaluated photocatalysts (Chapter 4, Figure 8 and Chapter 6, Figure 12). (1) In the absence of UV–Vis light irradiation, neither activation of the photocatalytic sites nor NO oxidation took place, consequently the concentration of NO was kept constant at 3 ppm. (2) Under UV–Vis light irradiation, the heterogeneous photocatalytic reaction occurred and the oxidation of the pollutant began. The decrease in NO concentration reached its maximum and became practically constant in this period of time, indicating complete activation of the photocatalytic sites. In parallel, NO_2 gas appeared in some extent as a product of the reaction, increasing the inlet NO_X concentration as much as it corresponds to the sum of both gases: NO and NO_2. It was noticed that the "deactivation" observed for the Au/N-TiO_2 particles deposited on glass did not take place under the experimental conditions employed in this case. The short time of analysis and the high amount of photocatalyst employed ensured that the effect of the acid nitric produced in the process was negligible. (3) Finally, when the irradiation was off, the NO concentration returned to its initial value.

The analysis of the second stage, related to the photoactivity region, leads to the NO conversion and selectivity data (Chapter 4, Table 4 and Chapter 6, Table 5). As expected, the inclusion of TiO_2 into the silica matrix transfoms into photocatalytic the inert starting material. The NO conversion values follow the same trends observed and discussed for the MB degradation results by AuCit/TiO_2 and Au/N-TiO_2 photocatalysts. For AuCit/TiO_2/SiO_2, the highest NO conversion was achieved for the intermedium gold content and the smallest Au size. For Au/N-

TiO_2/SiO_2 samples, it was observed that both, nitrogen doping and the presence gold increased the NO conversion, and the highest values were obtained for the photocatalysts prepared from P25 particles. Regarding the selectivity, it was improved as gold was included in the photocatalyst, especially for Au/N-TiO_2/SiO_2 samples, which confirmed that the AuNPs also promoted the simultaneous NO adsorption mechanisms previously described once they are integrated in the silica matrix.

FTIR spectra of photocatalyst before and after the NO test were recorded (Chapter 4, Figure S6), to obtain additional evidences of the formation of non-toxic nitrogen species. As can be seen, before irradiation, no bands concerning N-O vibration modes were detected. Only those related to the silica were observed, in particular the intense band at 1090 cm^{-1} with its shoulder at 1190 cm^{-1}, and the small peak at 1650 cm^{-1} can be assigned to the stretching of ≡Si-O-Si≡ in the silica structure and the deformation of adsorbed water, respectively. New bands in the 1300-1600 cm^{-1} range appear in the spectrum obtained after the NO test. In particular, according to [65] those located above 1500 cm^{-1} might correspond to monodentate and bidentate nitrates, while those between 1500 and 1300 cm^{-1} can be related to monodentate and bridging nitrites. These species could be eliminated in the form of soluble acids under the presence of rain in the potential application of our photocatalytic materials.

8.3. Au/TiO_2/SiO_2 photocatalysts on building materials

The developed photocatalysts were applied, as sol, by spraying onto three common building materials (limestone, granite and concrete) in order to evaluate the performance of the resultant photocatalytic building materials samples.

8.3.1. Characterization

8.3.1.1. Sol uptake and photocatalyst penetration

The sol uptake values (Chapter 3, Table 3; Chapter 5 Table 1; and Chapter 7, Table 2) were dependent on the substrate and sol viscosity. The uptake values for the granite samples were lower because the sol could not penetrate in its non-porous structure. By contrast, the sol can penetrate inside the porous substrates, limestone and concrete, producing higher uptakes. The surface finish also affected the sol uptake because the sol can fill holes and groves of the surface increasing the uptake. Indeed, we observed a really low uptake for a polished granite (Chapter 7, Table 2) because the sol did not penetrate in the substrate and produced a thin layer on the polished surface, on the contrary for bush-hammered granite the uptake was significantly higher (Chapter 5 Table 1). Regarding the effect of the sol viscosity, the uptake follows an inverse trend because the penetration inside the substrate porous structure diminish when the sol viscosity increases. This behaviour was clearly observed for AuD/TiO_2/SiO_2 (Chapter 3 Table 3) and Au/N-TiO_2/SiO_2 (Chapter 7 Table 2) photocatalysts. The photocatalysts penetration in the substrate was confirmed by direct observation of the cross section of the samples (Chapter 5, Figure 3 and Chapter 7, Figure S2).

8.3.1.2. Applicability evaluation

Some parameters must be satisfied to get suitable photocatalytic coatings for building materials. First, in order to preserve the photocatalytic properties, the coating must be well-adhered on the substrate and the TiO_2 particles must not be removed. The coating adhesion was evaluated by a peeling test employing an adhesive tape. The treatments significantly reduced the material removed by the peeling test in comparison with the untreated substrate (Chapter 3 Table 3). These results confirmed that the coatings presented an appropriate adhesion to the substrate and

they even produced an effective consolidation of the surface. Additionally, in order to evaluate the capacity of the silica matrix for preventing the TiO_2 removal, stone samples coated with only TiO_2 particles and with our TiO_2/SiO_2 photocatalysts were immersed in water and sonicated. First of all, a simple visual inspection of washing water allowed concluding that the TiO_2 sample produced higher turbidity than the TiO_2/SiO_2 one (Chapter 5, Figure S2). The increasing turbidity is related to the presence of TiO_2 particles which have an elevated refraction index. The composition of the material removed from the samples was studied by FTIR spectroscopy (Chapter 5, Figure 5). The main bands observed for both samples mainly matched those related to the substrate minerals. The TiO_2/SiO_2 sample only showed additional bands related to silica, but no TiO_2 signals were observed. On the other hand, the TiO_2 sample showed an evident absorption increase in the 400-800 cm^{-1} region that denote the TiO_2 removal from the substrate. The results demonstrated that the use of a silica matrix promotes the TiO_2 adhesion to the building materials. Thus, the developed treatments in this Thesis could lead to more durable materials than a TiO_2 particles based-treatment against the weathering.

The total colour differences of the substrates induced by the treatments can be relevant in certain applications, such as application on Cultural Heritage elements, where the material appearance should be preserved, being a value of 5 units the threshold [66]. This parameter was evaluated for all the building materials samples under study (Chapter 3, Table 3; Chapter 5, Table 1; and Chapter 7, Table 2). Briefly, the presence of AuNPs induced intense pink-purple colours in the photocatalysts. The colour variations were low for the $AuD/TiO_2/SiO_2$ photocatalysts with a small Au loading, whereas they were higher for $AuCit/TiO_2/SiO_2$ and $Au/N\text{-}TiO_2/SiO_2$ photocatalysts, showing a clear trend to increase as Au content in the sol was raised. As might be expected, the colour variations were also affected by the uptakes values and indeed, the granite samples showed low values always below the above 5 units. The other substrates presented higher colour changes being some of them above the accepted threshold. The main

reason of these strong colour variations is that we have employed quasi-white substrates (for better observation of stains produced for the photocatalytic evaluation) and the photocatalysts colour easily evolve. The impact in the aesthetic characteristics of the substrate can be reduced for other substrates, e.g. the colour variation produced by a Au/N-TiO_2/SiO_2 photocatalyst was reduced from 8.2 to 4.3 using a grey concrete substrate instead of a white one.

Also important and according to the price of gold, its impact on the cost of the catalysts was also evaluated for the optimized Au/N-TiO_2/SiO_2 photocatalysts. This cost associated to gold is directly related with the uptake values and the Au content in the sol, being in the range 0.01-0.07 €/m^2 for the granite, 0.19-0.70 €/m^2 for the limestone and 0.28-1.47 €/m^2 for the concrete (estimated from the current market value of gold 37 €/g). For comparison, the photocatalytic paint KEIM Soldalit®-ME [67] has a treatment cost of approximately 10 €/m^2 considering its price and its typical consumption. Therefore, the developed treatments can be commercially viable, especially for low absorbent substrates and low TiO_2/SiO_2 ratios. In addition, this cost can be further decreased reducing the sol uptake. Thus, the amount of photocatalyst applied on the substrate can be reduced applying an only silica sol as a primer before the Au/N-TiO_2/SiO_2 sol application. This strategy can also help to mitigate the problems associated to the substrate colour changes

8.3.1.3. Scanning Electron Microscopy

The SEM images of the building materials samples (Chapter 3, Figure S5; Chapter 5, Figure; and Chapter 7, Figure 4) showed that the photocatalyst produced a continuous and homogeneous coating that covered the original substrate surfaces. The absence of fractures in the coating demonstrates the role played by the n-octylamine to prevent the xerogel cracking [68] which promotes the adhesion, and the subsequent durability, of the coatings [69,70]. The higher magnification images allows confirming that the coatings were constituted by an

agglomeration of small particles corresponding to the silica particles produced via micelles inverse mechanism proposed for sols containing n-octylamine [61]. The TiO_2 particles were identified by their bigger size, increasing their presence in the coating surface as the TiO_2/SiO_2 ratio was raised, being especially visible for TiO_2/SiO_2 ratios of 25%.

8.3.2. Photocatalytic evaluation

8.3.2.1. Methylene blue degradation

The MB degradation was a reference test employed for testing the photocatalyst properties of all the samples evaluated. Previously, our research group had employed a methodology based on the colour measurement of the stained surface in order to determine the MB decolouration produced by the TiO_2 photoactivity [15,41,43,63,71]. However, the first studies of this Thesis revealed that this methodology was not convenient to study in-depth the MB degradation (Chapter 3, Figure 9a). The main drawback is that the colour coordinates are stablished according to the human visual perception of the colour and thus, the colour measurements are not directly related to the amount of dye. According to this, we employed a methodology based on applying the Kubelka-Munk theory to the UV-Visible reflectance spectra. The Kubelka-Munk theory [72,73] is commonly used to explain the light absorption in a thin layer of dye deposited on a non or low-absorbent substrate [74], situation that can be considered similar to that of MB deposited on the building materials samples. The following equation is specifically addressed for explaining these type of systems:

$$f\left(R_\infty\right)=\frac{\left(1-R_\infty\right)^2}{2R_\infty}=\frac{k}{s}$$

where $f(R_\infty)$) is equivalent to absorbance, R_∞ is the diffuse reflectance, k is the dye molar absorption coefficient and s the surface scattering coefficient.

From this equation, the experimentally obtained diffuse reflectance spectra can be converted into the corresponding absorbance spectra, being this absorbance directly related to the MB concentration, because the Kubelka-Munk equation fit the Lambert-Beer's law. In this way, we obtained new MB degradation profiles where each sample is clearly differenced (Chapter 3, Figure 10a), whereas the profiles made from the colour measurements showed a significant overlapping. Additionally, as we had information about the MB concentration, we could study the degradation of specifics forms of MB (Chapter 3, Figures 10,b and c) or the kineticss of the process (Chapter 3, Table 4), as extensively discussed in Chapter 3.

A series of common results for the different samples were observed. The MB on untreated substrate was slowly degraded and this effect was associated to the MB photolysis. The samples with an only silica coating showed a considerably increase of MB degradation rate even though no photoactive components were present. This significant difference was attributed to the combination of three factors: (1) MB is deposited in different form in the untreated stone, mainly as dimer, and predominantly as monomer in the treated stones (Chapter 3 Figure S7), being faster the monomer degradation [75,76]; (2) the coating restricts the MB penetration into the substrate and it has a large surface area compared with the stone, promoting the MB exposition to light, oxygen and humidity; and (3) the stone has a greater absorption in the UV range than the silica coating (Chapter 3, Figure S10), reducing the amount of high energy light available to produce the MB photolysis. The incorporation of TiO_2 to the coating enhanced the MB degradation as a result of its photocatalytic properties. Finally, the highest MB degradation rates corresponded to the $Au/TiO_2/SiO_2$ coatings, confirming the AuNPs role to promote the photocatalytic effect of TiO_2.

For the $AuD/TiO_2/SiO_2$ photocatalysts the maximum performance corresponded to the intermedium gold content evaluated, 0.12%. We can explain this as a consequence of the

influence of the structure and the texture of the coatings on their photoactivity [63]. In particular, photocatalysts showed a better distribution of the photoactive components in the matrix and the highest pore volume and surface area, as previously discussed. We also evaluated the benefits of using gold instead of silver for promoting the TiO_2 photoactivity. We found that our best AuD/TiO_2/SiO_2 photocatalyst showed higher performance than the Ag/TiO_2/SiO_2 photocatalysts previously developed by our group (Chapter 3, Figure 9b) [71]. It was needed a 3.2% wt. of silver to achieve a MB degradation equivalent to that corresponding to a 0.12% wt. of gold, furthermore, the high silver loading induced an excessive colour variation in the substrate. Therefore, the results obtained for these photocatalysts confirmed the adequacy of gold for enhancing the activity of TiO_2/SiO_2 coating. However, due to the differences in textural parameters induced by the water during the synthesis, we could differentiate the contribution of gold and textural parameters to this enhancement.

AuCit/TiO_2/SiO_2 sol were prepared employing the same water content and the differences in the textural parameters for the photocatalysts not very significant. In this way, we can conclude that the obtained photoactivity enhancement was effectively produced by the AuNPs. The coatings with the lowers in size AuNPs were more effective than those containing the largest AuNPs and the maximum activity was reached for the coatings with the intermedium Au content. These trends perfectly agree with the previously discussed results for MB degradation using AuCit/TiO_2 particles and for the NO degradation using the powdered AuCit/TiO_2/SiO_2.

In the case of Au/N-TiO_2/SiO_2 samples we also investigated the application on different substrates and coating with different TiO_2/SiO_2 ratios. Firstly, the granite samples showed considerably lower MB degradation rates than those corresponding to limestone and concrete samples, which is related to the low uptake that showed granite according to its texture. On the other hand, there was an evident increase of the MB degradation rate as the TiO_2 content was

raised, which was the expected behaviour since the TiO_2 is the photoactive component of the nanocomposite. However, other photocatalysts parameters, such as their textural properties, also affect their photoactivity. Indeed, it was previously reported that a TiO_2/SiO_2 ratio of 25% produced a drastic fall in the samples performance due to the low surface area and pore volume of the photocatalyst [15]. Therefore, the synthesis modification incorporating isopropanol allowed increasing the TiO_2/SiO_2 ratio of the coating, which promoted its photoactivity. Finally, all the Au/N-TiO_2/SiO_2 coatings showed higher activity than the equivalent AuCit/TiO_2/SiO_2 photocatalysts prepared from P25. This fact is related to: (1) the preparation method, the catalyst prepared using preformed AuNPs generally gives lower activities than those prepared from gold deposition methods [2]; (2) the AuNPs size, the small size implies a higher number of particles increasing the TiO_2-Au contact and smaller particles shift the fermi level promoting the charge separation [21]; (3) the nitrogen doping promotes the TiO_2 photoactivity for reducing the charge carriers recombination rate [31], producing a synergic effect with gold [12].

Although under our experimental conditions the MB mineralization should be favoured, we employed the mass spectroscopy to study the gases released during this process (Chapter 3, Figure 11 and Chapter 5, Figure 7) in order to confirm that the MB photobleaching is not due to other process, such as the reduction to the uncoloured leuco-MB [19]. The sample illumination induced a gradual increase in the concentration of carbon dioxide and water in the gas phase until reaching a maximum value. The effect must be associated with the photocatalytic process as far as after switching off the lamp, the CO_2 and H_2O signals decreases to residual values. Moreover, in the case of Au/TiO_2/SiO_2 samples, the effect was significantly more intense than that occurring in untreated or TiO_2/SiO_2 samples. These results confirm the efficiency of the proposed materials and are of interest because the wide majority of experimental evidences in literature regarding activity or mechanism of photobleaching of organic dyes have been obtained in aqueous medium and not in gas phase [77].

8.3.2.2. Self-cleaning properties

Soot, a common staining agent of building, was chosen in order to evaluate the self-cleaning properties of the developed photocatalysts. This evaluation was really tedious due to the difficulty for obtaining a proper staining of the treated building materials samples. The staining by using water or solvent soot dispersions was unsuitable because the soot was not homogeneously deposited. The soot deposition by flame produced homogeneous stains but it was difficult to control or determine the amount of soot deposited. The amount of soot deposited was also a key parameter, thick soot layers had strong light absorption and no degradation was observed whereas the colour variations of substrates was not effectively measured for very thin layers.

Despite these problems, we managed to get some results about soot degradation (Chapter 3, Figure 12 and Chapter 5, Figure 8). We observed that the soot degradation was slower than the MB degradation denoting the higher stability of soot. Nevertheless, we have proven the disappearance of soot stains for the TiO_2-containing samples demonstrated that the photocatalytic properties of the developed coatings has the capacity to remove real stains, producing the self-cleaning effect. This self-cleaning performance was higher for the coating containing the AuNPs, which confirms that the gold promotes the self-cleaning effect.

The self-cleaning properties of building materials is also associated to the wetting properties that can favour the elimination of dirt deposited on their surfaces by the water, such as the rain action. Specifically, the TiO_2 increased the hydrophilicity of the coating, so promoting the removal of oil-based stains by water (Chapter 3, Figure 13 and Video S1).

8.3.2.3. NO depolluting properties

As previously mentioned, one of the main purposes of this Thesis is producing depolluting building materials by employing the developed photocatalysts. Therefore, it was crucial to evaluate the NO removal activity of the treated building materials samples.

First, we evaluated the AuCit/TiO_2/SiO_2 samples according to a stationary method described in Chapter 5 instead of using the flow methodology described in the ISO standard, due to the sensibility of the analyser employed. It was observed that the concentration of NO detected was reduced after the samples irradiation (Chapter 5, Figure 9), calculating the NO conversion from the area of the obtained NO curves (Chapter 5, Table 3). A NO conversion around 10% in the presence of the untreated stones was measured, which was attributed to NO adsorption in the sample or chemical photoreactions. When the test took place using the TiO_2/SiO_2 samples, the NO degradation was noticeably increased demonstrating the photocatalytic oxidation produced by the coating. Regarding the AuCit/TiO_2/SiO_2 coated stones, the NO degradation was near the double of that corresponding to the TiO_2/SiO_2 coatings confirming that an enhancement of NO conversion induced by AuNPs was also observed for the coated materials. These results confirmed that the treated building materials samples had the capacity to oxidize NO, being possible their application for NO removal.

Finally, the depolluting properties of the optimized Au/N-TiO_2/SiO_2 photocatalysts was evaluated according to the ISO standard (Chapter 7, Figure 6 and Table 3). The photoactivity of the samples was evidenced by the immediate and sharp decrease in NO concentration, continuing with a slight increase during the test. Simultaneously, NO_2 was generated causing that the NO_x concentration maintains higher than the NO one. This apparent activity reduction associated to HNO_3 accumulation, which was observed for the Au/N-TiO_2 particles, is frequently observed for long duration tests [35]. According to the measured NO_x elimination

percentages, two clear trends (which were in accordance with those resulting from the MB degradation study) were observed. Thus, the amount of NO_x removed was increased as (1) the TiO_2/SiO_2 ratio was raised and (2) the AuNPs were included in the coating. This effect of AuNPs was produced by the combination of TiO_2 photoactivity enhancement and the activation of O_2 and NO via adsorption, as previously discussed. Regarding the different substrates, the low activity of granite samples was related to the relatively low amount of photocatalyst deposited onto this material. By the contrary, the concrete samples showed the highest activity being the amount of NO_x removed by them nearly 3 times that of the limestone samples. In addition to the higher amount of photocatalyst deposited in this substrate, this fact is attributable to its different acid-base behaviour. Both, limestone and concrete, have an alkaline nature but concrete basicity is significantly higher and even the treated surfaces showed a pronounced basic behaviour, as demonstrated by a simple phenolphthalein test (Chapter 7, Figure S4). The basic medium can promote the HNO_3 elimination in the form of nitrates enhancing the amount of NO_x removed. In this sense, the addition of an alkali, such as CaO, can be a viable strategy to optimize this type of photocatalysts for NO_x removal specific applications. Finally, to put the obtained results in perspective, a previous study of Zouzelka and Rathousky [78] was employed for comparison. In that work the NOx photodegradation of concrete samples coated with a P25-based photocatalytic paint was tested under the same conditions employed in the present work. Specifically, the samples had a TiO_2 loading of 5 mg/cm^2 and showed an initial NO_x photodegradation rate of 176 $\mu mol \cdot m^{-2} \cdot h^{-1}$. By contrast, the initial degradation rate for the S25Au/N-TiO_2/C sample, calculated from the first 30 minutes of test, was 344 $\mu mol \cdot m^{-2} \cdot h^{-1}$ and its TiO_2 loading was only 1 mg/cm^2. Therefore, the developed Au/N-TiO_2/SiO_2 coatings practically duplicate the NO_x depolluting performance of a common TiO_2 coating reducing by a fifth the amount of TiO_2 necessary, which demonstrates the potential of these photocatalysts for depolluting purposes.

8.4. References

[1] M.L.A. Gil, C. Garrido, J.M. Cantoral, V.E. González-Rodríguez, M. Carbu, L.M. Cubillana-Aguilera, J.L. Hidalgo-Hidalgo De Cisneros, I. Naranjo-Rodríguez, M.J. Luna, R. Zarzuela, J.M. Palacios-Santander, Synthesis of Gold Nanoparticles Using Aged Drago Leaf Extract (Dracanea Draco L.): Manufacturing Process and Using, 2015.

[2] A. Primo, A. Corma, H. García, Titania supported gold nanoparticles as photocatalyst, Phys. Chem. Chem. Phys. 13 (2011) 886–910.

[3] B. Cojocaru, Ş. Neaţu, E. Sacaliuc-Pârvulescu, F. Lévy, V.I. Pârvulescu, H. Garcia, Influence of gold particle size on the photocatalytic activity for acetone oxidation of Au/TiO_2 catalysts prepared by dc-magnetron sputtering, Appl. Catal. B Environ. 107 (2011) 140–149.

[4] B. Tian, J. Zhang, T. Tong, F. Chen, Preparation of Au/TiO_2 catalysts from Au(I)-thiosulfate complex and study of their photocatalytic activity for the degradation of methyl orange, Appl. Catal. B Environ. 79 (2008) 394–401.

[5] J. Turkevich, P.C. Stevenson, J. Hillier, A study of the nucleation and growth processes in the synthesis of colloidal gold, Discuss. Faraday Soc. 11 (1951) 55–75.

[6] R.P. Santos, L.S. Mendes, B.M. Silva, P.G. De Pinho, P. Valentão, P.B. Andrade, J. a. Pereira, M. Carvalho, Phytochemical profiles and inhibitory effect on free radical-induced human erythrocyte damage of Dracaena draco leaf: A potential novel antioxidant agent, Food Chem. 124 (2011) 927–934.

[7] R. Zanella, S. Giorgio, C.R. Henry, C. Louis, Alternative methods for the preparation of gold nanoparticles supported on TiO_2, J. Phys. Chem. B. 106 (2002) 7634–7642.

[8] C.C. Hu, T.C. Hsu, L.H. Kao, One-step cohydrothermal synthesis of nitrogen-doped titanium oxide nanotubes with enhanced visible light photocatalytic activity, Int. J. Photoenergy. 2012 (2012) 1–9.

[9] Y. Ruzmanova, M. Stoller, M. Bravi, A. Chianese, A novel approach for the production of nitrogen doped TiO_2 nanoparticles, Chem. Eng. Trans. 43 (2015) 721–726.

[10] F. Peng, L. Cai, H. Yu, H. Wang, J. Yang, Synthesis and characterization of substitutional and interstitial nitrogen-doped titanium dioxides with visible light photocatalytic activity, J. Solid State Chem. 181 (2008) 130–136.

[11] S.A. Ansari, M.M. Khan, M.O. Ansari, M.H. Cho, Nitrogen-doped titanium dioxide (N-doped TiO_2) for visible light photocatalysis, New J. Chem. 40 (2016) 3000–3009.

[12] B. Tian, C. Li, F. Gu, H. Jiang, Synergetic effects of nitrogen doping and Au loading on enhancing the visible-light photocatalytic activity of nano-TiO_2, Catal. Commun. 10 (2009) 925–929.

[13] I. Chiu, Z. Shen, R. Wu, Promotion Effect of Au on N/TiO_2 for Hydrogen Generation from Water Splitting, 14 (2014) 7125–7130.

[14] X. Li, T. Fan, H. Zhou, B. Zhu, J. Ding, D. Zhang, Microporous and Mesoporous Materials A facile way to synthesize biomorphic N-TiO_2 incorporated with Au nanoparticles with narrow size distribution and high stability, Microporous Mesoporous Mater. 116 (2008) 478–484.

[15] L. Pinho, M.J. Mosquera, Photocatalytic activity of TiO_2-SiO_2 nanocomposites applied to buildings: Influence of particle size and loading, Appl. Catal. B Environ. 134–135 (2013) 205–221.

[16] G.S. Anjusree, A. Bhupathi, A. Balakrishnan, S. Vadukumpully, K.R. V Subramanian, N. Sivakumar, S. Ramakrishna, S. V. Nair, A.S. Nair, Fabricating fiber, rice and leaf-shaped TiO_2 by tuning the chemistry between TiO_2 and the polymer during electrospinning, RSC Adv. 3 (2013) 16720–16727.

[17] V. Amendola, R. Pilot, M. Frasconi, O.M. Maragò, M.A. Iatì, Surface plasmon resonance in gold nanoparticles: a review, J. Phys. Condens. Matter. 29 (2017) 203002.

[18] A. Ayati, A. Ahmadpour, F.F. Bamoharram, B. Tanhaei, M. Mänttäri, M. Sillanpää, A review on catalytic applications of Au/TiO_2 nanoparticles in the removal of water pollutant., Chemosphere. 107 (2014) 163–174.

[19] A. Mills, J. Wang, Photobleaching of methylene blue sensitised by TiO_2: an ambiguous system?, J. Photochem. Photobiol. A Chem. 127 (1999) 123–134.

[20] A. Houas, Photocatalytic degradation pathway of methylene blue in water, Appl. Catal. B Environ. 31 (2001) 145–157.

[21] V. Subramanian, E.E. Wolf, P. V. Kamat, Catalysis with TiO_2/gold manocomposites. effect of metal particle size on the fermi level equilibration, J. Am. Chem. Soc. 126 (2004) 4943–4950.

[22] P. V Kamat, D. Meisel, Nanoparticles in advanced oxidation processes, Curr. Opin. Colloid Interface Sci. 7 (2002) 282–287.

[23] Y. Zhou, D.M. King, X. Liang, J. Li, A.W. Weimer, Optimal preparation of Pt/TiO_2 photocatalysts using atomic layer deposition, Appl. Catal. B Environ. 101 (2010) 54–60.

[24] X. Zhang, Y.L. Chen, R.S. Liu, D.P. Tsai, Plasmonic photocatalysis., Rep. Prog. Phys. 76 (2013) 046401.

[25] S. Mubeen, G. Hernandez-Sosa, D. Moses, J. Lee, M. Moskovits, Plasmonic photosensitization of a wide band gap semiconductor: converting plasmons to charge carriers, Nano Lett. 11 (2011) 5548–5552.

[26] C. Langhammer, Z. Yuan, I. Zorić, B. Kasemo, Plasmonic properties of supported Pt and Pd nanostructures, Nano Lett. 6 (2006) 833–838.

[27] V.P. Zhdanov, C. Hägglund, B. Kasemo, Relaxation of plasmons in nm-sized metal particles located on or embedded in an amorphous semiconductor, Surf. Sci. 599 (2005) L372–L375.

[28] X. Chen, H. Zhu, J. Zhao, Z. Zheng, X. Gao, Visible-light-driven oxidation of organic contaminants in air with gold nanoparticle catalysts on oxide supports, Angew. Chemie Int. Ed. 47 (2008) 5353–5356.

[29] J. Lee, T. Javed, T. Skeini, A.O. Govorov, G.W. Bryant, N.A. Kotov, Bioconjugated Ag nanoparticles and CdTe nanowires: Metamaterials with field-enhanced light absorption, Angew. Chemie Int. Ed. 45 (2006) 4819–4823.

[30] V. Subramanian, E. Wolf, P. V. Kamat, Semiconductor−Metal composite nanostructures. To what extent do metal nanoparticles improve the photocatalytic activity of TiO_2 films?, J. Phys. Chem. B. 105 (2001) 11439–11446.

[31] K. Yamanaka, T. Morikawa, Charge-carrier dynamics in nitrogen-doped TiO_2 powder studied by femtosecond time-resolved diffuse reflectance spectroscopy, J. Phys. Chem. C. 116 (2012) 1286–1292.

[32] M. Rochkind, S. Pasternak, Y. Paz, Using dyes for evaluating photocatalytic properties: A critical review, Molecules. 20 (2015) 88–110.

[33] N. Barbero, D. Vione, Why dyes should not be used to test the photocatalytic activity of semiconductor oxides, Environ. Sci. Technol. 50 (2016) 2130–2131.

[34] L. Yang, A. Hakki, L. Zheng, M.R. Jones, F. Wang, D.E. Macphee, Photocatalytic concrete for NOx abatement: Supported TiO2 efficiencies and impacts, Cem. Concr. Res. 116 (2019) 57–64.

[35] A. Mills, S. Elouali, The nitric oxide ISO photocatalytic reactor system: Measurement of NO_x removal activity and capacity, J. Photochem. Photobiol. A Chem. 305 (2015) 29–36.

[36] Y. Ohko, Y. Nakamura, N. Negishi, S. Matsuzawa, K. Takeuchi, Photocatalytic oxidation of nitrogen monoxide using TiO_2 thin films under continuous UV light illumination, J. Photochem. Photobiol. A Chem. 205 (2009) 28–33.

[37] Z. Wu, Z. Sheng, Y. Liu, H. Wang, N. Tang, J. Wang, Characterization and activity of Pd-modified TiO_2 catalysts for photocatalytic oxidation of NO in gas phase, J. Hazard. Mater. 164 (2009) 542–548.

[38] W. Zhu, S. Xiao, D. Zhang, P. Liu, H. Zhou, W. Dai, F. Liu, H. Li, Highly efficient and stable Au/CeO_2–TiO_2 photocatalyst for nitric oxide abatement: Potential application in flue gas treatment, Langmuir. 31 (2015) 10822–10830.

[39] D. Zhang, M. Wen, S. Zhang, P. Liu, W. Zhu, G. Li, H. Li, Au nanoparticles enhanced rutile TiO_2 nanorod bundles with high visible-light photocatalytic performance for NO oxidation, Appl. Catal. B Environ. 147 (2014) 610–616.

[40] R. Aelion, A. Loebel, F. Eirich, Hydrolisis of Ethyl Silicate, J. Chem. Soc. 72 (1950) 5705–5712.

[41] L. Pinho, F. Elhaddad, D.S. Facio, M.J. Mosquera, A novel TiO_2–SiO_2 nanocomposite converts a very friable stone into a self-cleaning building material, Appl. Surf. Sci. 275 (2013) 389–396.

[42] American Coating Association, Optimum Viscosity for Paint Application, https://www.paint.org/article/optimum-viscosity-paint-application/ (accessed March 28, 2019).

[43] L. Pinho, M.J. Mosquera, Titania-silica nanocomposite photocatalysts with application in stone self-cleaning, J. Phys. Chem. C. 115 (2011) 22851–22862.

[44] M. Thommes, K. Kaneko, A. V. Neimark, J.P. Olivier, F. Rodriguez-Reinoso, J. Rouquerol, K.S.W. Sing, Physisorption of gases, with special reference to the evaluation of surface area and pore size distribution (IUPAC Technical Report), Pure Appl. Chem. 87 (2015) 1051–1069.

[45] K.A. Cychosz, R. Guillet-Nicolas, J. García-Martínez, M. Thommes, Recent advances in the textural characterization of hierarchically structured nanoporous materials, Chem. Soc. Rev. 46 (2017) 389–414.

[46] C.J. Brinker, Hydrolysis and condensation of silicates: Effects on structure, J. Non. Cryst. Solids. 100 (1988) 31–50.

[47] D. Balköse, Effect of preparation pH on pore structure of silica gels, J. Chem. Technol. Biotechnol. 49 (2007) 165–171.

[48] T. Takeda, S. Okazaki, Adsorption of various amines on titanium(IV) oxide from aqueous solution, Chem. Soc. Japan. 270 (1983) 608–611.

[49] I.A. Polunina, A.A. Isirikyan, K.E. Polounine, S.S. Mikhailova, Water influence on the

surfactant adsorption on TiO_2, Colloids Surfaces A Physicochem. Eng. Asp. 160 (1999) 141–146.

[50] L.-F.F. Liao, W.-C.C. Wu, C.-C.C. Chuang, J.-L.L. Lin, FTIR study of adsorption and reactions of methylamine on powdered TiO_2, J. Phys. Chem. B. 105 (2001) 5928–5934.

[51] I.A. Mudunkotuwa, V.H. Grassian, Citric acid adsorption on TiO_2 nanoparticles in aqueous suspensions at acidic and circumneutral pH: Surface coverage, surface speciation, and its impact on nanoparticle−nanoparticle interactions, J. Am. Chem. Soc. 132 (2010) 14986–14994.

[52] Y. Yamauchi, F. Takeuchi, S. Todoroki, Y. Sakka, S. Inoue, Spherical Mesoporous Silica Particles with Titanium Dioxide Nanoparticles by an Aerosol-assisted Coassembly, Chem. Lett. 37 (2008) 72–73.

[53] N. Suzuki, X. Jiang, L. Radhakrishnan, K. Takai, K. Shimasaki, Y.T. Huang, N. Miyamoto, Y. Yamauchi, Hybridization of photoactive titania nanoparticles with mesoporous silica nanoparticles and investigation of their photocatalytic activity, Bull. Chem. Soc. Jpn. 84 (2011) 812–817.

[54] P. Zhang, J. Tian, R. Xu, G. Ma, Hydrophilicity, photocatalytic activity and stability of tetraethyl orthosilicate modified TiO_2 film on glazed ceramic surface, Appl. Surf. Sci. 266 (2013) 141–147.

[55] H.F. Ting, C.M. Chen, F.H. Lu, S.Y. Suen, Adsorption and photodegradation of methylene blue using a bulk Ti material with porous titania layer prepared by chemical oxidation, J. Taiwan Inst. Chem. Eng. 45 (2014) 617–624.

[56] A.H. Jawad, N.S.A. Mubarak, M.A.M. Ishak, K. Ismail, W.I. Nawawi, Kinetics of

photocatalytic decolourization of cationic dye using porous TiO_2 film, J. Taibah Univ. Sci. 10 (2016) 352–362.

[57] J. Zhang, L.R. Grabstanowicz, S. Gao, N.S. Hosmane, B. Huang, Y. Dai, D. Liu, T. Xu, Visible-light photocatalytic SiO_2 /TiO_{2-x} C_x/C nanoporous composites using $TiCl_4$ as the precursor for TiO_2 and polyhydroxyl tannin as the carbon source, Catal. Sci. Technol. 2 (2012) 390–399.

[58] I. Sopyan, M. Watanabe, S. Murasawa, K. Hashimoto, A. Fujishima, A film-type photocatalyst incorporating highly active TiO_2 powder and fluororesin binder: photocatalytic activity and long-term stability, J. Electroanal. Chem. 415 (1996) 183–186.

[59] D. Fattakhova-Rohlfing, J.M. Szeifert, Q. Yu, V. Kalousek, J. Rathouský, T. Bein, Low-temperature synthesis of mesoporous titania−silica films with pre-formed anatase nanocrystals, Chem. Mater. 21 (2009) 2410–2417.

[60] E. Beyers, E. Biermans, S. Ribbens, K. De Witte, M. Mertens, V. Meynen, S. Bals, G. Van Tendeloo, E.F. Vansant, P. Cool, Combined TiO_2/SiO_2 mesoporous photocatalysts with location and phase controllable TiO_2 nanoparticles, Appl. Catal. B Environ. 88 (2009) 515–524.

[61] D.S. Facio, M. Luna, M.J. Mosquera, Facile preparation of mesoporous silica monoliths by an inverse micelle mechanism, Microporous Mesoporous Mater. 247 (2017) 166–176.

[62] S. Linic, P. Christopher, D.B. Ingram, Plasmonic-metal nanostructures for efficient conversion of solar to chemical energy, Nat. Mater. 10 (2011) 911–921.

[63] L. Pinho, J.C. Hernández-Garrido, J.J. Calvino, M.J. Mosquera, 2D and 3D

characterization of a surfactant-synthesized TiO_2–SiO_2 mesoporous photocatalyst obtained at ambient temperature, Phys. Chem. Chem. Phys. 15 (2013) 2800–2808.

[64] N. Balázs, D.F. Srankó, A. Dombi, P. Sipos, K. Mogyorósi, The effect of particle shape on the activity of nanocrystalline TiO_2 photocatalysts in phenol decomposition. Part 2: The key synthesis parameters influencing the particle shape and activity, Appl. Catal. B Environ. 96 (2010) 569–576.

[65] R.V. Mikhaylov, A.A. Lisachenko, B.N. Shelimov, V.B. Kazansky, G. Martra, G. Alberto, S. Coluccia, FTIR and TPD analysis of surface species on a TiO_2 photocatalyst exposed to NO, CO, and NO−CO mixtures: Effect of UV−Vis light irradiation, J. Phys. Chem. C. 113 (2009) 20381–20387.

[66] C. Miliani, M.L. Velo-Simpson, G.W. Scherer, Particle-modified consolidants: A study on the effect of particles on sol-gel properties and consolidation effectiveness, J. Cult. Herit. 8 (2007) 1–6.

[67] KEIM Soldalit®-ME, https://www.keimpaintshop.co.uk/shop/view/9-Soldalit-ME-/405-White (accessed March 14, 2019).

[68] J.F. Illescas, M.J. Mosquera, Surfactant-Synthesized PDMS/Silica Nanomaterials Improve Robustness and Stain Resistance of Carbonate Stone, J. Phys. Chem. C. 115 (2011) 14624–14634.

[69] C. Mendoza, A. Valle, M. Castellote, A. Bahamonde, M. Faraldos, TiO_2 and TiO_2–SiO_2 coated cement: Comparison of mechanic and photocatalytic properties, Appl. Catal. B Environ. 178 (2015) 155–164.

[70] G. Borsoi, R. Veiga, A.S. Silva, Effect of nanostructured lime-based and silica-based

products on the consolidation of historical renders, in: 3rd Hist. Mortars Conf., 2013: pp. 1–9.

[71] L. Pinho, M. Rojas, M.J. Mosquera, Ag–SiO_2–TiO_2 nanocomposite coatings with enhanced photoactivity for self-cleaning application on building materials, Appl. Catal. B Environ. 178 (2015) 144–154.

[72] P. Kubelka, F. Munk, Ein Beitrag zur Optik der Farbanstriche, Z. Tech. Phys. 12 (1931) 593–601.

[73] P. Kubelka, New Contributions to the Optics of Intensely Light-Scattering Materials. Part I, J. Opt. Soc. Am. 44 (1948) 448–457.

[74] M.P. Fuller, P.R. Griffiths, Diffuse reflectance measurements by infrared Fourier transform spectrometry, Anal. Chem. 50 (1978) 1906–1910.

[75] K. Murugan, T.N. Rao, A.S. Gandhi, B.S. Murty, Effect of aggregation of methylene blue dye on TiO_2 surface in self-cleaning studies, Catal. Commun. 11 (2010) 518–521.

[76] K. Murugan, J. Joardar, a. S. Gandhi, B.S. Murty, P.H. Borse, Photo-induced monomer/dimer kinetics in methylene blue degradation over doped and phase controlled nano-TiO_2 films, RSC Adv. 6 (2016) 43563–43573.

[77] K. Rajeshwar, M.E. Osugi, W. Chanmanee, C.R. Chenthamarakshan, M.V.B. Zanoni, P. Kajitvichyanukul, R. Krishnan-Ayer, Heterogeneous photocatalytic treatment of organic dyes in air and aqueous media, J. Photochem. Photobiol. C Photochem. Rev. 9 (2008) 171–192.

[78] R. Zouzelka, J. Rathousky, Photocatalytic abatement of NO_x pollutants in the air using commercial functional coating with porous morphology, Appl. Catal. B Environ. 217

(2017) 466–476.

Chapter 9

Conclusions

According to the obtained results during the progress of the Doctoral Thesis, we can conclude that the here developed $Au/TiO_2/SiO_2$ photocatalysts can be applied as sol on building materials of different nature, where the sols spontaneously gel producing $Au/TiO_2/SiO_2$ photocatalytic coatings with self-cleaning and depolluting properties. Those corresponding to the coated building materials have been validated employing real pollutants, such as soot and NO, which demonstrates the potential use of the developed photocatalysts for real applications.

In addition, it is possible to stablish the following specific conclusions:

-The AuNPs enhance the TiO_2 photoactivity, allow the visible activation of TiO_2 and promote the selectivity of the NO photo-oxidation process. The AuNPs lowest size (5nm) are most adequate for enhancing the TiO_2 photoactivity. Intermedium gold loading (0.5 % wt.) shows the highest performance because some negative aspects (such as TiO_2 agglomeration or textural modification) are promoted for the highest loadings.

-The method of AuNPs incorporation to the photocatalyst determines its properties. The integration of AuNPs dispersed in water to the sol-gel synthesis gives rise to several disadvantages associated to the increase of water amount in the media synthesis. On the other hand, the integration of a preformed Au/TiO_2 in the sol-gel synthesis produces materials with better photocatalytic activity.

-There is a clear correlation between textural and structural properties of the photocatalysts and their performance. The photoactivity is promoted as the textural parameters (surface area and pore volume) are raised and it decreases when TiO_2 is agglomerated.

-The presence of reagent remnants from the AuNPs synthesis in the photocatalysts modifies their properties. Citrate and PVP change the pH behaviour of the photocatalysts and promote the TiO_2 agglomeration.

-The silica matrix promotes the TiO_2 adhesion to the substrates. Therefore, the developed treatments in this Thesis could lead to more durable materials than a bare TiO_2 particles based-treatment against the weathering.

-The double TiO_2 modification by AuNPs deposition and by nitrogen doping, both achieved by means of the deposition-precipitation synthesis method here proposed, produces a synergetic effect in the photoactivity enhancement. In addition, the obtained Au/N-TiO_2/SiO_2 photocatalysts are considerably more active than those prepared from preformed AuNPs.

-The substrate determines the final characteristics of the photocatalytic building material. The substrate porosity affects strongly the sol absorption, higher amounts of photocatalyst enhance the photoactivity but also induce higher colour variations of the substrates. The chemical composition of the substrate and therefore its acid-basic properties, can also modify the sample activity. In particular, the more alkaline behaviour of concrete in relation to limestone promotes the NO_x photodegradation.

-The promoted-TiO_2/SiO_2 ratio of the coating is directly related to its activity. On the other hand, the sol viscosity is increased as the TiO_2 loading is raised reducing the absorption and penetration in the substrate. The increase of the TiO_2 content also induces higher colour variations in the coated materials.